THE HONG KONG POLYTECHNIC UNIVERSITY

Department of Electrical Engineering

Investigations into the Use of Energy Storage in Power System Applications

Leung Ka Kit

Thesis submitted for the degree of
Doctor of Philosophy in Engineering

2001

ACKNOWLEDGEMENTS

I am indebted to my supervisor Professor Danny Sutanto for his invaluable guidance. He is the one who made me feel puzzled at the beginning and he is also the one who made me feel delightful at the end of my research. His thoughtful guidance and his enthusiasm on the research gave me the spiritual support on my work.

I wish to express my deepest appreciation to my bachelor degree supervisor Professor A.K. David for giving me the opportunity in his project that paved the way on now of my research work. I also thank for his encouragement during the early stage of my research.

I would like to thank my parents for their sacrifices and giving me private area at home for my work. I wish my brother, who is going to marry this month, has a wonderful new family. I would like to thank my dear Jenny, who brings me happiness and trouble that make my life excited.

I would also like to thank my roommate Divakar, Nelson and all of my friends for giving me encouragement.

Without their support, this project would not be completed.

John

September 2000

Abstract

This thesis embodies research work on the design and implementation of novel fast responding battery energy storage systems, which, with sufficient capacity and rating, could remove the uncertainty in forecasting the annual peak demand. They would also benefit the day to day operation by curtailing the fastest demand variations, particularly at the daily peak periods. Energy storage that could curtail peak demands, when the most difficult operational problems occur offers a promising approach. Although AC energy cannot be stored, power electronic developments offer a fast responding interface between the AC network and DC energy stored in batteries. The attractive feature of the use of this energy storage could most effectively be located near the source of load variations, i.e. near consumers in the distribution networks. The proposed, three-phase multi-purpose, Battery Energy Storage System will provide active and reactive power independent of the supply voltage with excellent power quality in terms of its waveform.

Besides the above important functions applied at the distribution side of the utility, several new topologies have been developed to provide both Dynamic Voltage Regulator (DVR) and Unified Power Flow Controller (UPFC) functions for line compensation. These new topologies can provide fast and accurate control of power flow along a distribution corridor. The topologies also provide for fast damping of system oscillation due to transient or dynamic disturbances.

Having demonstrated the various functions that the proposed Battery Energy Storage System can provide, the final part of the thesis investigates means of improving the performance of the proposed BESS. First, there is a need to reduce the switching losses by using soft switching instead of hard switching. A soft switching inverter using a parallel resonant dc-link (PRDCL) is proposed for use with the proposed BESS. The proposed PRDCL suppresses the dc-link voltage to zero for a very short time to allow zero voltage switching of inverter main switches without imposing excessive voltage and current stresses.

Finally, in practice the battery terminal voltage fluctuates significantly as large current is being drawn or absorbed by the battery bank. When a hysteresis controller is used to control the supply line current, the ripple magnitude and frequency of the controlled current is highly dependent on the battery voltage, line inductance and the band limits of the controller. Even when these parameters are constant, the switching frequency can vary over quite a large range. A novel method is proposed to overcome this problem by controlling the dc voltage level by means of a dc-dc converter to provide a controllable voltage at the inverter dc terminal irrespective of the battery voltage variations. By proper control of the magnitude and frequency of the output of the DC-DC converter, the switching frequency can be made close to constant. A mathematical proof has been formulated and results from the simulation confirm that using the proposed technique, the frequency band has been significantly reduced and for the theoretical case, a single switching frequency is observed. The main disadvantage is the need to have an extra dc-dc converter, but this is relatively cheap and easy to obtain.

List of Figures

List of Tables

List of Acronyms

ADC	Analog to digital converter
ARCPI	Auxiliary resonant commutated pole inverter
BESS	Battery energy storage system
DAC	Digital to analog converter
DSP	Digital signal processing
DVR	Dynamic voltage regulator
EMI	Electro-Magnetic Interference
EPRI	Electrical Power Research Institution
ESPRC	Engineering and Physical Science Research Council
ESPSS	Energy storage power system stabilizer
FACTS	Flexible ac transmission system
GTO	Gate-turn-off thyristor
HVDC	High voltage direct current
I/O	Input/output
IEA	International Energy Agency
IGBT	Insulated gate bipolar transistor
KCL	Kirchhoff's current law
PCS	Power conversion system
PRDCL	Parallel resonant dc-link
PREPA	Puerto Rico Electric Power Authority
PV	Photovoltaics

PWM	Pulse width modulation
RDCLI	Resonant dc-link inverter
RPI	Resonant pole inverter
SMES	Super-conducting magnetic energy storage
SOC	State of charge
SPFC	Storage power flow controller
SPSS	Single phase soft-switching
SSR	Subsynchronous resonance
STATCON	Static condensor
SVC	Static var compensator
THD	Total-harmonic-distortion
TSCS	Thyristor Series Compensation Systems
UPFC	Unified power flow controller
UPS	Un-interruptible power supply
VPC	Voltage per cell
VSI	Voltage source inverter
YMC	Young members committee
ZCS	Zero current switching
ZVS	Zero voltage switching

Title: - Investigations into the Use of Energy Storage in Power System Applications

Table of Contents

CHAPTER 1 INTRODUCTION

Uncertainty is painful for all people, and for all men.

Napoleon Bonaparte (1769-1821)

Political Aphorisms, Moral and Philosophical Thoughts of the Emperor Napoleon, collected by Cte. Ate. G. De Liancourt.

CHAPTER 1 INTRODUCTION

The consumer expects an electricity supply, which is available at all times and having a tight regulation of voltage and frequency for all appliances. Since, all consumers are free to alter their demands at any time, coupled with the inability to store AC power, this is a factor associated with the following power system operation and control problems, which all relate to uncertainty:

- It is impossible to precisely forecast demands even from hour to hour,
- Power system planning hinges on forecast of annual peak growth that is not known a priori,
- It is not possible to predict the numerous disturbances that do occur,
- Generator availability can vary unpredictably from day to day,
- System configuration constantly alters with outages of lines, cables and substation equipment.

The present method of handling uncertainty is very expensive because it requires redundancy of system equipment and use of additional generation to allow for unexpected outages as well as excessive demand than expected. The greatest difficulties are posed by the daily peak periods, when not only the highest demand occurs but also the fastest rates of load change. The largest demand forecasting errors are at peak periods, a serious problem as the power system becoming more susceptible to disturbances as loading increases.

Power systems throughout the world have also been affected by financial constraints (due to the worldwide economic downturn) as well as the community's environmental expectations. Both these factors have impeded the establishment of new power stations and additional transmission lines, which are needed to maintain the existing levels of power system reliability. The constant threat to the reliability of electricity is posed by the uncertainty associated with power system operation, namely, the continually varying loads and the numerous perturbations and disturbances to the power system, many times these have led to serious interruptions of services. As an example, the extensive system collapse which interrupted New York in 1977, was costed at $US350 million, 20% of the value of New York's electrical network (Dobie, W.C., 1998).

The conventional capital intensive approach for achieving reliability of supply had required long term financial decisions that are no longer possible with the uncertain rates of electricity demand growth coupled to the prevailing world economic uncertainties. The present situation undermines system security as well as reliability of supply to consumers so there is a need for a new approach which would be able to reduce uncertainty.

Although there are different aspects to power system uncertainty, the major problem is set by the difficulty of demand forecasting. Demand forecasting has two aspects: short term for day to day operation; and the annual peak demand on which the major cost commitments, both capital and operational, are focussed in the continuing development of the power system. Daily peak periods, because of their short duration, are associated

with only a small amount of the daily energy consumption, even on the day of annual peak demand.

This thesis embodies research work on the design and implementation of novel fast responding battery energy storage systems, which, with sufficient capacity and rating, could remove the uncertainty in forecasting the annual peak demand. They would also benefit the day to day operation by curtailing the fastest demand variations, particularly at the daily peak periods. Energy storage that could curtail peak demands, when the most difficult operational problems occur offers a promising approach. Although AC energy cannot be stored, power electronic developments offer a fast responding interface between the AC network and DC energy stored in batteries. The attractive feature of the use of this energy storage could most effectively be located near the source of load variations, i.e. near consumers in the distribution networks. The proposed, three-phase multi-purpose, Battery Energy Storage System (BESS) will provide active and reactive power independent of the supply voltage with excellent power quality in terms of its waveform.

Conventional BESS (Bhargava, B. and Dishaw, G., 1998; Hurwitch, H.J. and Carpenter, C.A., 1991; Kunisch, H.J. and Kramer, K.G., 1981; Nitschke, H.J., 1987; Voigt, B., Kunisch, H.J. and Kramer, K.G., 1989) employs voltage mode control for the inverter voltage manipulation. By manipulating the magnitude and phase of the inverter voltage, independent active and reactive power outputs of the inverter can be controlled. However, harmonic filters are usually required and the transient response is usually quite slow.

In the proposed BESS, current mode control based on hysteresis technique has been employed to increase the speed of response and to provide a controllable source current. By proper control, almost constant current will be drawn from the source and hence improved load factor can be obtained. By controlling the wave-shape of the ac source current, active filtering, power factor correction and harmonic control can automatically be provided. The fast responses provided by the current state-of-the-art power electronics and microprocessor control within BESS offer a wide range of additional power system applications, such as back-up supply, spinning reserve, improved damping both during dynamic and transient disturbances, energy management, and the ability to provide 'negative load shedding' during emergency operating conditions. In one device, the proposed BESS can provide several functions, which can provide significant improvement to power system performance.

The other contribution from the research is summarized below. Several new topologies have been developed for the BESS to provide Unified Power Flow Controller (UPFC) functions. These new topologies provide control for power flow through a distribution corridor, protect against temporary voltage sag and swell during short-term disturbance, and compensate for voltage drop in a long line. Although the configuration looks similar to the traditional UPFC configuration, the performance and control strategy are significantly different, as the energy used during the peak period has to be returned at low load period to ensure energy balance. Since active power is now available, we can have significant improvement in terms of performance when compared to the standard UPFC. One of the proposed topologies can now control not only the flow in the line but also the source current, and hence as far as the supply is concerned, the load always

appears constant and sinusoidal in nature, irrespective of the changes in the load both in magnitude and waveform.

Having demonstrated the various functions that the proposed BESS can provide, the final part of the thesis investigates the means of improving the performance of the proposed BESS. First, there is a need to reduce the switching losses by using the soft switching instead of the hard switching technique. A soft switching inverter using a parallel resonant dc-link (PRDCL) and a single phase soft switching (SPSS) technique (Venkataramanan, G. and Divan, D.M., 1993) is proposed for use with the proposed BESS. The proposed PRDCL suppresses the dc-link voltage to zero for a very short time to allow zero voltage switching of the inverter main switches without imposing excessive voltage and current stresses. In addition, the voltage stresses of all the inverter switches are limited by the battery voltage only. The PRDCL provides not only variable link pulse width but also variable pulse position thereby increasing the capability of the proposed PRDCL converter.

Finally, the hysteresis control scheme adopted in this project provides for fast-response current loop and inherent peak current limit capability without requiring any information on the system parameters. However, the use of a fixed hysteresis band has the disadvantage that the switching frequency varies within a band because peak-to-peak current ripple is required to be controlled at all points of the fundamental frequency wave. As a result, the controlled current contains excess harmonics. To deal with this problem, many papers utilized a controllable band, such as sinusoidal band (Rahman, K.M., Khan, M.R., Choudhury, M.A. and Rahman, M.A., 1997) and variable-band

(Tripathi, A. and Sen, P.C., 1992) to fix the switching frequency. However, these papers assumed that the dc voltage is constant at all time, whereas actually the battery voltage in the worst case may vary by a factor of two from full discharging to full charging. Experimental results show that the switching frequency tends to vary with the variation of battery voltage making the proposed techniques described in the above papers unsuitable for the BESS used in this research project. A novel method to overcome this problem is proposed, where the dc voltage level is continuously controlled by means of a dc-dc converter to provide a suitable instantaneous voltage at the inverter dc terminal at each instant of time. The controllable voltage is designed in such a way that a constant switching frequency can be obtained, even when fixed hysteresis band is used. A mathematical proof of this novel proposal has been formulated and the results from the simulation confirm that using the proposed technique, the switching frequency band has been significantly reduced and when an ideal case is considered, only a single switching frequency is observed. The main disadvantage is the need to have an extra dc-dc converter, but this is relatively cheap and easy to obtain.

ORGANIZATION OF THE THESIS:

In this thesis a brief literature review on the applications of Battery Energy Storage Systems for improving power system performance will be given in Chapter 2. Actual implementations and the applications, in which these implementations have been used will be provided. Most of these implementations are, however, limited in nature, in that each BESS can provide only one or two functions. With the current technology of microprocessors and fast switching power electronic devices, the thesis will explore the

possibility of having one BESS which can provide a comprehensive multi-function as such that all the potential benefits of the BESS can be fully realized.

Chapter 3 will introduce the proposed BESS for connection with the utility grid. The use of hysteresis controller to control the supply current to be constant will be described. Results from laboratory tests using single-phase system will be shown to demonstrate the capabilities of the proposed BESS, in particular the load leveling, active filtering, power factor compensation, un-interruptible power supply (UPS) operation and energy management functions.

Chapter 4 will extend the implementation to a 3-phase system and discuss the efficiency that can be obtained. Results from laboratory experiments will be discussed.

Chapter 5 will discuss several new topologies that can utilize BESS to operate as a Unified Power Flow Controller (UPFC). The chapter will also demonstrate how the proposed topologies can provide all the functions of UPFC such as providing voltage control both in sending and receiving end, series compensation and phase angle regulation. Results from laboratory tests will be provided to show the operation of the proposed topologies when connected to the utility grid through two transmission lines with unequal impedance.

Chapter 6 will discuss means of improving the performance of the BESS. Section 6.1 will describe the proposed soft switching technique to reduce switching losses based on parallel resonant dc-link (PRDCL) and single-phase soft switching (SPSS). Sections 6.2 – 6.3 will discuss the novel proposal of using a DC-DC converter to provide a constant switching frequency even when a fixed frequency band is used in the hysteresis controller.

SUMMARY OF ORIGINAL CONTRIBUTIONS AND PUBLICATIONS

The following portions of this thesis are considered as the original contributions to the state of scientific at the present time to the author's best knowledge:

1. The design and implementation of a single and a three-phase Battery Energy Storage System with multi-function capability for connection to the utility grid to improve power system performance and reliability.

2. The use of hysteresis technique to control the utility current (waveform and magnitude) through a BESS has never been reported by other researchers.

3. Three novel topologies have been designed and developed that can provide tight control of transmission line power flow and have more advanced capability than the recently developed Unified Power Flow Controller (UPFC).

4. A mathematical formulation has been developed to demonstrate that the BESS can provide all UPFC functions in particular: Series compensation, phase shifting capability and reactive power compensation.

5. The improvement of the BESS performance by employing the soft-switching instead of the hard switching technique, as far as the author is aware, is the first time that a parallel resonant dc-link inverter has been used to improve BESS performance.

6. The means of reducing the switching frequency band when hysteresis technique is used have been proposed, which has never been reported before. This overcomes one of the most difficult drawbacks of the hysteresis technique.

Based on the above-mentioned idea, papers published and under review are listed as follows:

Implementation of a single-phase Battery Energy Storage System based on the hysteresis current control with multi-function capability as described in Chapter 3 are recorded in:

K.K. Leung and D. Sutanto, "Improving Power System Operations & Control utilizing Energy Storage," published at the International Conference on Power Conversion and Intelligent Motions (PCIM) - Oct.14-17, 1997, Hong Kong.

K.K. Leung and D. Sutanto, "Novel Controllers utilizing Energy Storage," published at the International Conference on Australian Universities Power Engineering (AUPEC) Sept. 29-Oct. 1, 1997, Sydney, Australia.

K.K. Leung and D. Sutanto, "Novel Power System Controllers utilizing Energy Storage," published at the International Conference on Advances in Power System Control, Operation & Management (APSCOM) Nov. 14-17, 1997, Hong Kong.

K.K. Leung and Sutanto, D., "A new topology of a battery energy storage system" Proceedings of International Conference on Energy Management and Power Delivery, 1998. EMPD'98, Volume: 1, 1998, Page(s): 253 –258.

K.K. Leung and D. Sutanto, "A Novel Implementation of a Battery Energy Storage System to Improve Power System Performance" International Conference on Power System Computation Conference (PSCC) 28 June - 2 July, 1999, Norway.

K.K. Leung and D. Sutanto, "Using energy storage to improve power system operations and control." Submitted to IEEE Transactions on Energy Conversion.

K.K. Leung and D. Sutanto, "Three-phase implementation of Battery Energy Storage System with multi-function capability in a single controller." Submitted to IEE Power Engineering Journal.

The invention of Storage Power Flow Controller (SPFC) having the capability to provide FACTS facilities as described in Chapter 5 are presented:

K.K. Leung and D. Sutanto, "A Storage Power Flow Controller (SPFC) using Battery Storage" International Conference on Power Electronics and Drive Systems (PEDS) July 26-29, 1999, Hong Kong.

K.K. Leung and D. Sutanto, "A Novel Power Flow Controller using Battery Energy Storage" Submitted to IEEE Transactions on Power System.

K.K. Leung and D. Sutanto, "The Implementation of Storage Type Power Flow Controller using Battery Storage" Submitted to Journal of Power Electronics (JPE) and is currently being revised following the comment of the reviewer.

A novel current controller for Battery Energy Storage System with fixed-hysteresis band and constant switching frequency as described in Chapter 6 is submitted to:

K.K. Leung and D. Sutanto, "A Novel Current Controller for Battery Energy Storage Systems (BESS) with Fixed-Hysteresis Band and Constant Modulation Frequency" Submitted to IEEE Transactions on Power Electronics.

CHAPTER 2 LITERATURE REVIEW ON BATTERY ENERGY STORAGE SYSTEM

If you are not a part of the solution, you are a part of the problem.

CHAPTER 2 LITERATURE REVIEW ON BATTERY ENERGY STORAGE SYSTEM (BESS)

2.1 Introduction

The history of electrical energy storage systems can be traced back to the early days of power generation with lead-acid accumulator batteries supplying the residual loads on the DC networks (Woodbridge, J.L., 1909). The DC supply systems based on battery energy storage was then a state-of-the-art technology. In the 1930's, battery storage plant power had grown to some 100MW, with all these plants running in parallel with the DC supply system (Berdelle, J., 1932). With the subsequent development of the AC electricity supply industry using large generating stations employing synchronous machines and extensive development of transmission and distribution networks radically only a few battery storage applications remain, mainly to perform relatively slow power regulation, such as load levelling or peak shaving. (Nitschke, H.J., 1987; Walker, L.H., 1990; Hunt, G.W., 1999). There is now a growing recognition that the fast responses provided by the power electronics within BESS offer a wide range of additional power system applications, such as area regulation, area protection, spinning reserve, power factor correction, thermal unit minimum loading and the ability to absorb qualifying facilities (Hurwitch and Carpenter, March 1991).

In the last decade or so, the battery energy storage system (BESS) has emerged as one of the most promising storage techniques for use in power systems that offer solutions to

many operational problems faced by today's power systems. The technology has been available commercially for some years now, though until the present time only a relatively small number of utilities have adopted it. Some BESS(s) have been installed as demonstration projects and some for commercial applications.

Power utilities throughout the world are facing increasingly tough financial and environmental restrictions which impede the building of new power stations and transmission lines. As a consequence, this has imposed operational difficulties in maintaining the current levels of reliability and security, especially during peak periods. Moreover, power stations located within city load centres are being progressively retired without being replaced, imposing more operational difficulties due to the need to transfer power from remote power stations to the load centres. As it can offer some solution to the problems, BESS has been proposed in the literature.

2.2 Literature review

There have been some research and development efforts on the use of BESS in power systems with the literature in the areas of economics, technology and applications. In the economics area, works have been done, for examples, in the economic models (Reckrodt, December 1990) and battery system breakeven costs (Sobieski and Bhavaraju, December 1985). The following literature review will emphasize on the technical aspects of the applications of BESS in power systems.

2.2.1 Use of Energy Storage in Power Systems

2.2.1.1 Load Leveling or Peak Shaving

BESS is traditionally viewed by power utilities as an option for providing relatively slow regulation to supply peak power through load levelling (DelMonaco *et al*, September 1982). In this view, low cost electric energy during off-peak periods would be used to charge the batteries and during peak periods the batteries could deliver back the stored energy into the system to offer a cost benefit. It is obvious that load curve characteristics, storage efficiency and tariff structures are important parameters that determine the feasibility of BESS for this purpose.

The large fluctuation of demand with time is the cause of all the power system operational problems. To meet the short but very high peak demand, many utilities must run generating units fuelled by expensive oil, such as gas turbines, whereas at off-peak periods, base-load generation, such as cheap coal and nuclear power plants, is constrained from operating at more efficient heavy output. BESS is capable of replacing gas turbines or other expensive combustion units and filling light load troughs.

However, the economic benefit of BESS for load levelling alone might not be justified if the difference in energy cost between during the peak and off-peak periods is small. To be economically viable, dynamic benefits have to be assessed. These include area regulation, area protection, spinning reserve, power factor correction, thermal unit minimum loading and the ability to absorb qualifying facilities (Hurwitch and Carpenter, March 1991). Current practice has large base-load power plants operating below their

rated capacity to provide spinning reserve and load following, even though providing such a reserve is quite costly. Hurwitch and Carpenter in March 1991 reported that " ... the West German utility Bewag has been able to save over $6.3 million annually in fuel costs and has achieved a 2-year payback on its 17 MW/14 MWh lead-acid battery energy storage plant which is used for maintaining load frequency control and for providing instantaneous reserve power".

2.2.1.2 Reactive Power Support

The roles of BESS in electric utilities, especially when installed in urban areas, has been given another perspective by (Lachs and Sutanto, 1992) in the form of reactive power loss reduction and voltage control. They argued that the installation of BESS in urban areas would significantly increase power system levels of reliability and security. They illustrate the point by providing a quantitative analysis of the reduction of reactive power losses of an urban supply system. The losses are examined separately for each supply segment: 330 kV lines, 330/132 kV transformers, 132 kV lines, 132/33 kV transformers, 33 kV lines and 33/11 kV transformers, under three loading situations: heavy loading (640 MW), peak loading (800 MW) and emergency (960 MW). Emphasis is given on the dramatic increase of MVAr losses during the heaviest loading which, though occurs only for short duration and corresponds to very small percentage of the daily energy, can reduce operational security. They pointed out that if 160 MW BESS is available at the 11 kV distribution network, which can be increased to 320 MW in emergency, it can reduce lines and transformers loading so that reduce the series losses considerably and ease the operational problems. In addition to its voltage control ability the BESS would eliminate the need for 170 MW of peaking generation, a significant cost benefit. As

reliability and security are measured by the flexibility and resilience built into the network by having reserve or emergency capacity in both transmission and generation, BESS in the urban areas provides that reserve capacity for the limited time needed to control emergencies. Load shedding, which interrupts consumers, is the most effective means to control emergencies. Lachs and Sutanto pointed out that a fast increase of BESS output would give the same effect without disturbing consumers. BESS in the urban areas can assist with voltage control 24 hours/day. During light load condition when voltage control could be difficult, BESS is charged to increase the loading and hence increase series MVAr losses to help absorb surplus line and cable charging besides, the BESS can absorb MVAr power.

2.2.1.3 Spinning reserve

Being an energy storage system, a sufficient number of BESS(s) connected on line can provide spinning reserve capability. This application requires rapid response and sufficient storage capacity to provide constant power for at least 30 minutes to cover the 'trip-out' generating unit and to prepare for the alternate power turbine to start (Eckroad, S. and Radimer, B., 1991). This application has been demonstrated by Puerto Rico Electric Power Authority in 1994.

2.2.1.3.1 Daily Operation

Short term operation is concerned with the day to day issues. Not only does the generator availability change from day to day, but different lines, cables or transformers may also be out of service. In addition, operational security must allow for the possibility of severe disturbances, particularly at the daily peak period and make the

necessary provisions to ensure that with its prevailing disposition, the power system would not be disrupted. Operational provisions are based on a daily load forecast of demand for each of the next 24 hours, with particular concern for the daily peak period (Kunisch, H.J. and Kramer, K.G., 1981). This is based on the daily generator schedule which ensures that at any time sufficient generators are running to meet the expected load. In addition, generating reserve is maintained to ensure that the demand can continue to be met should the largest generator be lost. At peak periods, the fast changes of demand are met by running up less efficient and more costly peaking generators, whereas at the overnight light load periods, some generators are shut down and then re-started for the morning load pick-up. Although this operational approach assures reliability of supply to consumers, it creates problems:

i. When thermal generators provide spinning reserve, they operate below their most efficient output, so producing a higher level of emissions.
ii. When thermal generators are required to track portion of the load changes, not only does it lower their efficiencies and increase emissions, but there is an increased mechanical wear on the boiler and turbine equipment, subsequently causing increased outage times.
iii. Peaking turbines have higher operating costs and produce a higher level of emissions than base load thermal units.
iv. Thermal units on cycling duty (shut down overnight) are subject to greatly increased wear and in spite of greater maintenance efforts, have reduced availability. Substantial amount of fuel used in the morning startup which produces emissions without energy output.
v. The cost of staffing power stations must be met, even if some do not operate every day.

The greatest single component of electricity cost is due to generation. This cost component, particularly on thermal units, could be significantly reduced if generators could be held continuously at their most efficient outputs. Not only would this also reduce the level of emissions but it would lower wear and maintenance requirement, improve availability as well as extending the life of the thermal power stations. All these potential benefits are sacrificed by the need to maintain reliability of supply when tracking the continually varying system demand.

The daily peak period, when the fastest load changes occur poses the greatest difficulties, and at that time the cost of production is often made higher by the need to start up peaking generators. Further costs are often incurred at peak periods by operating measures, such as constraints on transmission line loadings, to assure the security of the power system (Lo, C.H. and Anderson, M.D., 1999). By the use of a battery energy storage system, the required peak-load energy and peak power are substituted by stored, renewable produced energy. The smoothing of system load by the use of storage leads to an improved use of the existing system capacity and, thus, to a delay in system extension measures. At the same time the transmission losses in the system and the costs for the reserve are reduced. The cost advantages, that are achieved by the reduction of the primary energy use and the optimal use of power station and grid capacities, are given on to the consumers through power contracts agreed with the utilities.

2.2.1.4 Frequency control.

The conventional method of performing load frequency control is by running quick-acting turbo-generator units, without re-heater, fed by a drum type boiler. Unfortunately, such units have poor efficiency and high operating cost.

With sufficient BESS on line, the BESS can quickly alternate between charge and discharge to ensure that the frequency can be maintained constant. If the frequency try to rise, the BESS can act as a braking load which force the frequency to come down, and when the frequency try to reduce, the BESS can act as a generator to provide sufficient active power to increase the frequency. In this way a very effective damping to load frequency variation can be obtained. In BEWAG generation mixed base-load energy can be produced some 40 percent cheaper than energy coming from load frequency control units (Alt, J.T., Anderson, M.D. and Jungst, R.G., 1997).

2.2.1.5 Power system stabilization.

It is possible by using an energy storage power system stabilizer (ESPSS), which is different from a conventional power system stabilizer, to change the power output of the power source rather than the voltage or the reactive power output. The installation of the ESPSS (Bhargava, B. and Dishaw, G., 1998) at the Chino BESS power station in United State of America is used to modulate the existing BESS active power output to damp the inter-area oscillations between the Northwest and Southwest at about 0.3 Hz and between California and Arizona at about 0.7 Hz. The ESPSS triggers whenever the frequency deviation exceeds the set dead band value. Once triggered the BESS will provide power regulation within +/- 10 MW depending upon the ESPSS signal level and

the set gain. The dead band can also be adjusted and is presently set at +/- 0.03 Hz. The ESPSS can function on the frequency deviation at the local 12.5 kV bus or also on the compensated value for a remote bus location. The field tests and operation responding to system disturbances are included in this paper to verify the concept of providing damping for power system swings using the ESPSS.

A field experiment of stabilization by a Super-conducting Magnetic Energy Storage (SMES) system for a small hydro power plant in a transmission line of Kyushu Electric Power Co., Japan, was presented (Irei, F., Takeo, M and et al, 1992) in 1992. The SMES system is composed of two 30 kVA converters which can be controlled in the full area of a P-Q plane, and a super-conducting magnet system with an energy capacity of 30 kJ at 100A. The hydro power plant with a rating of 60 kW at 3.3 kV is connected to a 6.6 kV commercial power distribution line via a transformer. The purpose of this experiment is to demonstrate the applicability of the SMES stabilization system to practical transmission lines. In this study a sudden insertion of two inductors in series with the transmission line is used to simulate the system fault. To confirm the compensation for a short period of voltage dip and the stabilization of the generator speed fluctuation following the system disturbance, different input signals, such as generator speed deviation, active power flow of the transmission line and generator terminal voltage, can be used to control the active and reactive power output of the SMES system. In this experiment, a comparison of the control characteristics obtained by different choices of control variables is made. This paper concluded that generator speed deviation control strategy is more effective than that of using active power of the transmission line. However, for practical application in which a transmission line is connected with many

generators, the control strategy using active power of the transmission line as the input signal is simpler because it needs only the active power to be measured. Besides, this paper also pointed out that a small SMES power rating which is less than 15% of the generator power output is already effective to stabilize the system. This result might give a good support to the introduction of the energy storage, not only SMES but also BESS, for stabilizing the practical power system. The application of the SMES and BESS to compensate for voltage dips might be another attractive use of the energy storage in power systems.

2.2.1.6 Integration with renewable.

Renewable energy sources are increasingly being exploited for electricity generation. In the case of wind generation, the present installed capacity world-wide totals around 6000MW. In the UK as of March 1998, there are a total of 43 wind farms with 725 operational turbines, totally 309 MW installed (YMC Delegation, 1996). This is only around 0.5% of the UK total electricity generation capacity, but it is likely that the proportion will continue to increase, because the resource is plentiful and the generation cost at around 3.5 p/kWh is already competitive with gas. Denmark has at present a total installed wind generation capacity of 1100 MW, over 10 % of the total generation capacity, and has an ambitious target of 4000 MW offshore wind generation capacity by 2030 (Windpower monthly, July 1997).

The utilization of wind energy for electricity generation has already been shown to be attractive in both environmental and economic terms, and is likely to extend offshore in the near future. The intermittent nature of wind means that power is not always

available, and although accurate wind speed forecasting can improve the predictability of wind power from each generator, an energy storage system is usually required to maintain network stability and reliability.

Other renewable energy sources with intermittent or cyclic behavior include photovoltaics (PV). PV generators have daily cycles where the theoretical maximum output is within a clearly defined envelope. However, there is considerable seasonal variation. The energy from day to day can vary by a factor of ten, and the actual power at any particular time of a day may be much less than the theoretical maximum, and subject to abrupt changes. PV generators are still considered expensive for grid connected application, but may soon become economically attractive, especially when they have a secondary purpose as a building cladding material, or where the generated power partly matches a building load demand, e.g. for air-conditioning. One of the examples, as Dipl-Ing M. Rothert (ISET, Germany) described, the successful operation of a 215V and 2200Ah gel battery with tubular positive plates and negative copper grids, was installed at a solar power plant at Flanitzhutte, Germany, as early as 1992.

The economic exploitation of renewable energy sources such as wind, wave, and solar for electrical power generation can be limited by the variable and intermittent nature of the supply. Energy storage can address these problems, by smoothing the net power supplied to the grid, or by enabling the energy to be stored and dispatched later (for example to supply peak demands), thus giving a higher value to the generated power.

The reliable supply of renewable energy at peak-load hours by means of energy storage is therefore an ecological and economic alternative for the operation of fossil peak-load power stations because such units show relatively low power efficiency. High power lead acid batteries help to overcome unreliability of renewable energy sources and have proven themselves in various utility applications.

2.2.1.7 Improving Security

The much faster responses of the BESS inverters, than turbo-generator governors, would react to quickly control the effects of any disturbance. At present these disturbance effects have time to be amplified before the slower mechanical devices can respond to suppress them. Consequently the power system has to be made much more robust to survive severe disturbances. With the fast BESS responses, the vulnerability of power system would be reduced (Sutanto, D. 1996).

The major difficulty facing power systems is the occurrence of extremely severe system disturbances which may threaten to disrupt the power system's integrity and cause loss of supply to numerous consumers. The first line of defense against power system outages is the flexibility and resilience built into the network by having reserve or emergency capacity in both transmission and generation. Conventional means of improving reserve and emergency capacity of system elements, and so raising levels of reliability and security, are cost intensive for a utility. There is a less expensive option for gaining emergency capacity, namely, the shedding of loads. With timely (fast) load shedding in localities affected by a disturbance the loadings of lines, generators and

transformers can be reduced to less than their continuous ratings (Lachs, W.R. and Sutanto, D., 1992).

2.2.1.8 Improving Reliability

With the tremendous advantages of locating BESS in distribution networks, back-up supply would be closed at hand even if the BESS was not in the consumer's installation. This would make a major impact on consumer reliability as 90% of interruptions to individual consumers are currently due to disturbances in the distribution networks.

2.2.1.9 Impact on Generation

With sufficient quantities of BESS to curtail daily peak demands, peaking power stations do not have to be manned nor be run up. At light load periods, re-charging the energy storage allows base load generators to be run at higher, more efficient outputs and avoids the need to shut units down. When suitable inverter controls are developed, energy storage would be able to take over frequency control from generators which would reduce mechanical wear at the power stations. Further, with a sufficient amount of energy storage, it would no longer be necessary to carry much spinning reserve on the generators (Anderson, M.D., and Carr, D.S., 1993).

2.2.1.10 Electricity Forecasting

At present demand forecasting is the area of greatest uncertainty, particularly the fast changes at peak periods. With sufficient energy storage to curtail the peak periods, the need for half hour to half hour demand forecasting would virtually be eliminated. There would only be a need to forecast the following 24 hours energy demand, to allow the day

by day scheduling of generation. By removing demand uncertainty, it would be possible to have uniform daily electricity generation costs, thereby greatly simplifying consumer tariffs (Lo, C.H. and Anderson, M.D., 1999).

2.2.1.11 Power System Planning

With a "competitive electricity market" allowing generating costs to vary every half hour it becomes extremely difficult to make realistic financial projections which are needed for power system planning decisions. By using energy storage to curtail daily peak periods, not only will it assure greater generator reliability, but it will allow a single daily generating cost, based almost entirely on the more easily assessable energy forecast. This stability in generating costs will make much easier the financial projections on which planning decisions are based. The planning process would be further aided by the fact that energy storage will constrain the annual increase of peak demands, delaying the introduction of new high capital cost power system equipment (Lee, T.Y. and Chen, N.M., 1995).

2.2.1.12 Additional Facets

Inverters associated with energy storage can allow an undreamed level of flexibility. There are many other aspects of power system operation which will be solved by developing the necessary inverter controls to fulfill the needed functions. Some possibilities are back-up power and "clean supplies" for consumers, interruptible loads, improved emergency responses, etc, which make the advent of energy storage for power systems such a promising avenue.

2.2.2 Actual Implementation of BESS in Power Systems

The BESS at Bewag, operated since January 1987, is the first large commercial application of battery storage in a power system. According to (Kunisch, H.J. and Kramer, K.G., 1981), the political situation (at that time) did not allow the power system of West Berlin to be connected with the surrounding grid. Consequently, the 2251 MW installed capacity with 1588 MW peak load power system faced four major problems: peak load coverage, spinning reserve, voltage regulation and load frequency control. After investigating several options of storage technology, only steam storage and BESS turned out to be the feasible ones. Lead-acid batteries, being cheap and available, has been chosen over the other battery technologies (NiCd, ZnCl, ZnBr, Redox, NaS, LiFeS). The Bewag's BESS was not justified for load levelling, because the load curve and tariff situation made gas turbines more economical than storage units. However, for this particular power system, BESS is well suited for load-frequency control and spinning reserve. Newly developed lead-acid batteries having high specific energy for short discharge periods (0.5 to 2 hours) and energy efficiency better than 80% have been achieved. The plant comprises two identical twelve-pulse converters with 8.5MW each. The rated DC voltage is 1180 V. The second inverter path operates as a reserve for the first in the load-frequency control mode and additionally enables an immediate reserve of a total 17MW. It provides rated output of 8.5 MW when frequency drops by 0.2 Hz and twice rated output for short periods when frequency drops below a preset limit. The battery is designed to deliver its maximum power (8.5MW) for at least 30 minutes under the worst operating conditions. The battery comprises of 7080 cells connected in 12

parallel strings of 590 cells each. It is equipped with electrolyte circulation by airlift pumps and a semi-automatic water filling system. The state of charge varies between 50 to 90% during frequency control operation to ensure at least 30 minutes rated power for spinning reserve purpose and the energy-efficiency of the battery be 87%.

While Bewag's BESS is intended for frequency regulation, the 10 MW/40 MWh BESS built in 1988 at Southern California Edison's Chino substation is intended for load levelling (Walker, January/February 1990). Along with the current trend in the use of solid-state converters for power system stabilisation, the dynamic regulation capability of the BESS was designed for rapid control of real and reactive power independently. This has been made possible by the use of self-commutating gate turn-off thyristors (GTOs) instead of conventional line-commutated thyristors. A bidirectional 18-pulse bridge voltage source converter topology and an appropriate control have been used to perform rapid control of real and reactive power output. The plant consists of two large battery buildings, joined by a common converter-control building in the center. The battery energy storage system comprises 8256 individual large lead-acid batteries specifically designed for deep discharge capability. The basic battery unit is a module of six cells connected in series. 172 modules are connected in series forming one battery string with a nominal voltage of 2064 V. A total of eight strings in parallel makes up the 40MWh of storage capacity. The plant has a transient response of 16 ms, which is fast enough for dynamic controls such as spinning reserve, damping or transient stability control.

The Puerto Rico Electric Power Authority (PREPA) (Torres *et al*, 1995) has commenced commercial operation of a 20 MW BESS in November 1994 primarily to assist with frequency control when generators are lost (Torres *et al*, 1995). In this island power system, sudden outages of more than 400 MW unit would cause instantaneous overload between 15 to 20%, resulting in a very fast frequency decline. Automatic load shedding has been used to cope with this problem, but this is no longer acceptable to PREPA. Alternative examination to BESS was found to offer the most economical answer after adding further benefits related to the transmission system (transmission losses and voltage control), as well as frequency control. Subject to review of the benefits of the first unit, it has been proposed to commission a further 4-20 MW BESS.

In May 1996, the Power Control Division of GNB Technologies (Hunt, G.W., 1999) commissioned a new facility, housing a 5-MW battery energy storage system (BESS) at GNB's Lead Recycling Center in Vernon, California. The Vernon BESS is the largest known installation of its kind in the world owned and operated by an industrial manufacturer (not owned by power utility) to support critical manufacturing process equipment, including the operation of emission control systems associated with handling lead dust. GNB's primary concern is to assure the continual operation of these systems during a power outage. Because the lead melting process at the GNB Recycling Center create lead dust, which is recovered via the use of several large exhaust control fans and large containers to collect the dust particles. When the plant lost of utility power, these fans must continue to run to avoid an environmental incident such as lead dust escaping into the air. To prevent this from occurring, GNB considered all the options available and decided to install a BESS.

In September 1997, Kashima-Kita (Shibata, A. and Sato, K., 1999) built a 200 kW x 4 hour-rate battery after having built both 2 kW and 10 kW prototype units. The battery is interconnected to the company's power plant grid system and has to date proved that a high efficiency heat power station system equipped with such an advanced electricity storage battery reusing byproducts of the power plant can be commercially viable. This design success verified that the vanadium battery was viable to store surplus electricity from the power plant at night and discharging it in the day to keep the operational load of the power plant constant and continuous.

In January 1998, a 6 MW (48 MWh) (Kodama, E. and Kurashima, Y., 1999) sodium-sulphur battery system consisting of 240 modules was built properly at Tsunashima substation of Tokyo Electric Power Co., Inc. The system has been proved to function as an electric energy storage system for load leveling. The construction and operating performance of the sodium-sulphur battery cell assembles in modules fitted with vacuum type enclosures and heaters in order to keep the temperature at 300°C. The modules for the 6 MW battery contain 3 units, each 2 MW. The first unit was operated in March 1997 and the other two units were operated late in the same year.

The European commission and the multi-national International Energy Agency (IEA) (Baker, J.N. and Collinson, A., 1999) coordinated all the storage programs in the United Kingdom, Netherlands, Spain, Germany and France. In the United Kingdom, a total amount of £1.5 million was launched by the Engineering and Physical Science Research Council (ESPRC) to seven energy storage projects in November, 1997. The seven

projects include four projects in novel batteries and materials, a flywheel-storage, a super-capacitor and a battery management project. In the Netherlands programs include NOVEM, TNO, EnergieNed and various distribution companies, have been established focusing mainly on storage applications, particularly in power quality. In Germany, various energy storage program activities are involving Federal and State Government, industrial, utility and academic with primary interest in battery storage, SMES, flywheel systems and hydrogen-based systems. In France and Spain, national program activities are centered on the utility with strategic interest in storage, as part of the overall concept of optimizing the energy system (Baker, J.N. and Collinson, A., 1999).

Table 2.1 records the commenced date, location, storage medium and rating of various battery energy storage systems. The plant's attributes are also indicated.

Table 2.1 Summary of battery energy storage system characteristics

Date of commence	Location of Plant and System	Storage medium	Rating	Attributes
	Germany			
October, 1986	Steglitz Battery Plant, West Berlin Network, Bewag (Germany)	Lead acid	17MW, 8.5MWh	Instantaneous power reserve, frequency control
1989	Berlin Subway	Lead acid	3.5MW/1M	Peak load power

	System (Germany)		Wh	demand
Early 1992	Installed at a solar power plant at Flanitzhutte (Germany)	Gel lead-acid battery	473kWh	Renewable integration
July, 1997	Hamburger Gaswerke GmbH (Germany)	Hydrogen	10MW	For urban supply of heat and electricity
	USA			
May, 1986	Keefe Avenue battery plant, Wisconsin (US)	Gelled lead acid	300kW, 600kWh	Load leveling, peak shaving
February, 1987	Automotive battery plant, Delco Remy Division, General Motors Corporation Muncie, Indiana (US)	Lead acid	300kW/600kWh (2hours)	Load-leveling, peak shaving
July, 1987	Crescent Electric, Statesville (US)	Lead acid	500kW/500kWh (1 hour)	Peak demand reduction
August,	South California	Lead acid	10MW/40M	Spinning reserve,

1988	Edison, Chino (US)		Wh (4 hours)	load leveling
February, 1989	Turn-key system, Brass foundry (US)	Lead acid	300kW/579k Wh (1.93hours)	Load-leveling, peak shaving
October, 1993	(Omnion PM250) Modular Generation Test Facility in San Ranon, California (US)	Lead Calcium	250kW/2.78k Wh (40 seconds)	Demand peak reduction
November, 1994	Sabana Llana substation, Puerto Rico Electric Power Authority (US)	Lead acid	20MW/13.3 MWh (40 minutes)	Spinning reserve, frequency control
November, 1995	GNB Battery Recycling Plant in Vernon, California (US)	Valve regulated lead acid	5MWe/10 seconds 5MVA, 2.5MWh	Voltage and frequency control
13th May 1996	GNB's Lead Recycling Centre in Vernon, California (US)	Valve-regulated lead-acid (VRLA)	5MW	Uninterrupted operation for large exhaust control fans and large

				container to collect lead dust particles
	Japan			
September 1997	Kashima-Kita (Japan)	Vanadium redox flow battery	200 kW x 4h	Load leveling
January 1998	Tsunashima substation, Tokyo Electric Power Co. (Japan)	Sodium-sulphur battery	6MW, 48MWh	Load leveling
	UK			
April, 1998	Caledonian Paper mill in Ayrshire, Scotland (UK)	Capacitors	2MVA to 10MVA	Dynamic Voltage Restorer
Will be completed late in 2000	Didcot power station (UK)	Redox flow cell (Regenerative fuel cell)	10MW, 100MWh	Provide load following, voltage control, frequency regulation, power system stabilisation, constant VAR control and constant AC power.

2.2.3 Development and Types of Battery for Power System Applications

According to (DelMonaco et al, 1982), five different batteries are considered to have the greatest potential: advanced lead-acid, zinc-bromide, zinc-chloride, sodium-sulfur and lithium-iron sulfide. In March 1991, (Hurwitch & Carpenter, 1991) mentioned only three types of batteries are suitable for power system applications: lead-acid, sodium-sulfur and zinc-bromide. The BESS(s) installed in Bewag, Chino and PREPA are all of lead-acid type. According to Hurwitch & Carpenter, lead-acid battery is suitable for short-term solutions to many utility needs, but it has limited applications due to factors such as uncertain return of investment, difficulty in quantifying benefits, lack of operating data and limited experience. It does have some good qualities, such as high rate performance, good low- and high-temperature performance, low maintenance and high efficiency, but lead-acid batteries have low energy density and relatively low cycle life, cannot be stored under discharged condition, and are costly. Alternatives to lead-acid battery, such as sodium sulfur and zinc-bromide, which have better performance at possibly lower costs, are under development in the US, Europe, Japan and Australia and are targeted for introduction in commercial markets by the late 1990's. Sodium-sulfur has some advantages over lead-acid, such as low potential cost, fast charge rate, high energy density, low footprint, flexible design, no self-discharge and long intrinsic life, but there are also some problems with this technology, such as safety aspects, difficult to maintain and low demonstrated lifetime (Hurwitch & Carpenter, March 1991). With Chloride Silent Power Ltd, Yuasa Battery Company and ASEA Brown Boveri are the leading developers of this battery. For rapid power regulation applications in power systems, the fast charge characteristic of sodium-sulfur battery is well suited for BESS

applications. From the same source, it is reported that zinc-bromide is of low cost materials, modularity and good energy density, despite having low efficiency, mechanical complexity, safety and lifetime. With Energy Research Corporation, Johnson Controls Incorporated and Meidensha Corporation are among developers of this battery technology.

Table 2.2 shows some of the typical batteries suitable for power system applications and a comparison of the main battery technology is listed.

Table 2.2 A comparison of the main battery technology

Battery	Advantages	Disadvantages	Comments
Lead-acid	Established technology; Low cost and fairly long life.	Low energy and power density	Horizon and other high performance batteries greatly improve the suitability for Battery Systems but must be made cheaper
Nickel-cadmium	Higher energy density and cycle life than lead-acid	Cadmium very toxic	Being used for second generation, purpose-built Battery Systems
Nickel-metal hydride	High power density, long cycle life. Twice the energy storage of lead-acid	Expensive	Promising mid-term option but currently over twice the cost of the USABC target
Zinc-bromide	High specific energy, low power density and an anticipated long cycle life. Inexpensive raw materials	Presence of toxic gases and need of purpose-built chargers	Probably best suited for Battery Systems where minimum battery size and high storage capacity are important
Lithium	High energy and power density.	Expensive	Research into scaling up to Battery System size will probably provide a mid-term battery
Sodium-sulphur	High efficiency and energy density	Thermal enclosure and thermal management is expensive. Corrosive components	Several technical issues to be resolved before this could become an option
Sodium nickel chloride	High energy and power densities. Long life	Thermal enclosure and thermal management is expensive	Promising mid-term option but currently over twice the cost of the USABC target
Zinc-air	High energy density. Rapid mechanical recharging (3 minutes)	Infra-structural needs	Interesting longer-term option for rapid recharging
Nickel-iron	High energy density. Long life	Hydrogen emitted – safety concerns. Periodic topping-up with water needed.	Research to increase efficiency and overcome disadvantages could lead to a long-term storage battery
Nickel-hydrogen	High energy density. Robust and reliable, no overcharge/over-discharge damage. Very long life	Fairly expensive (due to hand assembly)	Already used in communications satellites. Cost competitive for high cycle operations

2.3 Conclusion

The cost of providing a reliable and secure electricity supply to all consumers is substantially increased by the uncertainties imposed on power systems. The major cause of uncertainty is posed by the daily and annual peak demands and this is all the more serious as power systems become increasingly vulnerable to disturbances at periods of peak demand. Specifically to withstand a range of severe disturbances at the time of annual peak demand, heavy expenditures are committed for operations as well as equipment and controls for the entire power system. Most of this expenditure could be avoided, without reducing power system security, by curtailing the demand at peak periods.

Even though AC energy cannot be stored, fast responding inverters allow access to other forms of energy storage. Battery Energy Storage Systems (BESS), a mature technology can fulfill this function and inverters provide the ideal interface between the DC energy storage and the AC system. Capable of one cycle responses, the inverters can produce both active and reactive power, even though only drawing active power from the energy storage and their much faster responses are available without the mechanical wear suffered by turbo-generators. Of added importance, BESS can be located within distribution network, close to city consumers and fill the gap caused by the retirement of city power stations. In fact it has been the retirement of city power stations that has contributed to the growing difficulties faced by power systems throughout the world. City power stations had been largely able to shield the transmission grid from the fast load changes of city consumers during the daily peak periods. The impact on the

transmission system, following their retirement, has affected the security levels of the entire power system. The heavier and more volatile loadings have made the power system more susceptible to disturbances, and when the transmission grid is disrupted, many thousands of consumers may be interrupted for extensive periods, without any back-up power.

This chapter has provided a review of the various potential applications of BESS in Power Systems and actual implementations of BESS in recent years pointing out the attribute of each. Most of these implementations are, however, limited in nature, in that each BESS can provide only one or two functions. With the current technology of microprocessors and fast switching power electronic devices, the thesis has explored the possibility of having one BESS which can provide a comprehensive multi-functions such that the benefit of the BESS can be fully realized. Only by assessing the total value of the dynamic benefits of these additional functions, the cost-effectiveness of installing a BESS can be fully appreciated.

CHAPTER 3 THE IMPLEMENTATION OF BATTERY ENERGY STORAGE SYSTEM

Experiment is the sole source of truth. It alone can teach us anything new; it alone can give us certainty.

Poincare, Henri

Science and Hypothesis

CHAPTER 3 THE IMPLEMENTATION OF BATTERY ENERGY STORAGE SYSTEM

3.1 Introduction

Chapter 2 has shown that there are many functions that a Battery Energy Storage System (BESS) can provide, however, in many installations only one or two of these functions are usually realized. With the current state-of-the-art, fast acting power electronic devices and powerful microprocessors currently available in the market, the potential of having one BESS that can provide many of these functions can now become a reality. This chapter describes the implementation of a new BESS that can provide several functions in one device, such as power quality enhancement in the form active filtering, voltage regulation, power factor correction, balancing unbalanced load in a three-phase system, load leveling for daily load management, fast control of power flow, damping load fluctuations, and providing back up power supply during emergency conditions.

The following section describes the hardware and control system for the BESS implementation. Results from the laboratory experiments using single-phase and three-phase system will be discussed.

3.2 Battery Energy Storage System (BESS) Components

The BESS components include the storage component (battery subsystem), the power conversion system (PCS), the control system, transformers and various sensors. The battery subsystem includes the individual battery modules, wiring between modules and module containers to form a battery bank. The power conversion sub-system interfaces the DC battery bank to the ac utility and provides bi-directional control of power flow. High power Insulated Gate Bipolar Transistors (IGBT) are used to provide fast switching to meet fast dynamic changes. The control sub-system includes a digital signal processor which samples the required data through the control interfaces, and then processing them under a control rule to provide the control signals for the PCS to perform power transfer. The transformers are used to provide isolation and to match the output of the conversion system with the grid voltage.

3.2.1 The Battery Subsystem

'Endurance' range of valve regulated lead acid batteries have been selected for use with the BESS, because they require least maintenance and can withstand deep discharge (up to 80% depth of discharge). The construction of the 'Endurance' valve regulated lead acid batteries is shown in Figure 3.1. The gas recombination technology transforms the generated gas into water thus no topping up is required throughout the life of the batteries. In the event of overcharge the battery is fitted with a safe low pressure venting system that can automatically reseal after releasing any excess pressure.

3.2.1.1 Discharge characteristics

The discharge capacity varies depending on the discharge current, usually denoted by CA, for example, 0.1CA means that the battery is discharged with a current equal to 0.1 times the rating of the battery, i.e. if the battery is rated at 100Ah, 0.1CA means that the battery is discharged with 10A, and 1CA means that the battery is discharged with 100A. Figure 3.2 shows the constant current discharge characteristic of batteries when they are discharged to the final discharge voltage at various discharge currents at 20°C.

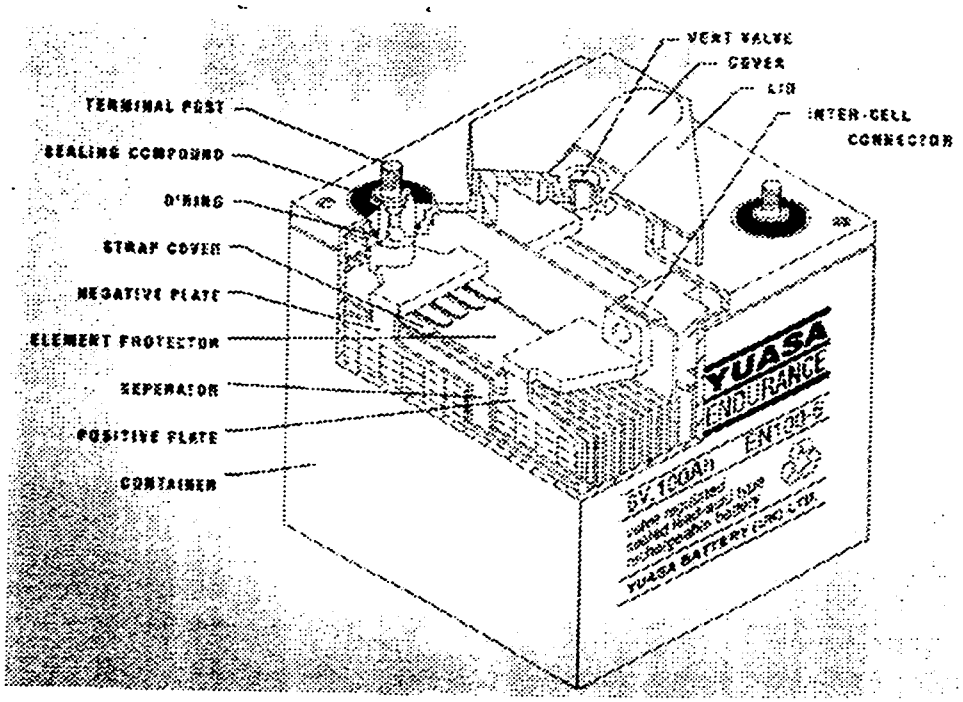

Figure 3.1 Construction of lead-acid battery

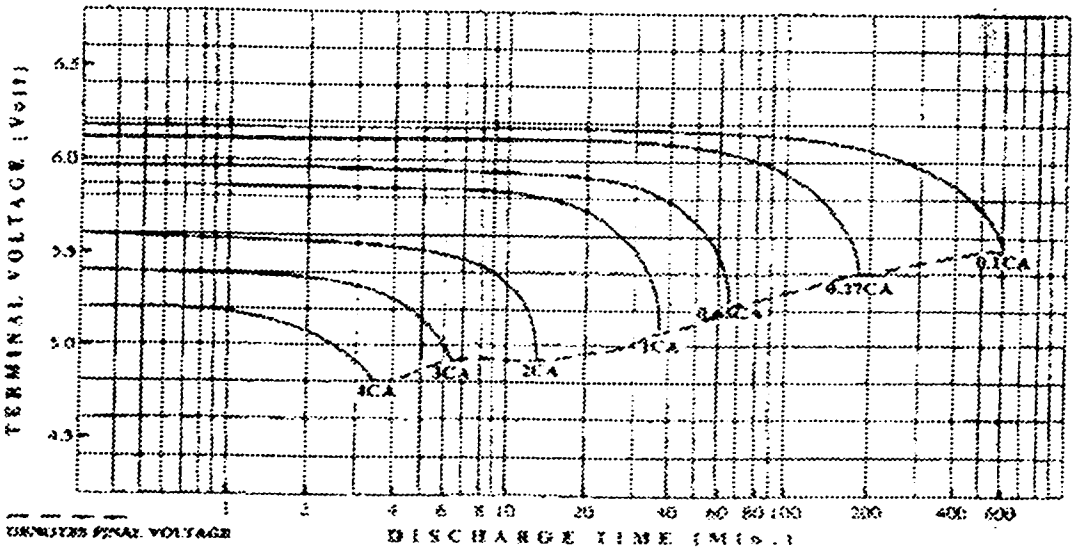

Figure 3.2 Discharge characteristic of battery

Discharge capacity also varies with battery temperature. The lower the temperature, the less the capacity. Since the selected batteries are located in an air-conditioned room with temperature ranging from 18°C to 23°C, temperature is not an important role in this study. In actual applications, the temperature can play an important factor in determining the remaining capacity of the battery. For instance, at 0.1CA discharge: a battery capable of discharging for 10 hours at 20°C will decrease the discharge duration to about 8 hours (84%) at −10°C and increase its capacity by about 2.5% at 30°C.

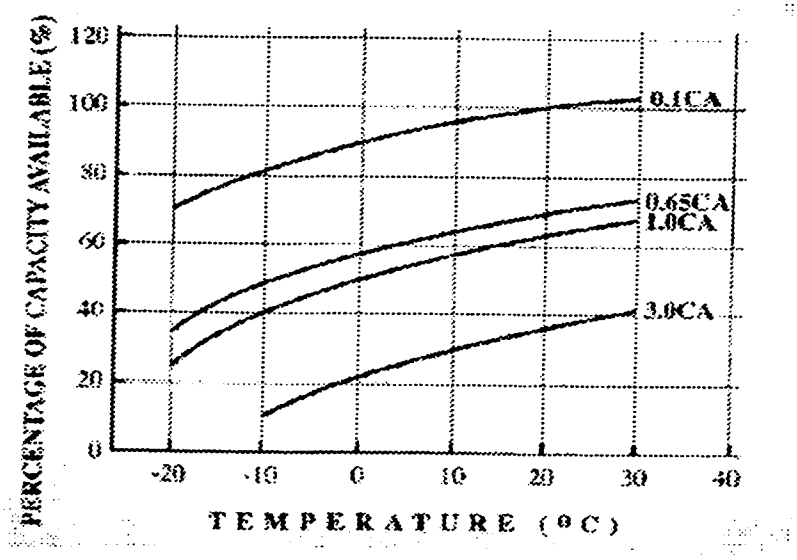

Figure 3.3 Relationship of temperature with capacity

3.2.1.2 Charge characteristics

The optimum charge voltage for the batteries is 2.26V/cell under normal temperature condition (20°C). The battery requires no equalizing charge, this is because of its low self-discharge rate resulting in a minimal variation among the cells in the battery bank and float charge at sufficient voltage to maintain it in a fully charged condition. Recovery charge after the battery has been discharged can be carried out at the float charge voltage of 2.26 V per cell. Figure 3.4 shows the charge characteristics at constant current (0.1CA) and constant voltages at 2.26 V at 10 hr rated capacity. As shown in Figure 3.4 charging a fully discharged battery by constant current and constant voltage of 0.1CA and 2.26 V respectively at 20°C will put back around 100% of the previous discharge in 24-hour. The time required to complete the charging varies by the amount of the previous discharge, initial charge current and temperature.

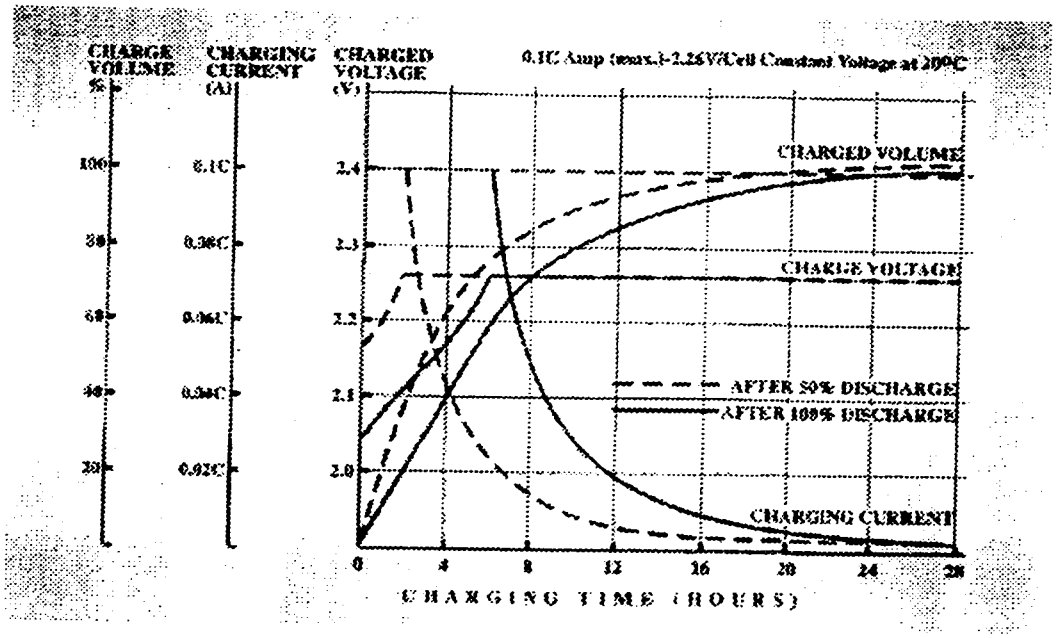

Figure 3.4 . Charge characteristic of constant current (0.1CA) & constant voltage at 2.26 V

The battery's characteristics provide important information for the management of the battery energy.

3.2.2 Power Conversion System (PCS)

The PCS initial design requires the specification of maximum voltage and maximum current for it to be operated, and the maximum power, both real and reactive, to be supplied with specified discharge and charge duration. Therefore, the determination of the PCS rating and the battery bank rating can not be treated separately. The determination of the PCS and the battery bank rating will be explained in section 3.2.2.1.

Since the solid-state devices in the PCS are required to make rapid and frequent changes between charge and discharge, the PCS, therefore, must be able to operate at high

transient voltage and current to prevent the batteries and the PCS components from being damaged. Moreover, in case of mal-operation, the PCS is well protected which is fast enough to disconnect (trip) the main supplies connected at both terminals of the PCS. The reasons for the selection of each component and the design of PCS will be described briefly in section 3.2.2.2.

In order to carry out the control task, fast interfacing devices are employed to convert the power signals, with filtering to prevent noise contamination, into digital signals for processing, as well as, adding dead-time to the processed signal before entering the driver circuit for power amplification. The required devices such as voltage sensor, current sensor and dead-time controller will be discussed in section 3.2.3.

3.2.2.1 The PCS design based on the battery characteristics

In the preliminary deliberation on the energy capacity of the batteries and the PCS to be built for the project, it was decided that for the load leveling and emergency supply applications, the BESS has to provide 2 kW DC from the battery for 10 hours (20 kWh) and 7.5 kW dc from the battery for 2 hours (15 kWh) respectively, and the maximum DC voltage allowable is 500 V DC.

In the selection of a cell for the given applications, the largest cell size available is generally chosen since the price per kWh of lead acid cells is lowest for the largest cells. In this case, the ampere-hour capacity of one vendor's cell is 100 Ah at the 10-hour rate, but only 72 Ah at the 2-hour rate. The end of discharge battery voltage is 1.75V and the end of charge voltage is 2.26V. The average cell voltage during discharge is 1.85 V per

cell, giving the energy capacities of 1.85 x 100 = 185 Wh and 1.85 x 72 = 133.2 Wh respectively. For 20 kWh and 15 kWh of battery capacities, 20k/185=108 cells and 15k/133.2=113 cells are required respectively. Since the cells are packaged three to a module, by choosing 113 cells, this is rounded up to 38 modules. The battery voltages are 1.75 V x 3 x 38 = 199.5 Vdc at the end of discharge, and 2.26 V x 3 x 38 = 257.64 Vdc at the end of charge. This meets the original specification on the battery for maximum voltage. Therefore, the valve regulated lead-acid batteries chosen for the project consist of 38 battery modules with 6 V per module are connected in series to provide a nominal voltage at 228 V and nominal capacity at 100 Ah battery bank. The battery bank capacity is sufficient to supply the amount of energy for the targeted applications.

In designing the custom-made PCS for the above application, we know that on average the current can vary from 10A (100Ah for 10hr) to 36A (72Ah for 2hr), and the power level on average can vary from 2kW (20kWh for 10hr) to 7.5kW (15kWr for 2hr). To meet this demand, the PCS is designed to operate at 5 kW normally and 25 kW with additional cooling. All the wires and terminals are sized at 50 A rating and the dc bus maximum voltage is limited at 500 V to allow a maximum of 25 kW operation. However, this is not recommended for continuous operation because of thermal consideration. Notwithstanding that, the PCS rating is large enough to operate at 7.5 kW for 2 hours and for a short period can be operated up to 15kW.

3.2.2.2 The PCS construction

A number of general decisions had to be made in regard to the design of the battery energy storage system. The most important issue was the decision concerning the type of converter circuit. The alternatives in question were self-commutated or line-commutated converters. Self-commutated converters were chosen because:

- four-quadrant operation can be obtained; this means that not only active power but also capacitive and inductive reactive power can be obtained from and fed into the three-phase mains.
- the mains voltage can be controlled.
- harmonic currents can be reduced.
- reactive power compensation can be provided.
- no anti-parallel converter circuit is required for current reversing operations.
- simple control can be used.
- no bulky inductor is required on the dc main.

The circuit diagram of the PCS chosen for the BESS is shown in Figure 3.5. The conversion system is a bi-directional voltage source self-commutated converter which consists of: (i) dc bus capacitors, (ii) heat sink, (iii) power semiconductor switches and (iv) gate drive circuits. The converter is connected to the ac grid through the (v) three ac interface inductors and a three-phase transformer.

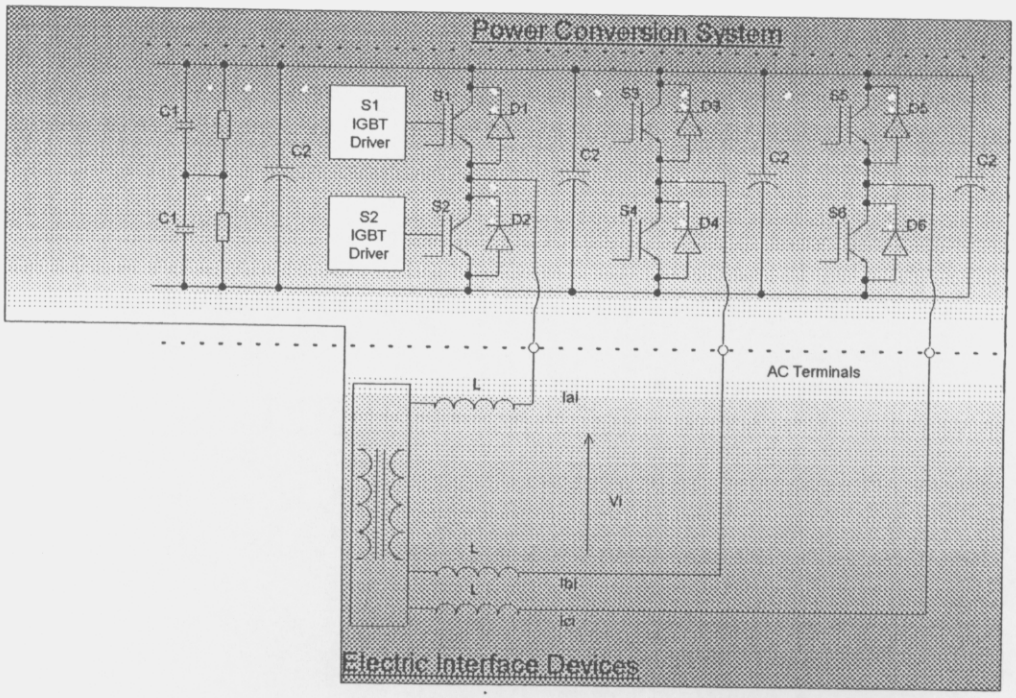

Figure 3.5 The Power Conversion System and the Electrical Interface

3.2.2.2.1 Capacitors

Two types of capacitors (C1 and C2) are used. C1's are electrolytic capacitor to smooth the dc voltage, and C2's are polypropylene capacitors to absorb switching transients. These capacitors protect the batteries from high current stress and voltage stress while turning on and off the switches.

3.2.2.2.2 Heat sinks

Heat sink can bring heat away from the switching element in order to prevent overheating of the power electronics devices. Normally, a thin uniform coat, such as G746 (Shin-Etsu Silicone) or SC102 (Toray Silicone) or YG6260 (Toshiba Silicone) is painted between the two surfaces to ensure good thermal conduction between the switch

and the heat sink. In this inverter, YG6260 is used to make good contact between the two surfaces to aid the heat conduction.

3.2.2.2.3 Power electronics switching devices

The power electronics switching devices used in the PCS employ the third-generation insulated gate bipolar transistors (IGBTs), each rated at 600 V, 50A and connected in parallel with a reverse diode to give the converter the capability of handling power flow in reverse directions. The IGBT devices chosen have very fast switching speed and lower conduction and switching losses, allowing the converter to be switched at a high switching frequency, typically higher than 15 kHz, to avoid audible noises. Like the power MOSFET, the IGBT is turned on when a positive voltage is applied to the gate (voltage controlled device).

3.2.2.2.4 Drive circuits for the Power electronics switching devices

The drive circuits determine the performance of the power switching devices. In this case, all of the switches in the PCS system are power IGBTs (2MBI50N-060) rated at 600 V 50 A. The drive circuits are designed such that they are able to drive isolated power IGBTs and switch up to 50 A current at a frequency from 15 kHz to 25 kHz. The designed gate drive circuit, shown in Figure 3.6, uses gate component EXB841. The EXB841 is a hybrid IC capable of driving up to 400 A for 600 V IGBT. Since the signal delay in the drive circuit is 1us or less, the hybrid IC is suitable for switching at up to 40 kHz. In addition, EXB841 has 4-A peak current driving capability and has de-saturation protection when there is a device over-current or shoot-through fault. The fault signal is coupled through an opto-coupler, TLP621, to control the interface. An on-board power

supply, NMD120515S, is shown in the figure to provide proper isolation between power ground and signal ground.

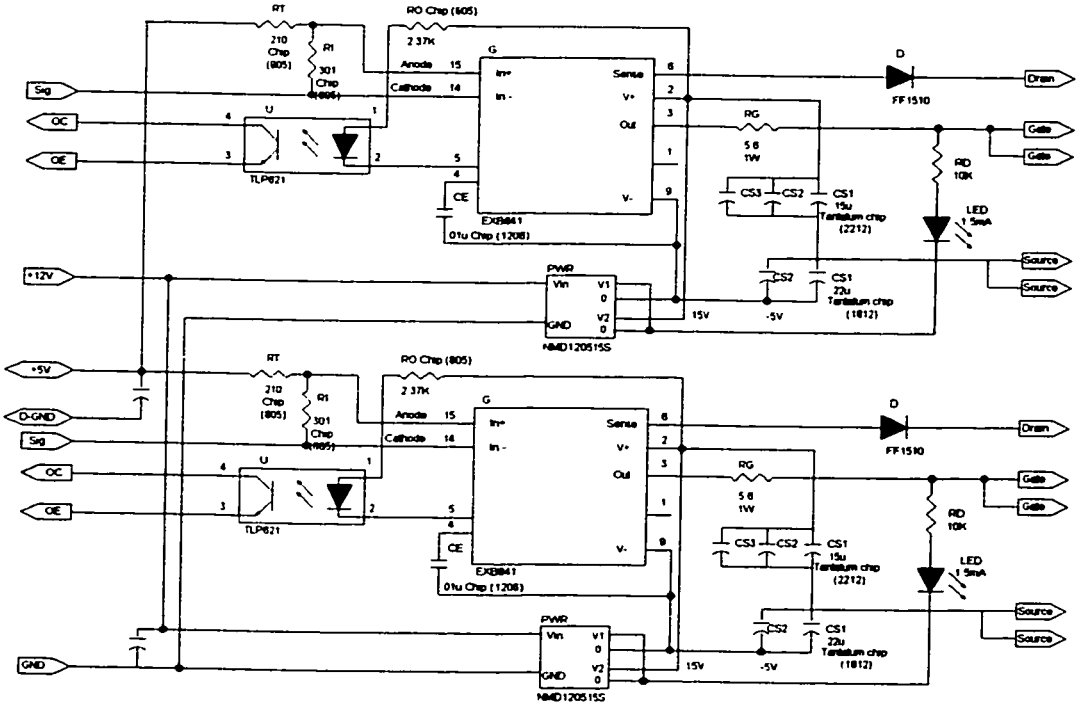

Figure 3.6 IGBT drive circuit using EXB841

3.2.2.2.5 PCS inductors and transformers

The PCS ac terminals are connected to the ac supply system through three inductors aimed to reduce the current ripples. The three-phase transformer is used to provide electrical isolation between the BESS and the three-phase ac system, as well as interfacing the two voltages.

3.2.3 Digital Signal Processor (DSP) and the control interface for the BESS

3.2.3.1 DSP Board

A DSP Board, DSpace DS1102, as shown in Figure 3.7 is employed for data processing, data capturing, and control functions. The DS1102 is based on the Texas Instruments TMS320C31 3rd generation floating-point Digital Signal Processor (DSP). The TMS320C31 supports a total memory space of 16M 32-bit words including program, data and Input/Output (I/O) space. Moreover, all off-chip memory and I/O can be accessed by the host, even while the DSP is running, thus allowing simple system setup and monitoring. In addition, the DS1102 board contains 128K words memory and is fast enough to allow zero wait state operation. Several peripheral subsystems are implemented to support a wide range of digital processing applications. The DS1102 hardware is designed for flexible use at maximum program overhead by implementing functions in hardware otherwise often performed by software. The host interface contains a bus-width converter mapping two 16-bit host accesses into a single 32-bit transfer on the DSP-bus to avoid data transfer inconsistencies.

The DSP has been supplemented by a set of on-board peripherals frequently used in digital control systems. Analog to digital (A/D) and digital to analog (D/A) converters, a DSP micro-controller based digital-Input/Output (I/O) subsystem and incremental sensor interfaces make the DS1102 an ideal single board solution for the proposed control tasks.

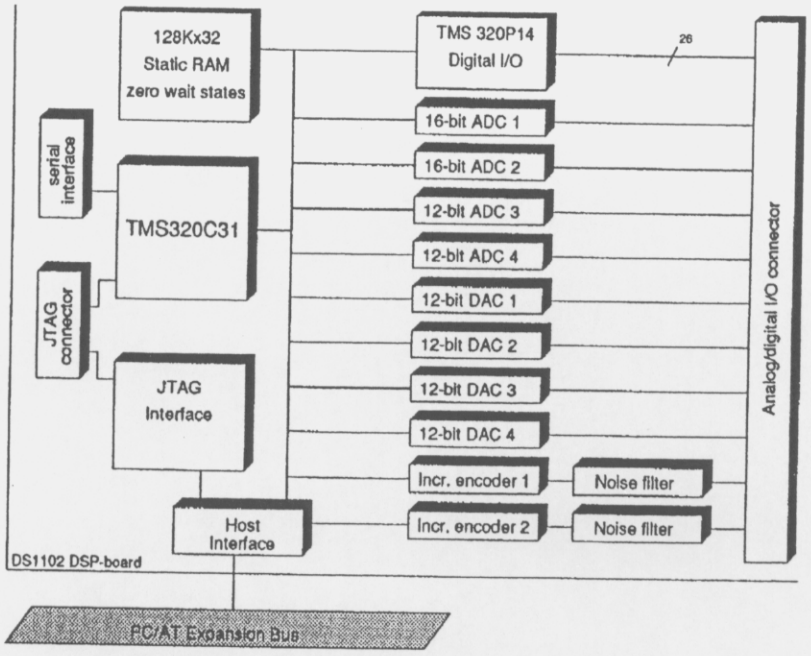

Figure 3.7 Block Diagram of the digital signal processor

The DS1102 contains two types of analog-to-digital converter (ADC):

a) Two 16-bit charge redistribution AD converters with integrated sample/holds. Each of the ADCs contains a 16-bit successive approximation type AD converter, a sample/hold circuit and a micro-controller-based auto-calibration circuit. These converters achieve a conversion time of 10 us.

b) Two 12-bit charge distribution successive approximation ADCs with integrated sample/holds circuits and a digitally controlled offset calibration unit. Each converter achieves a conversion time of 3 us.

All ADCs have single ended bipolar inputs with ±10 V input span. All return lines are connected to the system ground. To avoid ground loops, separate return lines are used for all connected sensors and the sensor grounds are isolated from each other.

The DS1102's digital-I/O subsystem is based on the TMS320P14 DSP micro-controller. Beside a 16-bit fixed point DSP core, it features a bit-selectable parallel-I/O port, four timers, six PWM circuits, four capture inputs and a serial interface. The TMS320P14 contains firmware making all on-chip peripherals accessible by the TMS320C31. After power-up, the DSP executes an I/O server firmware residing in its built-in PROM. This PROM has been augmented by an external program RAM providing a program download feature, which allows application specific DSP programs to be executed in parallel to the TMS320C31. This feature allows the customization of the digital-I/O subsystem depending on the applications need. The TMS320P14 incorporated 16-bit parallel I/O port consisting of 16 individually bit-selectable I/O pins. All 16 I/O pins are accessible via the I/O connector. Each line features a 10KΩ pull-up resistor to 5V.

3.2.3.2 Voltage sensor

Figure 3.8 shows four voltage sensors and one dc current sensor used in the BESS. The three analog voltage sensors provide an analog output of 1V for every 100V measurement. The scaled down analog signals are in the range of ±10V. These signals are then read into the DSP-board through the AD converters. The digitized signals can be used as the control variables in the controller.

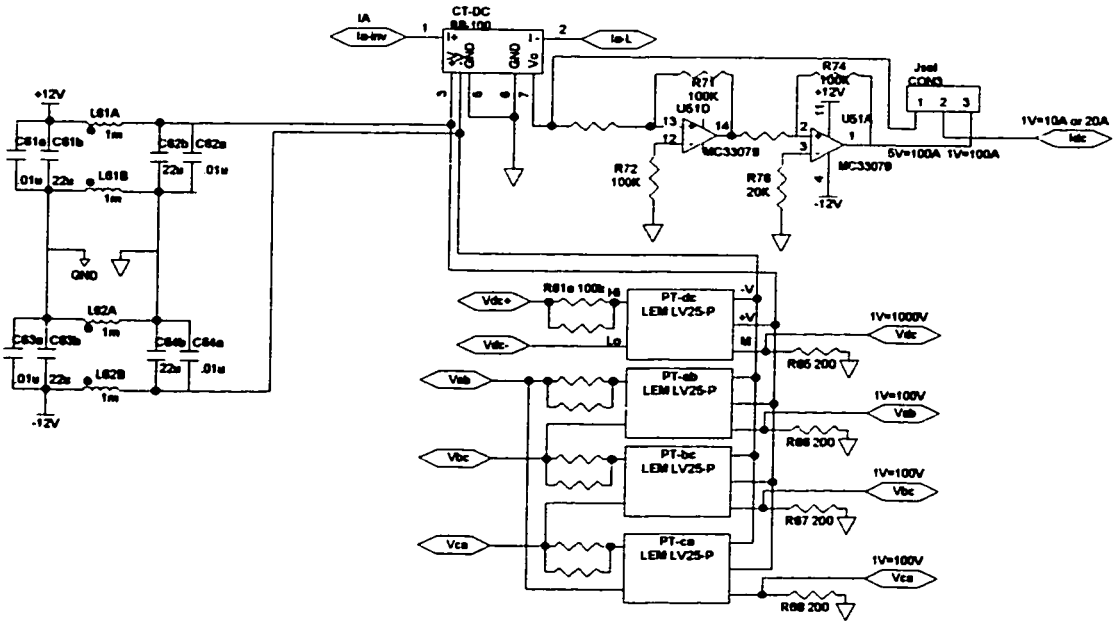

Figure 3.8 Voltage sensors

3.2.3.3 Current sensor

The ac current sensor schematic is shown in Figure 3.9. The three analog current sensors provide analog outputs of 1V for an actual current of 20A. However, the signal conditioning circuit provides an option of giving out 1V signal for actual currents of 10A. This is to reduce noise effect and to take full advantage of the DSP analog signal voltage range. These current signals are to be used by the current controller and have been well filtered before entering the DSP controller.

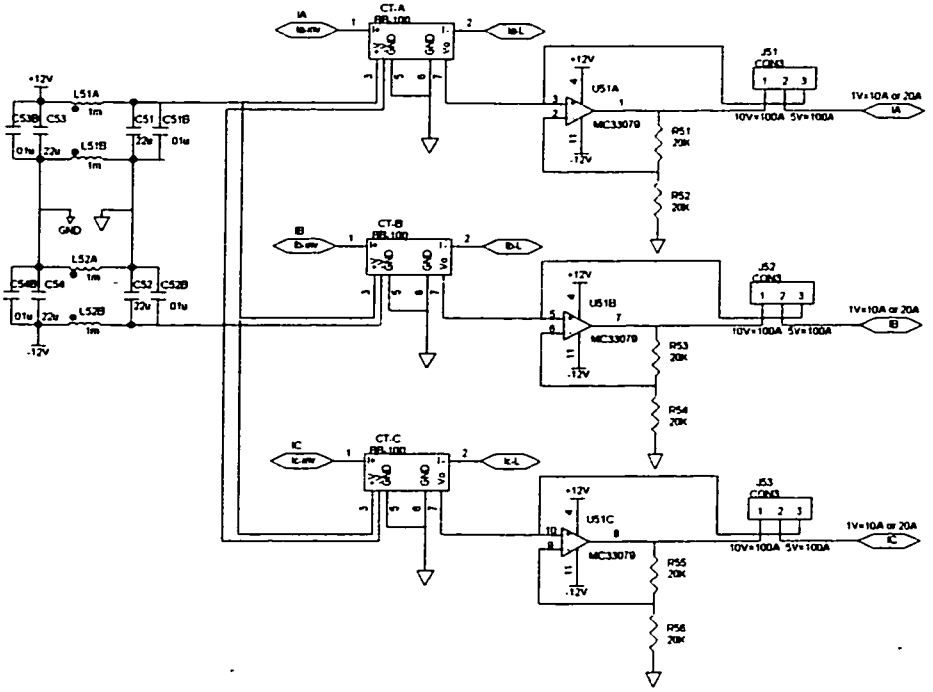

Figure 3.9 Current sensors

3.2.3.4 Dead-time controller (IXDP630)

In the design, the only gate control signals required are those for three upper switches S_1, S_3, and S_5. The dead-time controller (IXDP630) will automatically generate gate signals for lower switches S_2, S_4, and S_6. This reduces some burden of the DSP from calculating the dead-time period. The dead-time controller automatically inserts a 2.5us dead-time, that can be adjusted through the use of $R_{osc}C_{osc}$ oscillator, during which time both S_1 and S_2 are turned off, and S_2 is then turned on after the dead time. The implementation of the circuit is shown in Figure 3.11.

In Figure 3.10, the IXDP630 uses a Schmitt trigger inverter oscillator, 74HC14, two external components, $R_{osc}=R_t$ and $C_{osc}=C_t$, to determine the clock frequency and consequently the dead-time. This design allows a significant cost reduction over a

standard crystal oscillator. The initial accuracy and drift are a function of the external component tolerance and temperature coefficients, supply voltage, and IXDP630 internal parameters. At frequencies under 1MHz, assuming the external components were perfect, the IXDP630 would introduce an initial accuracy error of 5%, and a temperature dependence of –400ppm. The shift in frequency over the V_{cc} range of 4.5V to 5.5V is typically less than 5%.

At higher frequencies and with resistor values below 1kΩ, the IXDP630 internal parameters become more important. This results in greater frequency variation from one device to another, as well as with temperature and supply voltage variations.

$F_{osc} = 0.95/(C_{osc}*R_{osc})$ is the highest allowable clock frequency, including the effects of initial accuracy, tolerance, temperature coefficient, etc. When choosing oscillator components, special attention to resistor and capacitor construction is mandatory. For instance, the material used in carbon composition resistors is hydroscopic, causing resistors above 100 KΩ to 1 MΩ to change value with relative humidity. Instead, precision metal film resistor construction is used, with initial tolerances of 1 % and better with temperature coefficients of ±100 ppm. The construction of C_{osc} is also critical to circuit operation. C_{osc} is a good quality metallized polypropylene timing capacitor. The layout of the external components is also critical. The components are placed as close to the device as possible, minimizing stray capacitance and inductance.

The dead-time obtained from the IXDP630 is exactly 8 clock periods, $DT=8/F_{osc}$, of the calculated clock frequency, F_{osc}.

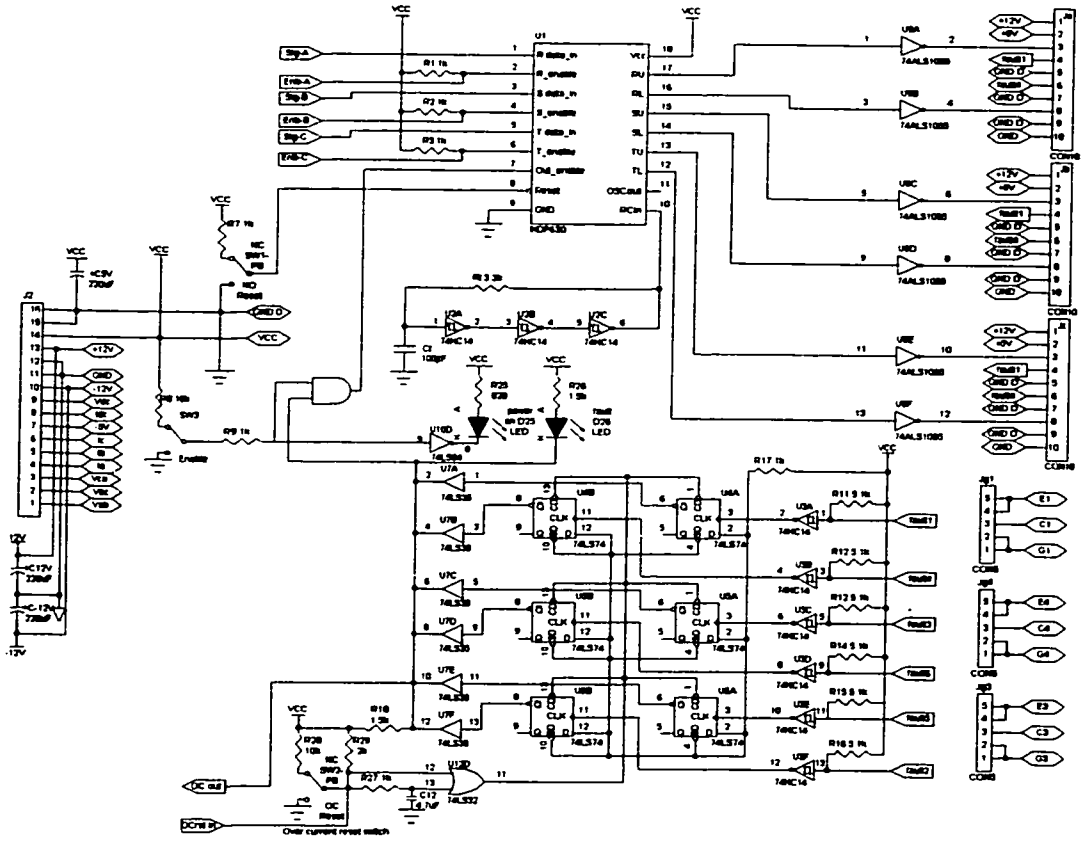

Figure 3.10 Dead-time controller

3.3 Control implementation using DSP

The BESS control implementation is shown in Figure 3.11. Figure 3.11 shows that the DSP-Board sampled two voltages and two currents from the analog-to-digital converters (ADCs) and then output three PWM signals from the input/output (I/O) pins to the dead-time controller. Finally, six PWM signals are sent to the power conversion system for control.

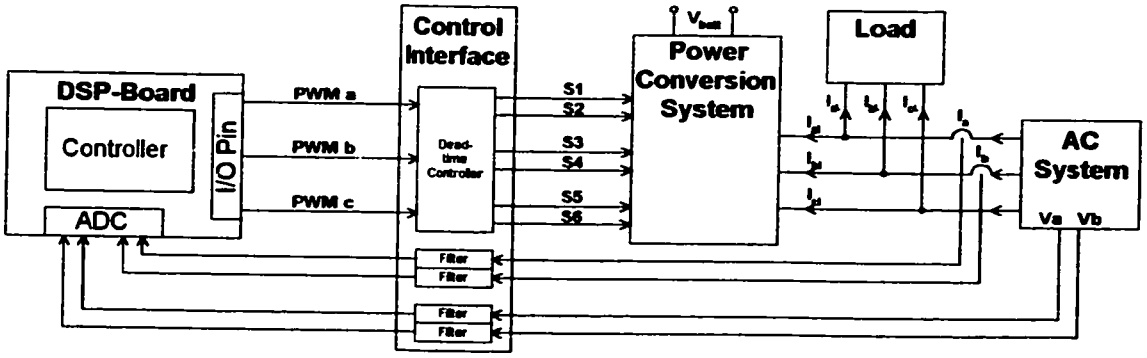

Figure 3.11 The BESS control implementation

While processing the input and output signals, the DSP-Board executes the programmed control process. The written software is first compiled into a machine code and then loaded into the memory for execution. The software consists of instructions that direct the DSP-Board to carry out the designed tasks such as to initialize the DSP-board, to activate the ADCs and I/O pins, to take control action while fetching the control variables (i.e. voltage and current), to monitor and provide a facility to alter the control references at any time even while the DSP is running.

The control strategy comprises a hysteresis band controller and a phase shift controller. Figure 3.12 shows the structure of the controller in a three-phase BESS system. The operating principle of each component will be described in the following sections.

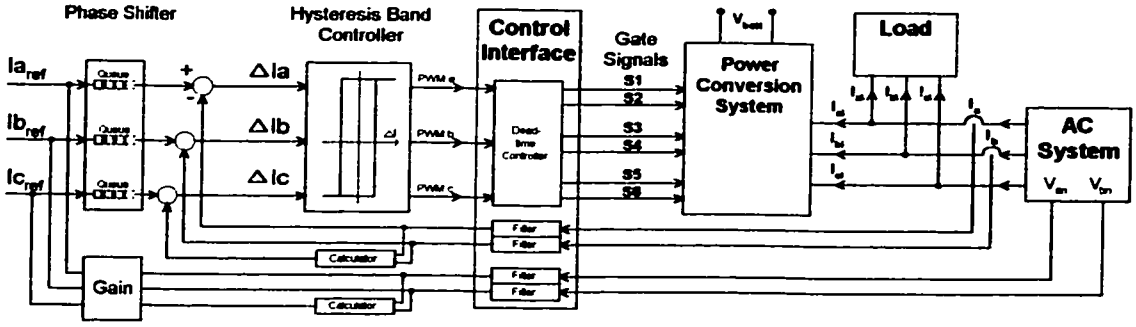

Figure 3.12 The BESS control setup

3.3.1 The hysteresis band controller

In this application, a hysteresis band controller is used to control the power supply currents connected to the power conversion system and the load. The hysteresis band control is illustrated in Figure 3.13, for a sinusoidal reference current I_{aref}. The actual current, I_a, is compared with the band around the reference current associated with that phase. If the actual current in Figure 3.13 tries to go beyond the upper band, S_1 is turned on (i.e., S_2 is turned off). The opposite switching occurs if the actual current tries to go below the lower band. Similar actions take place in the other two phases.

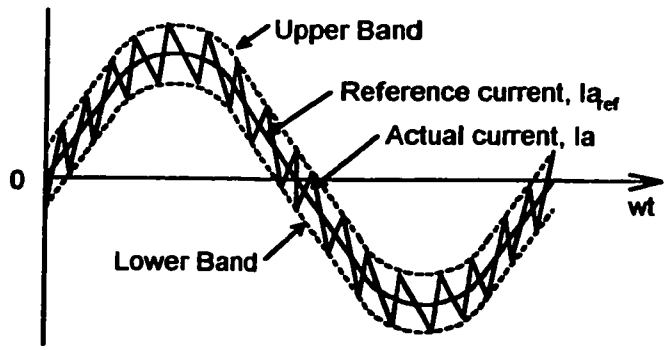

Figure 3.13 Hysteresis band

The hysteresis control of BESS is most easily interpreted if the converter is regarded as a single leg inverter. The single leg inverter, as shown in Figure 3.14, represents one phase leg of the three-phase converter connected with a single-phase ac system. It shows the current, I_s, in the source is sampled by the analog to digital converter (ADC). The sampled signal is then compared with a reference waveform to provide the ON and OFF signal for the IGBTs to ensure that the BESS will supply or absorb the required current to force the source current, I_s, to follow the reference waveform both in magnitude and phase. As the reference waveform is independent of the load current (I_L) in Figure 3.14, the source current waveform will be kept sinusoidal, even though the load current is non-sinusoidal. For the three-phase system control, the digital signal processor (DSP) provides an environment for the software-based controller to manipulate the magnitude and phase of the reference signal.

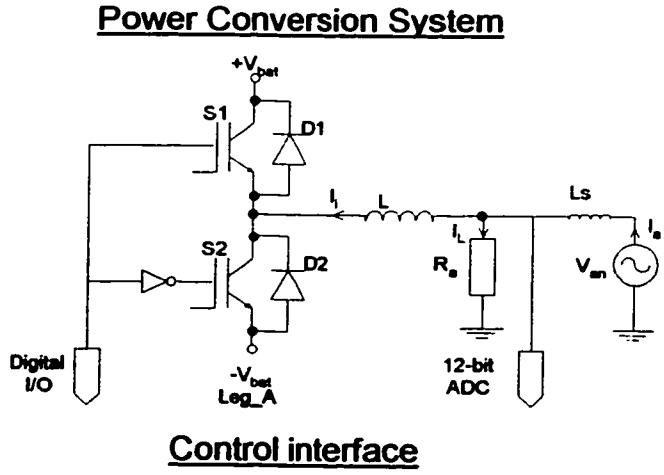

Figure 3.14 Control Strategy of BESS

3.3.2 The phase shift controller

The phase shift controller is implemented by a programming technique called linked-list. The linked-list is a data structure consisting of a group of nodes. For instance, in an array, each data element occupies a consecutive memory location. Nodes, on the other hand, may be spread out over many different locations within memory and consist of a link field. The link field contains a pointer that shows which other node the current node is connected to. The connection of node to node forms a queue.

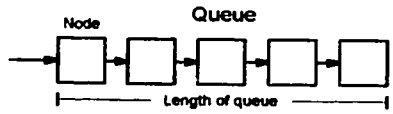

(a)

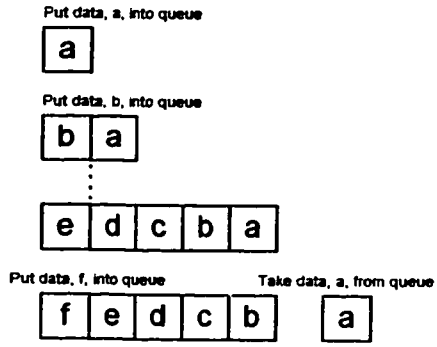

(b)

Time(sec.) (Time Step=0.00033sec)	Data Input (sampled by the ADC)	Data Shifted with an angle of 30° (0.00165sec)
T	a	X
T+0.00033	b	X
T+0.00066	c	X
T+0.00099	d	X

T+0.00132	e	X
T+0.00165	f	a
T+0.00198	g	b
T+0.00231	h	c
.	i	d
T+t		

(c)

Figure 3.15 Phase Shifter operations (a) Queue (b) Queue operations (c) Time evaluation

In this application, the length of the queue determines the angle shifted between the supply voltage and the source current. If the length of the queue is set, the data (sampled supply voltage) sampled by the ADC is entered into the left-end of the queue, on the other hand, the data at the right-end of the queue will become the reference signal of the source current. Figure 3.15(a) shows that the queue is formed by connection of five nodes and Figure 3.15(b) shows in each operation a new data (sampled supply voltage) is put into the queue with a newly created node located at the left-end of the queue. While the data at the right-end is taken away from the queue, it becomes the reference signal, and the node contains that data will be discarded. For instance, the third row of Figure 3.15(b) shows the queue (with five nodes) is full with data captured from ADC represented by letters a to e. When the next cycle starts, as shown in the last row of Figure 3.15(b), a new data (letter f) is sampled from ADC and the data at the right-end of the queue (letter a) is taken as the reference signal. After that the node will be discarded. In this regard, it forms a time delay between the data arrived at the left-end

and the data left from the right-end of the queue. The angle shift, θ_s, is corresponded to the time delay, t_{delay}, which can be calculated as:

$$t_{delay} = Length\_of\_queue \times \Delta t$$

$$\theta_s = \frac{t_{delay}}{t_f} \times 360^o$$

where Δt is the time step of each execution cycle.

t_f is the time period of a cycle (i.e. 20 msec.).

For instance, as shown in Figure 3.15(c), if the time step is equal to 0.000325 second and angle shift required is 30°, then applying the above equations, t_{delay} can be calculated as 0.00165, and length_of_queue is finally calculated as 5. Figure 3.15(c) shows the phase shift operation evaluated in time when 30° shift is needed, and based on the calculation five buffers are formed in order to obtain the required time delay (0.00165sec.). So data 'a' is shifted from T=T to T=T+0.00165 and the above data is substituted which is represented by X.

The following flow chart, in Figure 3.16, represents the flow of the two controllers (Hysteresis and Phase shift controllers). The flow chart shows one of the phases is being controlled according to the predefined conditions, such as the hysteresis band width, the magnitude and the phase angle. The whole process is implemented using DSP, which allows the predefined conditions to be changed even the DSP is running. So real-time control of the system is possible.

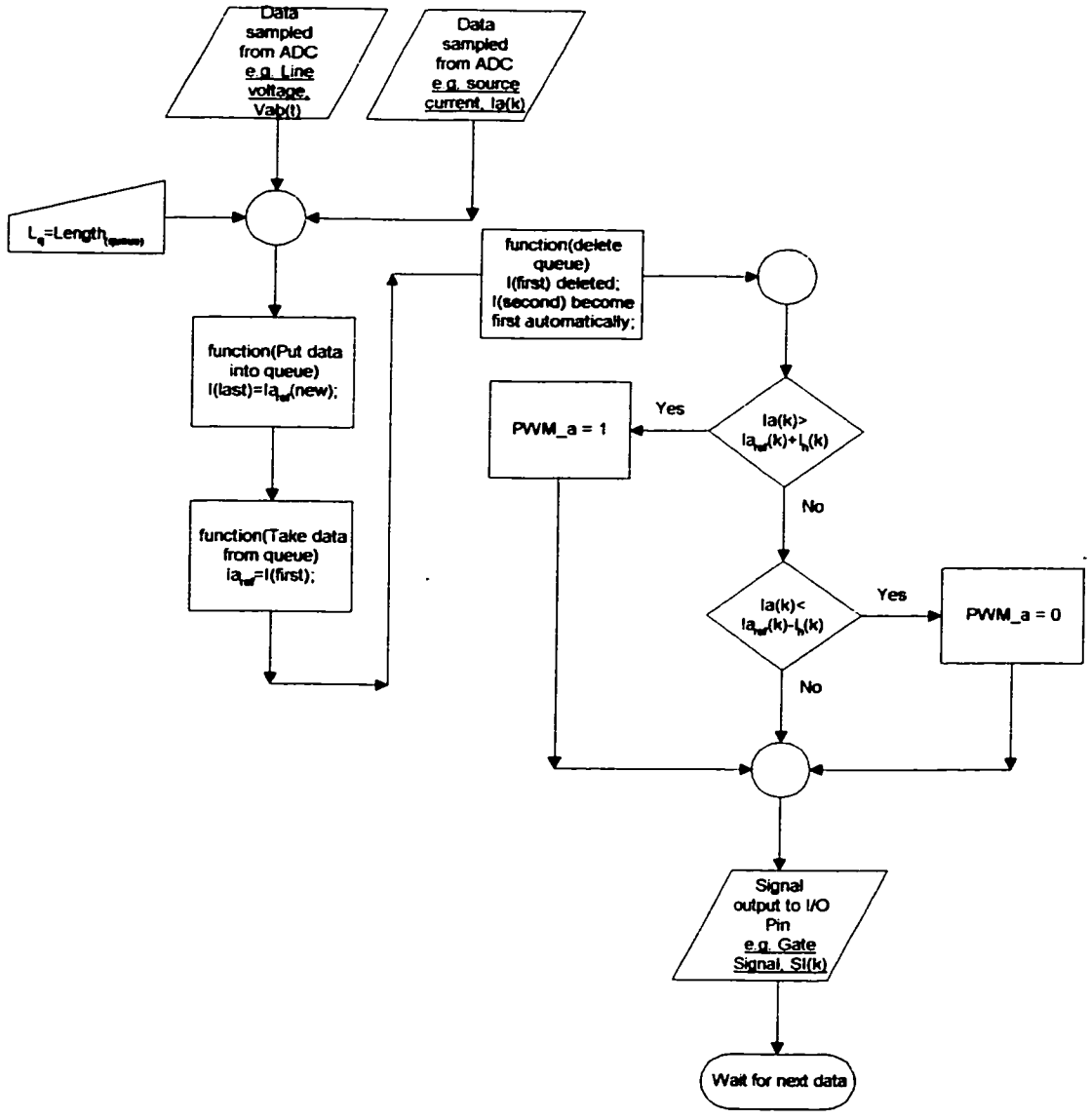

Figure 3.16 Flow Chart of the control system

3.4 BESS for Single-phase implementation

The BESS was first implemented in a single-phase system. To test the multi function capability of the BESS, the following five tests were carried out: - (i) BESS during zero-

current conditions, (ii) fast control of active and reactive power, (iii) BESS used for load leveling, (iv) active filtering, and (v) damping load fluctuations.

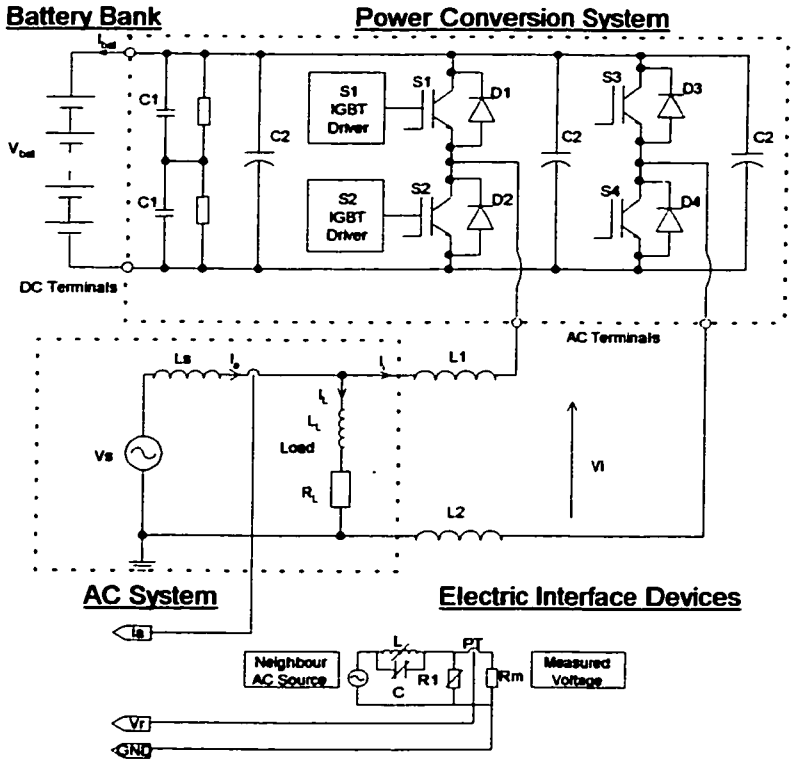

Figure 3.17 Single-phase system configuration

The system configuration is shown in Figure 3.17. In this figure, a single-phase hysteresis controller is used, and the phase shift controller is implemented using a parallel LC circuit instead of the software implementation as described in the previous section. As the capacitor (C) and inductor (L) are varied, a shifted waveform of the reference signal can be obtained. In this way the power factor of the supply can be varied, from 45° lagging to 45° leading, while at the same time the BESS can be made to provide or absorb active power.

The reference signal is sampled across the resistor R_m. When the circuit is inductive, the voltage across R_m is lagging the source voltage. The lagging voltage across R_m is then sampled by the ADC and used as the current reference to compare with the actual current, forcing the current in the source to become lagging.

3.4.1 BESS at zero-currents conditions

3.4.1.1 Operation when the source current is controlled to be equal to the load current (i.e. inverter current equals to zero)

Initially the load current is set to be 5A rms with unity power factor, i.e. pure resistive load. The magnitude of the reference waveform is also set to be 5A rms in phase with the supply voltage. To ensure that the reference current be sinusoidal, the reference current is taken from a neighboring supply source, with pure sinusoidal waveform. The results are shown in Figure 3.18(a)-(c). Figure 3.18(a) shows the source current waveform. It has a slight ripple due to the hysteresis control, but the waveform follows closely the reference waveform both in magnitude and phase. Figure 3.18(b) shows the inverter current waveform. Although in theory, the BESS will supply zero current but due to the hysteresis control, a small current still flows, which is equal to the difference between the controlled source current and the load current.

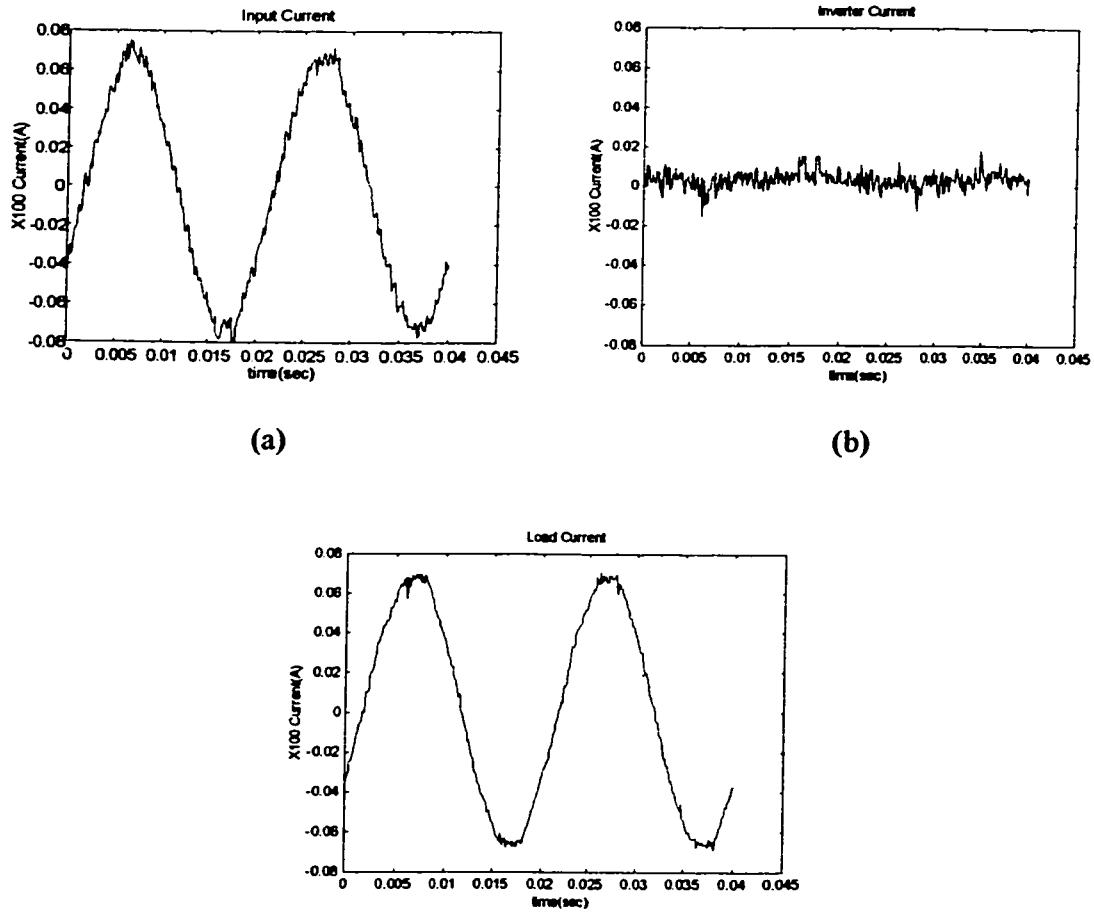

Figure 3.18 (a) Source current, I_s; (b) Inverter current, I_i; (c) Load current, I_L

3.4.1.2 Operation when the load is disconnected (i.e. load current equals to zero)

The load current is then reduced to zero by disconnecting the load. The reference current is kept constant as before. The results are shown in Figure 3.19(a)-(c). No effect is seen on the source current as the load is disconnected. It is maintained at 5A rms with unity power factor (Figure 3.19(a)), but now the BESS absorbs all the source current as shown in Figure 3.19(b). This corresponds to the case of light load at night, where the source

current is used to charge the batteries associated with the BESS and this is observed by recording a negative current going to the inverter.

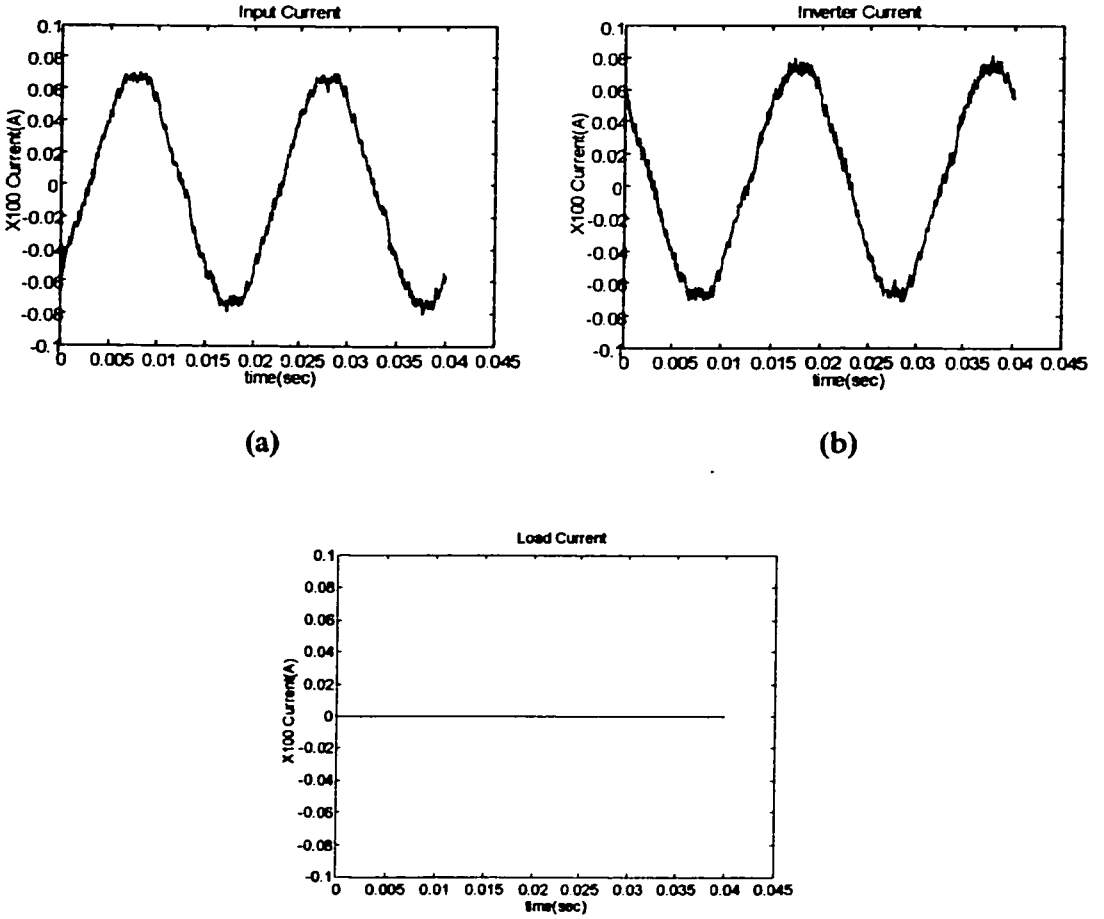

Figure 3.19 (a) Source Current, I_s; (b) Inverter Current, I_i; (c) Load current, I_L

3.4.1.3 Operation when the reference current is set to zero (i.e. source current equals to zero)

The load current is maintained at 5 A rms with unity power factor (Figure 3.20(c)) and the reference waveform magnitude is now reduced to 0A. In this way the BESS is now

supplying all the load current. As expected the source current contains ripples due to the hysteresis control with an average of 0 A (Figure 3.20(a)), and the inverter current is roughly equal to the load current (Figure 3.20(b)), and the addition of source current and inverter current waveform will form the load current waveform in accordance with Kirchhoff's current law. If BESS has sufficient energy it can be used to supply the load current during peak period.

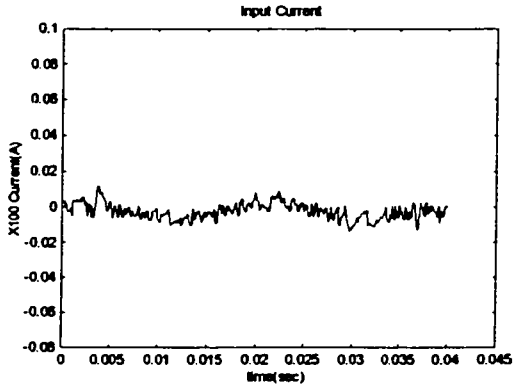

(a)

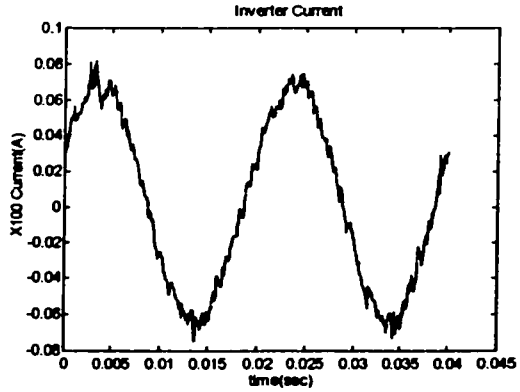

(b)

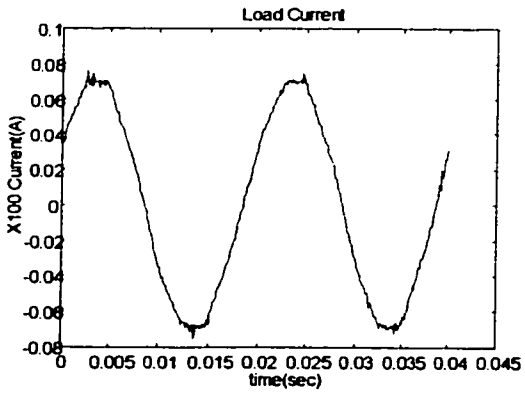

(c)

Figure 3.20 (a) Source Current, I_s; (b) Inverter Current, I_i; (c) Load Current, I_L

3.4.2 Fast control of BESS active power from generating to absorbing power

Figure 3.21 and Figure 3.22 show the response of the BESS following a sudden change in the polarity of the reference signal from positive to negative value. Initially the source current is controlled at 4A in phase with the supply voltage. The load current is lagging the supply voltage and in terms of phasor, $I_L = 4.5\angle -18°$ as shown in Figure 3.21(c). Therefore the BESS is supplying part of the load current as shown in Figure 3.21(d). When the polarity of the reference waveform is reversed, the input current is now 180° apart from the supply voltage as shown in Figure 3.22(a) & (b). BESS is now not only supplying the load but also pumping power back to the supply as shown in Figure 3.22(d). The load current remains the same as before. This demonstrates that the output of BESS can vary from positive value to negative value. As the response is very fast, such a capability can be used to damp oscillation by charging and discharging BESS to

counter the rising and reducing acceleration. It can be used to provide damping for transient disturbances as well as negative load shedding.

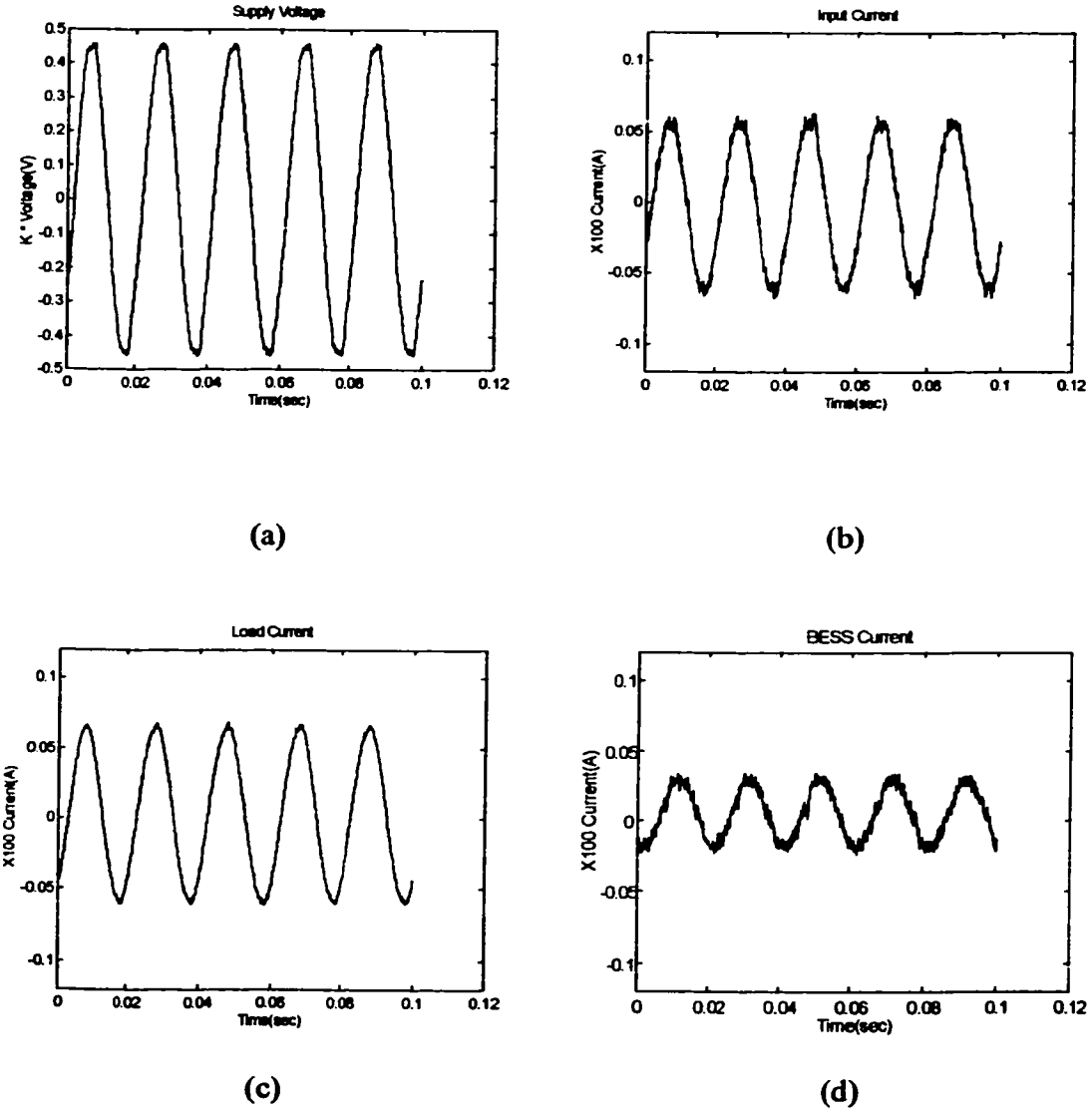

Figure 3.21 Fast control of BESS active power at generating (a) Supply voltage; (b) Source current, I_s; (c) Load current, I_L; (d) Inverter current, I_i.

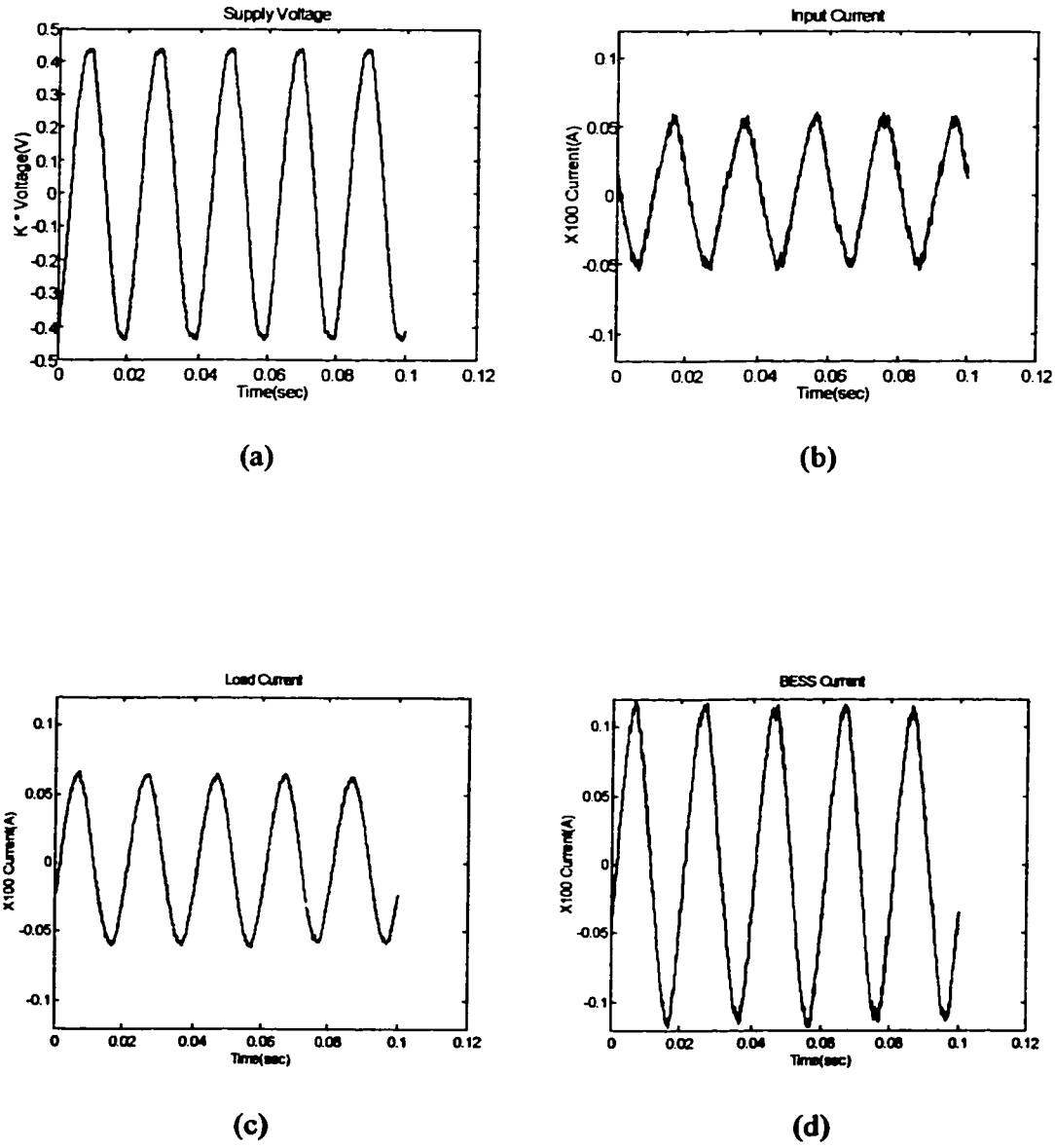

Figure 3.22 Fast control of BESS active power at absorbing (a) Supply voltage; (b) Source current, I_s; (c) Load current, I_L; (d) Inverter current, I_i.

3.4.3 Applying BESS for load levelling

Figure 3.23 shows the potential operation of the BESS for load levelling. There are three divisions of time: early morning time, day-time, and night time. As can be seen from the load current curve, the load is the highest during the day-time (I_L = 8.0A during the day and 1.6A at night). Without BESS, the source current will have to follow the load current and therefore the maximum demand will be 8A, which can be even higher if there is a sudden change in load during its peak load. With the BESS installed, the source current can be controlled to be maintained at 5.6A throughout the day and night giving a load factor of 1. During the day the BESS is used to supply the load, and during early morning time and at night-time when the load is low, the batteries are charged. The level of the source current is controlled by the reference signal and can be adjusted to ensure that the losses associated with charging and discharging be taken care of, i.e. more energy is available to charge than to discharge. This is taken care of by the microprocessor controller, which will also monitor the battery state-of-charge to avoid total discharge of the battery. As the reference signal is controlled in its magnitude, phase and waveform, the source current is maintained sinusoidal even when the load is distorted as shown in the next section.

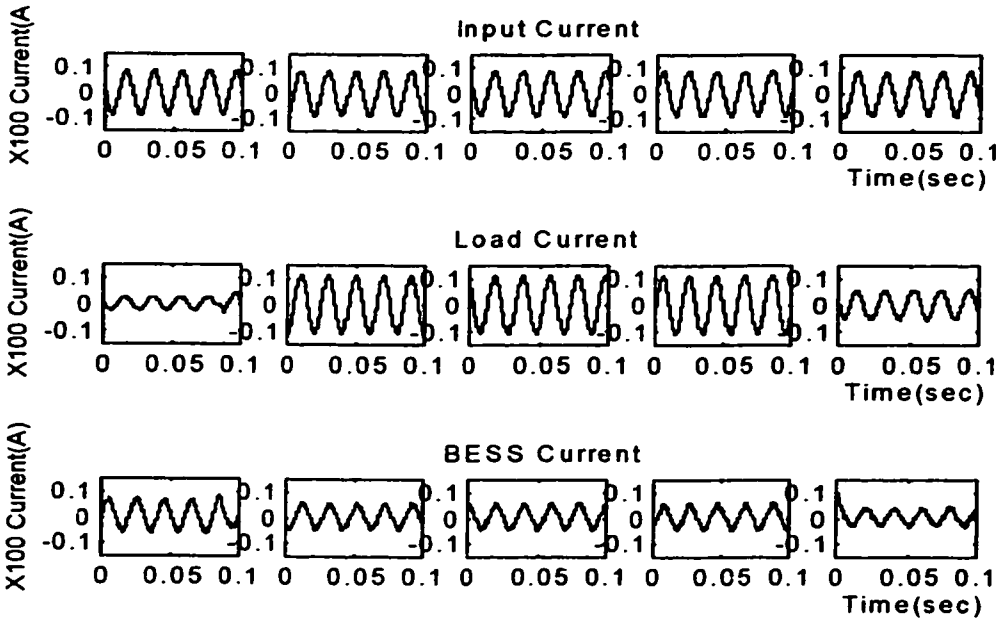

Figure 3.23 BESS for load levelling

3.4.4 Active filtering Action of the BESS

To prove the active filtering capability of the BESS, the load is distorted artificially using a diode in series with the load, as shown in Figure 3.24 with the same resistance value as before. The reference current is set to 5A rms in phase with the supply. Figure 3.25(a)-(c) show the results of the experiment. The load current is clipped whenever the supply voltage goes positive, but the source current is maintained to be sinusoidal following closely the reference current. The BESS absorbs current during the positive cycle to ensure that the source current remains sinusoidal. This demonstrates that the BESS is acting as an active filter naturally without any requirement for extra control strategy.

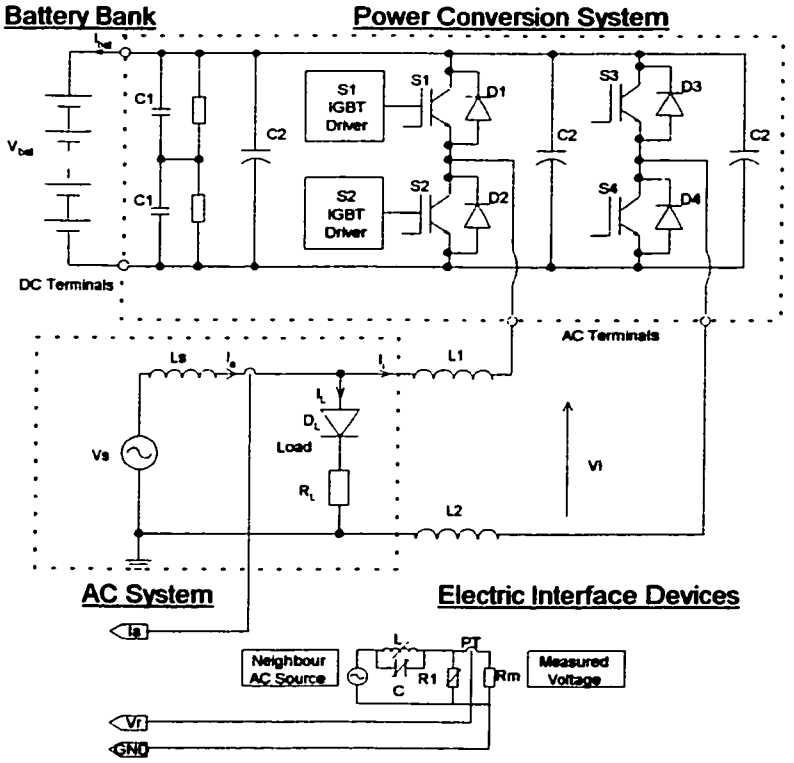

Figure 3.24 Circuit for distorted load

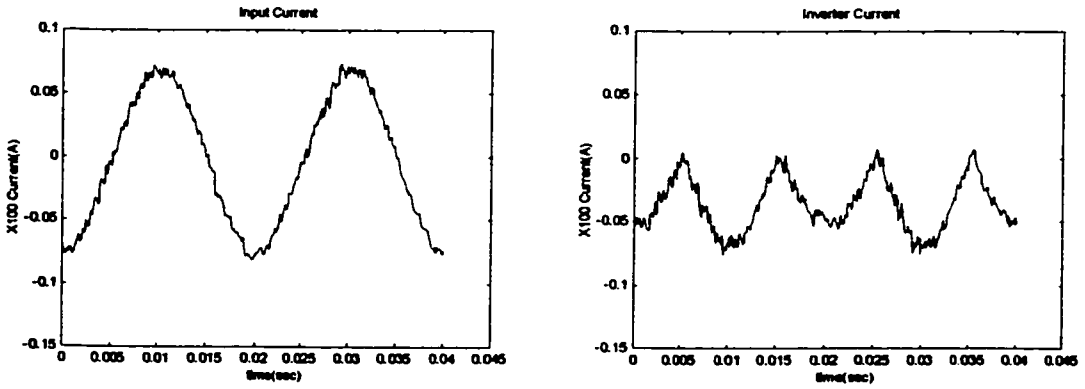

(a) (b)

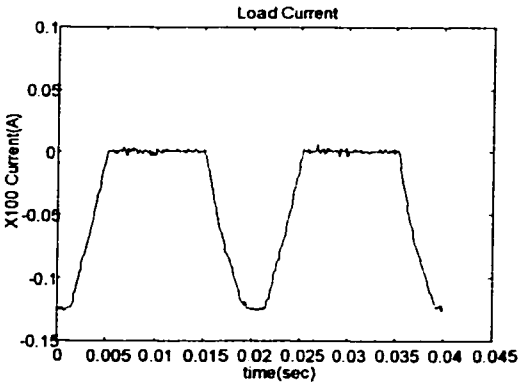

(c)

Figure 3.25 (a) Source Current, I_s; (b) Inverter Current, I_i; (c) Load Current, I_L

3.4.5 Using the BESS to damp load fluctuation

Figure 3.26 shows the effect of load fluctuation on the power system. As the load magnitude varies, the source current and hence the voltage at the point of common coupling will vary and this can cause voltage flicker to the neighboring load.

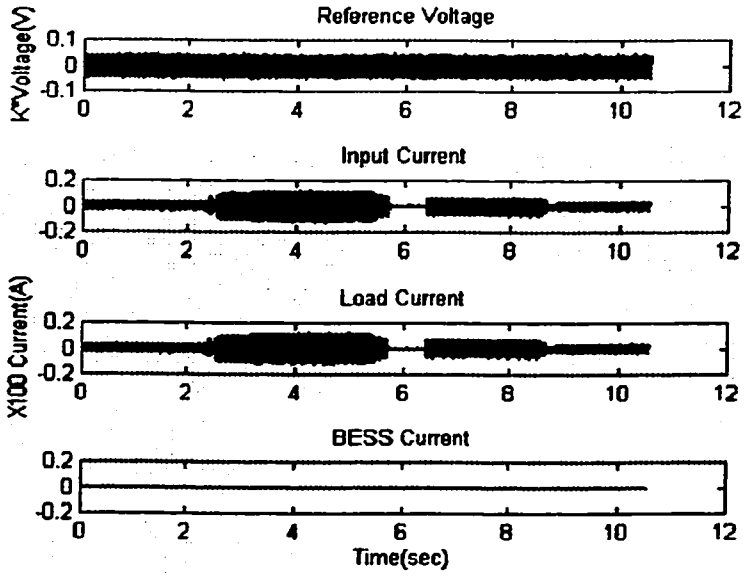

Figure 3.26 Effect of load fluctuation without BESS

When the BESS is connected to the power system, the BESS guarantees rock solid control of the source current as shown in Figure 3.27. As the load fluctuates, the source current remains constant and unaffected by the load fluctuations, ensuring that the voltage at the common coupling will not experience flickers due to the load fluctuation.

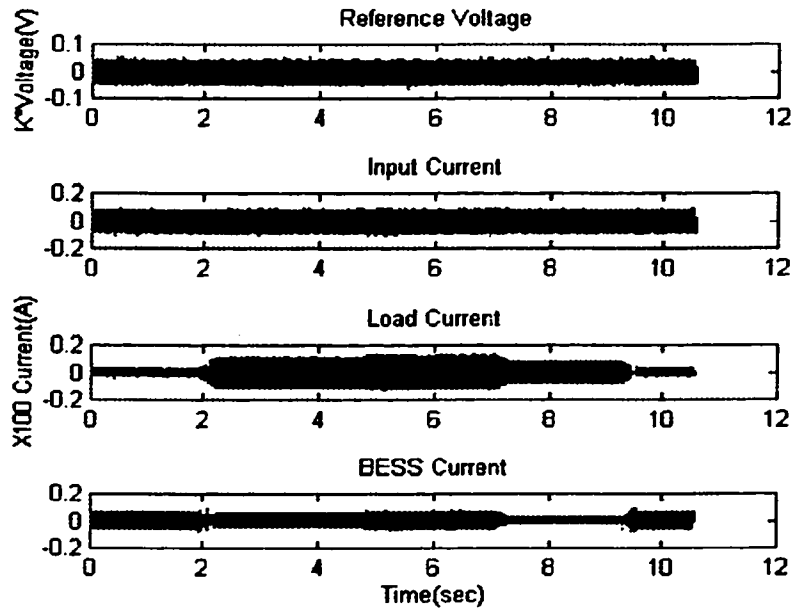

Figure 3.27 Effect of load fluctuation with BESS

3.5 Conclusion

This chapter presented the design procedure of the system including the selection of the battery bank, the design of the power conversion system and the implementation of the control system. Building up of the whole system hinged on the application tasks

requiring the relationship between the battery bank and the PCS rating. In addition, the PCS construction and the implementation of the control system based on the control interface were explained. Finally, the implementation of the designed control strategy based on the DSP environment has been described.

Based on the above-mentioned work, the system has been implemented in single-phase for physical test. The use of BESS for power factor correction, active filtering, damping load fluctuations and fast control of charge and discharge conditions have also been demonstrated.

The next chapter will show the BESS for three-phase implementation with more useful attributes being studied.

CHAPTER 4 THREE-PHASE IMPLEMENTATION

Much testing; accuracy and precision in experiment; no guesswork or self-deception.

Ehrlich, Paul

In Martha Marquardt

CHAPTER 4 THREE-PHASE IMPLEMENTATION

4.1 Configuration

Figure 4.1 shows a three-phase implementation of the proposed BESS system connected with the utility grid. The ac system is a three-phase four-wire star system, with 110 V line to line voltage. The BESS is connected to the ac utility grid through three inductors and an isolating three-phase transformer.

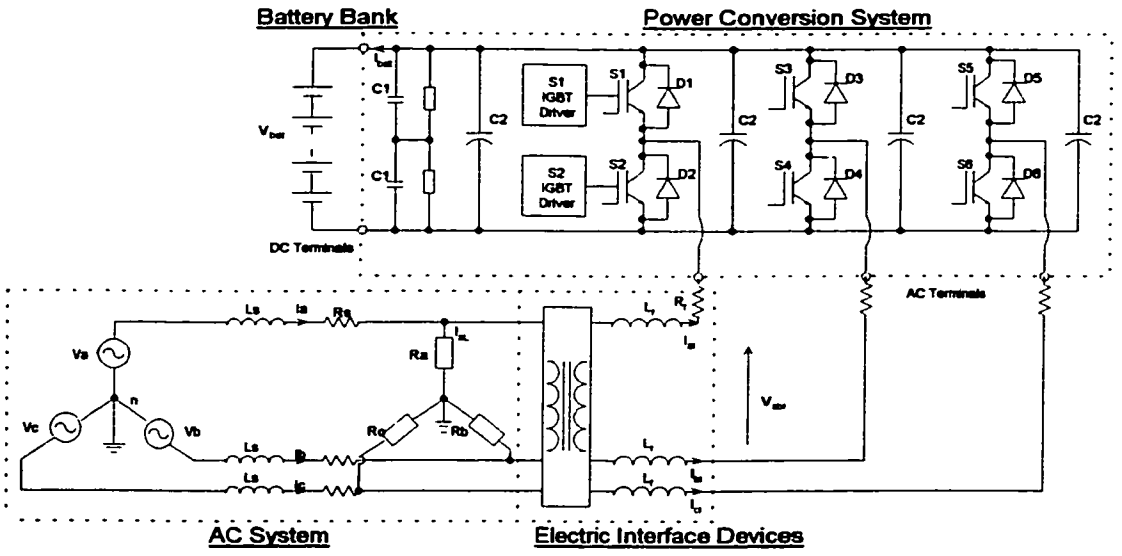

Figure 4.1 Three-phase system configuration

To understand the operation of the circuit in Figure 4.2, a mathematical analysis has been developed, consisting of the battery model and the system model and will be described in Section 4.1.1. The mathematical analysis can be used to simulate the

operation of the BESS before the actual implementation of the actual circuit in the laboratory. Results from the simulation are shown in Section 4.1.1.3.

After confirmation of the system operation by Pspice simulation, the system was built and the control system was implemented using DSP. Various experiments have been carried out to show the multi-function capabilities of the BESS. The efficiency of the BESS under various operating conditions will be discussed in Section 4.2.

4.1.1 Circuit Analysis

The BESS shown in Figure 4.1 can be modeled by differential equations based on circuit analysis, however some assumptions should be made before the system is modeled. The following assumptions have been made:

1. The system grid can be represented by a three-phase balanced, sinusoidal voltage source.
2. The filter inductors L are assumed to be linear and saturation is not considered.
3. The diodes and IGBTs are assumed to be ideal switches.
4. The ESR of the capacitors is negligible.

Let d_a, d_b and d_c be the switching functions of the converter representing upper switches of phase leg A, B and C respectively, we have

$$V_a = V_{Cdc} d_a \tag{4.1}$$

$$V_v = V_{Cdc} d_b \tag{4.2}$$

$$V_w = V_{Cdc} d_c \tag{4.3}$$

In this way, the system can be separated into two models, the battery bank model and the three-phase model as shown in Figure 4.2.

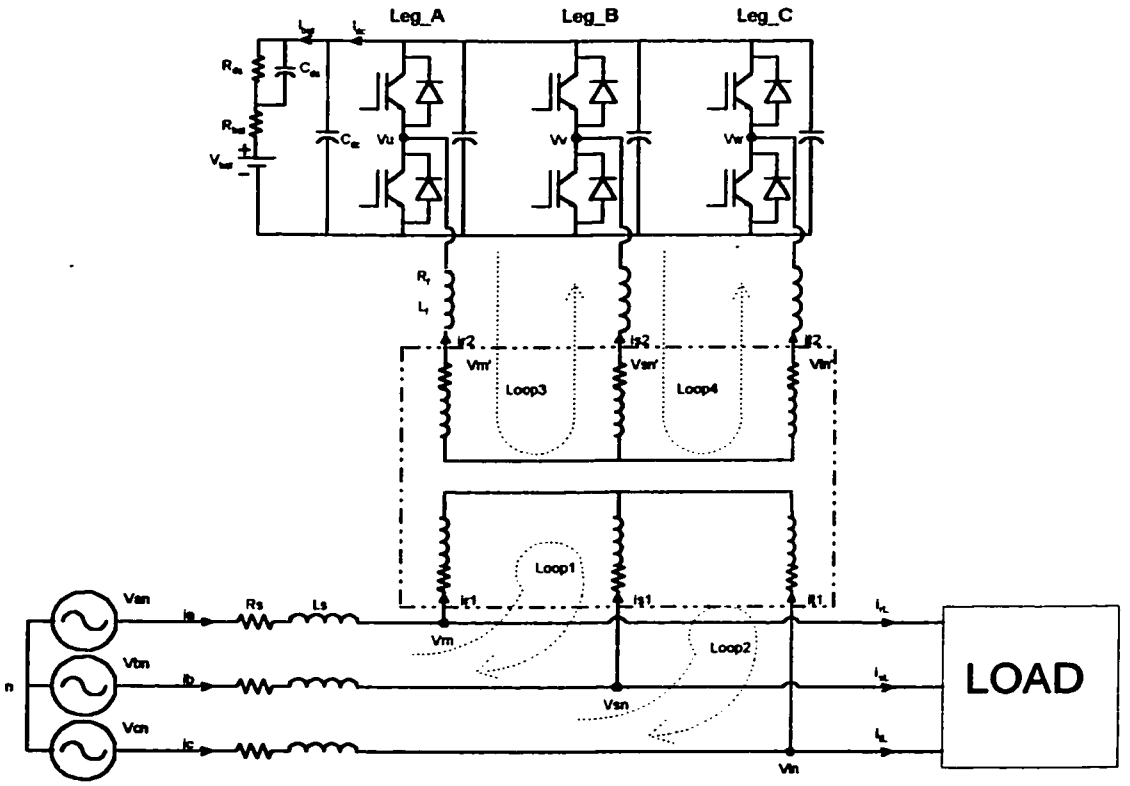

Figure 4.2 System model

4.1.1.1 Mathematical model of the battery bank

There are many available battery models in literature (Salameh, Z.M., Casacca, M.A. and Lynch, W.A., 1992). The simplest model to use is the Thevenin equivalent circuit shown in Figure 4.2, where the battery bank is represented by the internal resistance, R_{bat},

in series with a parallel circuit consisting of a capacitance, C_{ds}, and an overvoltage resistance, R_{ds}. C_{ds} represents the capacitance of the parallel plates and R_{ds} represents the non-linear resistance contributed by the contact resistance of the plates to the electrolyte.

The battery model can be represented by the following differential equations:

$$\frac{dV_{Cdc}}{dt} = \frac{d_a}{C_{dc}} i_{r2} + \frac{d_b}{C_{dc}} i_{s2} + \frac{d_c}{C_{dc}} i_{t2} - \frac{1}{C_{dc} R_{bat}} V_{Cdc} + \frac{1}{C_{dc} R_{bat}} V_{bat} + \frac{1}{C_{dc} R_{bat}} V_{Cds} \quad (4.4)$$

$$\frac{dV_{Cds}}{dt} = \frac{i_{bat} - V_{Cds}/R_{ds}}{C_{ds}} \quad (4.5)$$

$$i_{bat} = \frac{(V_{Cdc} - V_{Cds} - V_{bat})}{R_{bat}} \quad (4.6)$$

4.1.1.2 Mathematical model of the BESS

By using the Kirchhoff's current law and Kirchhoff's voltage law, from Figure 4.2, the following dynamic equations can be formulated:

$$i_a = i_{r1} + i_{rL} \quad (4.7)$$

$$i_b = i_{s1} + i_{sL} \quad (4.8)$$

$$i_c = i_{t1} + i_{tL} \quad (4.9)$$

$$N = \frac{V_m}{V_m'} = \frac{V_{sn}}{V_{sn}'} = \frac{V_{tn}}{V_{tn}'} = 1 \quad (4.10)$$

First part: - (Loop 1 & Loop 2)

$$V_{ab} = R_s(i_a - i_b) + L_s(\frac{di_a}{dt} - \frac{di_b}{dt}) + V_{rs} \quad (4.11)$$

$$V_{bc} = R_s(2i_b + i_a) + L_s(\frac{di_a}{dt} + 2\frac{di_b}{dt}) + V_{st} \quad (4.12)$$

$$i_c = -(i_a + i_b) \quad (4.13)$$

Second part: -(From Loop 3 & Loop4)

$$V_{rs}' = R_f(i_{r2} - i_{s2}) + L_f(\frac{di_{r2}}{dt} - \frac{di_{s2}}{dt}) + V_{uv} \quad (4.14)$$

$$V_{st}' = R_f(i_{s2} - i_{t2}) + L_f(\frac{di_{s2}}{dt} - \frac{di_{t2}}{dt}) + V_{vw} \quad (4.15)$$

$$i_{t2} = -(i_{r2} + i_{s2}) \quad (4.16)$$

From Equations 4.11 to 4.16 and with reference to Figure 4.3, we have

$$\frac{di_a}{dt} = \frac{V_{an} - V_{nn}}{L_s} - \frac{i_a R_s}{L_s} \quad (4.17)$$

$$\frac{di_b}{dt} = \frac{V_{bn} - V_{sn}}{L_s} - \frac{i_b R_s}{L_s} \quad (4.18)$$

$$\frac{di_c}{dt} = \frac{V_{cn} - V_{tn}}{L_s} - \frac{i_c R_s}{L_s} \quad (4.19)$$

$$\frac{di_{r2}}{dt} = \frac{3V_{nn}' - (2V_{uv} + V_{vw})}{3L_f} - \frac{i_{r2} R_f}{L_f} \quad (4.20)$$

$$\frac{di_{s2}}{dt} = \frac{3V_{sn}' - (V_{vw} - V_{uv})}{3L_f} - \frac{i_{s2} R_f}{L_f} \quad (4.21)$$

$$\frac{di_{t2}}{dt} = \frac{3V_{tn}' - (-2V_{vw} - V_{uv})}{3L_f} - \frac{i_{t2} R_f}{L_f} \quad (4.22)$$

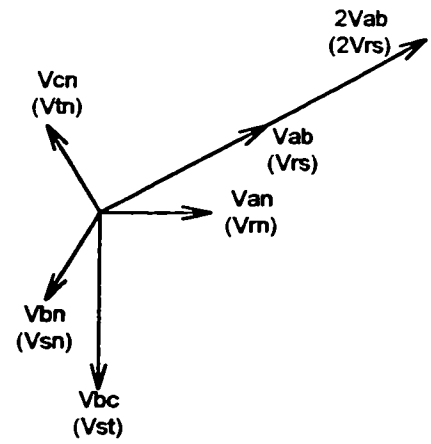

Figure 4.3 Phasor diagram of balanced three-phase voltage

From Equations 4.1, 4.2 and 4.3, rearranging Equations 4.20, 4.21 and 4.22 we have

$$\frac{di_{r2}}{dt} = \frac{3V_m' - V_{Cdc}(3d_a - \sum_{x=a,b,c} d_x)}{3L_f} - \frac{i_{r2}R_f}{L_f} \tag{4.23}$$

$$\frac{di_{s2}}{dt} = \frac{3V_{sn}' - V_{Cdc}(3d_b - \sum_{x=a,b,c} d_x)}{3L_f} - \frac{i_{s2}R_f}{L_f} \tag{4.24}$$

$$\frac{di_{t2}}{dt} = \frac{3V_{tn}' - V_{Cdc}(3d_c - \sum_{x=a,b,c} d_x)}{3L_f} - \frac{i_{t2}R_f}{L_f} \tag{4.25}$$

The system can be represented by the following Equations 4.4 to 4.10, 4.17 to 4.19 and 4.23 to 4.25. Rewritten as:

$$\frac{dV_{Cdc}}{dt} = \frac{d_a}{C_{dc}} i_{r2} + \frac{d_b}{C_{dc}} i_{s2} + \frac{d_c}{C_{dc}} i_{t2} - \frac{1}{C_{dc}R_{bat}} V_{Cdc} + \frac{1}{C_{dc}R_{bat}} V_{bat} + \frac{1}{C_{dc}R_{bat}} V_{Cdc} \tag{4.26}$$

$$\frac{dV_{Cds}}{dt} = \frac{i_{bat} - V_{Cds}/R_{ds}}{C_{ds}} \tag{4.27}$$

$$i_{bat} = \frac{(V_{Cdc} - V_{Cds} - V_{bat})}{R_{bat}} \tag{4.28}$$

$$i_a = i_{r1} + i_{rL} \tag{4.29}$$

$$i_b = i_{s1} + i_{sL} \tag{4.30}$$

$$i_c = i_{t1} + i_{tL} \tag{4.31}$$

$$\frac{di_a}{dt} = \frac{V_{an} - V_{rn}}{L_s} - \frac{i_a R_s}{L_s} \tag{4.32}$$

$$\frac{di_b}{dt} = \frac{V_{bn} - V_{sn}}{L_s} - \frac{i_b R_s}{L_s} \tag{4.33}$$

$$\frac{di_c}{dt} = \frac{V_{cn} - V_{tn}}{L_s} - \frac{i_c R_s}{L_s} \tag{4.34}$$

$$N = \frac{V_{rn}}{V_{rn}'} = \frac{V_{sn}}{V_{sn}'} = \frac{V_{tn}}{V_{tn}'} = 1 \tag{4.35}$$

$$\frac{di_{r2}}{dt} = \frac{3V_{rn}' - V_{Cdc}(3d_a - \sum_{x=a,b,c} d_x)}{3L_f} - \frac{i_{r2}R_f}{L_f} \tag{4.36}$$

$$\frac{di_{s2}}{dt} = \frac{3V_{sn}' - V_{Cdc}(3d_b - \sum_{x=a,b,c} d_x)}{3L_f} - \frac{i_{s2}R_f}{L_f} \tag{4.37}$$

$$\frac{di_{t2}}{dt} = \frac{3V_{tn}' - V_{Cdc}(3d_c - \sum_{x=a,b,c} d_x)}{3L_f} - \frac{i_{t2}R_f}{L_f} \tag{4.38}$$

where R_s and R_f are the series resistances in one phase, and

d_x (x = a, b, or c) is the switching function of the switching device S_x.

When the S_x is on, d_x=1. Otherwise, d_x=0.

Because no specific restriction was imposed on the switching function d_x during the derivation, this mathematical model is a general one and is universally applicable to six-step inverter, various forms of pulse-width modulation or to other switching strategies. It provides an exact solution at any moment if the switching function d_x is defined, and it is especially useful in a computer simulation to obtain a detailed waveform in the time domain.

Using Equations 4.26 – 4.38, the circuit in Figure 4.2 can then be simulated. The results obtained from the Pspice simulation will be discussed in the next section.

4.1.1.3 Simulation Results

Three control circuits to control the magnitude and phase of three individual currents based on hysteresis control have been simulated using the BESS circuit shown in Figure 4.2. This technique aims to control the three-phase system source current very close to the reference current. A hysteresis band of 0.5A has been used. Figure 4.4(a) shows the circuit diagram of the control circuit for one of the phases. The input signal V_e (proportional to the actual current signal) is applied to the inverting input. At the non-inverting input the reference voltage v_{ref} is given by the voltage divider principle to be:

$$v_{ref} = v_o R/(R + R_f) = kv_o$$

The output v_o is ideally one of the saturation levels ±VCC. Thus, v_{ref} has one of two levels ±kVCC. If the error signal v_e is greater than the reference signal v_{ref}, the output v_o goes negative. In this application the negative output –VCC is to be a gate signal that

will lead to a change (less positive) of the error signal v_e. When the error signal v_e is negative and less than the reference signal v_{ref} (at present –kVCC) the comparator output shifts states to v_o = +VCC and the reference signal becomes v_{ref} = kVCC. The reference signal remains at +kVCC until the error signal v_e is greater than v_{ref}, at which point the cycle repeats. While the comparator output is v_o = +VCC, the output is to be a gate signal that will lead to a change (less negative) in the error signal. Figure 4.4(b) shows how the error signal as a function of time is transformed by the comparator to a square-wave output. The negative output voltage v_o becomes the gate signal to keep switch Sw.1 of the inverter in the on-state. The positive output voltage v_o is used to maintain switch Sw.2 on.

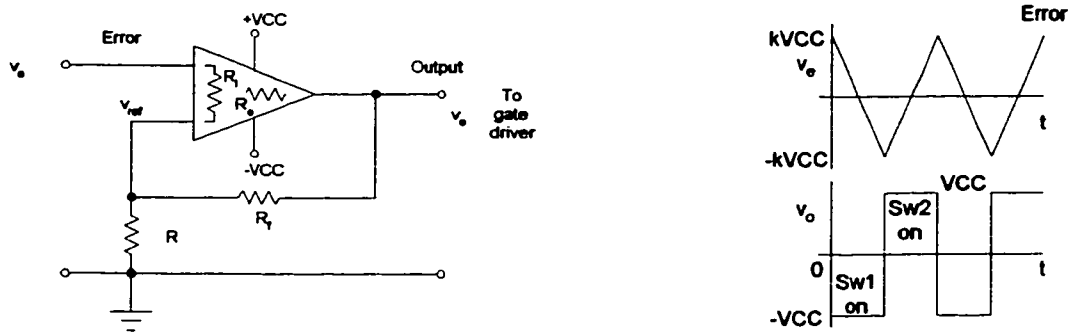

(a) (b)

Figure 4.4 PWM with band tolerance (a) comparator; (b) input and output signals.

Based on this technique, the whole BESS system is implemented and the simulated result is shown in Figure 4.5. The simulation result is based on a BESS with the following parameters: V_{bat}=230 V; V_{an}=65.5 $V_{(rms)}$; L_s=1m H; R_s=0.01 Ω; L_f=8m H; R_f=0.01 Ω; R_L=20 Ω; L_L=40m H. This result will be compared later with the experimental results described in Section 4.2.

Figures 4.5(a)-(f) show the simulation results when the system is normally operated with BESS controlling the ac source current, which is in phase with the phase voltage. The system is inductively loaded with the load current slightly less than the controlled source current.

Figures 4.5(a) and (b) show the line- and phase-voltage at the point of common coupling between the BESS and the ac utility grid. Figures 4.5(c) and (d) show the inverter line voltage and the inverter phase voltage at the inverter ac terminals. The inverter line voltage waveform is a set of switching pulses between ±228 V, where its fundamental can be represented by a 50 Hz sinusoidal waveform. Figures 4.5(e), (f) and (g) show the source current, the inverter current and the load current in phase-A. The magnitude and phase of the source current is controlled at 2.83 $A_{(rms)}$ and in phase with the phase voltage. It can be observed that the source current is equal to the sum of the inverter and the load currents. Figures 4.5(h) and (i) show the battery voltage and the battery current, and since the sign of battery current is positive, the current is flowing into (charging) the battery. This is because the source current is controlled to be slightly larger than the load current. By controlling the source current magnitude and phase at appropriate level during the day and at night, the battery state-of-charge can be controlled to be always optimum when required.

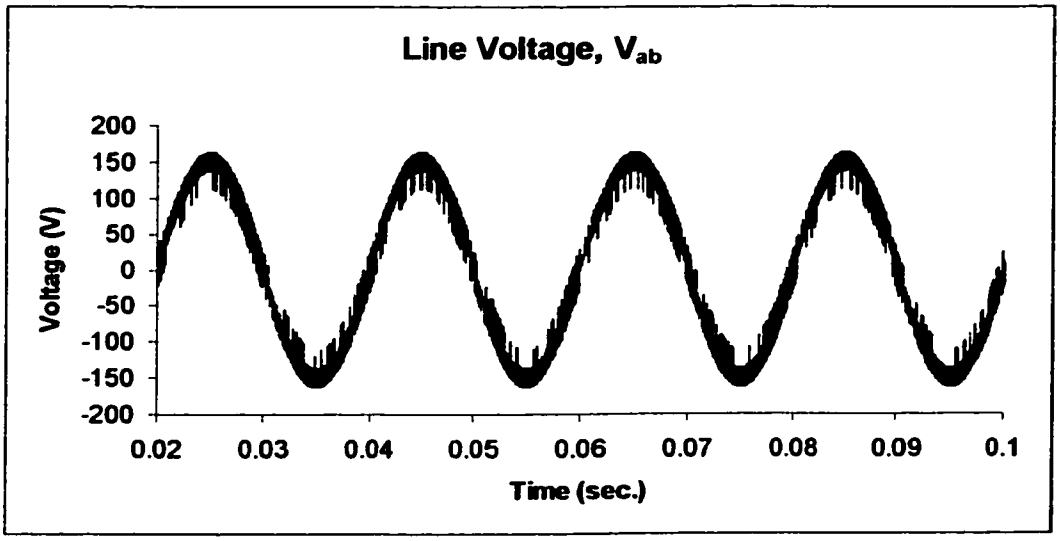
Line Voltage, V_{ab}
Voltage (V)
200
150
100
50
0
-50
-100
-150
-200
0.02
0.03
0.04
0.05
0.06
0.07
0.08
0.09
0.1
Time (sec.)

(a)

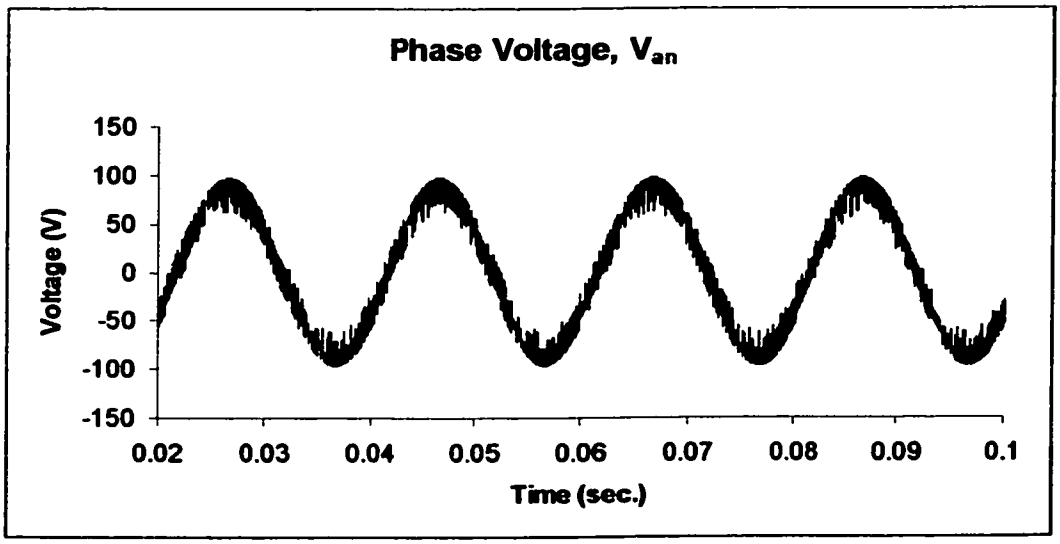
Phase Voltage, V_{an}
Voltage (V)
150
100
50
0
-50
-100
-150
0.02
0.03
0.04
0.05
0.06
0.07
0.08
0.09
0.1
Time (sec.)

(b)

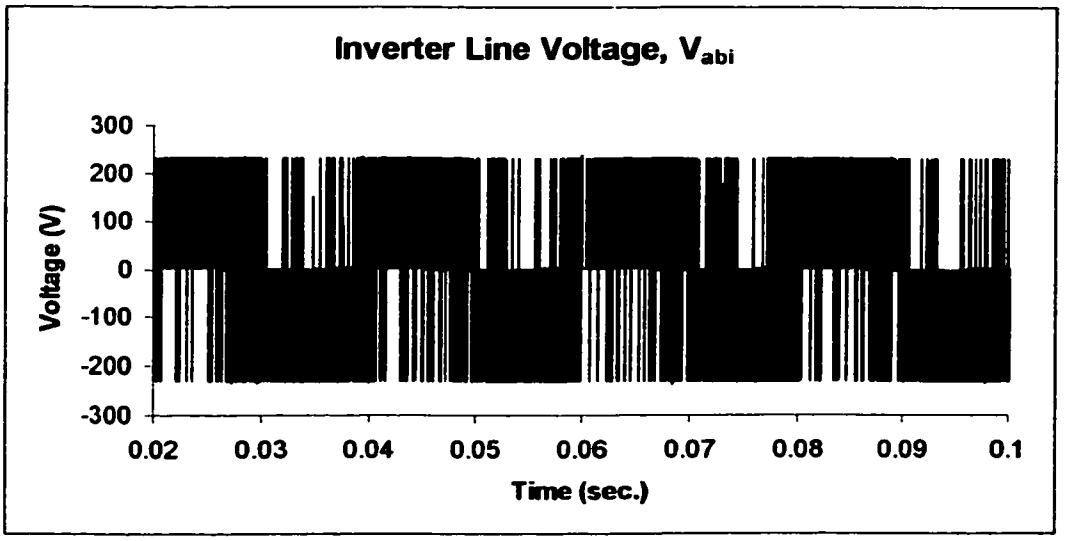
Inverter Line Voltage, V_{abi}
300
200
100
0
-100
-200
-300
Voltage (V)
0.02
0.03
0.04
0.05
0.06
0.07
0.08
0.09
0.1
Time (sec.)

(c)

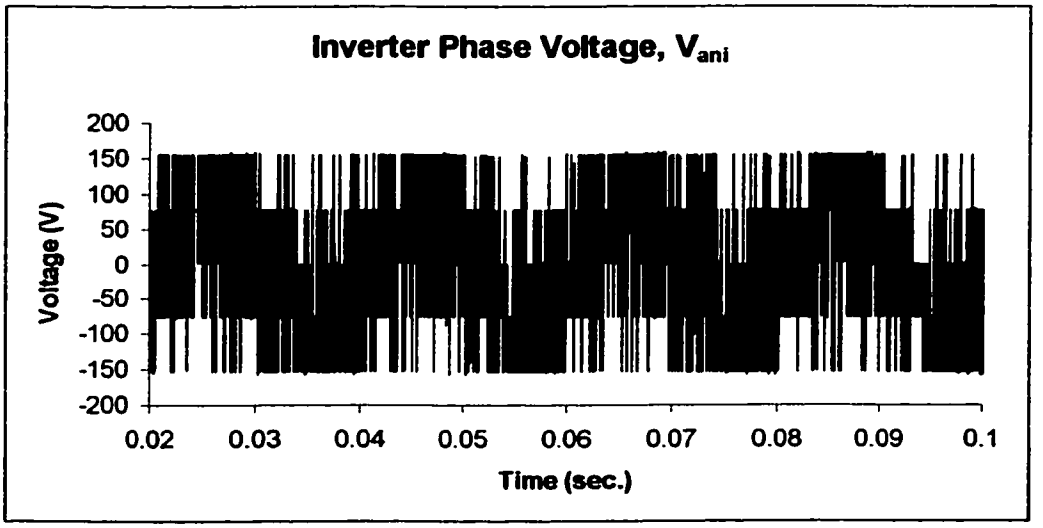
Inverter Phase Voltage, V_{ani}
200
150
100
50
0
-50
-100
-150
-200
Voltage (V)
0.02
0.03
0.04
0.05
0.06
0.07
0.08
0.09
0.1
Time (sec.)

(d)

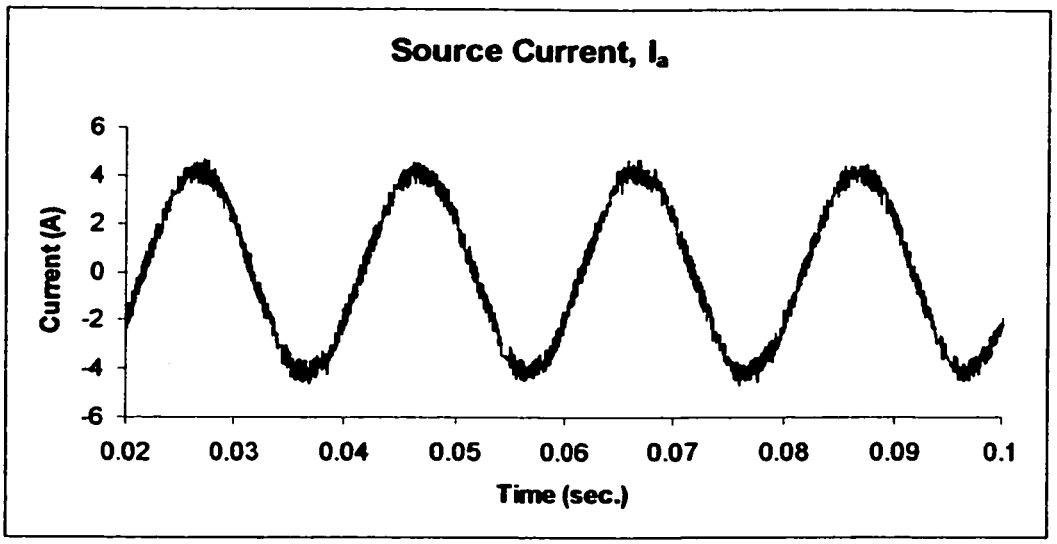
Source Current, I_a
Current (A)
6
4
2
0
-2
-4
-6
0.02
0.03
0.04
0.05
0.06
0.07
0.08
0.09
0.1
Time (sec.)

(e)

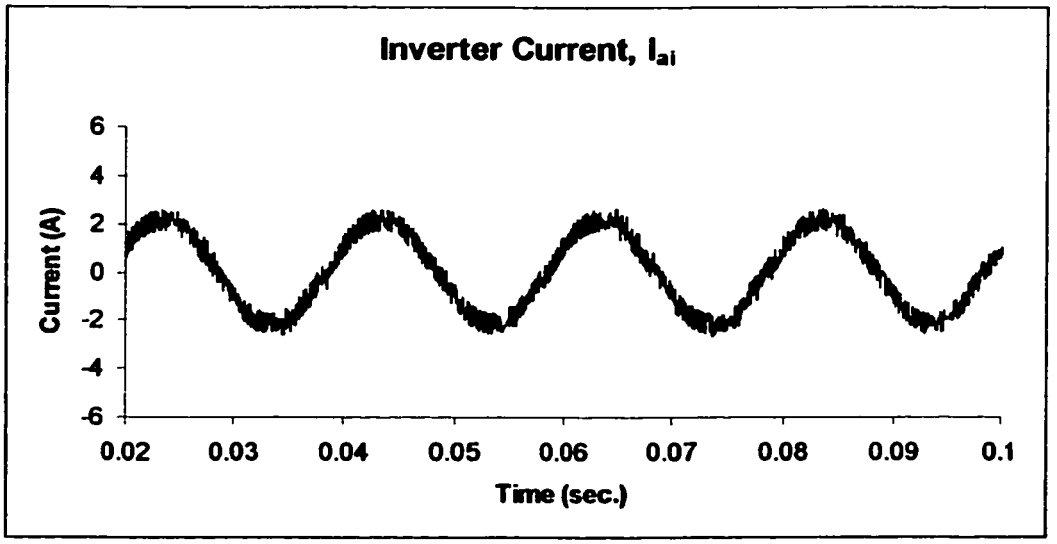
Inverter Current, I_{ai}
Current (A)
6
4
2
0
-2
-4
-6
0.02
0.03
0.04
0.05
0.06
0.07
0.08
0.09
0.1
Time (sec.)

(f)

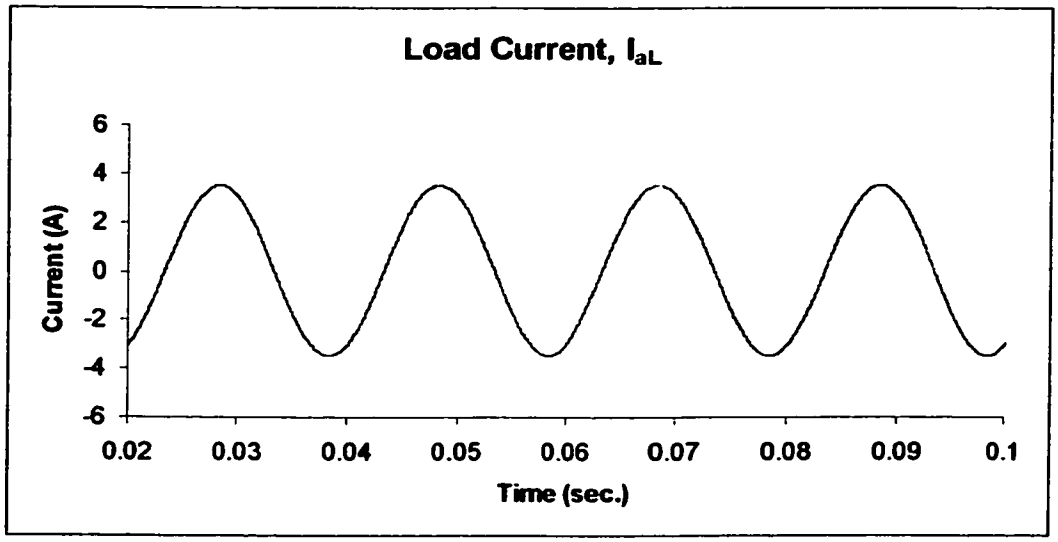
Load Current, I_{aL}
Current (A)
6
4
2
0
-2
-4
-6
0.02
0.03
0.04
0.05
0.06
0.07
0.08
0.09
0.1
Time (sec.)

(g)

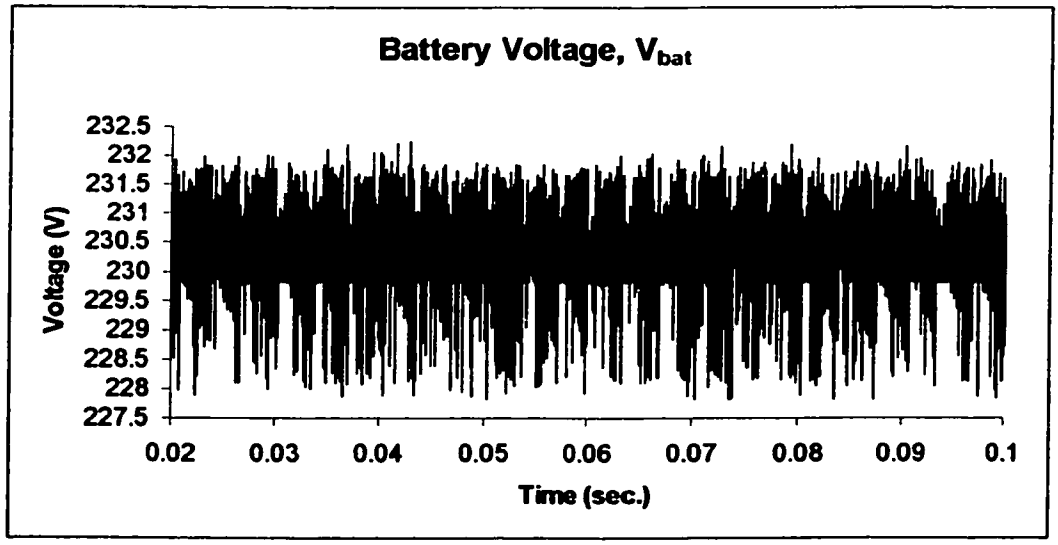
Battery Voltage, V_{bat}
Voltage (V)
232.5
232
231.5
231
230.5
230
229.5
229
228.5
228
227.5
0.02
0.03
0.04
0.05
0.06
0.07
0.08
0.09
0.1
Time (sec.)

(h)

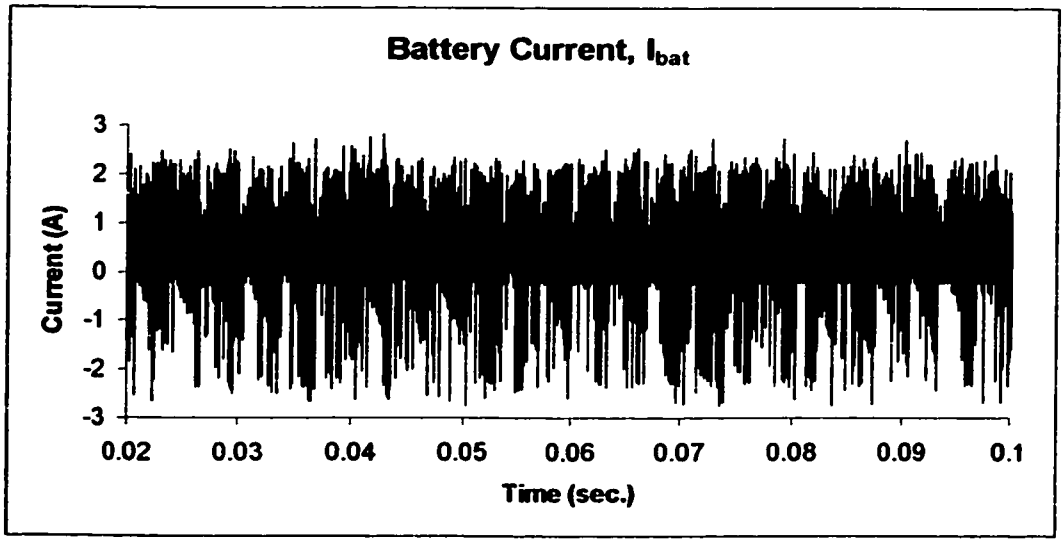

(i)

Figure 4.5 Simulation results (a) Line Voltage, V_{ab}; (b) Phase Voltage, V_{an}; (c) Inverter Line Voltage, V_{abi}; (d) Inverter Phase Voltage, V_{ani}; (e) Source Current, I_a; (f) Inverter Current, I_{ai}; (g) Load Current, I_{aL}; (h) Battery Voltage, V_{bat}; (i) Battery Current, I_{bat}.

4.2 Experimental Results

Having confirmed that the three-phase BESS and its control system are operating properly through simulation, the actual three-phase BESS is then implemented in the laboratory. To compare the simulation and laboratory results, the same three-phase experiment as described in Section 4.1.1.3 is initially carried out. The corresponding experimental results to those given in Figures 4.5(a)-(i) are shown in Figures 4.6(a)-(i).

Comparing Figures 4.5(a)-(b) with Figures 4.6(a)-(b), very similar results are shown. Both the line voltages and the phase voltages measured at the point of common coupling show high frequency components but no low harmonics are present. More spikes can be seen in the experimental results, but this is expected. Both voltages comprise fundamental frequency and high order harmonics, which can be filtered easily by the line inductance and system transformers. In Figures 4.6(c)-(d), the experimental waveforms have higher switching ripples compared with those in Figures 4.5(c)-(d), due to the inductances and capacitances in the system not modeled in the simulation. In Figure 4.6(e), the source current is controlled at the desired value, which is very close to that shown in Figure 4.5(e). With nearly the same load, both the inverter currents as shown in Figures 4.5(f) and 4.6(f) are almost the same, and the difference can be attributed to the slightly lower load current in the actual implementation. In Figures 4.6(h)-(i), the battery voltage and current are shown. As compared with that in Figures 4.5(h)-(i), the battery current has larger ripple than that in Figure 4.6(i), since the battery model assumes that there is no line inductance between the battery and the inverter.

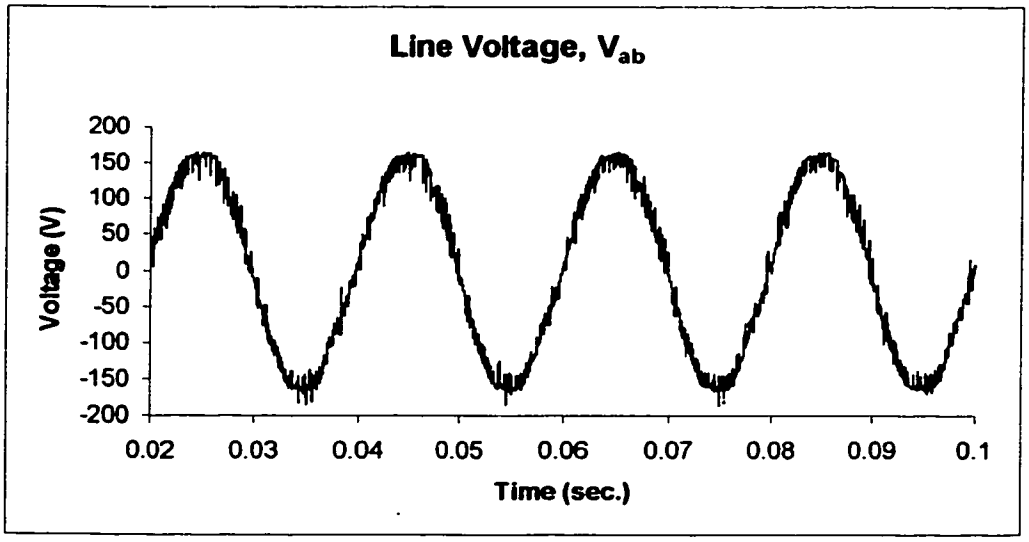
Line Voltage, V_{ab}
Voltage (V)
200
150
100
50
0
-50
-100
-150
-200
0.02
0.03
0.04
0.05
0.06
0.07
0.08
0.09
0.1
Time (sec.)

(a)

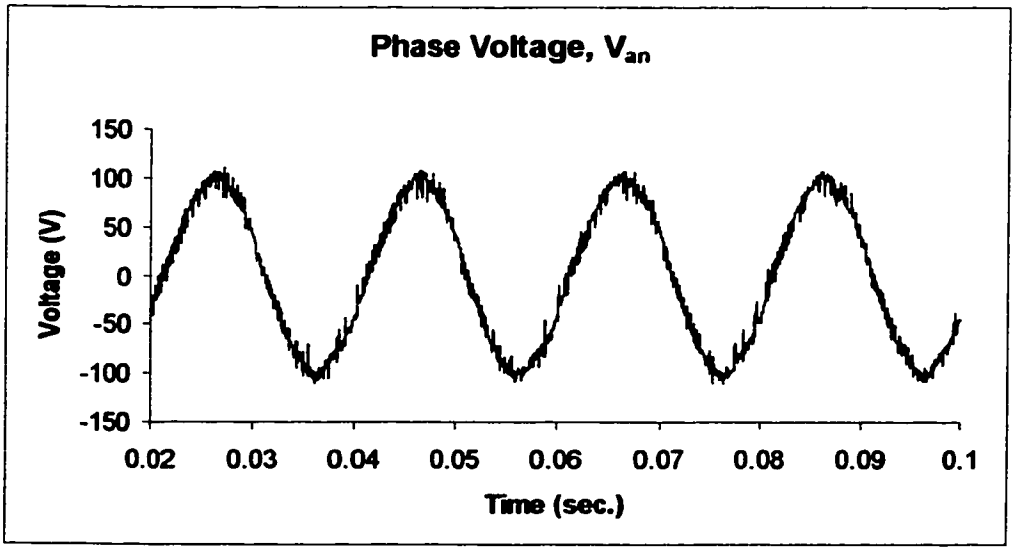
Phase Voltage, V_{an}
Voltage (V)
150
100
50
0
-50
-100
-150
0.02
0.03
0.04
0.05
0.06
0.07
0.08
0.09
0.1
Time (sec.)

(b)

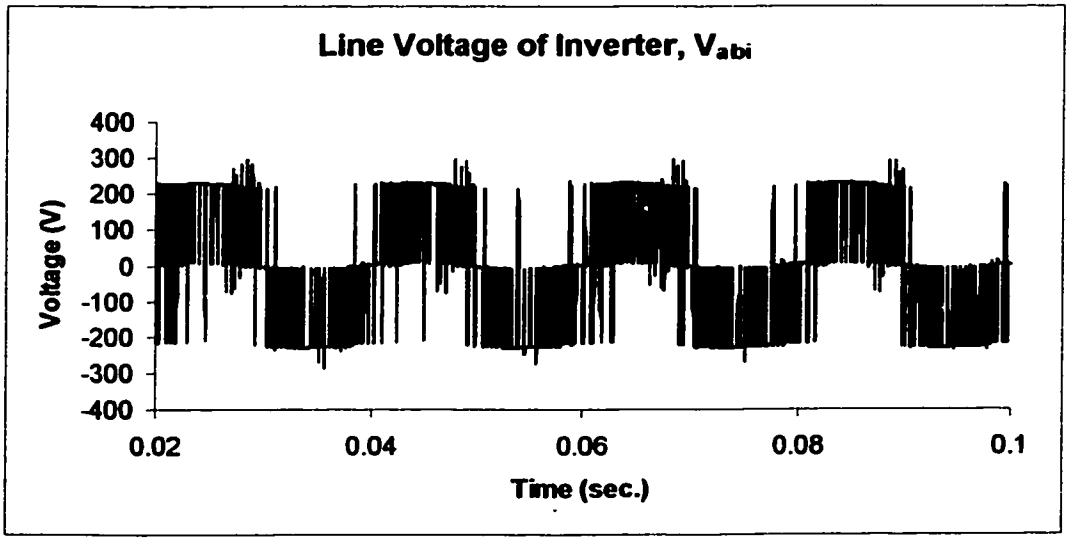
Line Voltage of Inverter, V_{abi}
Voltage (V)
400
300
200
100
0
-100
-200
-300
-400
0.02
0.04
0.06
0.08
0.1
Time (sec.)

(c)

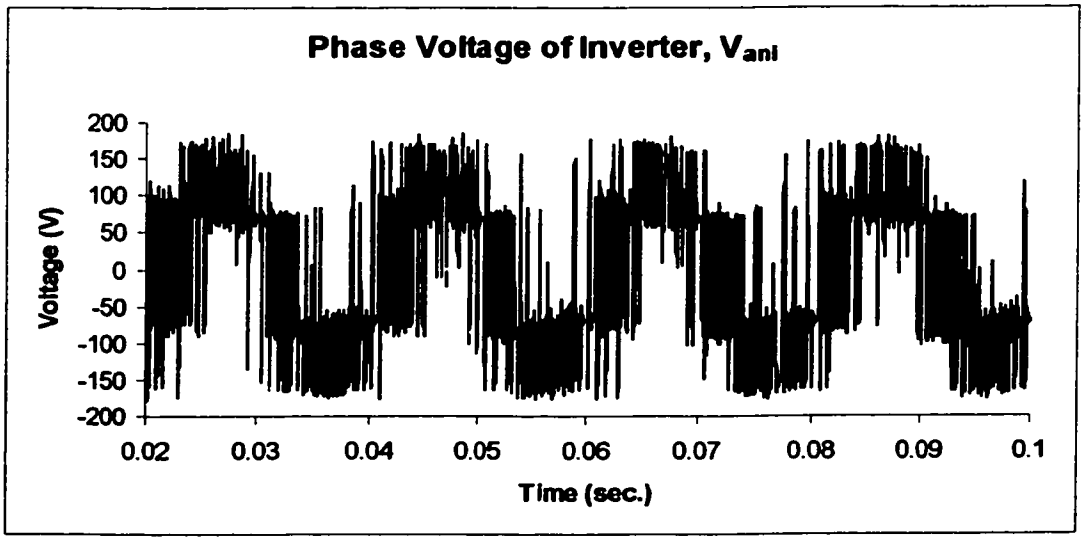
Phase Voltage of Inverter, V_{anI}
Voltage (V)
200
150
100
50
0
-50
-100
-150
-200
0.02
0.03
0.04
0.05
0.06
0.07
0.08
0.09
0.1
Time (sec.)

(d)

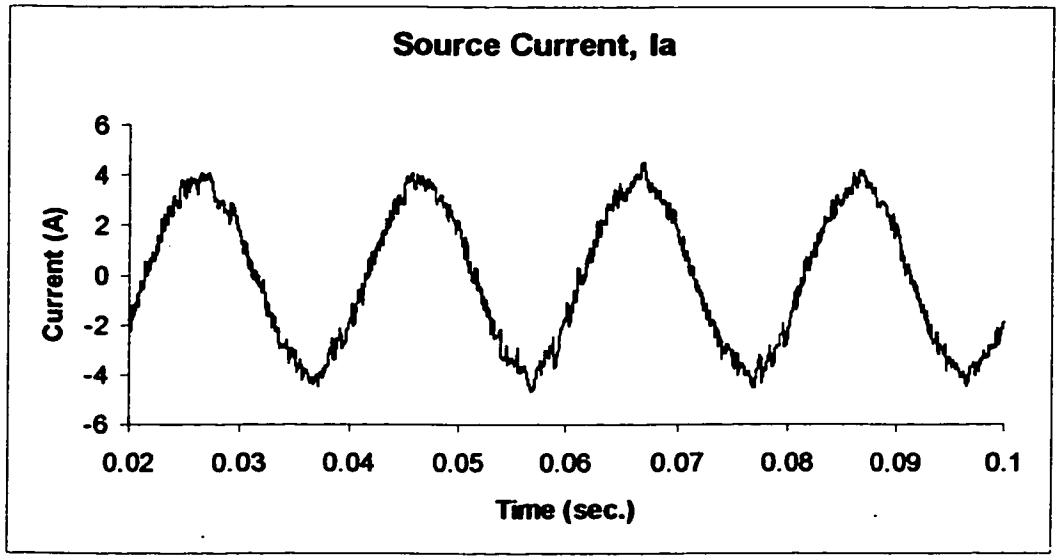
Source Current, Ia
Current (A)
6
4
2
0
-2
-4
-6
0.02
0.03
0.04
0.05
0.06
0.07
0.08
0.09
0.1
Time (sec.)

(e)

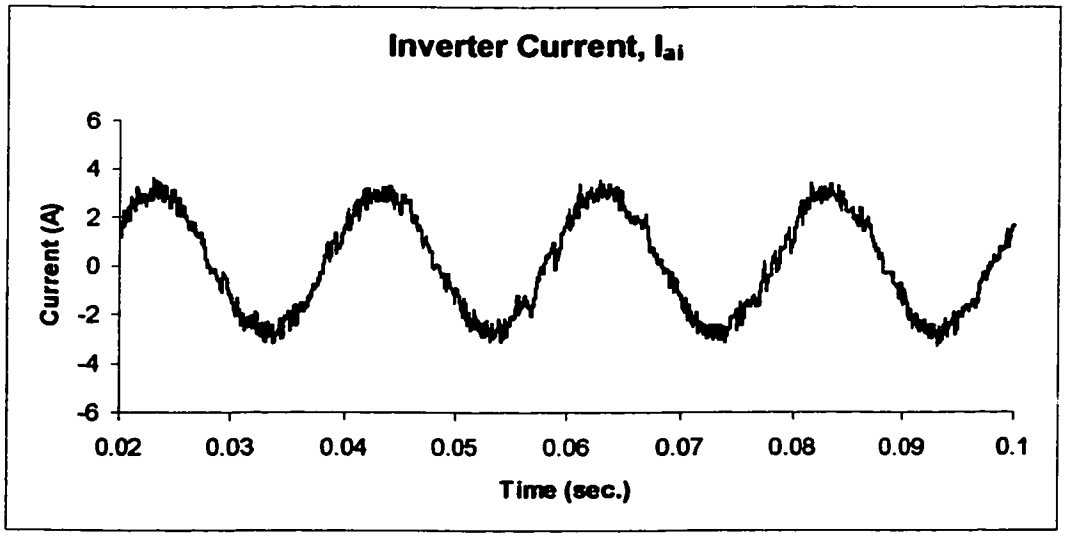
Inverter Current, Iai
Current (A)
6
4
2
0
-2
-4
-6
0.02
0.03
0.04
0.05
0.06
0.07
0.08
0.09
0.1
Time (sec.)

(f)

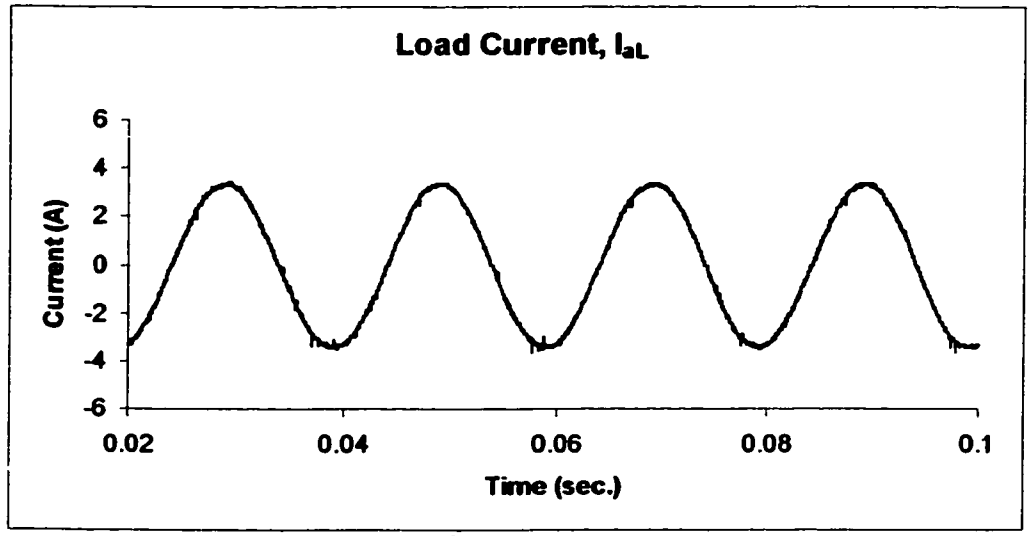
Load Current, I_{aL}
Current (A)
6
4
2
0
-2
-4
-6
0.02
0.04
0.06
0.08
0.1
Time (sec.)

(g)

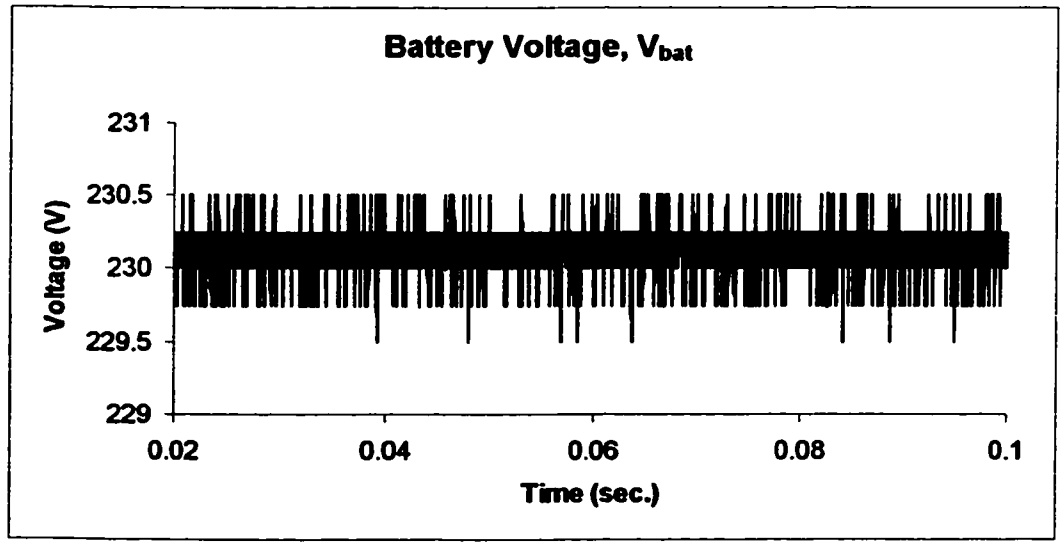
Battery Voltage, V_{bat}
Voltage (V)
231
230.5
230
229.5
229
0.02
0.04
0.06
0.08
0.1
Time (sec.)

(h)

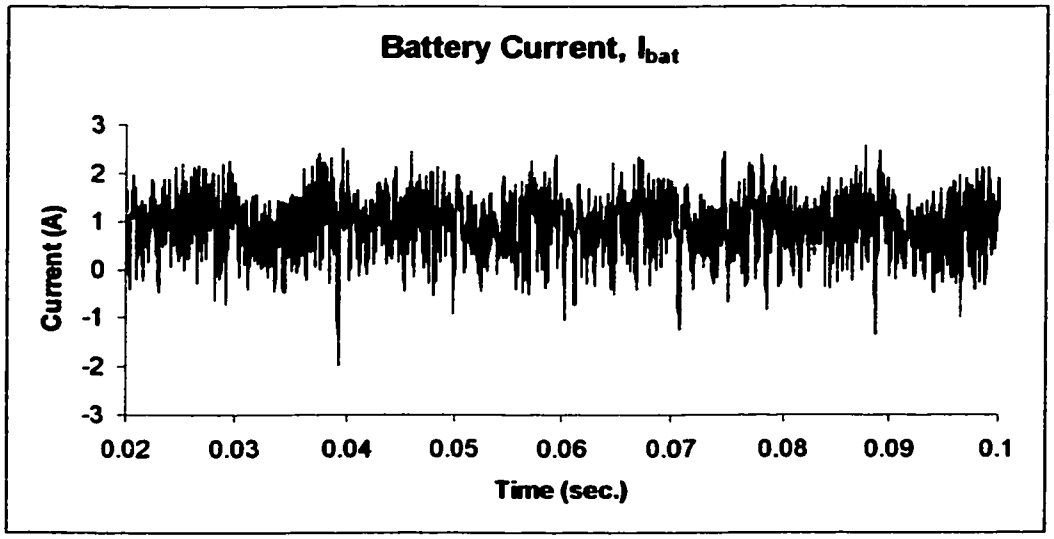

(i)

Figure 4.6 Experimental results (a) Line Voltage, V_{ab}; (b) Phase Voltage, V_{an}; (c) Inverter Line Voltage, V_{abi}; (d) Inverter Phase Voltage, V_{ani}; (e) Source Current, I_a; (f) Inverter Current, I_{ai}; (g) Load Current, I_{aL}; (h) Battery Voltage, V_{bat}; (i) Battery Current, I_{bat}.

4.2.1 BESS for Power Quality Control

In this section, several demonstrations on the use of BESS for power quality control are being studied. They include the use of BESS for (i) providing a balanced three-phase source currents even with unbalanced load currents, (ii) providing power factor correction, and (iii) active filtering.

4.2.1.1 Three-phase unbalanced current

Figure 4.7 shows the operation with unbalanced load currents in a three-phase system with current magnitude, I_b, less than the other two phases current I_a and I_c. This

operation is difficult to control because the loading is usually different in each phase, particularly in a high rise building where the three-phase supply is distributed to single phase circuits throughout the building. If a BESS is installed, the three-phase supply current can be controlled to be balanced irrespective of the unbalanced load. The BESS can control each source current individually as shown in Figure 4.7. Prior to the energisation of the BESS, the currents in three-phases are unequal but when the BESS is operated, the three currents can be made balanced almost instantly. Furthermore, the magnitudes and the phases can be controlled as required.

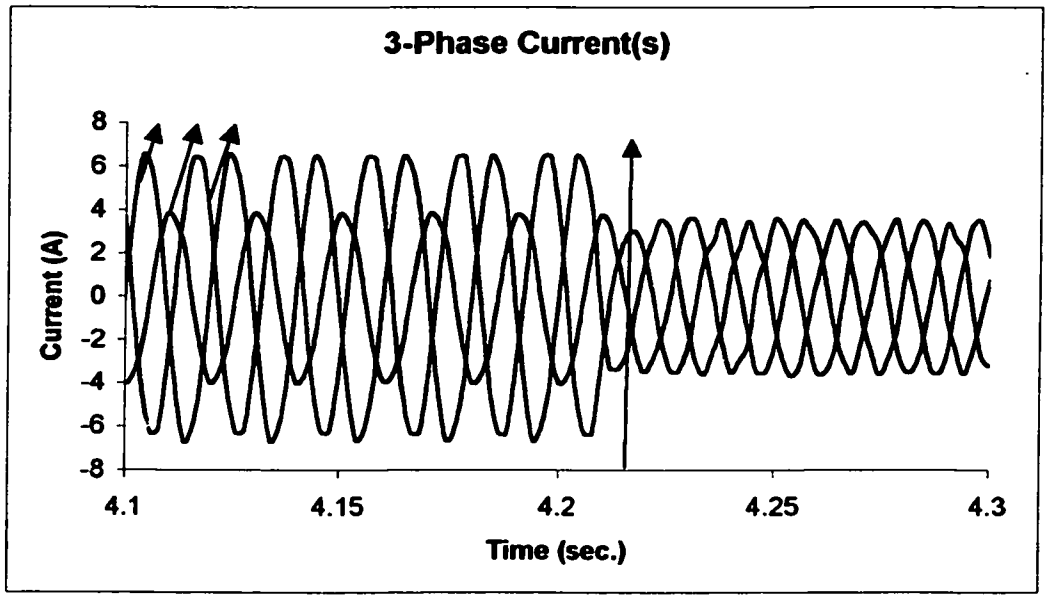

Figure 4.7 BESS for Three-phase balancing

4.2.1.2 Power factor correction

Figure 4.8 shows a single line diagram of the three-phase system, with a lagging load and a BESS is connected to the ac supply. Figure 4.9(a) shows the source current, I_s, is sinusoidal and in-phase with the phase voltage and hence the utility supplies the real

power only, with the BESS supplying the reactive power required by the load. Figure 4.9(b) shows that the load current, I_{aL}, is not affected by the BESS and is maintained to be lagging to the phase voltage by 45°. To achieve this, Figure 4.9(c) shows that the current in the BESS has to lead the phase voltage by 90°, i.e the BESS is operating in the capacitive mode.

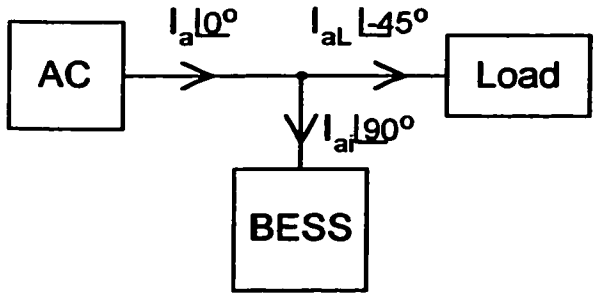

Figure 4.8 Single line diagram of the BESS system

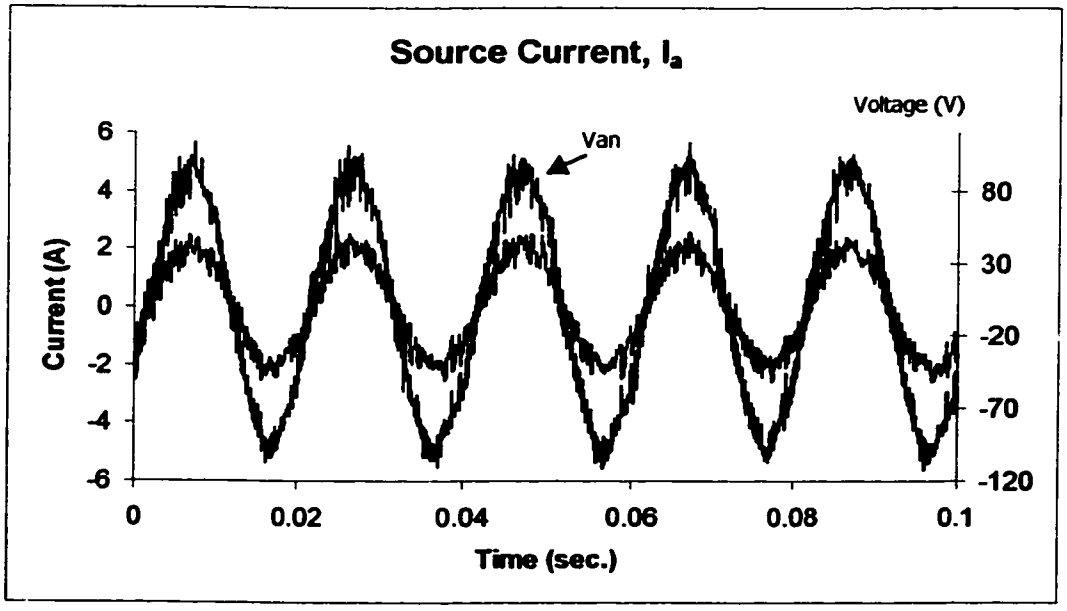

(a)

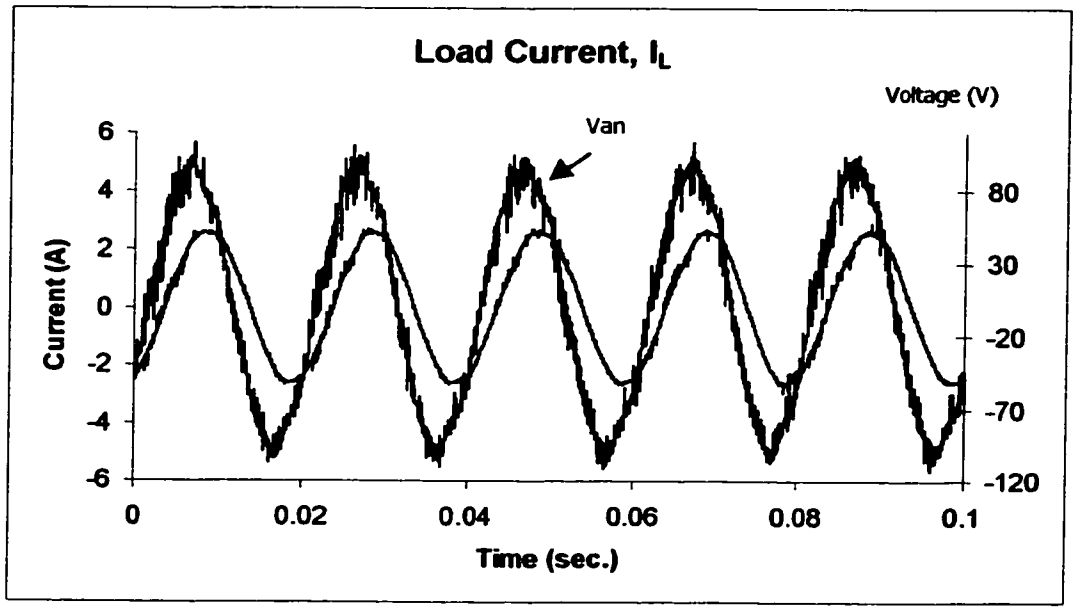

(b)

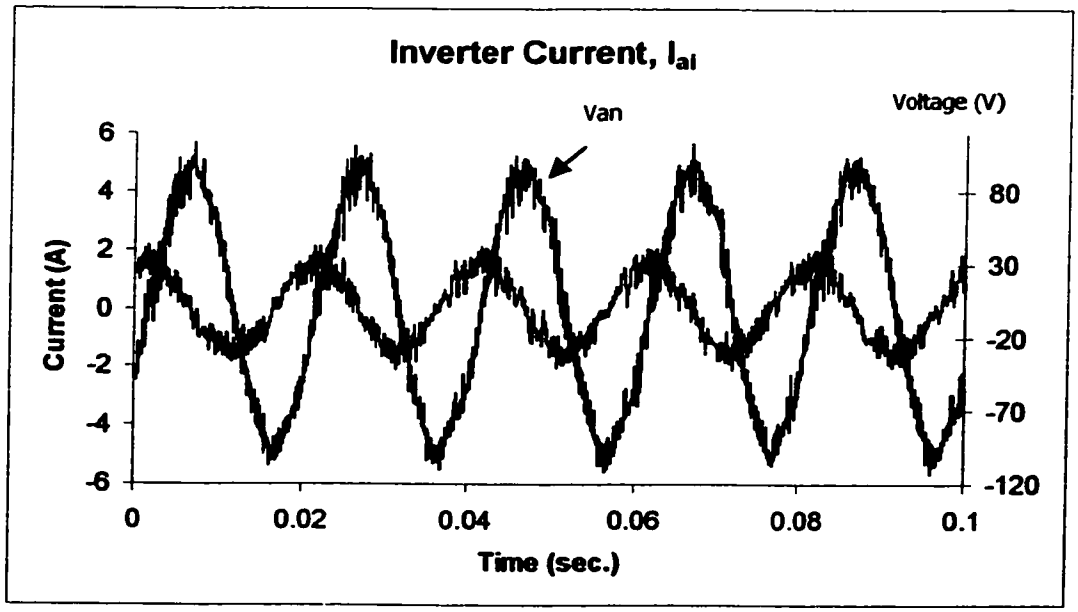

(c)

Figure 4.9 BESS for Power Factor Correction

4.2.1.3 Active filtering

Figure 4.10 shows a typical three-phase rectifier load, with the diodes making the input waveform non-linear. Such load contains significant low-order harmonic content that is large enough to distort the line voltage waveform.

Figure 4.11 shows the experimental results of the harmonic current for distorted load as shown in Figure 4.10.

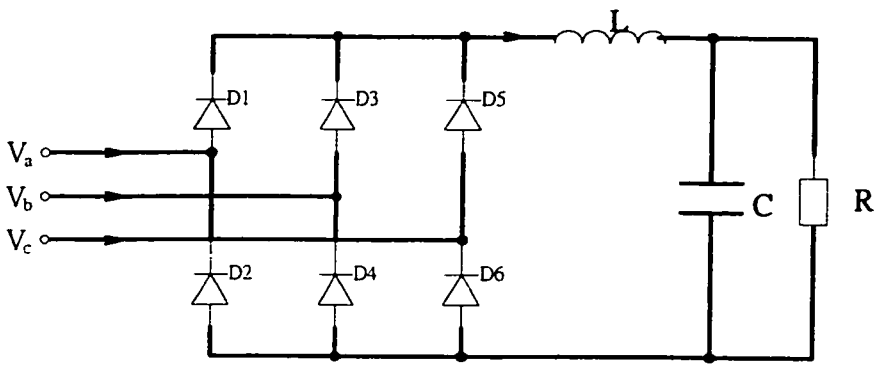

Figure 4.10 Distorted Load

Figures 4.11(a) and (c) show the line voltage, V_{ab}, and source current, I_a, when the load is connected to the ac grid without the BESS. The line voltage is slightly distorted at the zero crossing and the current is highly distorted. The frequency spectrum of the line current without the BESS, as shown in Figure 4.11(d), shows that the low-order harmonic contents are significant, causing the distorted voltage waveform in Figure 4.11(b).

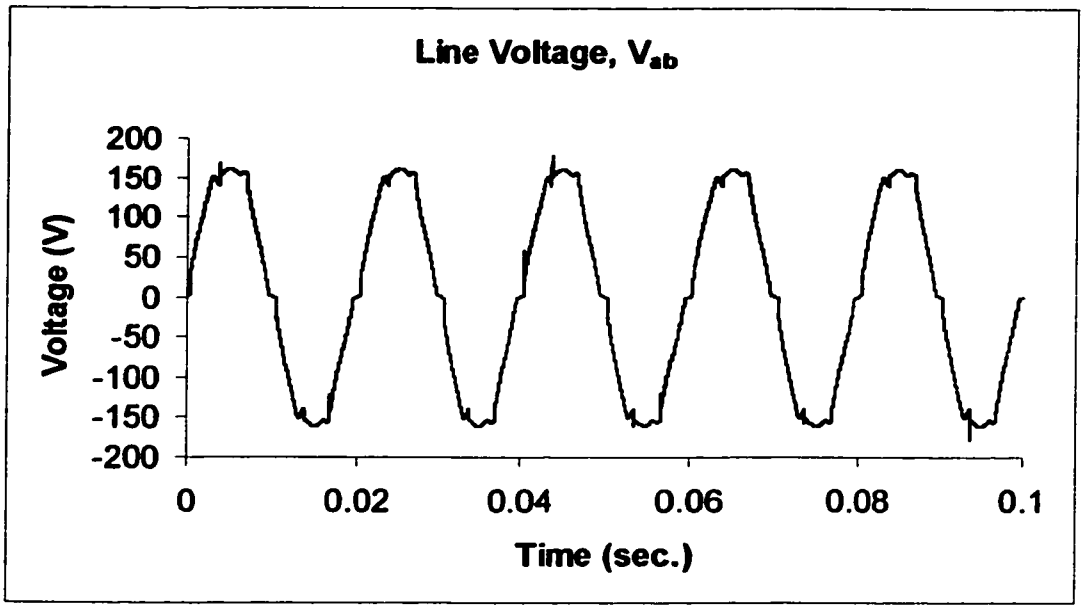
Line Voltage, V_{ab}
Voltage (V)
200
150
100
50
0
-50
-100
-150
-200
0
0.02
0.04
0.06
0.08
0.1
Time (sec.)

(a)

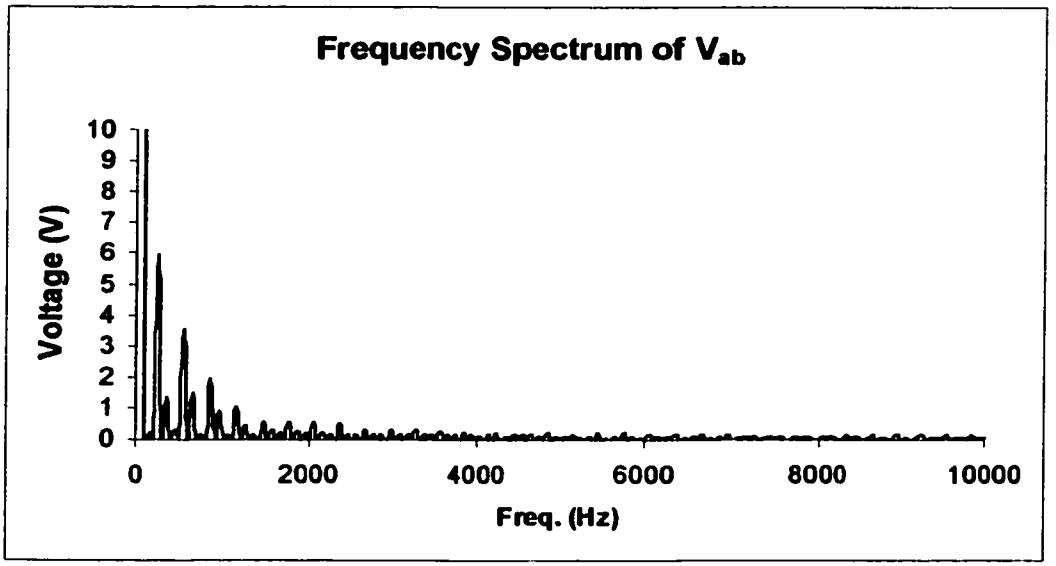
Frequency Spectrum of V_{ab}
Voltage (V)
10
9
8
7
6
5
4
3
2
1
0
0
2000
4000
6000
8000
10000
Freq. (Hz)

(b)

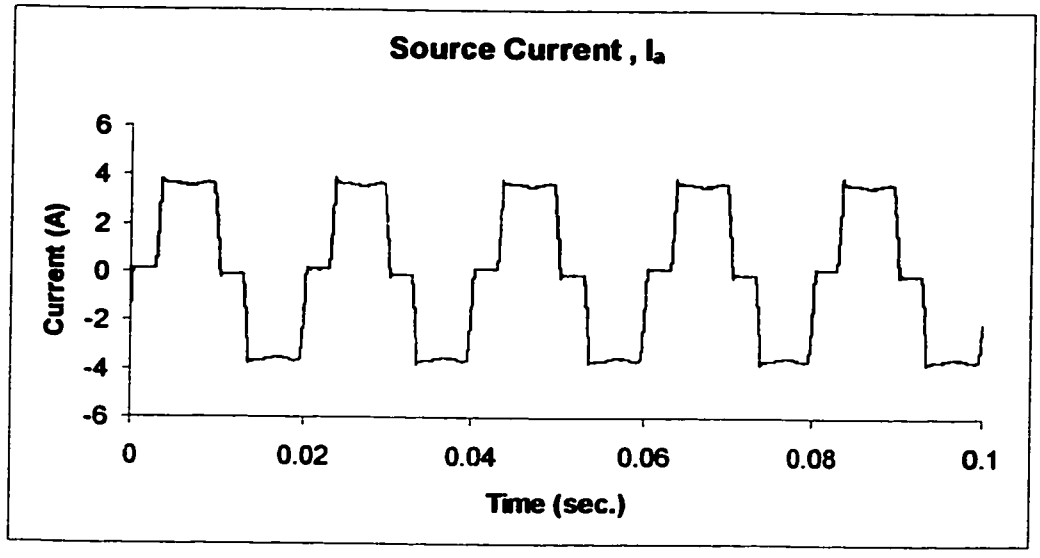

(c)

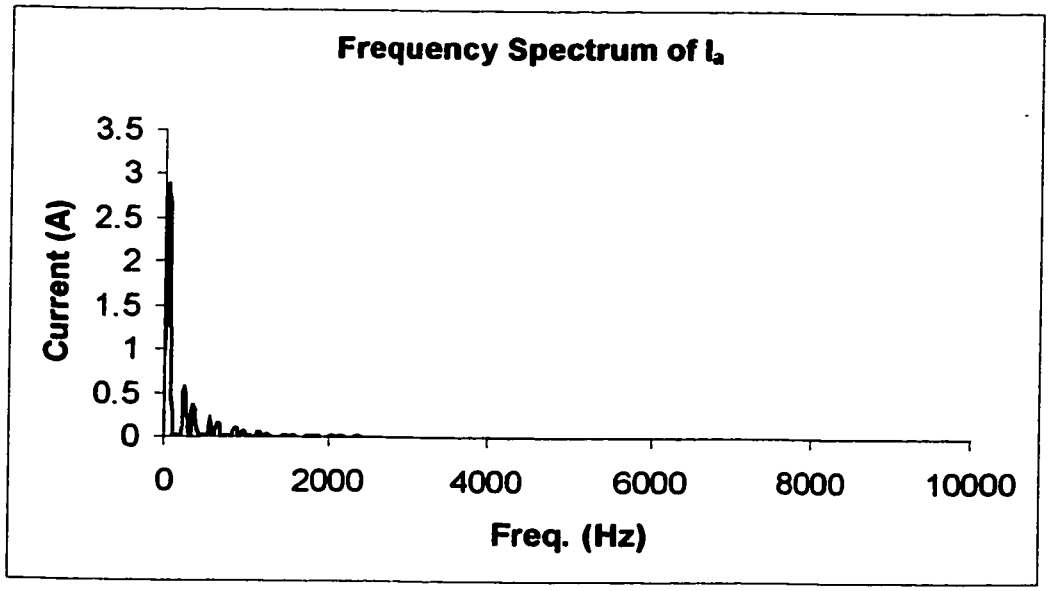

(d)

Figure 4.11 Waveforms of Distorted Load_1 (a) Line Voltage, V_{ab}; (b) Frequency Spectrum of V_{ab}; (c) Source Current, I_a; (d) Frequency Spectrum of I_a.

Once the BESS operates, the source current, I_s (in Figure 4.11(c)), can be controlled to have sinusoidal waveform although the load current remains distorted. The required low order harmonics are being supplied by the BESS. Figures 4.12(d) and (b) show that not only the frequency response of the source current is improved but also that of the line voltage.

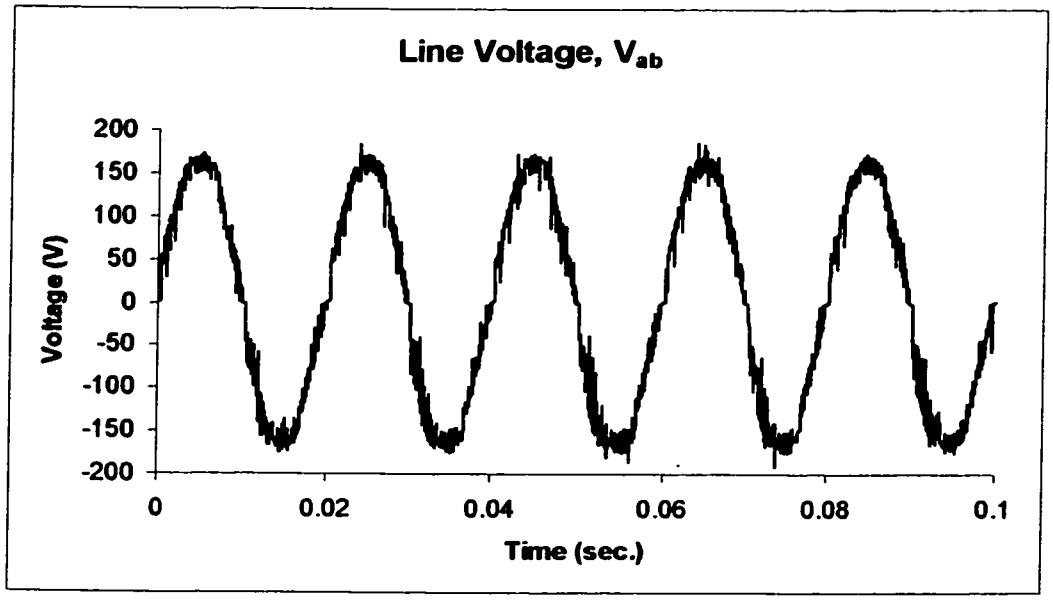

(a)

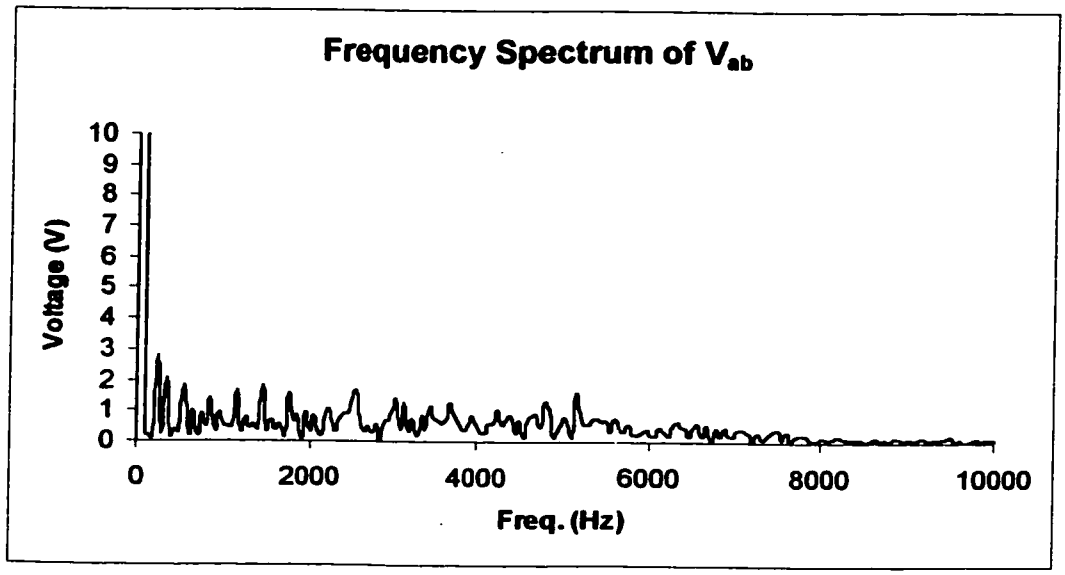
Frequency Spectrum of V_{ab}
Voltage (V)
10
9
8
7
6
5
4
3
2
1
0
0
2000
4000
6000
8000
10000
Freq. (Hz)

(b)

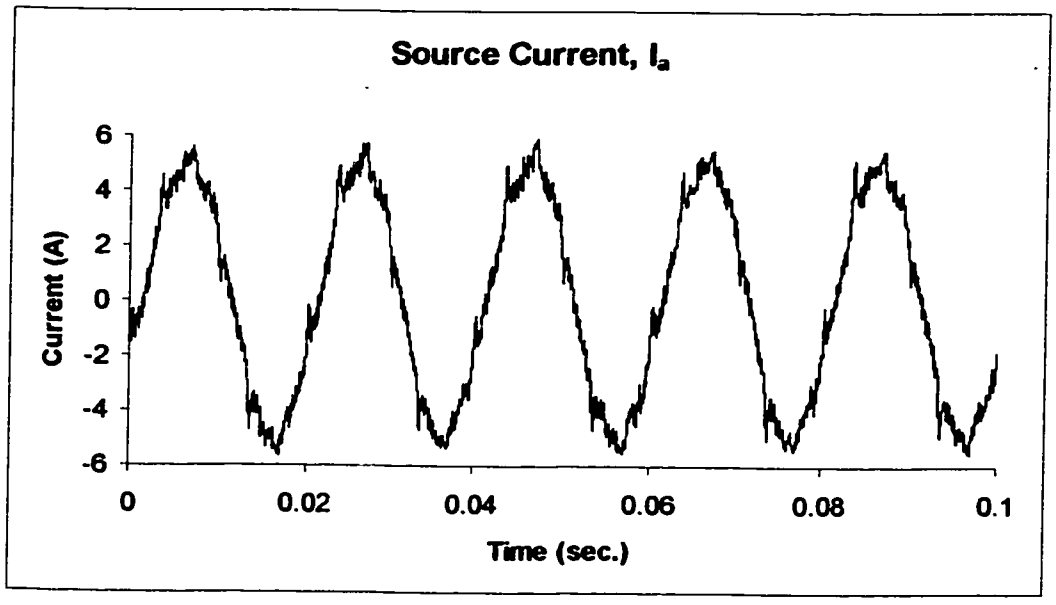
Source Current, I_a
Current (A)
6
4
2
0
-2
-4
-6
0
0.02
0.04
0.06
0.08
0.1
Time (sec.)

(c)

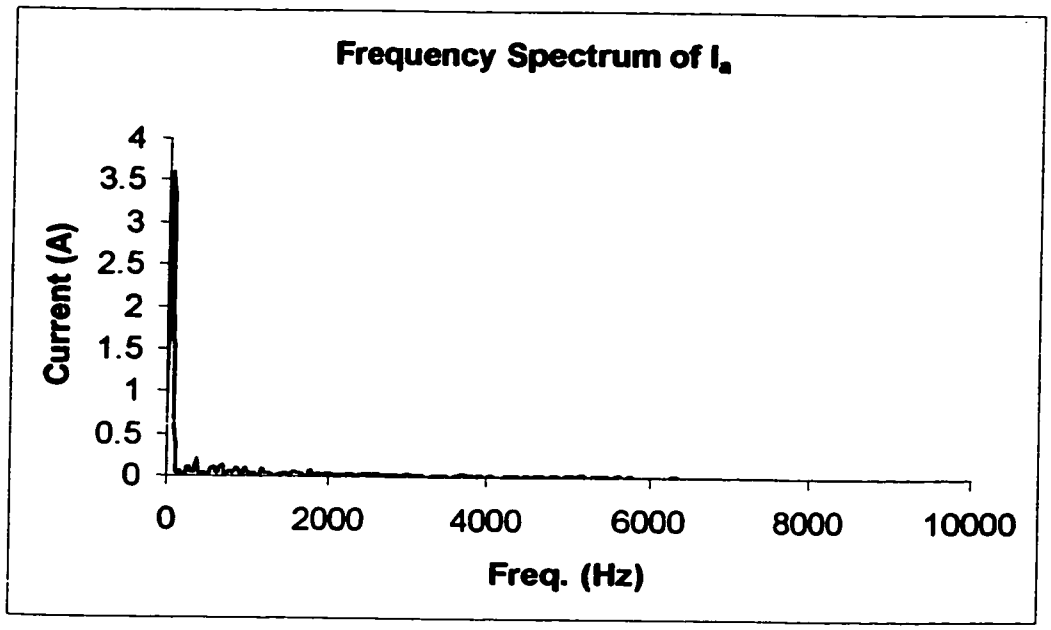

(d)

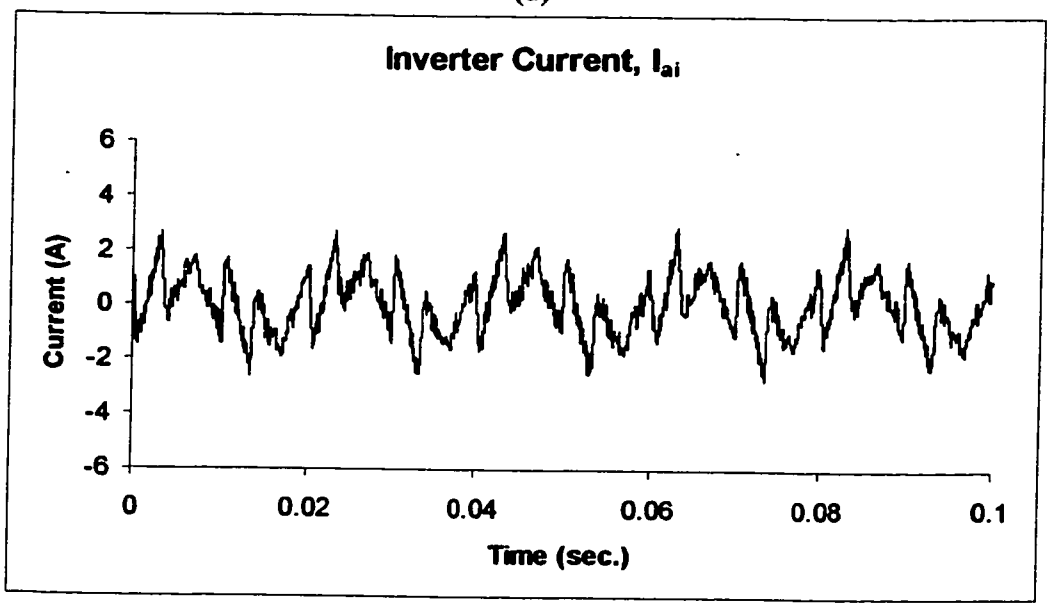

(e)

Figure 4.12 BESS for Active Filtering with Distorted Load_1 (a) Line Voltage, V_{ab}; (b) Frequency Spectrum of V_{ab}; (c) Source Current, I_a; (d) Frequency Spectrum of I_a; (e) Inverter Current, I_{ai}.

The capacity of the BESS energy is given by the time integration of the load curve at which the energy of the battery is being used during the peak shaving operation. It is important to ensure that for a forecasted load curve, a calculation is carried out of the expected amount of energy that can be charged at night, so that sufficient amount of energy can be provided to reduce the peak load to an expected level. The timing of the operation of the BESS has therefore to be planned ahead, otherwise there may not be enough energy to reduce the peak load at a later time. For example, Figure 4.13(a) shows that the BESS has been used extensively from 9 am to 1 pm to control the grid power, at 500W, and as a result it has no more energy to control the load after 1 pm. As a result, the maximum demand will now be 1100W as same as the load for the rest of the day. It would be better to start the operation of the BESS at 10am, as shown in Figure 4.13(b), say to control the maximum demand at 900W, and hence allowing it to have control throughout the day to ensure that the 900W maximum demand is not exceeded. So, good estimation of the battery state-of-charge (SOC) is very important for the daily BESS schedule (i.e. 24 hours).

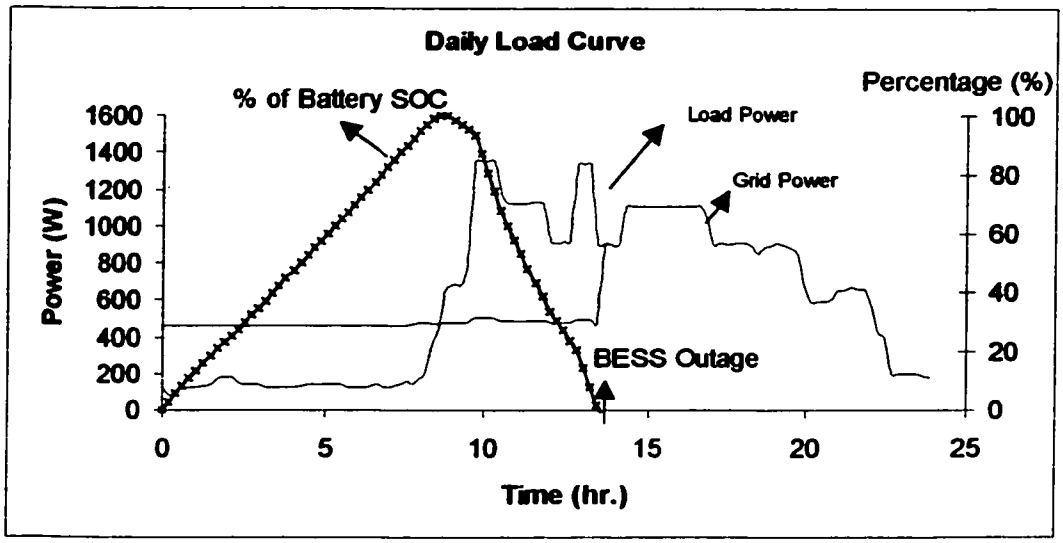

(a)

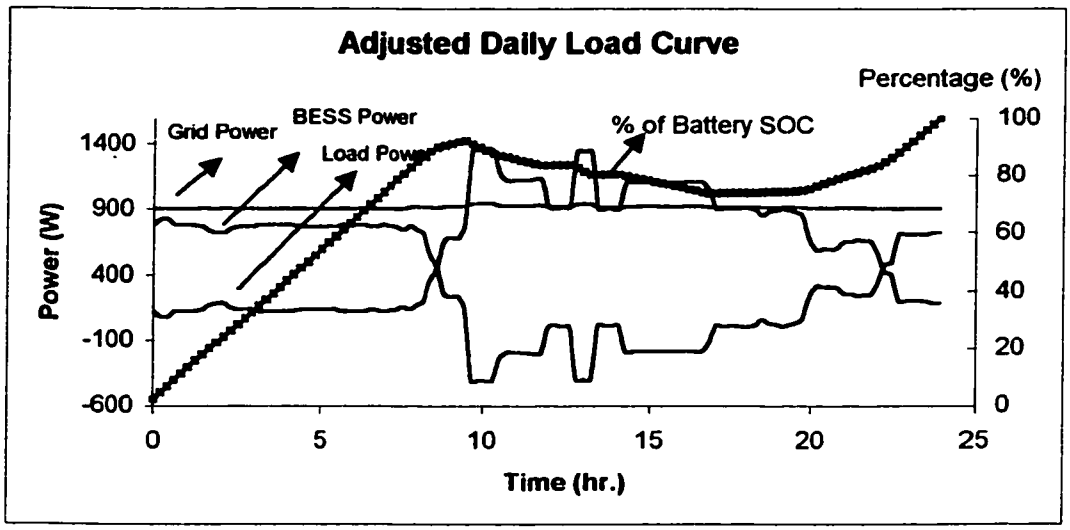

(b)

Figure 4.13 (a) Battery State-Of-Charge; (b) Adjusted Daily Load Curve

It is well known that the open circuit battery voltage, V_{soc}, can provide reliable information about the remaining energy stored in the battery. Figure 4.14 shows the

waveform of the open circuit battery voltage at constant current discharge conditions. Since the voltage for the fully charged battery bank and for the end of discharge is equal to 257.64 V (2.26 x 3 x 38) and 199.5 V respectively. According to these voltages, the state-of-charge of battery can be estimated as 100 % at V_{soc} = 257.64 V and 0 % at V_{soc} = 199.5 V. The calculated V_{soc} is monitored at all time to prevent the battery from over-charge or over-discharge consequently may damage the battery cells and may cause BESS outage.

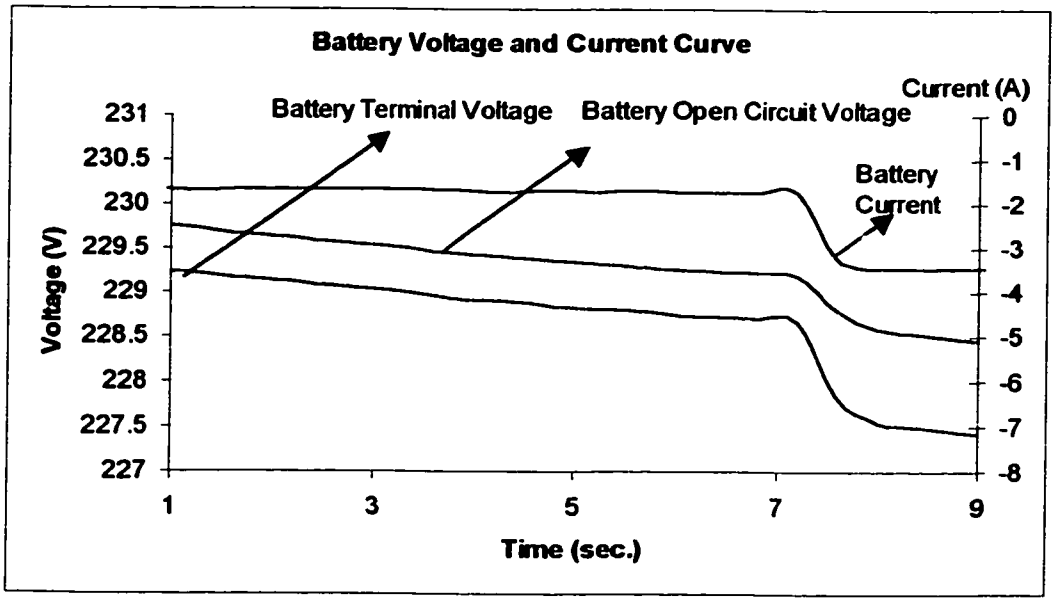

Figure 4.14 Battery open circuit voltage

Figure 4.15 shows a possible application of the BESS, where BESS absorbs power at night, and the energy is then released at day-time during heavy load condition. In this mode of operation, as far as the utility is concerned, the load is constant through the whole 24-hour period. In reality, the size of the BESS is quite small compared to the

load demand and therefore, the requirement is usually to reduce the maximum demand to a specified value and let the grid power varied at times when the load is below this value, and control is applied only when the load demand exceeds the specified value. The load factor can therefore be greatly improved. Depending on the shape of the load peaks and the tariff situation reasonable load reductions ranging from 5 % to 15 % of the peak load for peak periods shorter than 3 hours are possible.

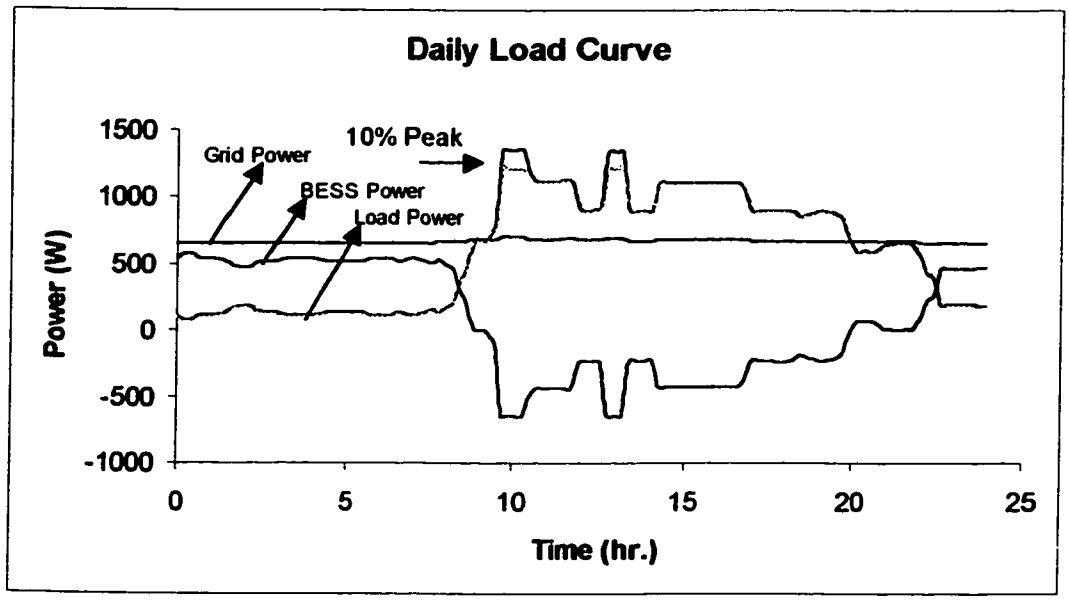

Figure 4.15 Daily Load Curve

4.2.3 System efficiency

An important consideration in planning for the application of the BESS is the losses associated with its operation.

Figure 4.16(a) shows an analysis of the BESS loss when it is operated with active power transfer only, i.e. when the inverter current is in-phase with the corresponding phase voltage. Based on this condition, Figure 4.16(a) shows the corresponding efficiency curve for the system. As shown in the figure, the efficiency is very low when the BESS is operating at low output, otherwise the efficiency is very good, between 75-95%. It is interesting to note that the efficiency is higher when it is generating power and lower when it is absorbing power.

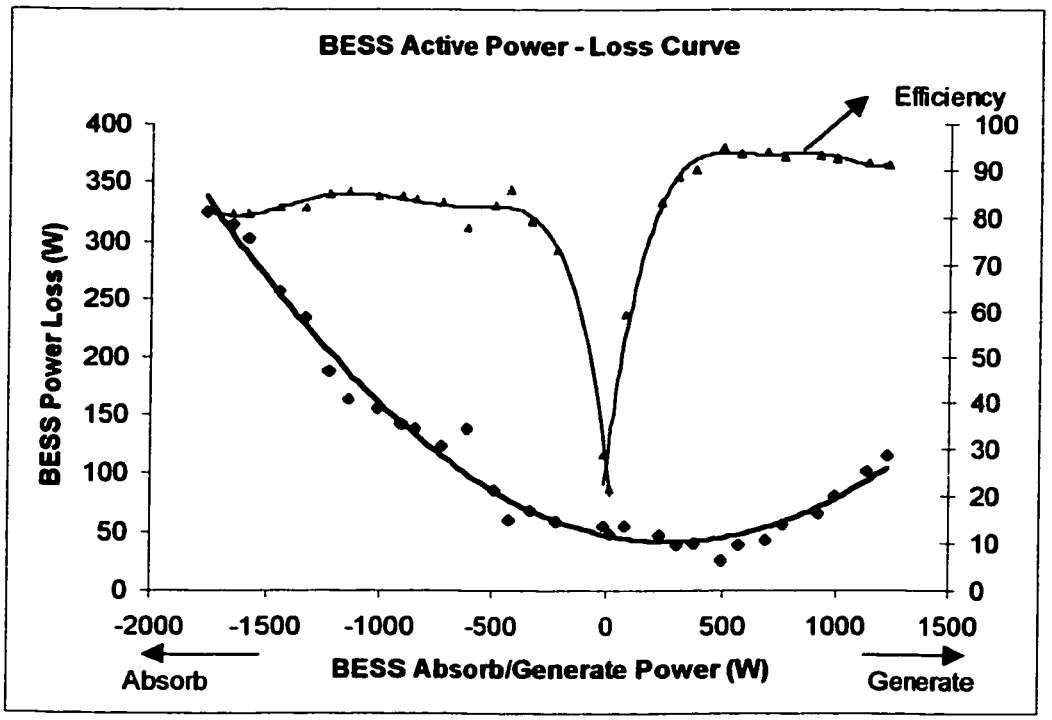

(a)

Figure 4.16(b) shows the result from the experimental study of BESS loss when it is operated with reactive power transfer only. When the BESS generates or absorbs reactive power to or from the system, there is power loss in the BESS because of the

current flowing through the inverter. In this case, efficiency has no real meaning, since the ac side does not consume real power (only reactive power). The loss is mainly due to I^2R losses and it is slightly lower than when real power is being delivered.

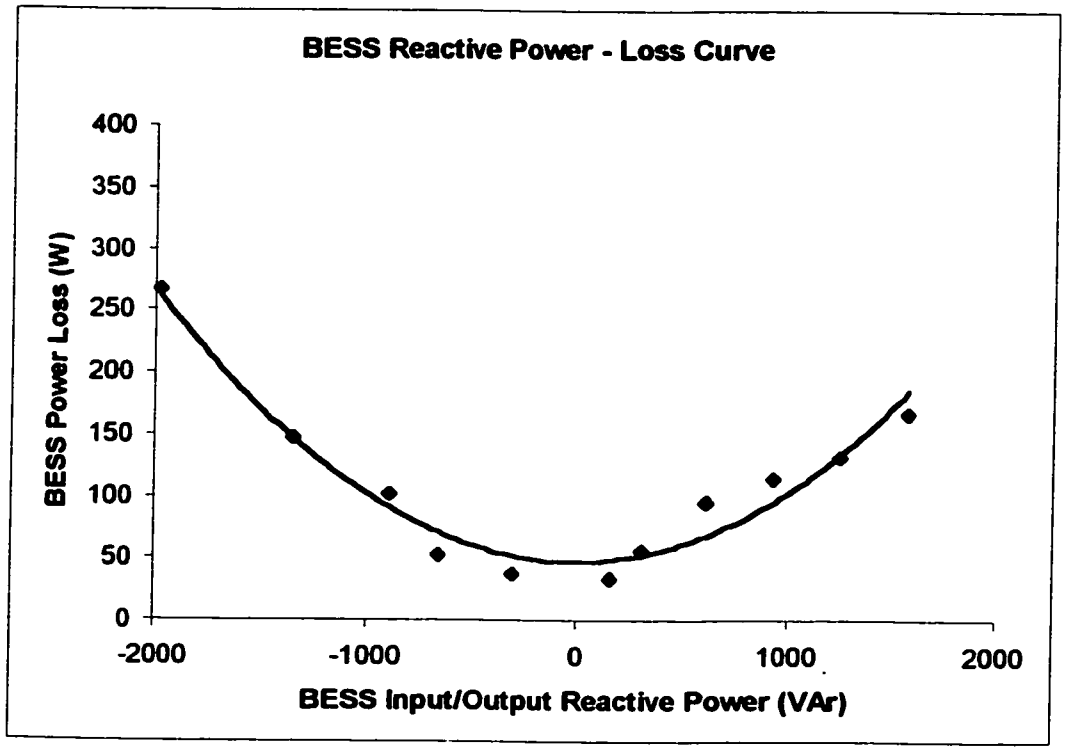

(b)

Figure 4.16 Efficiency of BESS for (a) Active Power Transfer; (b) Reactive Power Transfer.

4.2.4 BESS to Overcome Load Disturbance

4.2.4.1 Damping load fluctuation

Figures 4.17(a) and (b) show the effect of three-phase load fluctuation on the power system. As the load current magnitude varies, the supply current and hence the voltage

at the point of common coupling vary and this can cause voltage flicker to the neighboring load. When the BESS is connected to the power system, the BESS guarantees rock solid control of the supply current as shown in Figure 4.18(b). As the load fluctuates, the supply current remains constant and unaffected, ensuring that the voltage at the point of common coupling will not experience flickers due to the load fluctuation.

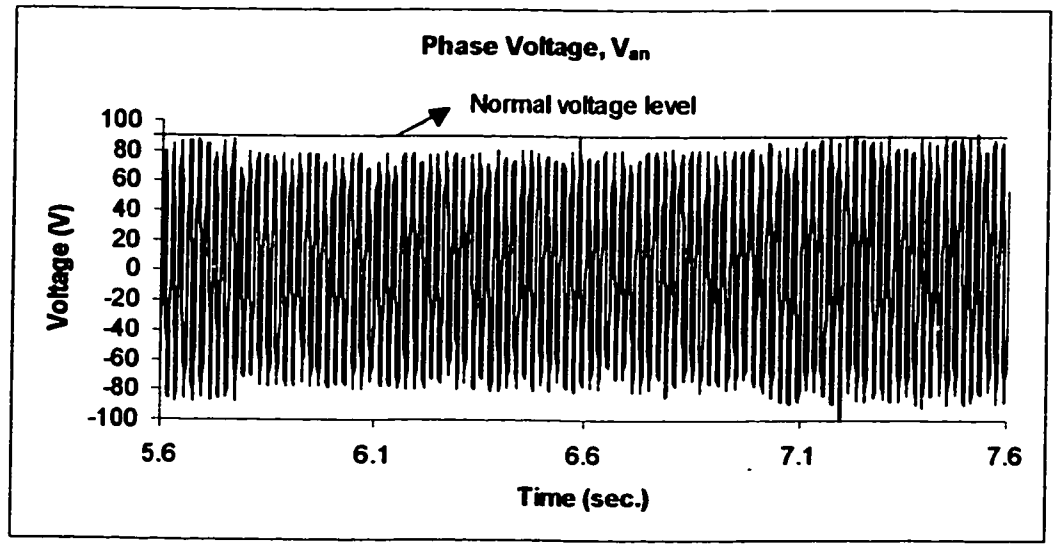

(a)

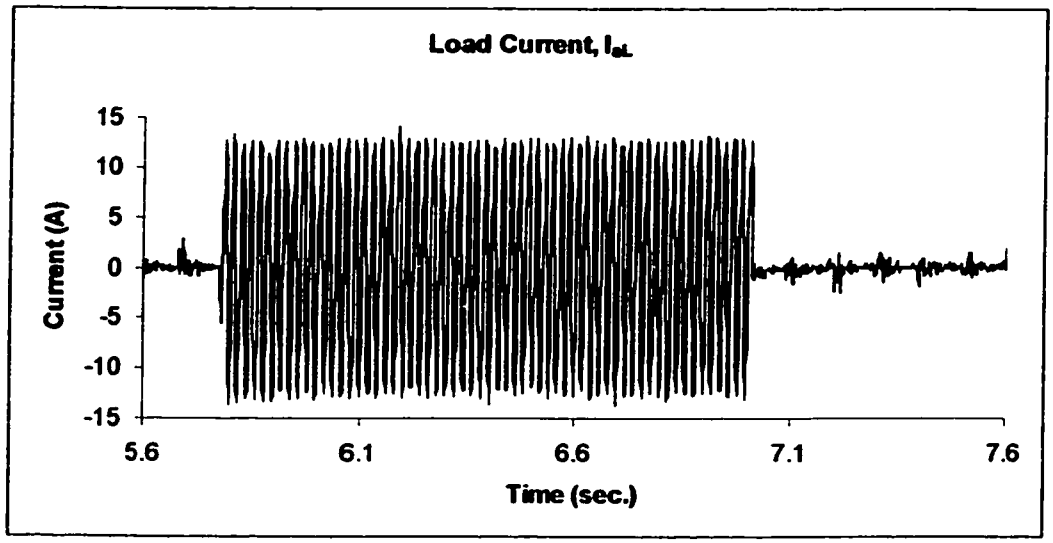

(b)

Figure 4.17 Voltage flicker due to load change (a) Phase voltage at point of common coupling; (b) Load current change.

Figure 4.18(a) shows the phase voltage, V_{an}, of the system captured in a 8-second period. Even with the significant load fluctuation, as shown in Figure 4.18(c), the source current (in Figure 4.18(b)) is still being controlled at a constant level. All the variation in the load current is compensated by the inverter current as shown in Figure 4.18(d).

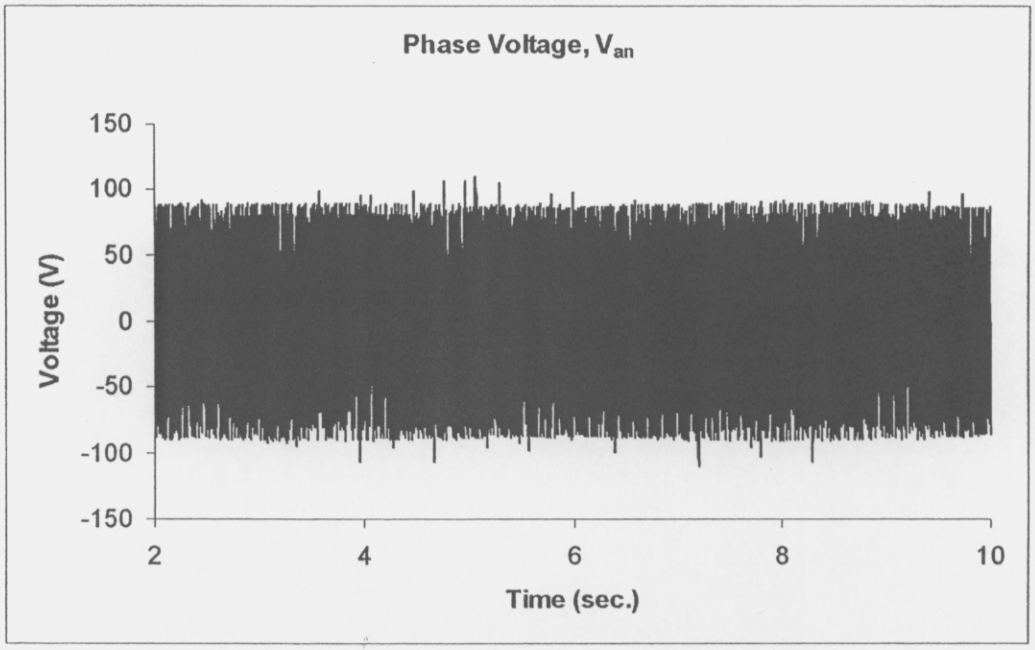
Phase Voltage, V_{an}
150
100
50
0
-50
-100
-150
Voltage (V)
2
4
6
8
10
Time (sec.)

(a)

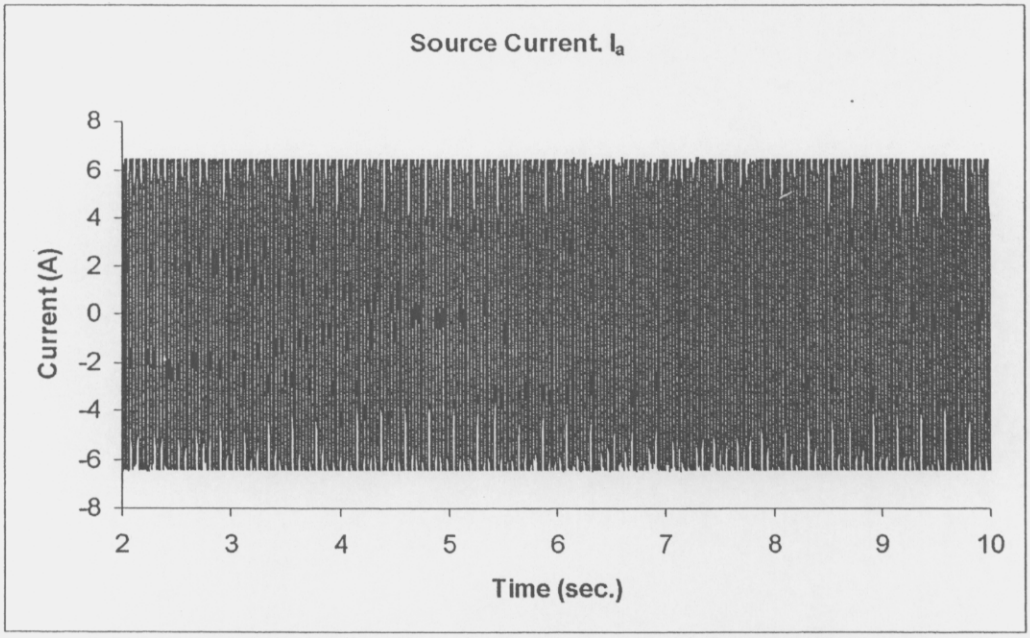
Source Current. I_a
8
6
4
2
0
-2
-4
-6
-8
Current (A)
2
3
4
5
6
7
8
9
10
Time (sec.)

(b)

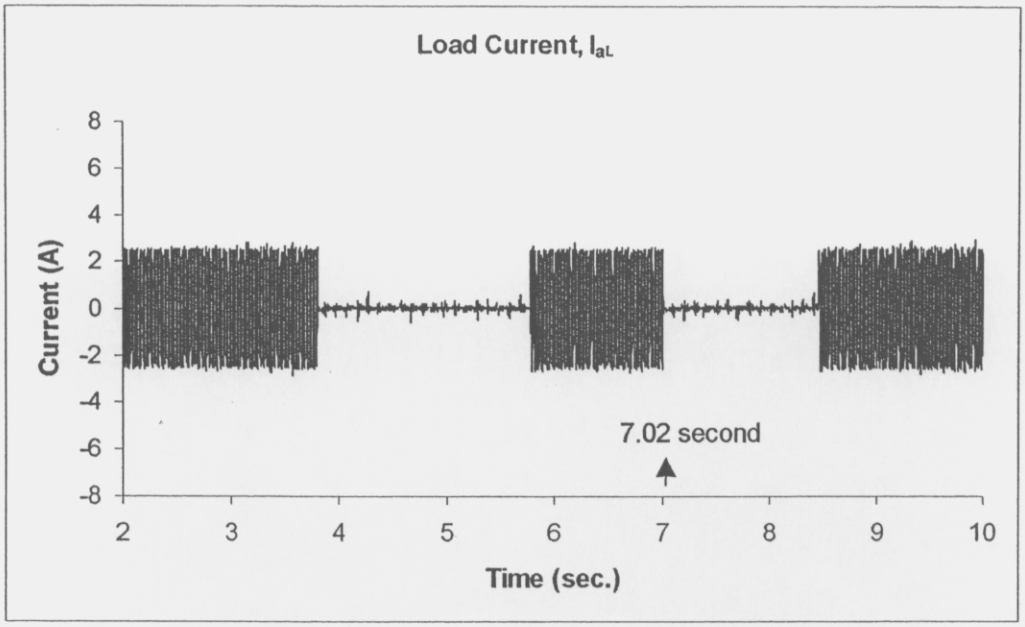

(c)

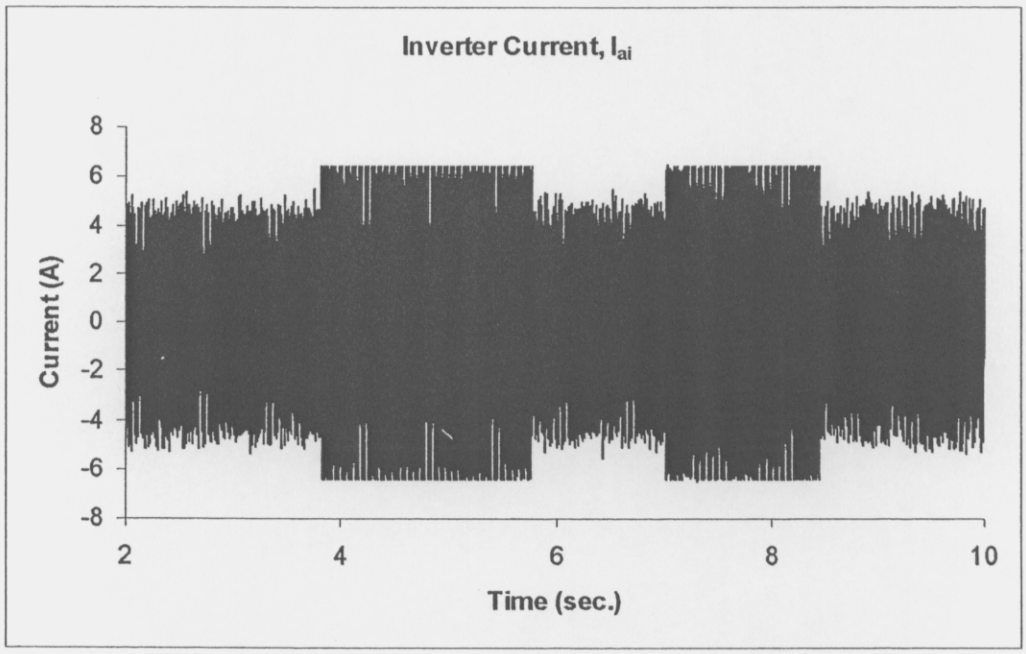

(d)

Figure 4.18 BESS for Damping Load Fluctuation (a) Phase Voltage, V_{an}; (b) Source Current, I_a; (c) Load Current, I_{aL}; (d) Inverter Current, I_{ai}.

Figures 4.19(a) to (d) show the close-up of Figures 4.18(a)-(d) at around seven-second, Figure 4.19(c) shows clearly that the load current drops at time 7.02 second, and the inverter current, as shown in Figure 4.19(d), increases almost instantaneously to maintain the source current (Figure 4.18(b)) constant. In this way, the voltage at the point of common coupling can also be maintained constant.

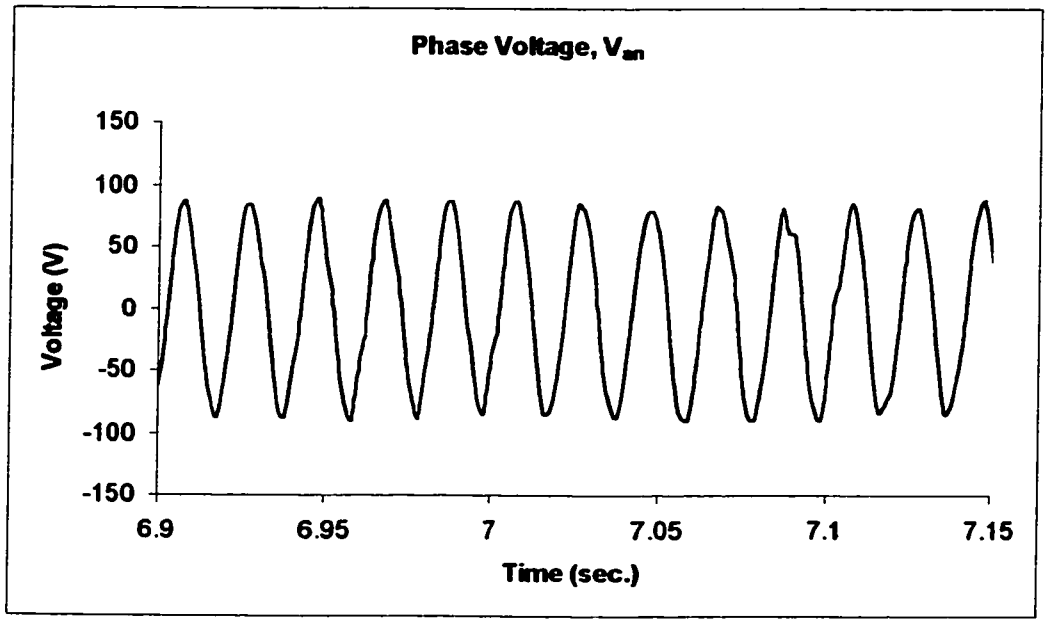

(a)

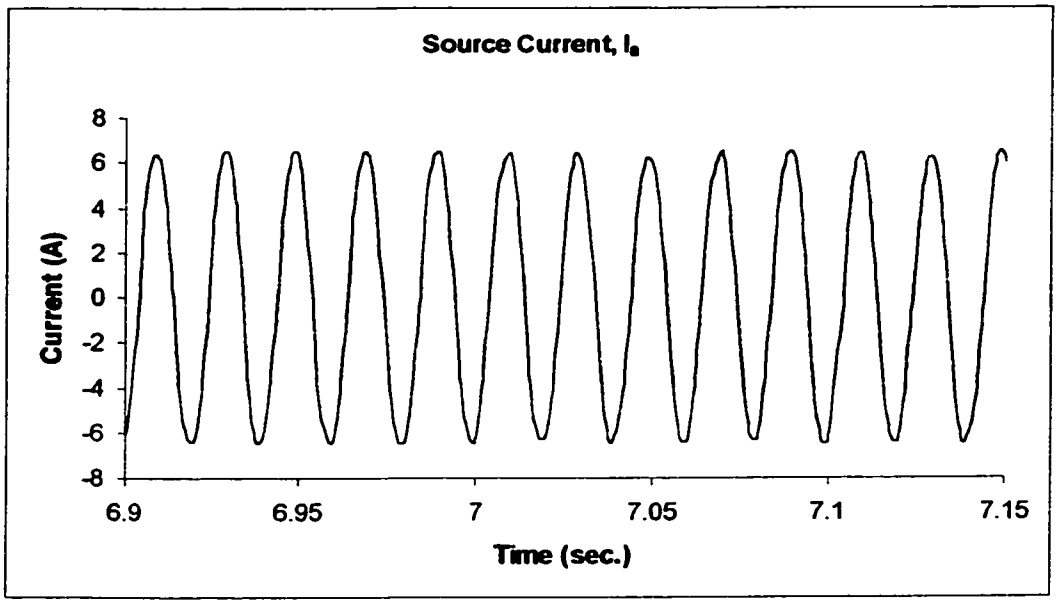
Source Current, I_a
Current (A)
8
6
4
2
0
-2
-4
-6
-8
6.9
6.95
7
7.05
7.1
7.15
Time (sec.)

(b)

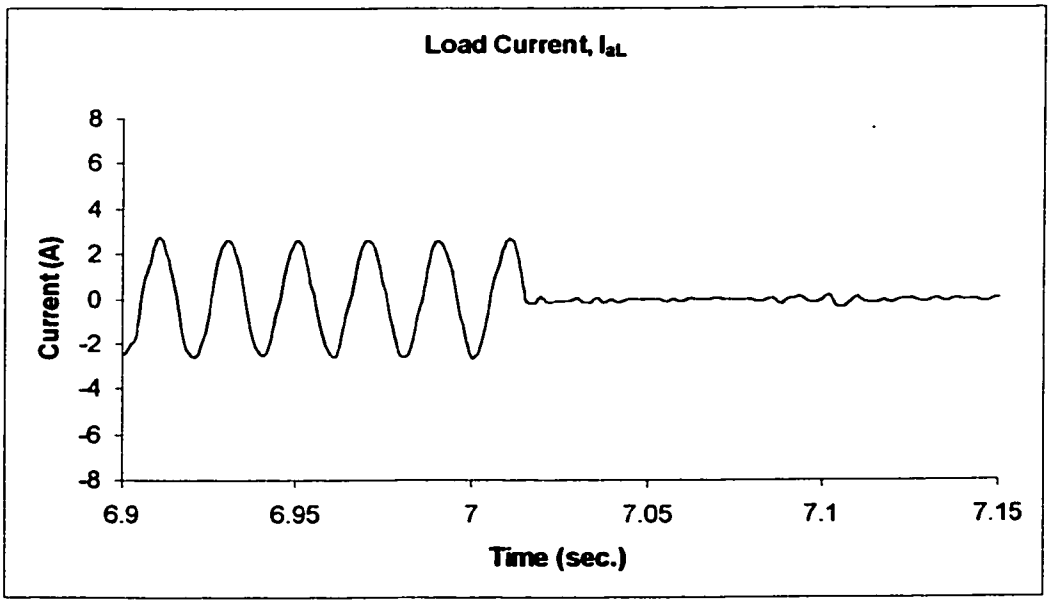
Load Current, I_{aL}
Current (A)
8
6
4
2
0
-2
-4
-6
-8
6.9
6.95
7
7.05
7.1
7.15
Time (sec.)

(c)

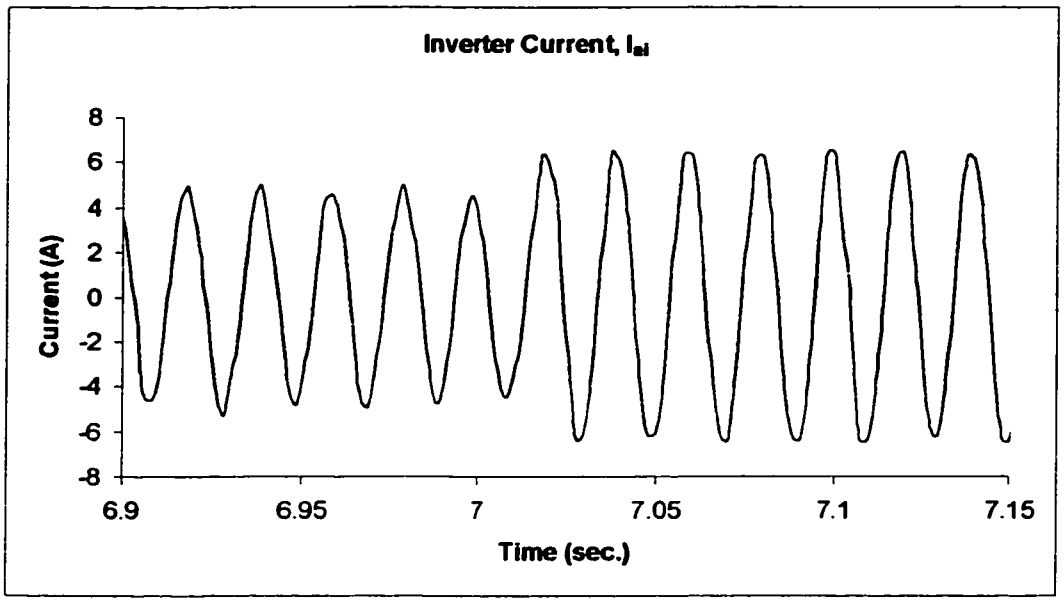

(d)

Figure 4.19 BESS for Damping Load Fluctuation (Zoom at range 6.9 - 7.15 sec.) (a) Phase Voltage, V_{an}; (b) Source Current, I_a; (c) Load Current, I_{aL}; (d) Inverter Current, I_{ai}.

4.2.4.2 From Unity to Lagging Power Factor

Load disturbance can also occur when the load suddenly becomes more lagging. This usually happens when an addition inductive load is switched on, causing an increase of current drawn from the supply, which gradually causes the supply line voltage to drop. Since BESS can provide both active and reactive power compensation, this type of load disturbance can be easily overcome by the BESS.

Figure 4.20(a) shows the experimental results of the utility phase voltage and source current, where the source current is controlled to be in phase with the phase voltage at all time. Even when there is a sudden increase of reactive power drawn by the load as

shown in Figure 4.20(b). At 2.85 second an inductive load is applied into the system causing a phase shift of the total load current with respect to the phase voltage. This kind of disturbance can create voltage dips for long period, but in this case with sufficient time response of the storage system, the system can generate or absorb active and reactive power to maintain constant current and voltage.

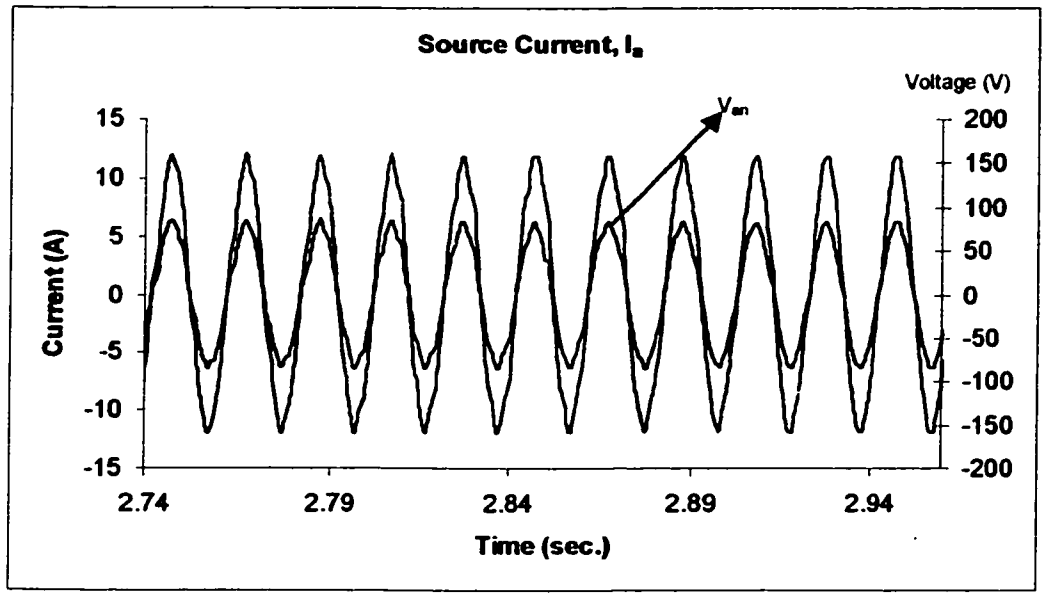

(a)

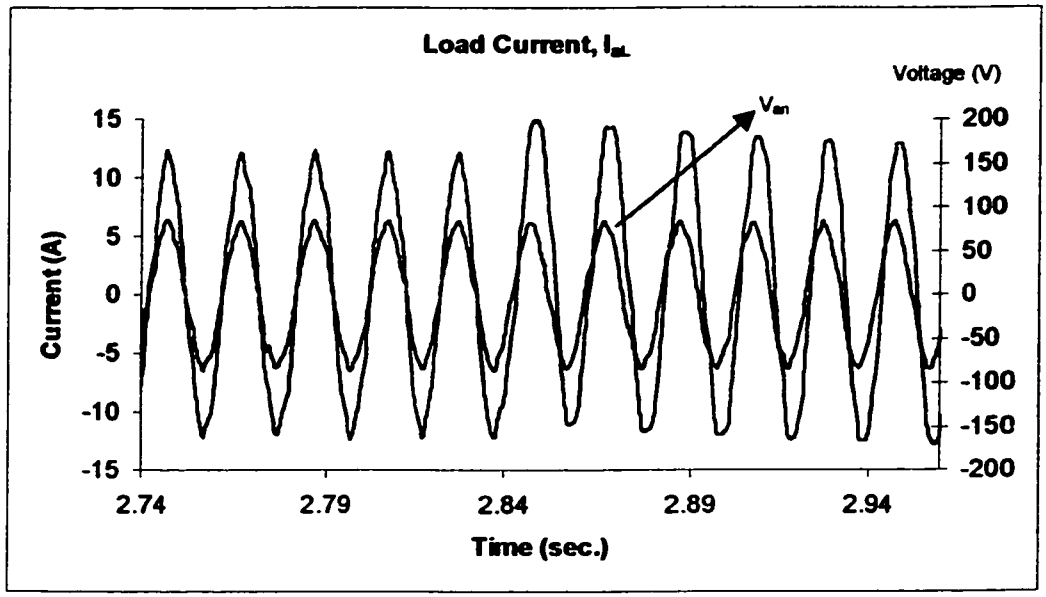

(b)

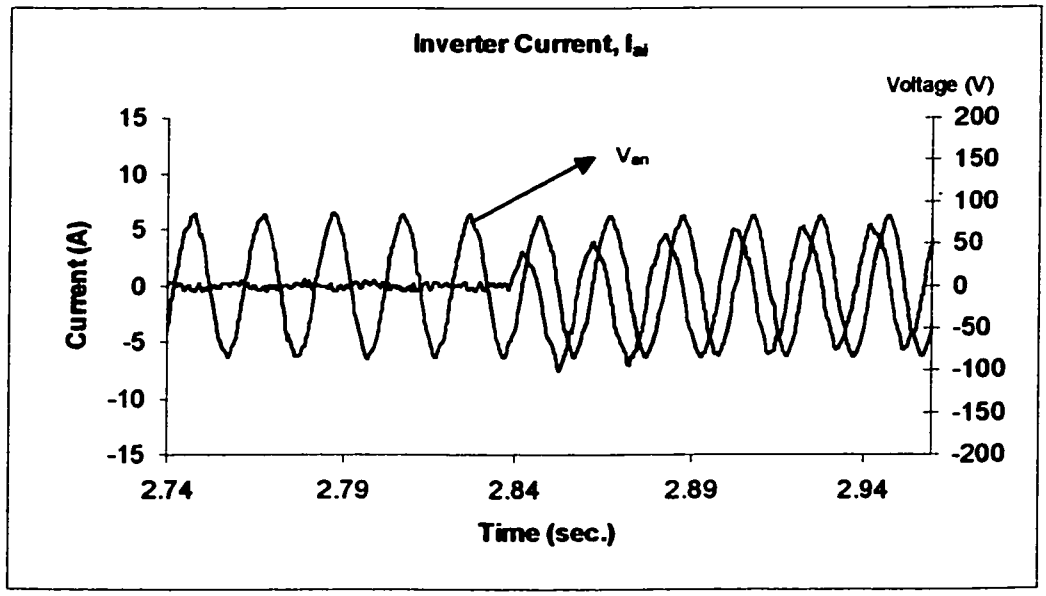

(c)

Figure 4.20 BESS for Reactive Power Fluctuation (a) Source Current, I_a; (b) Load Current, I_{aL}; (c) Inverter Current, I_{ai}.

4.2.4.3 Discharging to charging

Figure 4.21(a) demonstrates the case with an increase of battery voltage, V_{bat}, due to the rise of battery current from –2 A to +2 A as shown in Figure 4.21(b). The battery is initially discharging at –2 A, a sudden lost of load (see Figure 4.21(c)) reverses the power flow through the inverter (see Figure 4.21(d)) while the source current (see Figure 4.21(e)) is still maintained constant. As all the source current flows into the BESS, the amount of energy absorbed by the battery gives rise to an increase in the battery terminal voltage.

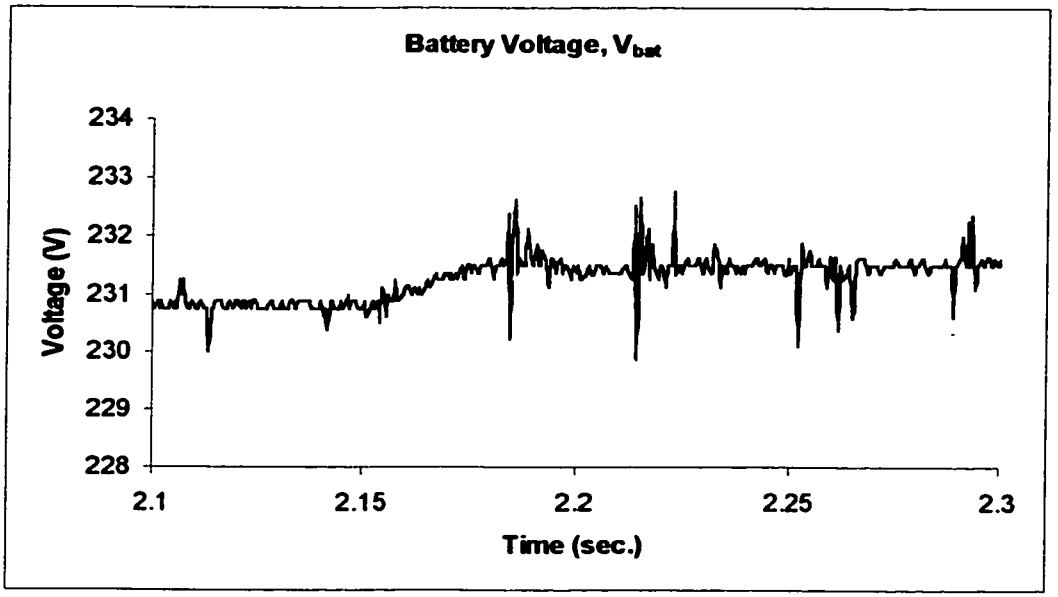

(a)

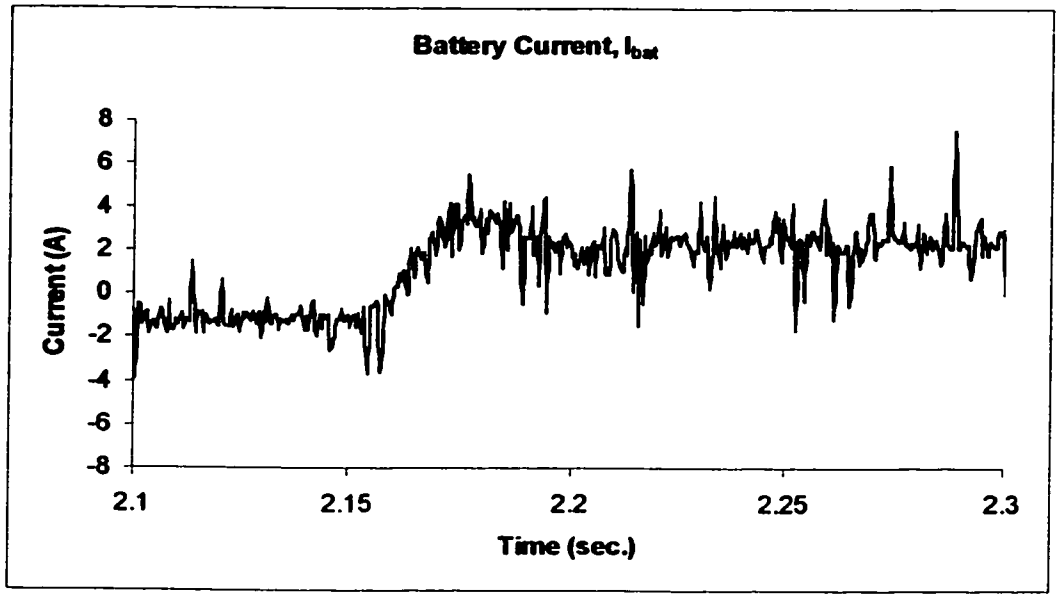
Battery Current, I_{bat}
Current (A)
8
6
4
2
0
-2
-4
-6
-8
2.1
2.15
2.2
2.25
2.3
Time (sec.)

(b)

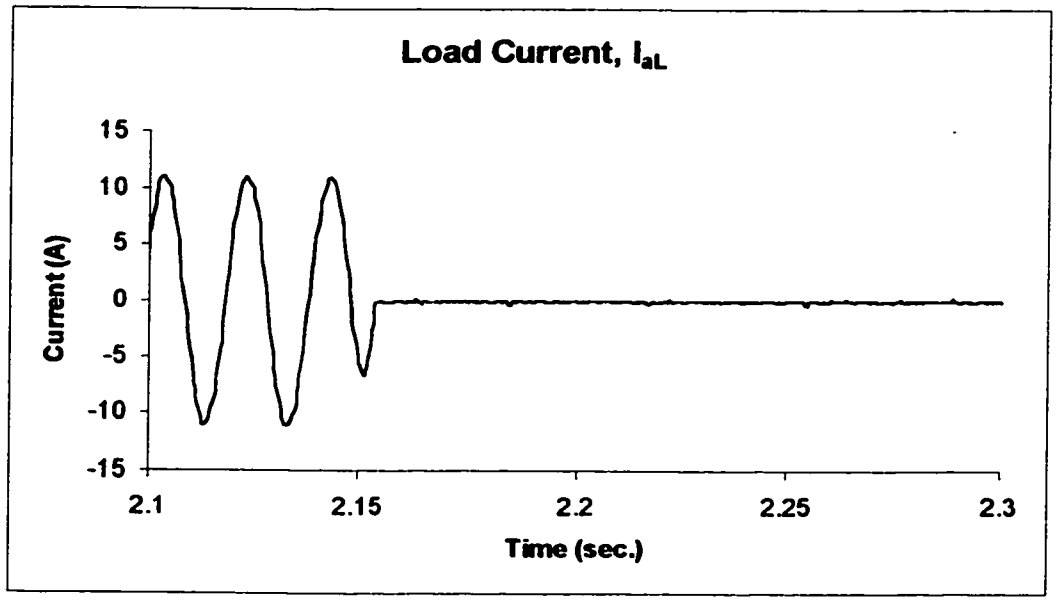
Load Current, I_{aL}
Current (A)
15
10
5
0
-5
-10
-15
2.1
2.15
2.2
2.25
2.3
Time (sec.)

(c)

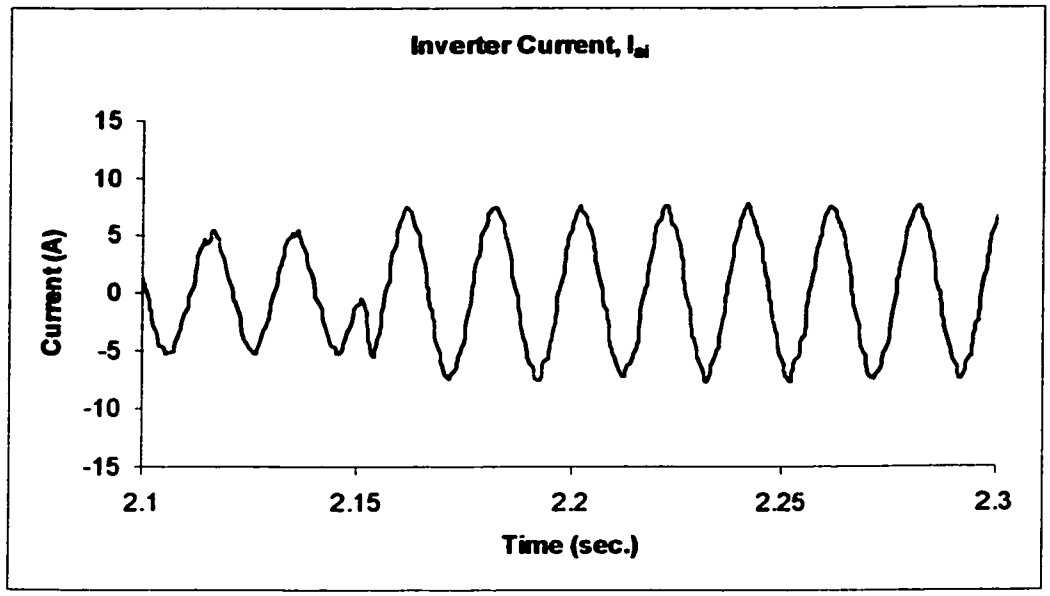

(d)

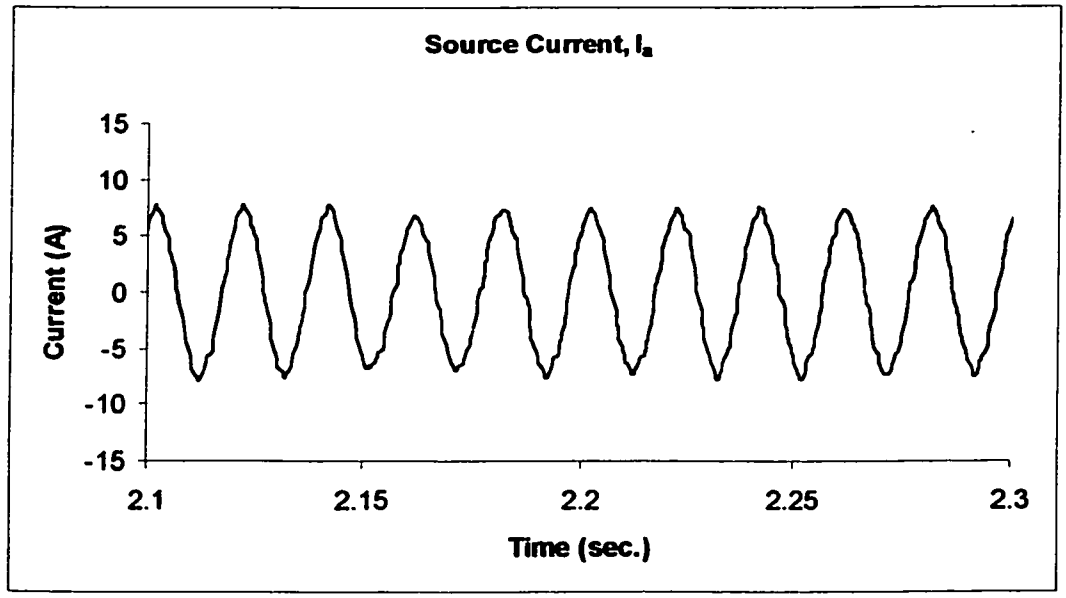

(e)

Figure 4.21 BESS form Fast Discharge to Charge (a) Battery Voltage, V_{bat}; (b) Battery Current, I_{bat}; (c) Load Current, I_{aL}; (d) Inverter Current, I_{ai}; (e) Source Current, I_a.

4.2.5 BESS operation when the reference current setting is changed

4.2.5.1 Magnitude change

To maintain power balance of the battery, the charging and discharging time needs to be evaluated with care. A time schedule should be designed to make sure the battery state-of-charge returns to its full capacity to supply the next day peak load. However, the daily load may change from day to day or season to season, some adjustment of the control setting (i.e. current reference, Ia_{ref}) should be made to ensure that the battery be fully charged before the next day begins.

To demonstrate the operation of the BESS control system when the reference current setting is changed, Figure 4.22(a) shows the experimental results when the source current setting is changed from 4 A peak to 14 A peak.

Figures 4.22(c), (d) and (e) show the inverter current, battery voltage and battery current are responding to the change of source current and they all show a very fast and stable result.

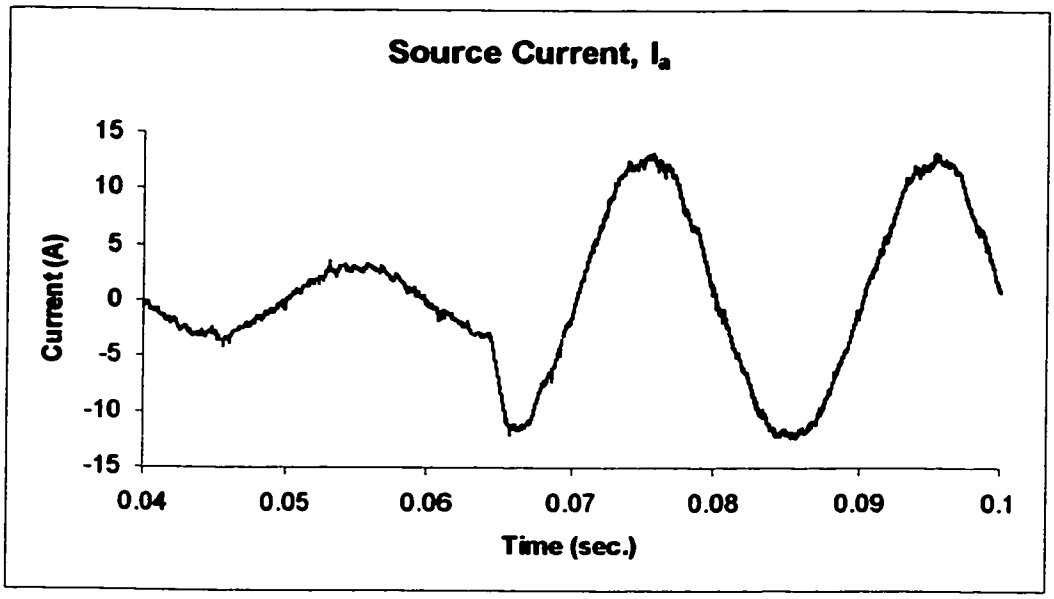
Source Current, I_a
Current (A)
15
10
5
0
-5
-10
-15
0.04
0.05
0.06
0.07
0.08
0.09
0.1
Time (sec.)

(a)

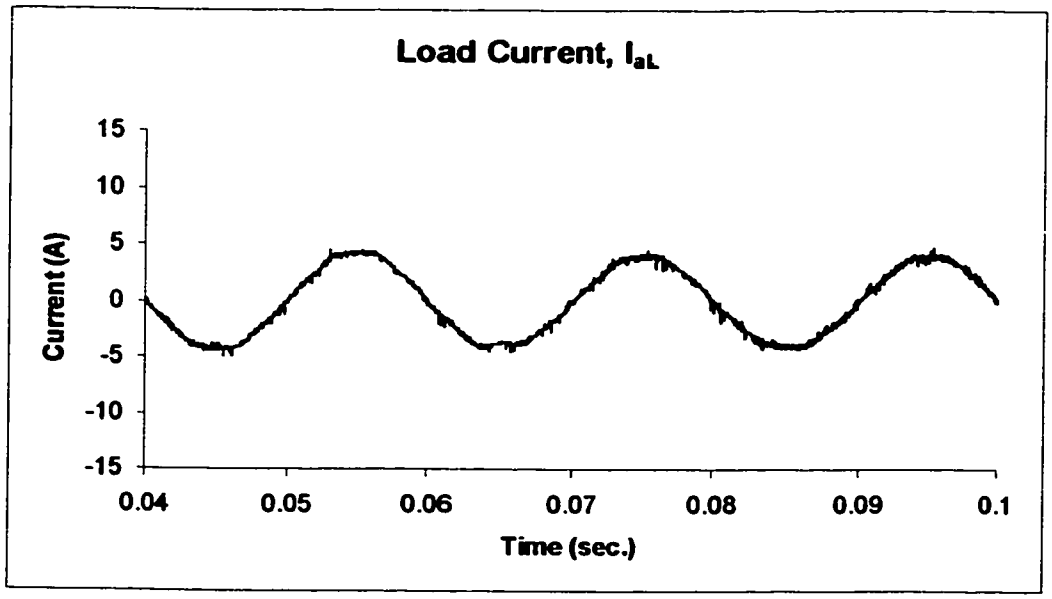
Load Current, I_{aL}
Current (A)
15
10
5
0
-5
-10
-15
0.04
0.05
0.06
0.07
0.08
0.09
0.1
Time (sec.)

(b)

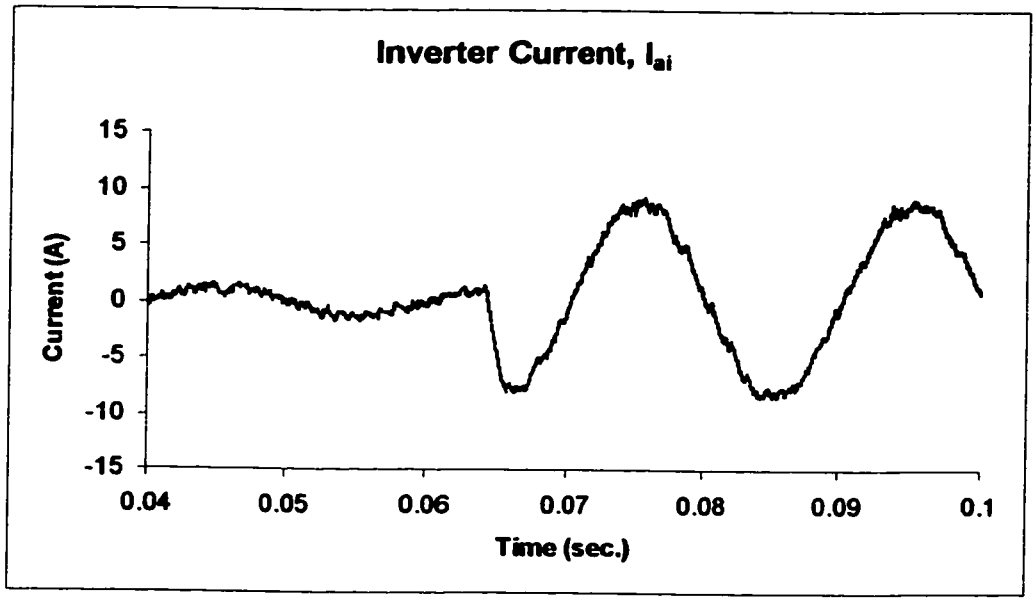
Inverter Current, I_{ai}
15
10
5
0
-5
-10
-15
Current (A)
0.04
0.05
0.06
0.07
0.08
0.09
0.1
Time (sec.)

(c)

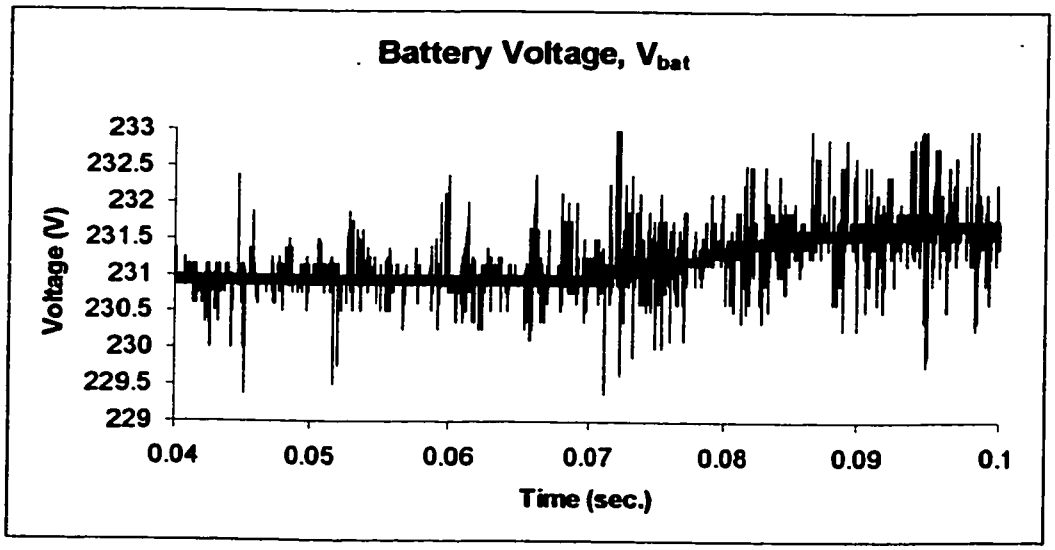
Battery Voltage, V_{bat}
233
232.5
232
231.5
231
230.5
230
229.5
229
Voltage (V)
0.04
0.05
0.06
0.07
0.08
0.09
0.1
Time (sec.)

(d)

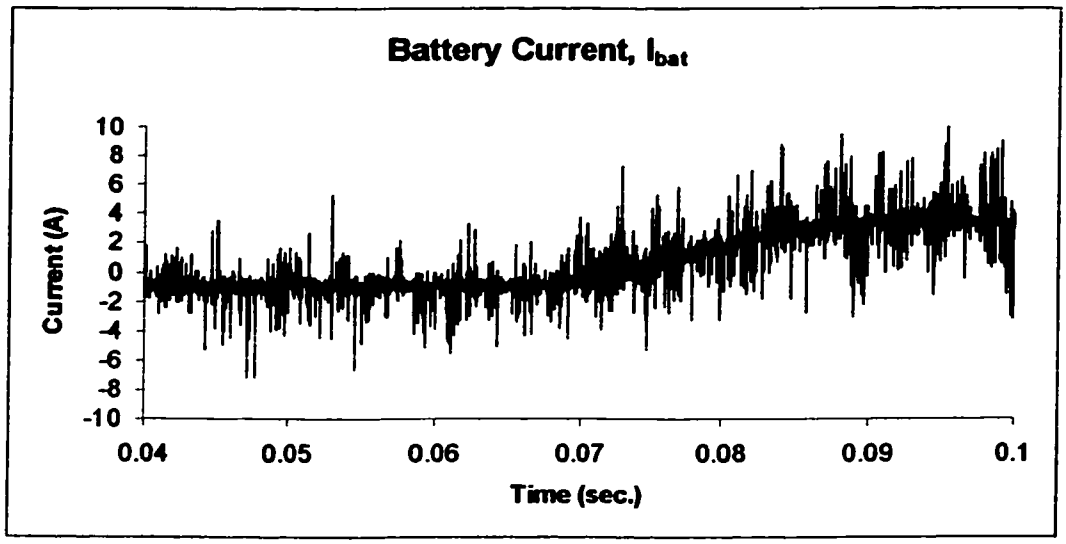

(e)

Figure 4.22 BESS for Source Current Magnitude Control (a) Source Current, I_s; (b) Load Current, I_{aL}; (c) Inverter Current, I_{ai}; (d) Battery Voltage, V_{bat}; (e) Battery Current, I_{bat}.

4.2.5.2 Phase change

Similarly it can also be demonstrated that the source current can be quickly varied from leading to lagging. Figure 4.23(a) shows the transition of source current from leading to lagging and Figure 4.23(b) recorded the load current which is in phase with the phase voltage during the experiment.

Figures 4.23(c), (d) and (e) show the inverter current, battery voltage and battery current are responding to the phase shift. By controlling the phase shift of the source current,

which causes a shift of the phase angle of the inverter current but not the magnitude, so it does not show any change in the battery voltage and current.

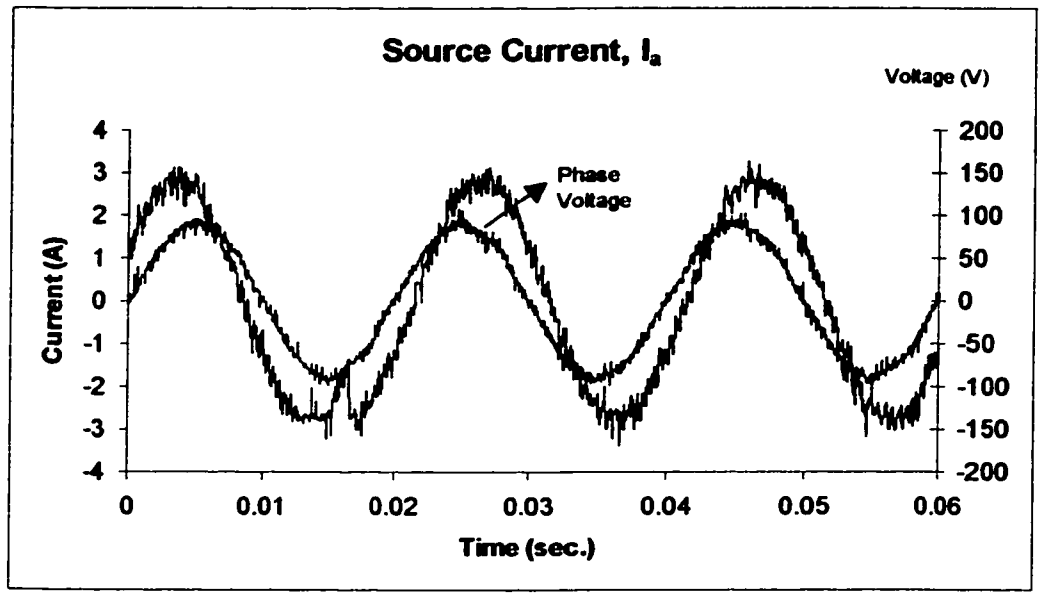

(a)

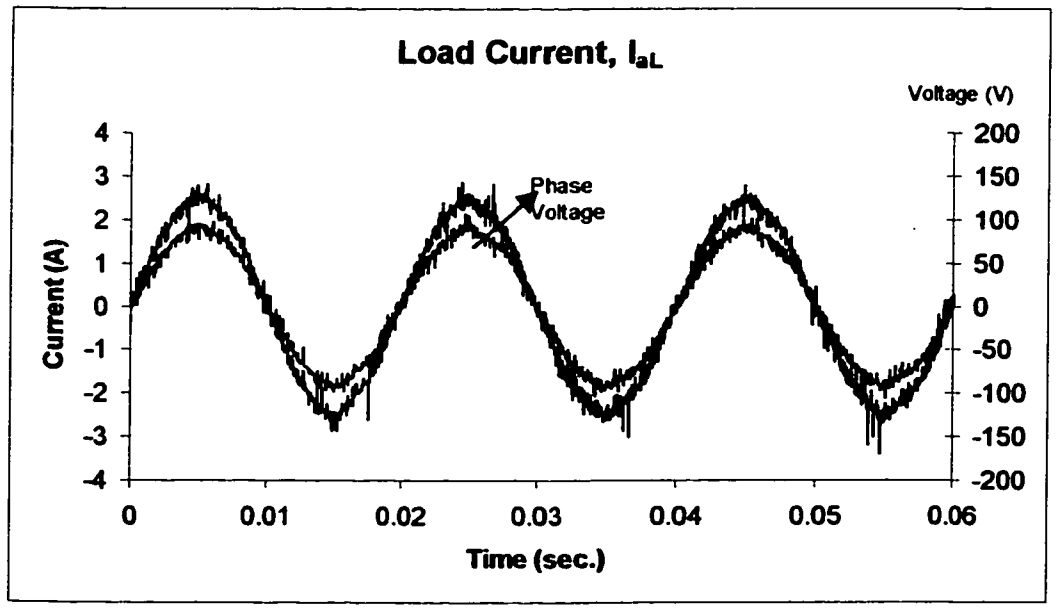

(b)

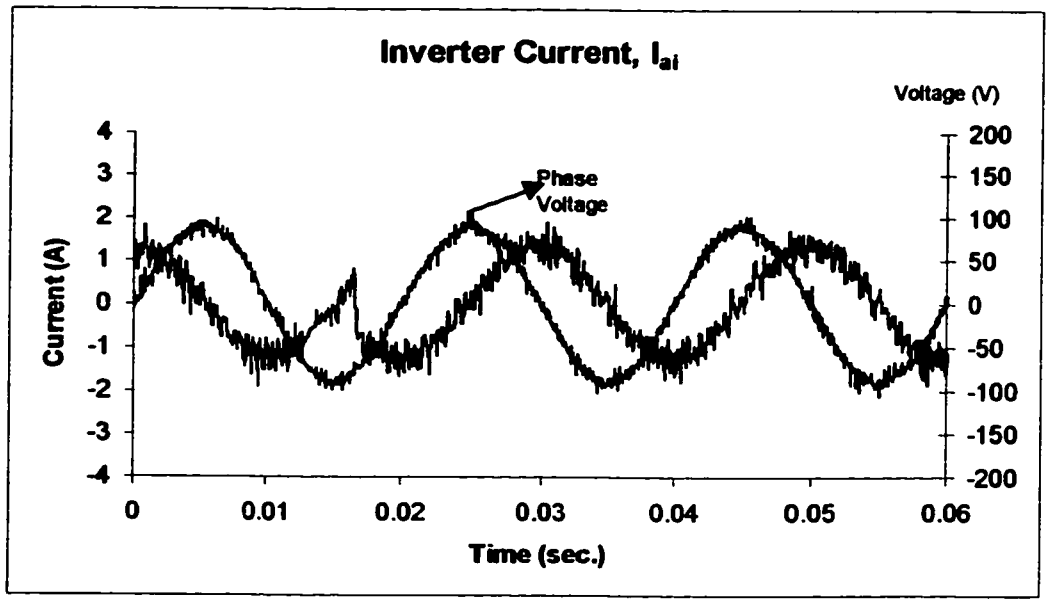
Inverter Current, I_{ai}
Voltage (V)
Current (A)
Phase Voltage
4
3
2
1
0
-1
-2
-3
-4
200
150
100
50
0
-50
-100
-150
-200
0
0.01
0.02
0.03
0.04
0.05
0.06
Time (sec.)

(c)

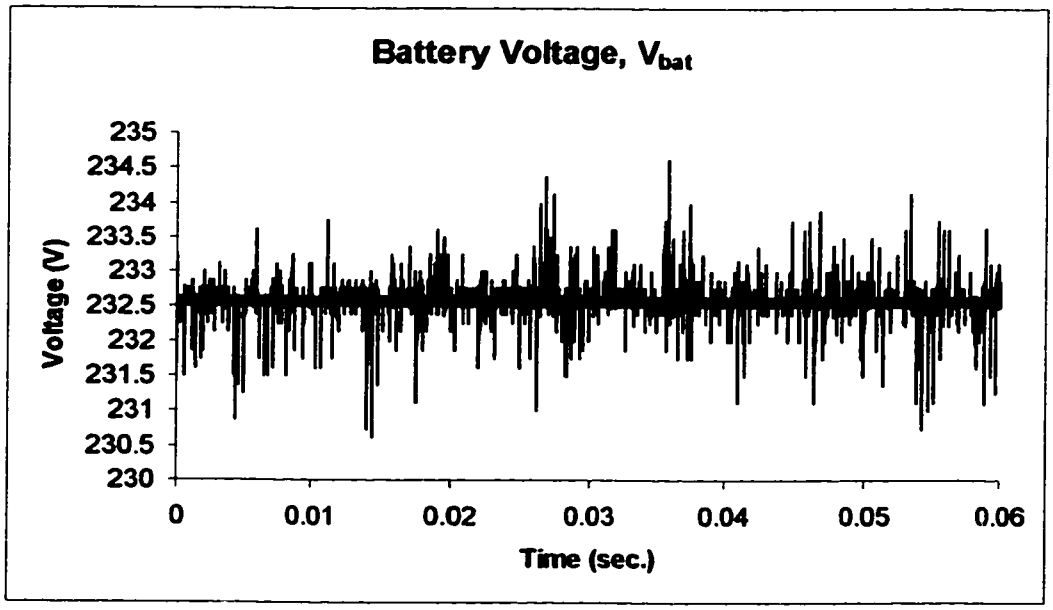
Battery Voltage, V_{bat}
Voltage (V)
235
234.5
234
233.5
233
232.5
232
231.5
231
230.5
230
0
0.01
0.02
0.03
0.04
0.05
0.06
Time (sec.)

(d)

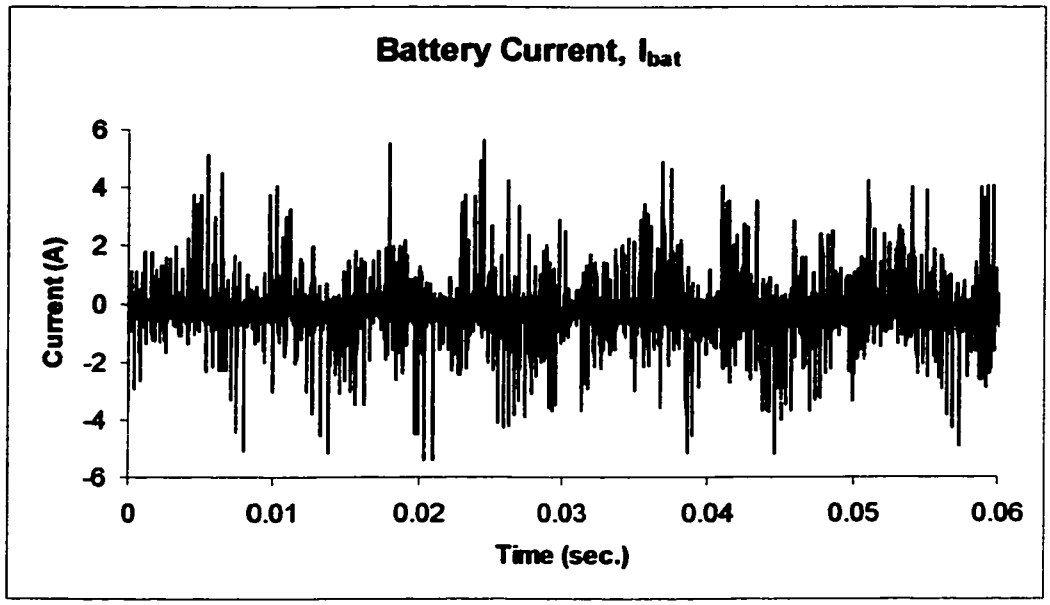

(e)

Figure 4.23 BESS for Source Current Phase Angle Control (a) Source Current, I_a; (b) Load Current, I_{aL}; (c) Inverter Current, I_{ai}; (d) Battery Voltage, V_{bat}; (e) Battery Current, I_{bat}.

4.2.6 Transient response time of the BESS

4.2.6.1 Real power response time

An important criterion in applying BESS is the response time following the magnitude change of the load demand or change in the current setting of the source current. To investigate the response time, the setting of the supply active power is changed from 0.68 kW to 0.15 kW. Figure 4.24 shows the experimental results with a 0.53 kW (0.68 kW – 0.15 kW) step response for the system. It only takes 4msec for the BESS to respond.

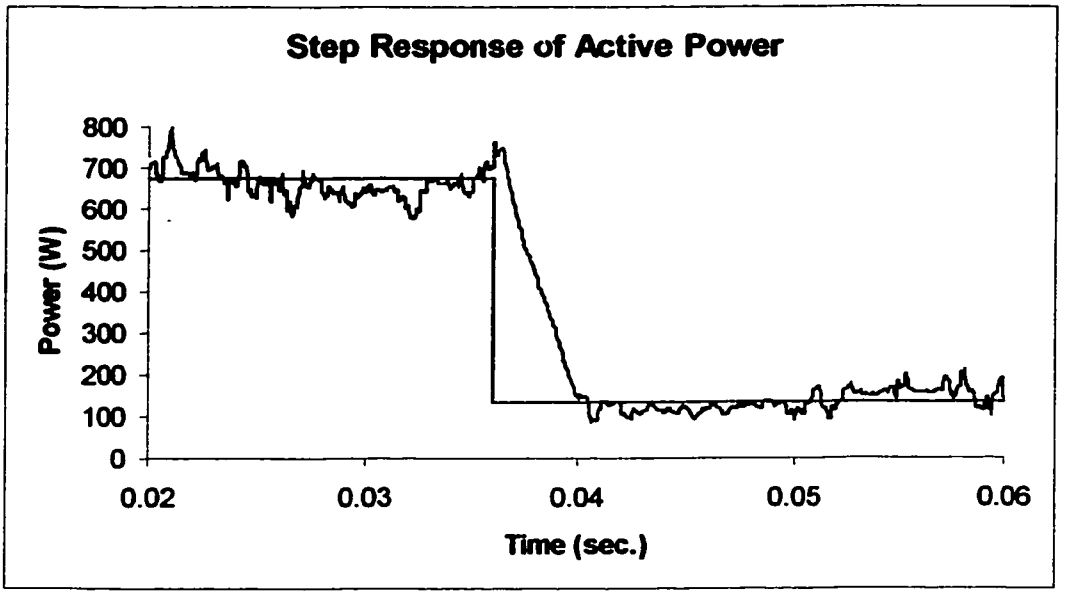

Figure 4.24 Response Time for Active Power Control

Since the response time is very dependent on the step change. From the experiment with different step levels, a set of response time is recorded as shown in Table 4.1.

Table 4.1 Recorded Step Response Time

Step Change (kW)	0.5	1	3	5	7
Response Time(sec.)	0.004	0.009	0.026	0.04	0.057

4.2.6.2 Reactive power response time

Figure 4.25 shows the reactive power step response of the system, a 0.56 kVAr (0.28 kVAr to –0.28 kVAr) step of reactive power change takes only 0.001 sec. or 1 msec.

Since the reactive power change is due to the phase angle variation of the source current, the displacement for phase angle variations is normally smaller than that for magnitude variations with the same power level. As a matter of fact, the response time is proportional to the step magnitude level.

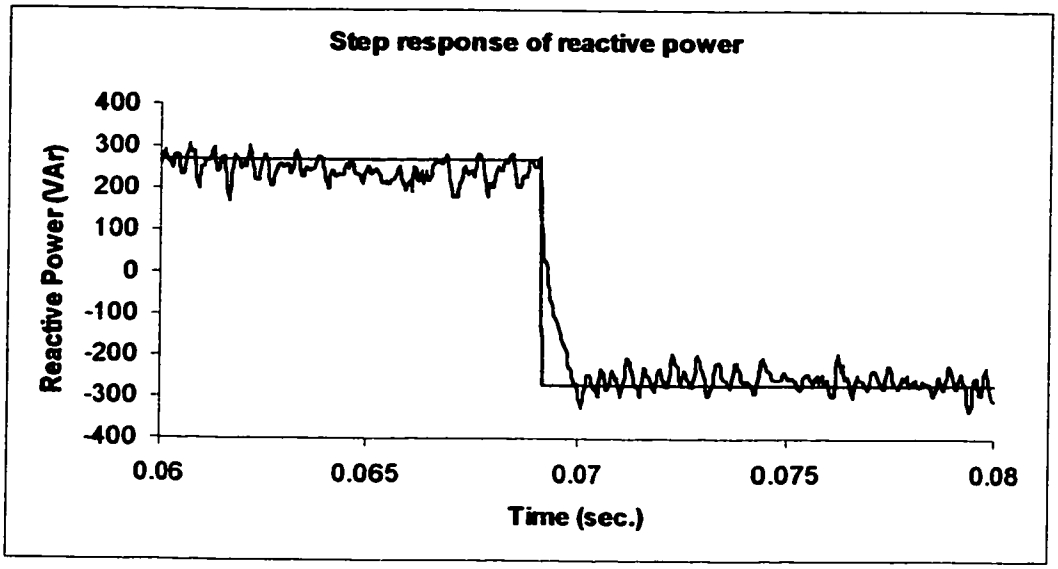

Figure 4.25 Response Time for Reactive Power Control

4.3 Conclusion

This chapter has described the operation of the proposed battery energy storage system under various operating conditions, such as load leveling, frequency control and harmonic elimination. A brief introduction of each component and the new configuration of the BESS were presented. In addition, the application of the new BESS system to improve the operation and control of a power system was demonstrated. Results from the laboratory experiments have been presented to show the effectiveness of the system.

For industrial applications, a three-phase system is usually used. A three-phase configuration has been simulated and implemented in the laboratory. Experimental and simulation results show that the proposed BESS can provide a continuous control of the active and reactive power in four quadrants. The system also demonstrated the control ability of the BESS to maintain constant voltage at a point of common coupling irrespective of fluctuation in load demand and the ability to damp any swing during transient and dynamic operation.

CHAPTER 5 A STORAGE POWER FLOW CONTROLLER USING BATTERY STORAGE

... in order to make an experiment meaningful one must have a theory as to what matters for the experiment.

Thomson, Sir George

The Inspiration of Science

CHAPTER 5 A STORAGE POWER FLOW CONTROLLER (SPFC) USING BATTERY STORAGE

5.1 Introduction

Power utilities throughout the world are facing increasing financial and environmental restrictions on the building of new power stations and transmission lines. This has imposed operational difficulties in maintaining the current levels of reliability and security, especially during peak periods.

The distribution of power on paralleling connected transmission line depends on the ratio of the line impedance rather than the line thermal rating, causing uneven loading of transmission line corridors. Furthermore, reactive power losses increases rapidly as more power is transferred through a line, causing severe reactive power deficit which can lead to voltage instability. In the last decade serious collapses have occurred in USA, France, Sweden and Japan.

Flexible AC Transmission Systems (FACTS) (Hingorani, N.G., 1993; Moore, P. and Ashmole, P., 1995; Moore, P. and Ashmole, P., 1996; Moore, P. and Ashmole, P., 1997; Moore, P. and Ashmole, P., 1998) have been recently introduced as a means of using power electronics to rapidly control the power flow along a transmission corridor in a predetermined manner. The power flow along a transmission corridor depends on the magnitude of the voltages at both sending and receiving end, the impedance of the

transmission line and the phase angle between the two voltages. FACTS devices are designed generally to control one or more of these variables, for example, Thyristor Series Compensation Systems (TSCS) control the impedance of a transmission line. The Unified Power Flow Controller (UPFC) (Moore, P. and Ashmole, P., 1998; Gyugi, L., 1992; Fuerte-Esquivel, C.R. and Acha, E., 1997; Hu, L. and Morrison, R.E., 1996) concept has been recently introduced to provide simultaneous control of the three principal parameters mentioned above using one device.

This chapter will describe a new proposal to utilize the state-of-the-art fast-switching power electronics, microprocessor control and energy storage for effective and fast control of power flow along a transmission or distribution corridor, in many ways acting like a UPFC devices, while at the same time providing additional benefits such as load leveling, damping of inter-area oscillations, damping transient stability, back-up electricity supply on loss of AC supply and also providing active power filtering to meet power quality standards. We have called this new device the Storage PFC (SPFC), but unlike UPFC, the SPFC is most suited for application in distribution systems. There are several topologies currently being explored to implement the above objectives using a Battery Energy Storage System connected to the grid. The proposed multi-purpose SPFC can provide high-speed control of active and reactive power along a transmission corridor independent of the supply voltage with excellent power quality in terms of its waveform. This chapter will also demonstrate that the proposed SPFC actually provides all the UPFC control functions, such as voltage drop compensation, phase angle control and reactive power compensation. Results from simulations and experiments will be provided and discussed.

5.2 Flexible AC Transmission System (FACTS)

Before the concept of FACTS was introduced, power electronic controlled devices, such as static VAR compensators (Hauth, R.L. and Moran, R.J., 1978) have been used in transmission networks for many years. In 1988, the concept of FACTS as a total network control philosophy was introduced by (Hingorani, N.G., 1991). The flexible transmission system is akin to high-voltage dc transmission, designed to overcome the limitations of the present mechanically controlled tap changers, phase shifters, switched capacitors, and reactors in the ac power transmission systems. By using reliable high-speed power electronics controllers, the technology offers utilities opportunities for increased efficiency:

- Control power so that the desired amount flows on the desired routes.
- Secure loading of transmission line near their steady-state and dynamic limits.
- Greater ability to transfer power between controlled areas so that the generation reserve margin can be reduced to 15 percent or less.
- Prevention of cascading outages by limiting the effects of faults and equipment failure.
- Damping of power system oscillations which could damage equipment and/or limit usable transmission capacity.

FACTS technology is not a single high power controller but rather a collection of controllers which can be applied individually or collectively to control the inter-related

parameters such as voltage, phase angle, impedance, current, reactive power and active power. However, there is no active power storage capability in the devices and each device can only provide control of few parameters only. Therefore, in a power transmission networks, many devices are required to provide entire control of the networks.

5.2.1 Static var compensator (SVC)

Since the mid-1970s, the first static var compensator has been used for stability control. Seven years later, the first application of SVC to voltage control was demonstrated on the Tri-State G&T System by General Electric Company. In addition, SVC developed by EPRI started operation in 1978 with voltage and stability control. Up to now, SVC can provide damping of oscillations, voltage control and var compensation.

SVC consists of a combination of fixed capacitors, thyristor-switched capacitors and thyristor-controlled reactors connected in parallel with the power system in most cases via a step-up transformer. The maximum SVC reactive currents are dependent on SVC terminal voltage. The reactive power produced or consumed by an SVC is generated or absorbed by passive reactive components. The controllable parameter in this equipment is the parallel capacitive or inductive susceptance. Within the SVC rating, its susceptance can be continuously controlled. When the SVC reaches it capacitive or inductive limit, it then acts as a parallel capacitor or reactor, respectively (Hingorani, N.G., 1991).

5.2.2 Resonance damper

NGH-SSR damper was invented by Dr. N. G. Hingorani to counter subsynchronous resonance (SSR). Subsynchronous resonance is created by the conventional use of mechanically controlled series capacitor added in the transmission corridor. While resonance damper consists of thyristor-controlled reactors providing a current path that bypasses the capacitor on the transmission line to prevent resonance occur between generators and the capacitors.

5.2.3 Thyristor-controlled series capacitor

Similar to the resonance damper, the thyristor switches are employed to control a number of capacitors so as to add variable positive impedance to a value above the line's natural positive impedance. In this regard, line impedance, power and current can be controlled. However, resonance damper and thyristor-controlled series capacitor require physical components adding on transmission line (Moore, P. and Ashmole, P., 1996).

5.2.4 Unified power flow controller (UPFC)

UPFC (Edris, A., Mehraban, A.S., Rahman, M., Gyugi, L., Arabi, S. and Rietman, T.R., 1998) consists of two converters with one connected in parallel and the other connected in series with the transmission line through transformers. This controller allows active power flow in the dc link from either direction between the two converters, for example, from the shunt converter to supply power required by the series converter for four-

quadrant voltage injection. The UPFC can provide magnitude and phase angle control of the voltage and independent reactive power compensation. However, the voltage vector has a much greater impact on the transmission line power flow, both active and reactive. In addition, the UPFC can only provide direct control of one line's power flow.

The UPFC topology, developed under the advanced FACTS initiative, is one which combines two voltage source inverters (VSIs) back to back using a common DC link (Gyugi, L., 1992). This topology not only has many advantages on the transmission network, but also on the distribution network that can operate at a higher speed and with a different control strategy.

The UPFC when located at the distribution network can operate at a higher speed and with a different control strategy. With two VSIs coupled by a common DC link it is possible to combine the fast voltage control achieved by a series connection with that of fast current control achieved by a shunt connection to the power system. With the shunt current control also regulating the DC link voltage, some energy required by the series connected voltage conditioning can be provided.

Additional energy is required for situations where the supply voltage is too low and for supply voltage outages. This differs from the series compensation alone, since not all the energy required for voltage compensation with the UPFC needs to come from an external energy store.

Series compensation -- Voltage conditioning with the series connected topology is only necessary when one or more of the load voltages start to extend beyond either the upper or lower allowable limits set by standards. For this the phase voltage across the load is compared with a reference value, any discrepancy is provided by the series connected converter. The DC voltage presented to the VSI is held constant by the shunt compensator, therefore real power is available through the UPFC.

Shunt compensation -- This system is at the commercial stage and has been used extensively in Japan (Akagi, H., 1996). Most incorporate IGBTs, however, a few high power, low switching frequency GTO based filters have been used to compensate for reactive power drawn by the Japanese "bullet" trains.

The instantaneous control necessary for the shunt compensation in the UPFC is very similar to that typically used for active filtering (Akagi, H., 1996; Watanabe, E.H., Aredes, M., 1995). That is based on the instantaneous active and reactive power methodologies using p-q co-ordinates (Akagi, H., 1996; Watanabe, E.H., Aredes, M., 1993; Kanazawa, A.Y., Nabae, A., 1984). However, an additional active power component, determined by the DC voltage level, is also incorporated into the UPFC control algorithm, since this value is indicative for power required by the series compensation. The DC voltage level, in conjunction with the knowledge of the active power being drawn by the shunt compensation, can be used to determine the energy required by the energy storage.

Table 5.1 FACTS Controllers

1. Damping of Oscillations	5. VAR Compensation
2. Series Impedance Control	6. Power Control
3. Transient Stability	7. Phase Angle Control
4. Voltage Control	8. Limiting Dynamic Over-voltages

FACTS Controller	1	2	3	4	5	6	7	8
NGH-SSR Damper	✔	✔	✔					
Static Var Compensation (SVC)	✔			✔	✔			
Thyrsitor Controlled Series Capacitor/Reactor	✔	✔	✔			✔		
Static Condensor (STATCON)	✔		✔	✔	✔			
Thyristor Controlled Phase Angle Regulator	✔		✔			✔	✔	
Unified Power Flow Controller (UPFC)	✔		✔	✔	✔	✔	✔	
Thyristor Controlled Dynamic Brake	✔		✔					
Thyristor Controlled Dynamic Voltage Limiter								✔

Table 5.1 summarizes the attributes of each FACTS controller. As mentioned earlier, all the controllers are power electronic devices which can be designed for use at different power levels. However, most of them have no active power component incorporated into the controller. This limits the functions of the controllers. A potential spin-off of the

FACTS and HVDC is to replace the capacitor with batteries to develop electricity storage, able to deliver short-term power to the grid as well as voltage boost. This has been implemented for example in Dynamic Voltage Regulator (DVR) or in STATCOM (Moore, P. and Ashmole, P., 1997).

Table 5.2 attempts to list both conventional and power electronic solutions to the various problems that are being met. It is believed that the proposed topologies can also solve some of the problems listed in Table 5.2.

Table 5.2 Conventional and power electronics solutions to problems

Problem	**Conventional solution**	**Power electronics solution**
1. low voltage at heavy load	Power factor correction	-
2. high voltage at low load	Breaker switched capacitor/reactor	-
3. low voltage on line outage	Breaker switched capacitor	SVC
4. large voltage variability	Tap changer	SVC
5. voltage variability but location unpredictable	-	Relocatable SVC or Statcom
6. very long line	Shunt reactor	TCSC or SSC
7. stability limit reached	Series capacitor	TCSC or SSC
8. sub-synchronous	Reduce series capacitor	TCSC or NGH damper

resonance		
9. long distance instability	Higher voltage, new lines stabilizing signal in generator excitation	-
10. inter area swings	Stabilizing signal in generator excitation	-
11. unstable interconnection	Series capacitor, excitation damping	HVDC back-to-back link
12. persistent loop flow	Open connections, series reactors	HVDC back-to-back link
13. unsynchronized systems	-	HVDC long distance
14. poor parallel line	Series capacitor/reactor or quad booster	-
15. poor post-fault	Breaker switched series capacitor or quad booster	-
16. continuous need to adjust	-	TCSC or SSC thyristor phase shifter
17. voltage variable and continuous poor	-	Unified power flow controller
18. fault level limits	Series reactors	HVDC back-to-back link
19. more power needed, but new line impossible	Cable, gas duct	Convert AC line to DC

5.3 The storage power flow controller (SPFC)

The Storage Power Flow Controller consists of a Battery Energy Storage System connected in shunt or series to the grid through inverters, whose operation is tightly controlled by a high-speed microprocessor.

Power flow along a transmission line is a function of the sending and receiving end voltages, as shown in Equation 5.1. Assuming that busbar magnitudes are maintained at fixed levels, in order to increase power flow, we must increase δ. However, increasing δ increases the risk of transient and voltage stability problems if a fault were to occur along the line. If both ends of the transmission line were connected to a generator, we could simply assess the post-fault transient stability conditions by using the equal area criterion and the voltage stability using AC transmission-line equations. Since power systems are far more complex than Figure 5.1, so too is the problem of stability and more complicated techniques need to be sought to assess stability in highly interconnected systems.

$$P = \frac{V_1 V_2}{X} \sin\delta \qquad (5.1)$$

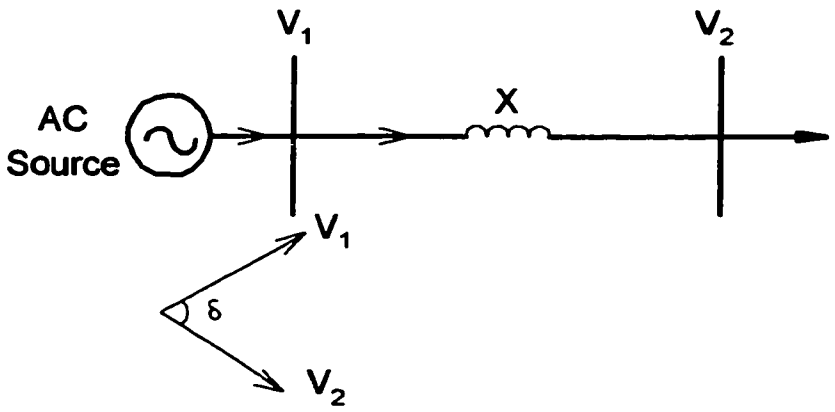

Figure 5.1 Power flow along a line

Consider a section of a power system, shown in Figure 5.2. If we consider the flows of active and reactive power from busbar V1 to busbar V2 in the two transmission lines, the flows are entirely determined by the line impedances and hence we have an inflexible AC Transmission System. In order to provide the required flexibility, we need to be able to control the power flow in at least one of the transmission lines at high speed, faster than any fluctuations that can occur including the fluctuations due to harmonics.

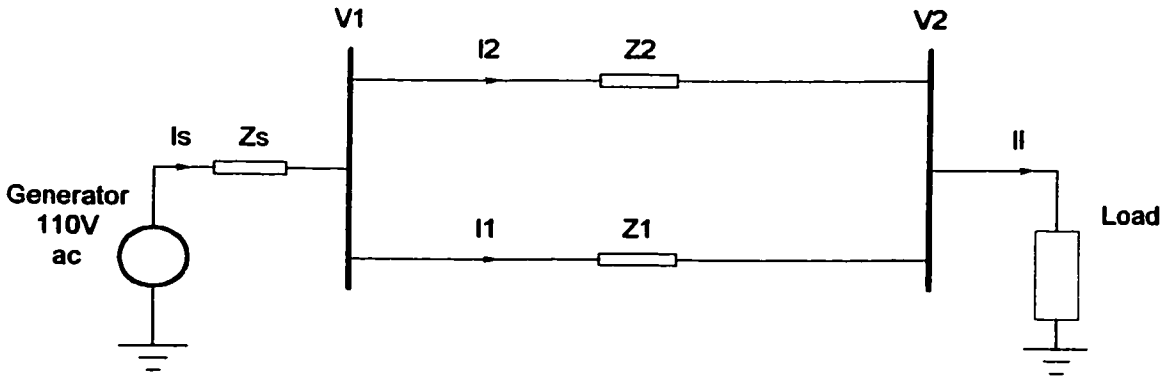

Figure 5.2 A simple power system

There are several topologies in which a Battery Energy Storage System can be utilized to meet this requirement:

a) One of the lines is disconnected from the supply and reconnected to the BESS as shown in Figure 5.5. Line active and reactive power can then be tightly controlled by the BESS at high speed.
b) The AC output of the inverter of the BESS is connected in series with the controlled line through a series transformer as shown in Figure 5.10.
c) The BESS is sandwiched between two inverters connected in series with the line as shown in Figure 5.15. The two inverters are then controlled independently so that two independent power flows can be obtained.

In this chapter, the power flow evaluation of the SPFCs have the following model assumptions:

- lossless transmission lines
- sending and receiving ends are stiff nodes and their voltages are equal in magnitude
- performance characteristics are drawn for midpoint location of control devices.

5.3.1 Controlling power flow using Shunt connected BESS (SPFC1 – SPFC type I)

5.3.1.1 Power Flow evaluation of SPFC1

Power flow controllers can utilize the physical principles, depending on their construction and operating mode, based on the concepts of controllable shunt current

injection. The concept of SPFC1 based on shunt current injection can be demonstrated using the system shown in Figure 5.3. I_i is the controllable shunt current injected to the midpoint of the transmission system. Figure 5.4 shows the vector diagram of the SPFC1 for the real and reactive current injection to the system.

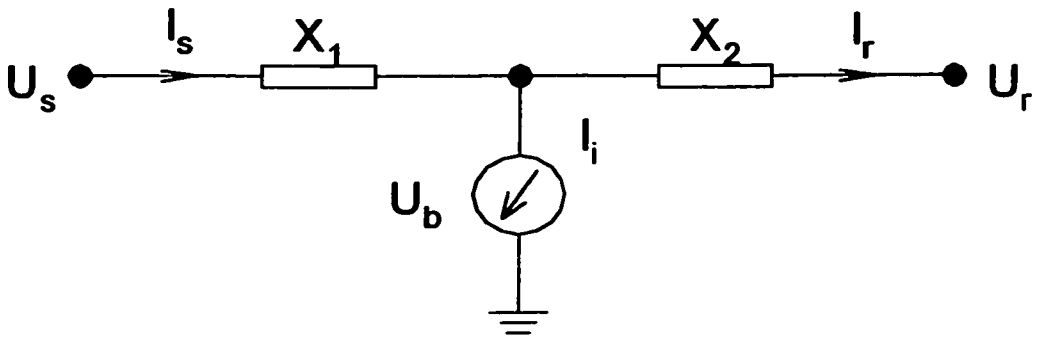

Figure 5.3 Line model of the system with SPFC1 (Shunt connected BESS)

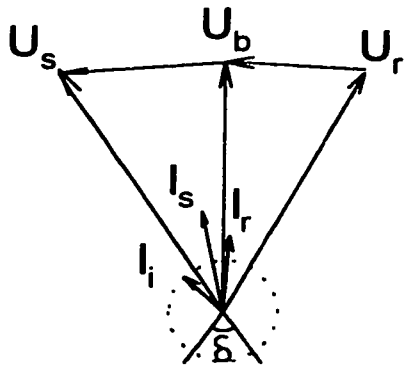

Figure 5.4 Vector diagram of the system with SPFC1

The power flow along the transmission line can be written in Equations 5.2 and 5.3.

$$P_s = \mathrm{Re}(V_s I_s) \tag{5.2}$$

$$Q_s = \mathrm{Im}(V_s I_s) \tag{5.3}$$

From Figure 5.3, the following equations can be written,

$$I_s = I_r + I_i \tag{5.4}$$

$$U_s = U_b + jX_1 I_s \tag{5.5}$$

$$U_b = U_r + jX_2 I_r \tag{5.6}$$

By rearranging Equations (5.4), (5.5) and (5.6), we get

$$I_s = \frac{U_s - U_r}{j(X_1 + X_2)} + \frac{X_2 I_i}{X_1 + X_2} \tag{5.7}$$

Substituting I_s into Equations (5.2) and (5.3), we have

$$P_s = \mathrm{Re}[U_s(\frac{U_s - U_r}{j(X_1 + X_2)} + \frac{X_2 I_i}{X_1 + X_2})] \tag{5.8}$$

$$Q_s = \mathrm{Im}[U_s(\frac{U_s - U_r}{j(X_1 + X_2)} + \frac{X_2 I_i}{X_1 + X_2})] \tag{5.9}$$

As can be seen from Equations (5.8) and (5.9), the real and reactive power can be controlled depending on the injected current I_i, and assuming that magnitudes of the sending end and receiving end voltages are the same, even if the impedance of the lines are not equal.

By using the concepts discussed above, it is possible to quantify the impact that SPFC1 has on power transfer capability and reactive power requirements in transmission systems. The reactive power balance is one of the many requirements that enforces a practical limit on how much active power P can be transferred over a system. In addition, the real power is another requirement for power system stability.

In addition, SPFC1 helps maintain the system voltage when transferred power is varied. SPFC1 can act as loads to absorb the real/reactive power surplus in case of reduced power transfer or open lines and also gives maximum security against over-voltages in the event of sudden load rejection or opening of lines.

5.3.1.2 Simulation results of SPFC1

In this topology, the BESS is connected at the sending end of the transmission line, and the line is disconnected from the supply as shown in Figure 5.5. The system, as shown in Figure 5.5, consists of a supply point (represented by a generator behind its transient impedance, a variable load, which can contain harmonics, and two lines having different impedances). Without the BESS, the current flow of each line is entirely determined by the line impedances, in this case, inversely proportional to the line impedances. During heavy load condition, the low impedance line may be severely overloaded and the high impedance will be under-loaded – a very inefficient way of utilizing valuable resources.

Further, if the load is nonlinear, the voltage at the supply terminal will be distorted and there will be non-sinusoidal currents flowing through the power system, an undesirable phenomenon.

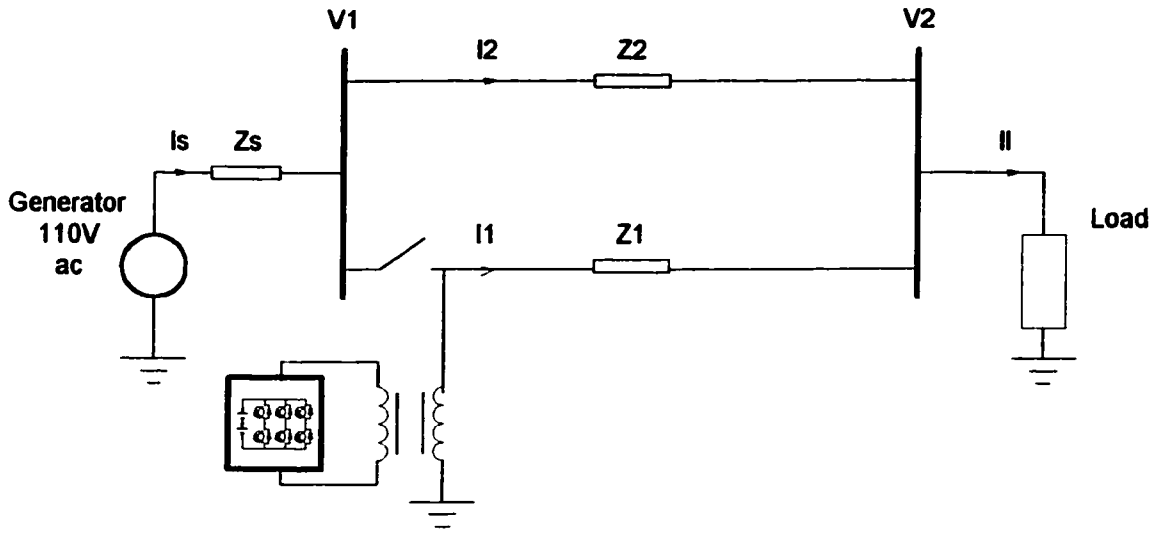

Figure 5.5 Topology for SPFC1

The switches in the inverter of the BESS is controlled at high-speed such that the current I_s (and hence I_2) is controlled both in its magnitude and waveform following a pre-determined reference current. Assuming that the supply voltage is constant, the active and reactive power flow from the generator is tightly controlled in sinusoidal waveform irrespective of any changes in the load or the load having non-linear characteristics. The BESS supplies the difference between the varying load demand and the controlled line power flow.

For example, if $Z_1=2 \times Z_2$,

Without the SPFC1:

$I_S = I_L$

$I_1 = 0.5 \times I_2 = 1/3\ I_L$

$I_2 = 2/3\ I_L$

And as load changes, I_S , I_L , I_1 and I_2 will all change.

With the use of SPFC1, I_S and I_2 can be controlled both in their magnitude and waveform, for example, it is possible to set I_2 and I_S to be 0.5 I_L. Because the current waveform can be controlled, the phase of I_2 and I_S can be set to be in phase with the supply voltage, in this way, the reactive power supplied from the source is zero, although the load may have very poor power factor, hence the SPFC1 can also provide power factor correction similar to the conventional UPFC, it also has the ability to provide active filtering. Once controlled in this way, the two currents will be fixed irrespective of the changes in the load demand. To ensure that the batteries of the BESS will not be fully discharged, at low load, the reference waveform can be set to be higher than the load current (but well below its thermal limit) such that the current is now flowing from the supply to the battery to provide the required charging.

Figure 5.6(a) shows the load current I_L and the supply voltage. Note that the current contains harmonics and has lagging power factor. Figure 5.6(b) shows the current I_1 and Figure 5.6(c) shows the current I_2. I_s is the same as I_2. Figure 5.6(c) shows that the current in the source is controlled to be in phase with the source voltage and sinusoidal in its waveform, even though the load current is distorted. Note that the voltage

waveforms have been scaled to half its size so that it will not interfere with the current waveform. Figure 5.6(b) shows that current I_1 from the BESS supplies all the harmonics of the load. Note that I_1 and I_2 are now independent of the line impedances.

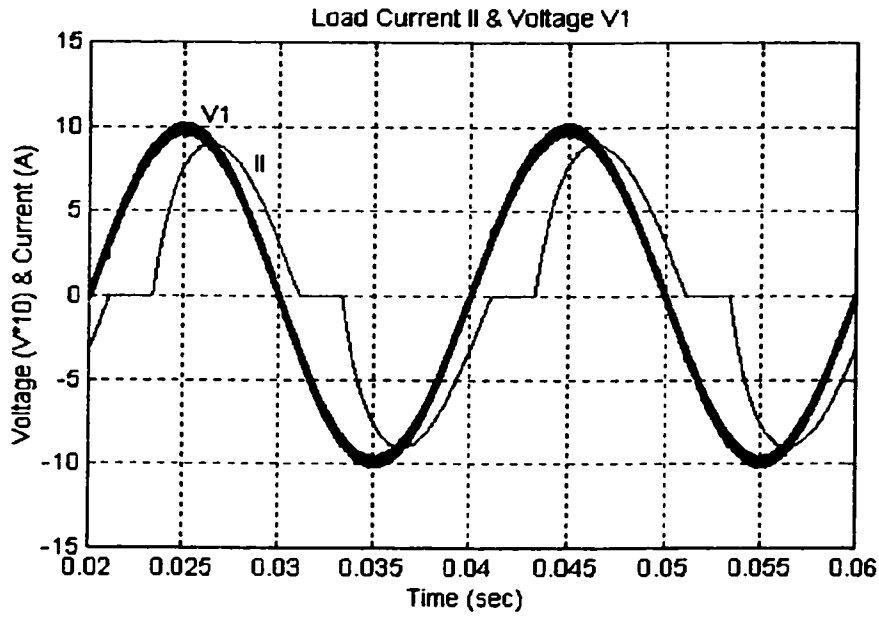

(a)

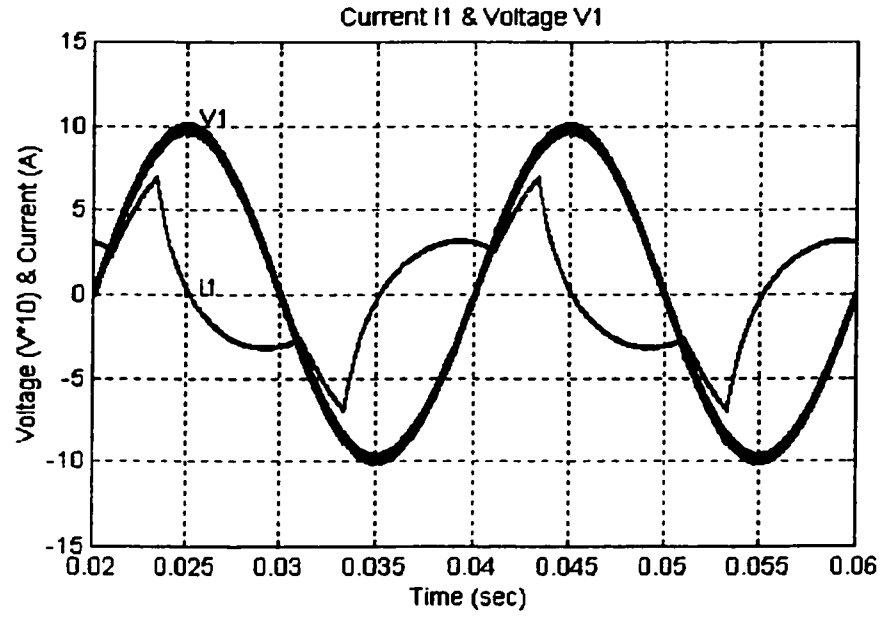

(b)

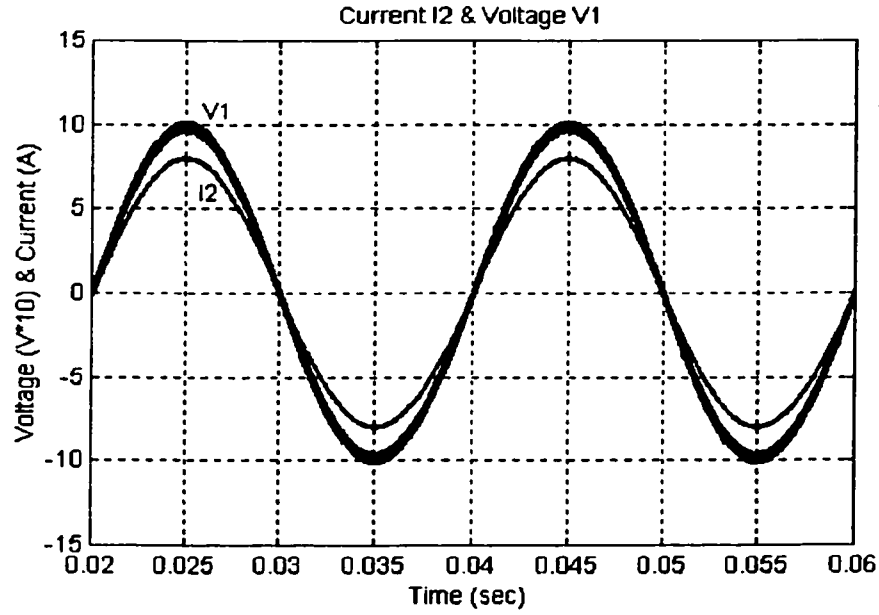

(c)

Figure 5.6(a) Load Current (I_L); (b) Current (I_1); (c) Current (I_2).

The SPFC1 can also provide extra damping for power system oscillation by modulating the BESS from generating to demanding at high speed. Being a static generating source, the SPFC1 can also provide temporary back up supply if the power system experiences a black-out situation, whilst at the same time it can act as a "negative load-shedding" during voltage instability situation, by generating extra active and reactive power beyond its rating for a short period.

5.3.1.3 Experimental results of SPFC1

In this experiment, the system is configured similar to Figure 5.5. Two air-core inductors with very low internal resistance are used as the transmission lines. The supply is a three-phase ac with 110 V line-to-line voltage connected to a distorted load (Figure 4.10) through the transmission line. Since the SPFC1 is connected at the other end of the parallel line, it compensates all the harmonics required by the distorted load. In Figure 5.7(a) the load current is shown with peak current equal to 5A. The result in Figure5.7(c) shows that the ac grid provides current which is in phase with the bus-bar voltage that can reduce the stress of the ac supply for reactive power transfer because the SPFC1 provides the harmonic current, as shown in Figure 5.7(b) through transmission Line-2. On the other hand, the grid current magnitude can be controlled to prevent over-current of the low impedance line in order to provide network security.

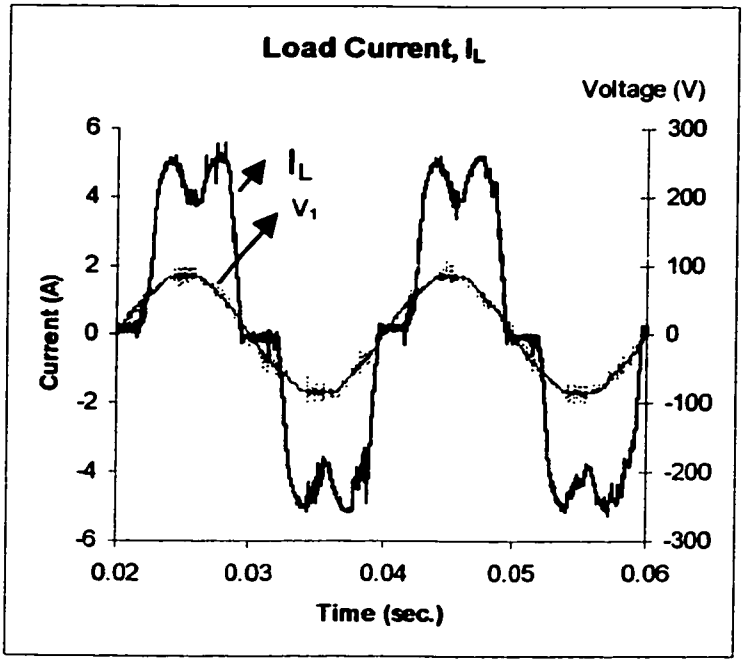
Load Current, I_L
Voltage (V)
I_L
V_1
Current (A)
Time (sec.)
6
4
2
0
-2
-4
-6
300
200
100
0
-100
-200
-300
0.02
0.03
0.04
0.05
0.06

(a)

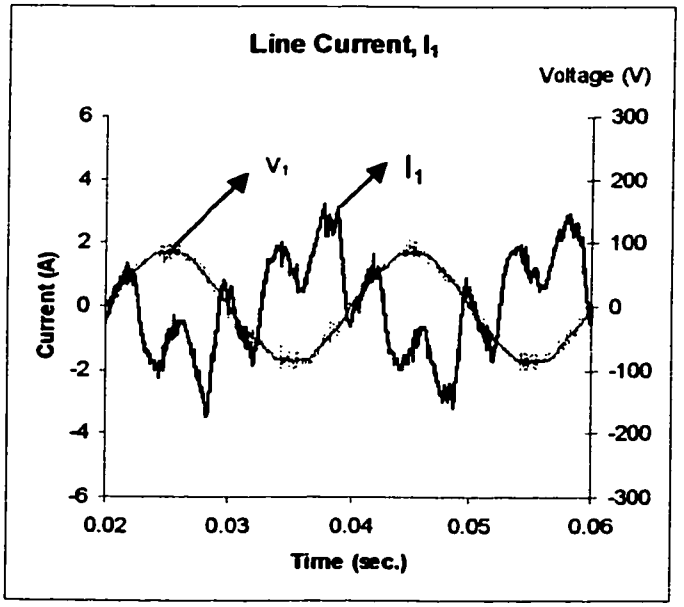
Line Current, I_1
Voltage (V)
V_1
I_1
Current (A)
Time (sec.)
6
4
2
0
-2
-4
-6
300
200
100
0
-100
-200
-300
0.02
0.03
0.04
0.05
0.06

(b)

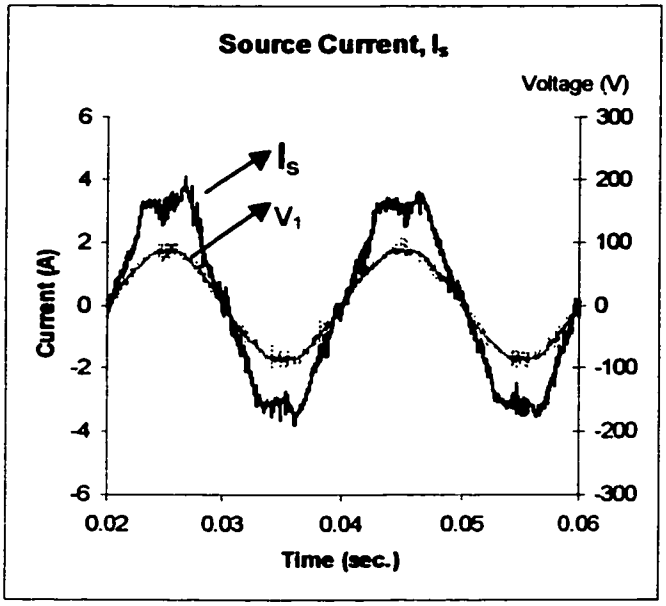

(c)

Figure 5.7 (a) Load Current, I_L; (b) Line Current, I_l; (c) Source Current, I_s

5.3.2 Controlling power flow using series connected BESS (SPFC2 – SPFC type 2)

5.3.2.1 Power flow evaluation of SPFC2

The series voltage of SPFC2 can be provided by a controlled voltage source. The series voltage device can be constructed such that the injected voltage's magnitude U_T and/or phase angle α can be varied. The impact on power flow can be investigated by using the transmission model and vector diagram shown in Figure 5.8 and Figure 5.9 respectively.

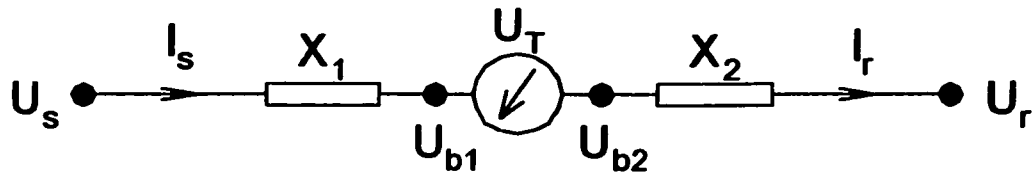

Figure 5.8 Line model of the system with SPFC2 (Series connected BESS)

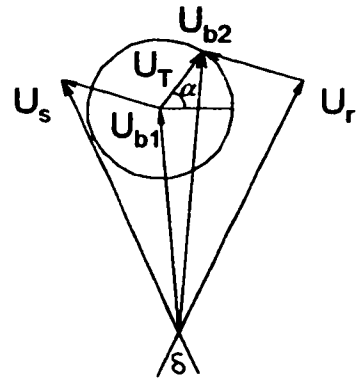

Figure 5.9 Vector diagram of the system with SPFC2

From Figure 5.8, Equations (5.10), (5.11) and (5.12) can be written

$$U_{b1} = U_r + jX_2 I_s - U_T \tag{5.10}$$

$$U_s = U_{b1} + jX_1 I_s \tag{5.11}$$

$$I_s = I_r \tag{5.12}$$

Since the SPFC2 only provides voltage injection along the line without tapping of the systems power, so the current I_s equals to I_r, and Equations (5.13) and (5.14) can be represented as:

$$P_s = \mathrm{Re}(U_s I_s) \tag{5.13}$$

$$Q_s = \mathrm{Im}(U_s I_s) \tag{5.14}$$

SPFC2 provides a specific amount of compensation in general enabling more active power to be transferred with less reactive power supply requirements as compared with SPFC1. However, there is limited compensating capability, for example active filtering is not capable, as compared with SPFC1.

5.3.2.2 Simulation results of SPFC2

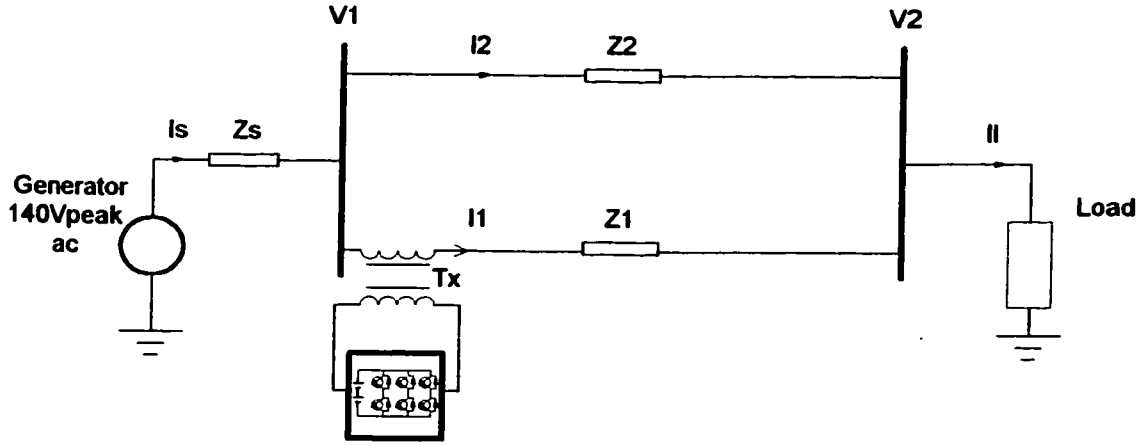

Figure 5.10 The topology for SPFC2

In this topology, the output of the BESS is connected in series with the controlled line through a series transformer as shown in Figure 5.10. In many ways the BESS here acts as the series inverter in the conventional UPFC. The output of the BESS can be controlled both in its magnitude and its waveform. It therefore provides reduction of voltage drop and phase shifting in controlling the power through the controlled line.

In this configuration, the SPFC2 can control the current I_1 and hence I_2 both in their magnitudes and waveforms, and if required the two can be made equal irrespective of the value of each line impedance. Figure 5.11(a) shows the load current and the supply voltage, whilst Figure 5.11(b) and (c) show I_1 and I_2. In this case, I_1 and I_2 are controlled to be half of the load current magnitude.

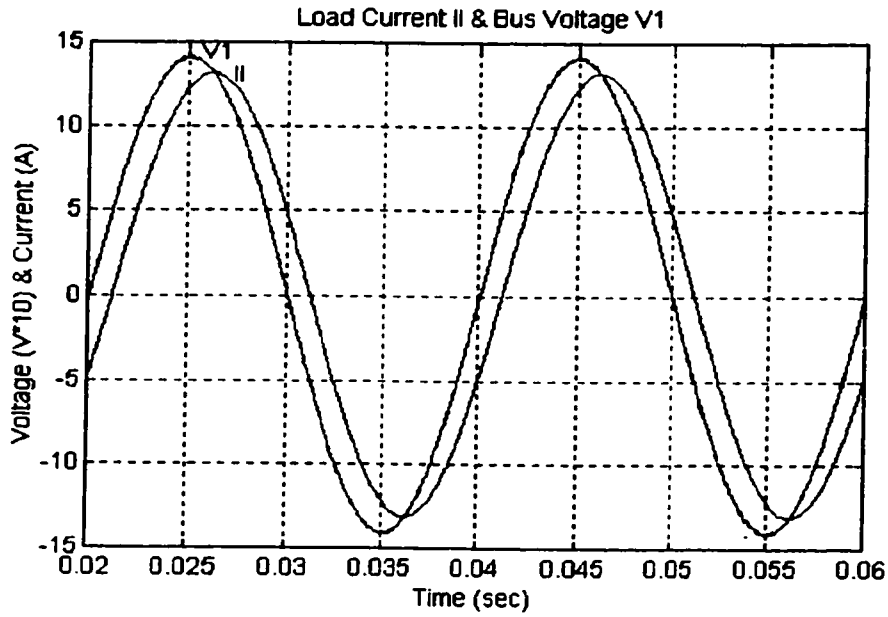

(a)

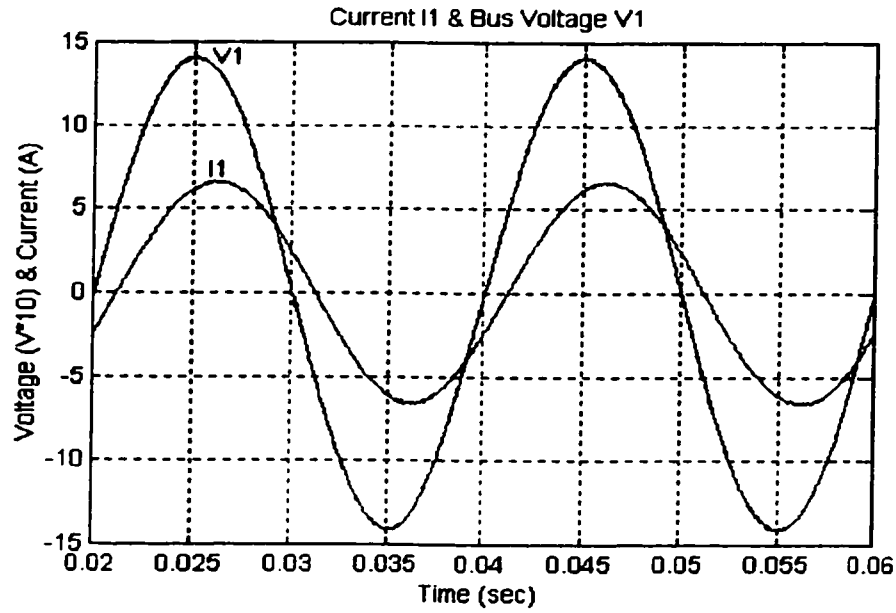

(b)

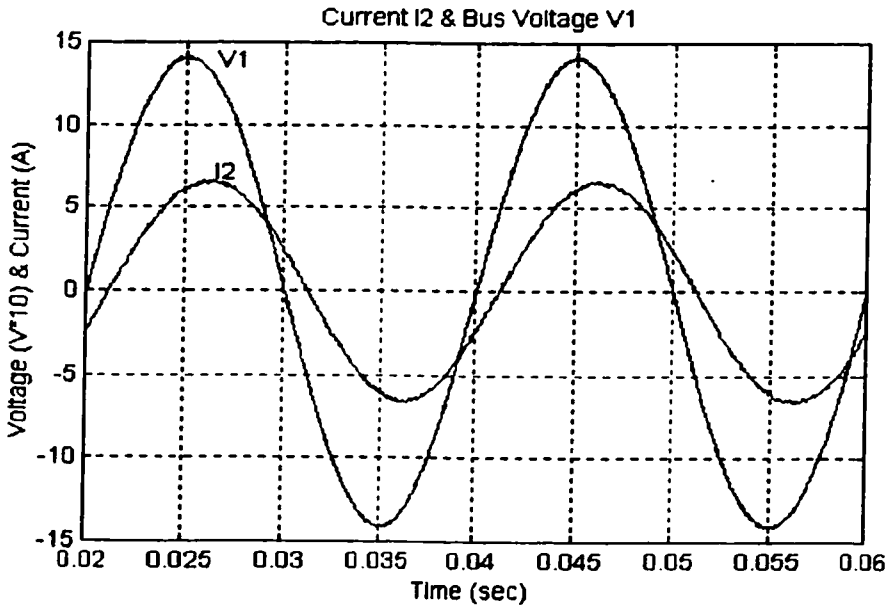

(c)

Figure 5.11 (a) Load Current (I_L) (b) Current (I_1)

(c) Current (I_2)

5.3.2.3 Experimental results of SPFC2

In this experiment, the system as shown in Figure 5.10 is connected with an inductive load. The load current, I_L, shown in Figure 5.12(a) is lagging bus-voltage, V_1, by 60 degree. If the high impedance line does not have voltage injection, more current will flow through the low impedance line and may exceed the thermal limit of the line. By voltage injection at the high impedance line, the line currents can be made balanced. The voltage injected is opposite to the voltage drop across the line allowing more current to flow through the line.

Figure 5.12(b) and (c) show the two line currents are nearly equal in magnitude and in phase with each other. They shared half of the load current which is not possible if there is no voltage injection across the line.

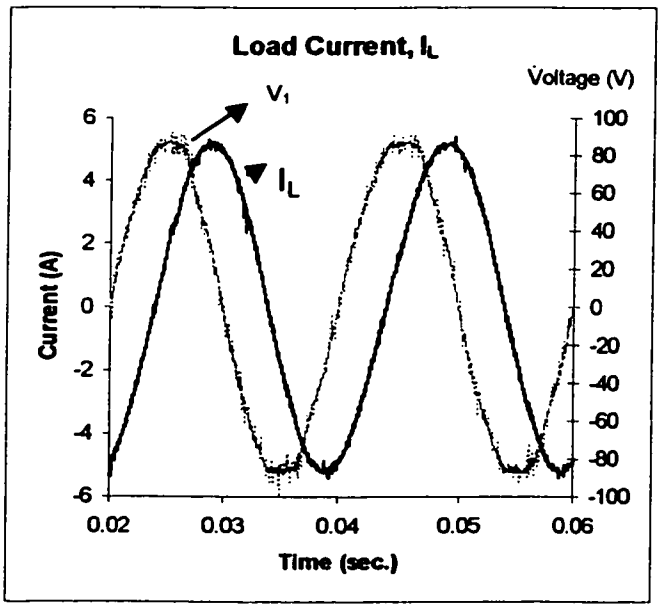

(a)

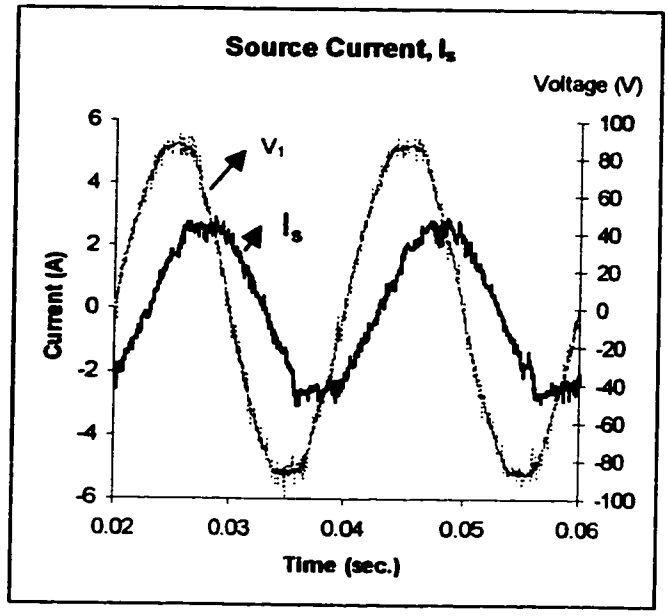

(b)

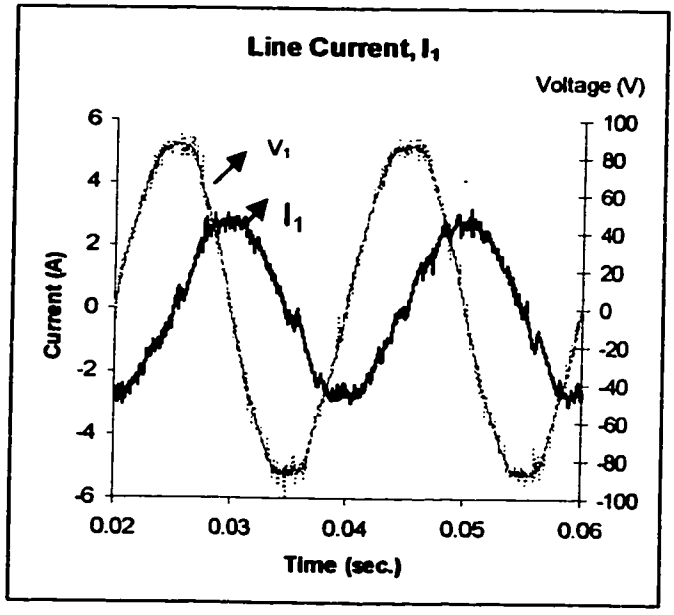

(c)

Figure 5.12 (a) Load Current, I_L; (b) Source Current, $I_s=I_2$; (c) Line Current, I_1.

5.3.3 Controlling power flow using BESS sandwiched between two inverters connected in series with the controlled line (SPFC3 – SPFC type 3)

5.3.3.1 Power flow evaluation of SPFC3

Figure 5.13 shows the SPFC3 model connected at the midpoint of a line, it is represented by two shunt injection devices connected separately at the terminals of a split line. The shunt devices provide control of two currents as well as the line parameters. It provides hypothesis voltage compensation across the split line like series voltage compensation devices.

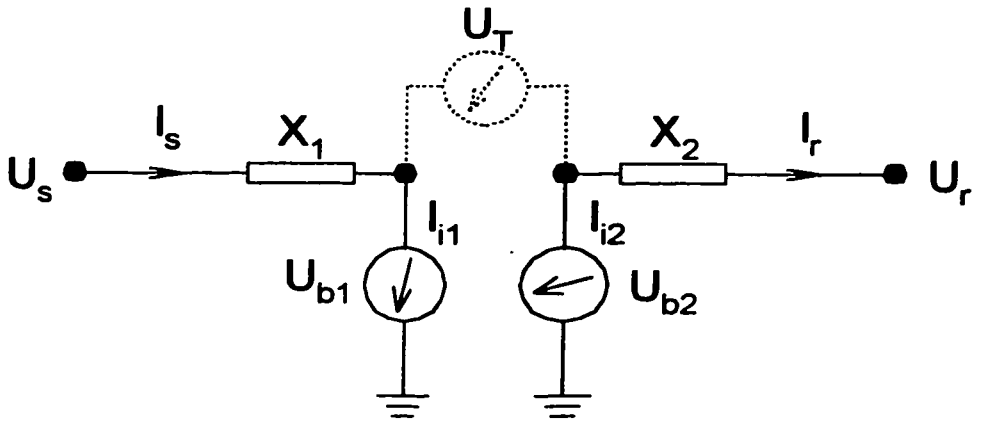

Figure 5.13 Line model of the system with SPFC3 (Two shunt connected BESSs)

Figure 5.14 shows the vector diagram of the system with SPFC3. It shows that the two currents along the lines are being controlled. And provide two current controllabilities for the system unlike normal FACTS devices.

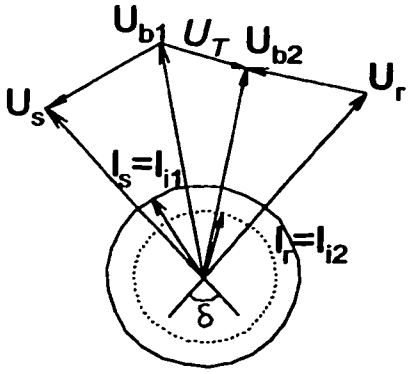

Figure 5.14 Vector diagram of the system with SPFC3

From Figure (5.13), Equations (5.15) – (5.18) can be written

$$U_s = U_{b1} + jX_1 I_s \tag{5.15}$$

$$U_{b2} = U_r + jX_2 I_r \tag{5.16}$$

$$I_s = I_{i1} \tag{5.17}$$

$$I_r = I_{i2} \tag{5.18}$$

Therefore, the power flow from the source can be represented by:

$$P_s = \mathrm{Re}(U_s I_{i1}) \tag{5.19}$$

$$Q_s = \mathrm{Im}(U_s I_{i1}) \tag{5.20}$$

5.3.3.2 Simulation results of SPFC3

In this configuration, we use back-to-back inverters with the BESS at the middle as shown in Figure 5.15. The two inverters are then controlled independently so that two independent power flows can be obtained, in contrast to SPFC1 and SPFC2 or the

conventional UPFC which can only control the power flow in **one** line only. As shown in Figure 5.15, for example, the inverter on the left controls the current I_1 and the inverter on the right controls the current I_S or I_2. In this way, I_S can be quite different from I_L and the difference is supplied by the BESS. Further, I_S can be controlled to be sinusoidal and in phase with supply voltage.

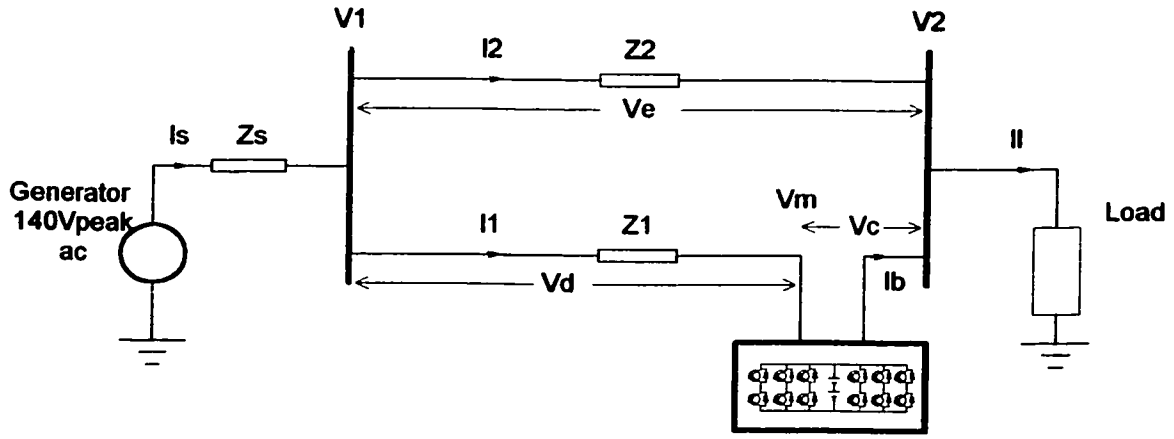

Figure 5.15 The topology for SPFC3

The main benefit of such an arrangement is that the battery can be charged at night by having I_S larger than I_L and during the day I_S is controlled to be smaller than I_L ensuring that the energy of battery is used to help the power system.

Figure 5.16(a) shows the load current I_L and the supply voltage. Note that I_L is non-sinusoidal and lags the supply voltage. Figure 5.16(b) shows the source current I_S and the source voltage. Notice that I_S is larger than I_L and is in phase with the supply voltage and sinusoidal. This clearly shows the reactive power compensation and active filtering capability of the SPFC3. Figures 5.16(c) and (d) show the currents I_1 & I_2 accordingly.

Note that I_1 is also sinusoidal and in phase with the supply voltage and its magnitude and waveform are also controlled tightly by the BESS. I_2 follows Kirchoff's current law and is therefore in phase and sinusoidal in its waveform. Figure 5.16(e) shows the current coming out of the BESS (I_b) to supply all the harmonics of the load. Since I_S is larger than I_L, the current is coming into the BESS and therefore the operation is in charging mode.

The configuration of SPFC3 has the most flexible arrangement as it provides all conventional UPFC capabilities, while at the same time gives additional benefits such as, ability to provide load leveling, damping of inter-area oscillations, help in damping transient stability, back-up electricity supply on loss of AC supply very similar to UPS applications and active power filtering to meet power quality standards.

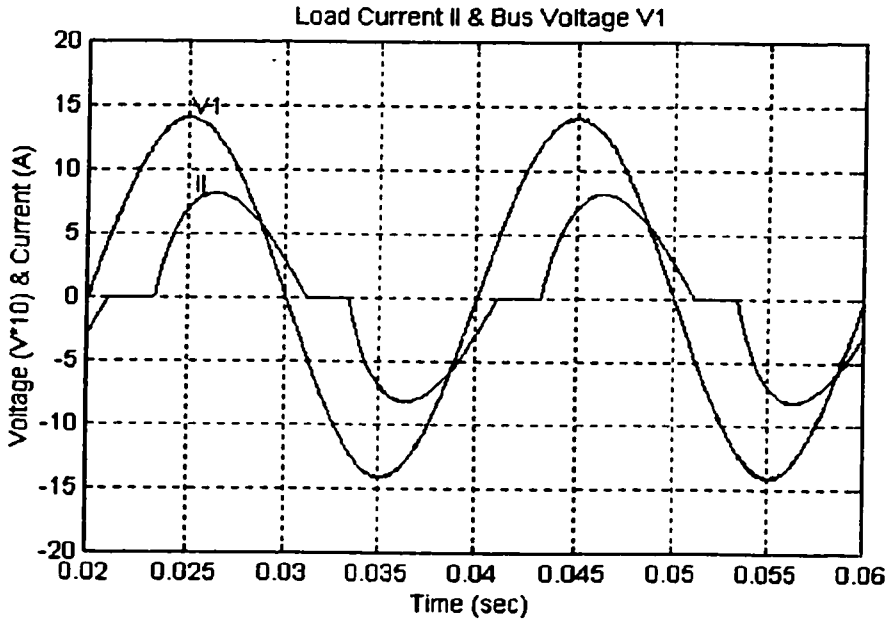

(a)

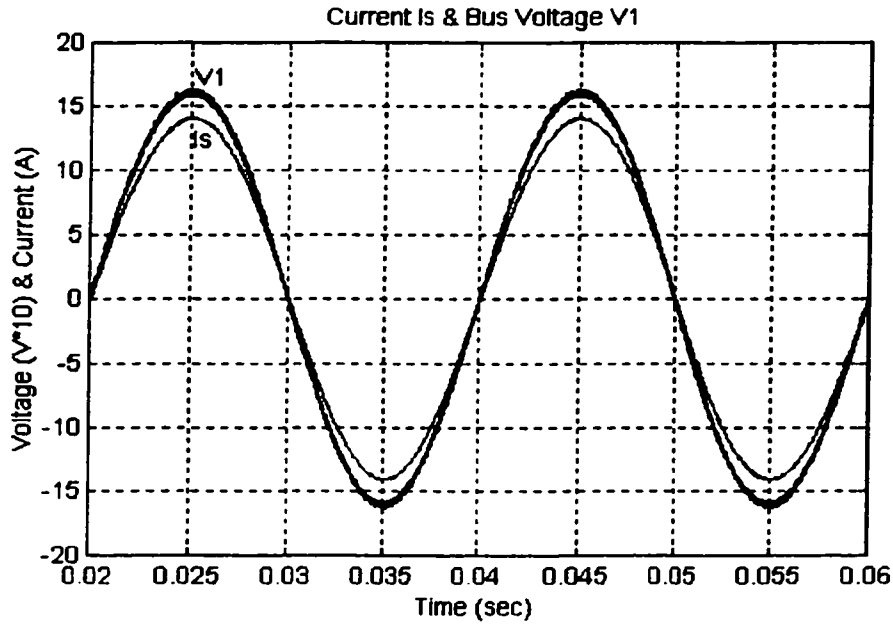
Current Is & Bus Voltage V1
V1
Is
Voltage (V*10) & Current (A)
Time (sec)
20
15
10
5
0
-5
-10
-15
-20
0.02
0.025
0.03
0.035
0.04
0.045
0.05
0.055
0.06

(b)

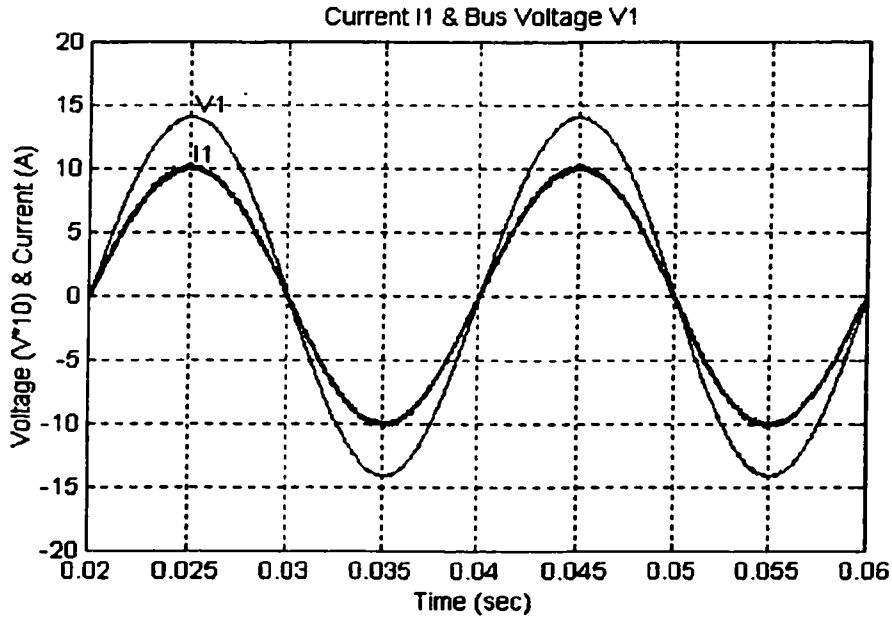
Current I1 & Bus Voltage V1
V1
I1
Voltage (V*10) & Current (A)
Time (sec)
20
15
10
5
0
-5
-10
-15
-20
0.02
0.025
0.03
0.035
0.04
0.045
0.05
0.055
0.06

(c)

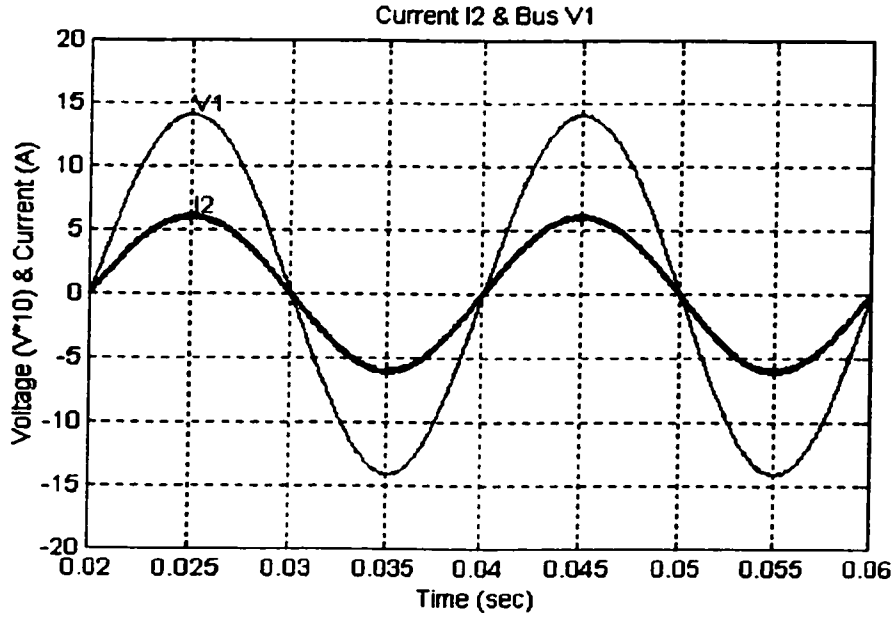

(d)

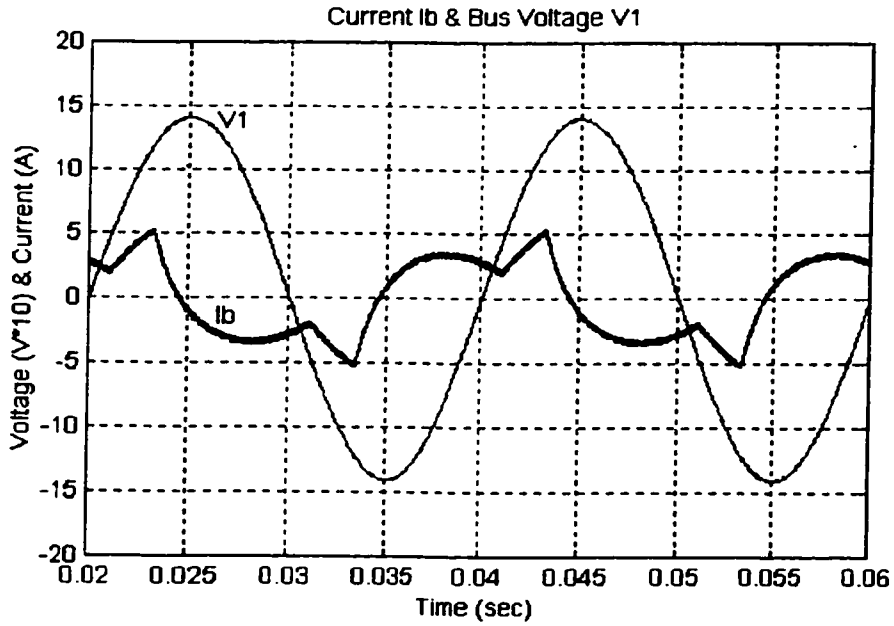

Figure 5.16(a) Load Current (I_L); (b) Source Current (I_S); (c) Current (I_1); (d) Current (I_2); (e) Current (I_b)

5.3.3.3 Experimental results of SPFC3

Figure 5.17 shows the experimental results from a laboratory implementation of SPFC3 as shown in Figure 5.15. To perform **two** currents controls of the transmission lines, one of the converter controls the source current, I_s, in phase with the bus-voltage, V_1, and the other converter controls the line current, I_2, in phase with the bus-voltage, V_1 as shown in Figures 5.17(a) and (c) respectively. The difference between the currents I_s and I_2 is the current, I_1, through line 1. In this case current I_2 is controlled almost equal to the fundamental value of the load current, I_L. Therefore, the converter at the right-hand-side provides harmonics current, as shown in Figure 5.17(d), required by the distorted load (Figure 5.17(e)).

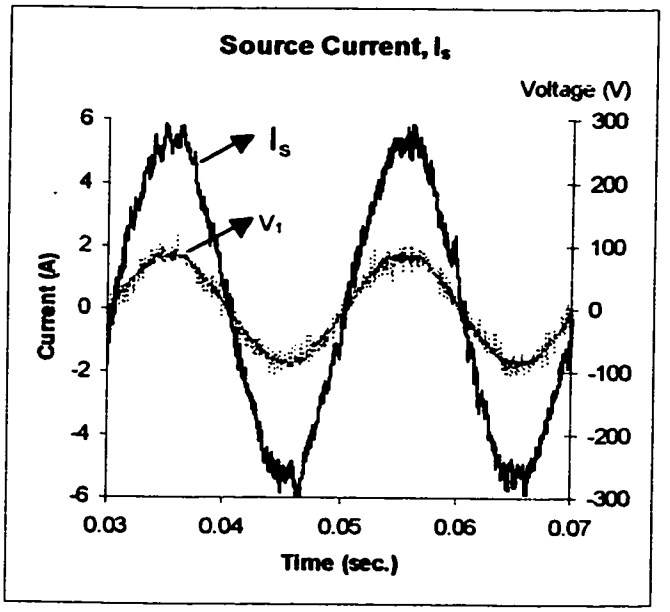

(a)

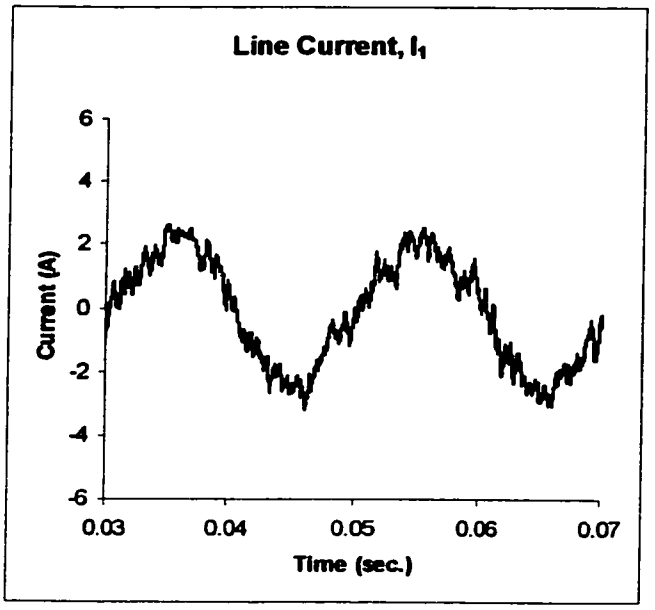
Line Current, I_1
Current (A)
6
4
2
0
-2
-4
-6
0.03
0.04
0.05
0.06
0.07
Time (sec.)

(b)

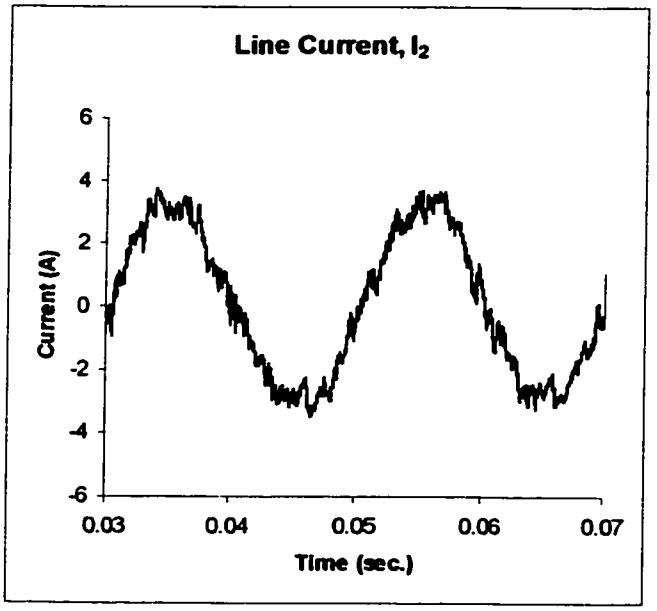
Line Current, I_2
Current (A)
6
4
2
0
-2
-4
-6
0.03
0.04
0.05
0.06
0.07
Time (sec.)

(c)

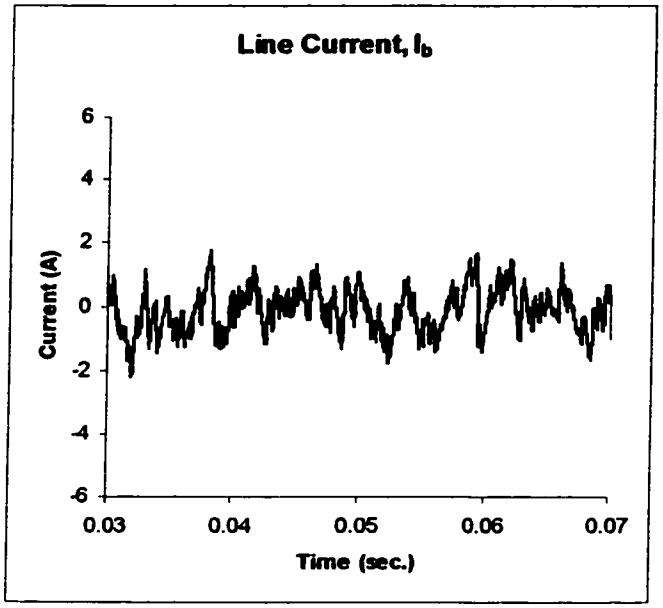

(d)

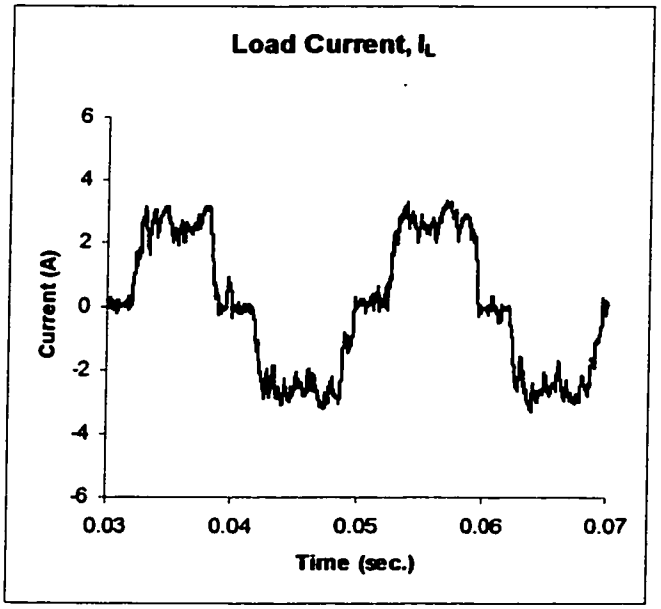

(e)

Figure 5.17 Experimental results of SPFC3 (a) Source Current, I_s; (b) Line Current, I_1; (c) Line Current, I_2; (d) Line Current, I_b; (e) Load Current, I_L.

5.4 Proof that SPFC3 provides UPFC control

This section shows that SPFC3 in Figure 5.15, provides the three main UPFC control functions, i.e. voltage drop compensation, phase shifting and shunt reactive power compensation. In addition, an experiment will show the actual waveforms when the two transmission lines are controlled with the same current magnitude and phase. As long as the line currents are being controlled the same, a set of vector diagrams will show the availability of the SPFC3 of the three main UPFC functions.

5.4.1 Voltage drop compensation

For a sinusoidal load, Figure 5.18 shows the vector diagram of V_d, V_e and V_c (see Figure 5.15) when I_1 and I_2 are controlled to be equal (a half of the load current). In this case $Z_1 = 2 \times Z_2$. Appendix 1 shows the main parameters in the calculation. Figure 5.18 shows clearly that the voltage across SPFC3, V_c, compensates for half of the voltage drop across Z_1 represented by V_d, such that $V_d - V_c = V_e$, where V_e is the voltage drop across Z_2. This means that the SPFC3 acts as a continuously controlled voltage drop compensator.

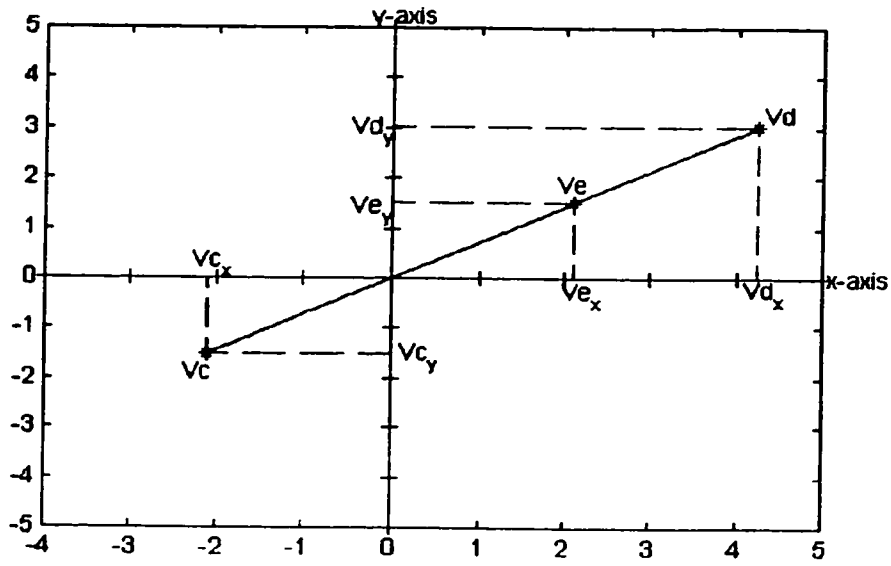

Figure 5.18 Vector diagram of V_d, V_e and V_c

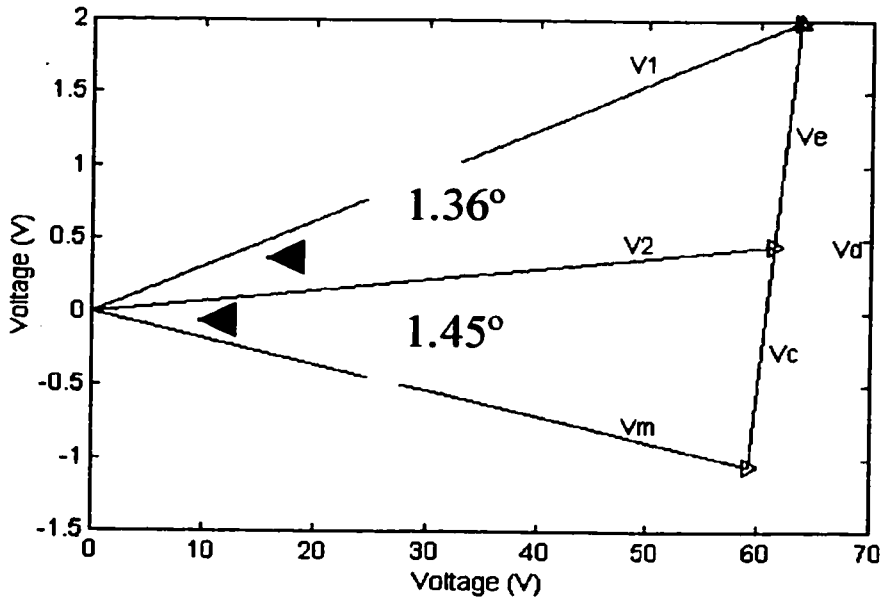

Figure 5.19 Phasor diagram of V_1, V_2 and V_m

5.4.2 Phase Angle Control

From the simulation, the values of V_1, V_2 and V_m (see Figure 5.15 and Figure 5.18) are as follows:

$V1=63.5\angle 1.79°$

$V2=61.3\angle 0.43°$

$Vm=59.2\angle -1.02°$

From this, we can conclude that the voltage across SPFC3, i.e. V_c, has shifted the angle across Z_l from (1.79°-0.43°) to (1.79°-(-1.02°)), i.e. from 1.36° to 2.81°. This shows that SPFC3 acts as a phase shifter. We need to note as well that the magnitude of the voltage has changed from V_2 to V_m, so actually the voltage across SPFC3 can be considered as a series voltage, whose magnitude and angle can be tightly controlled at high speed. This is exactly the definition of the output voltage of the series converter of the conventional UPFC.

5.4.3 Shunt Reactive Power Compensation

Since I_1 and I_s (hence I_2) in Figure 5.15 are tightly controlled irrespective of the load current I_L, any changes in reactive power load must be compensated by the BESS, i.e. the SPFC3 acts as a continuously variable shunt compensation that compensates for any changes in load reactive power. Actually it compensates for any changes in active power as well, a function not available in the conventional UPFC.

5.4.4 Experimental result of SPFC3 for providing UPFC functions

Figures 5.20(a)-(e) show the experimental results of the laboratory implementation of SPFC3 when the two line currents are controlled at the same current level. Figure 5.20(a) shows the source current is in-phase with the bus-voltage V_1 with peak current at 4 A. Where current I_1 and I_2 are in-phase and each is a half of the source current, I_s. In this experiment, an inductive load is used (see Figure 5.20(e)) with current peak at 6 A. The line current I_2 is in phase with the bus voltage V_1 and the reactive current is compensated by the SPFC3 which is shown in Figure 5.20(d).

Although in this case lines 1 and 2 are of unequal impedance, the currents flowing through them are almost the same. This is because line 1 is compensated by SPFC3 having voltage drop compensation and phase shift control capability that is exactly the same function provided by the conventional UPFC. On the other hand, even if the load is highly inductive, SPFC3 can also provide all the inductive part of the load without influencing the line currents.

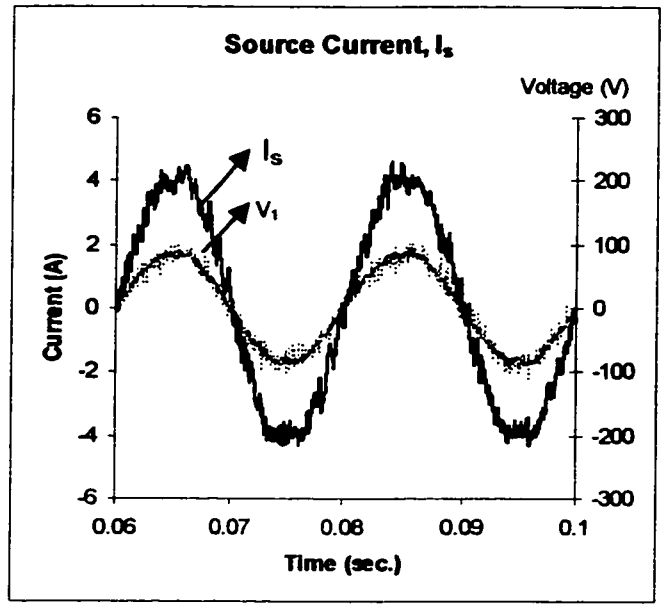
Source Current, I_s
Voltage (V)
I_S
V_1
Current (A)
Time (sec.)
6
4
2
0
-2
-4
-6
300
200
100
0
-100
-200
-300
0.06
0.07
0.08
0.09
0.1

(a)

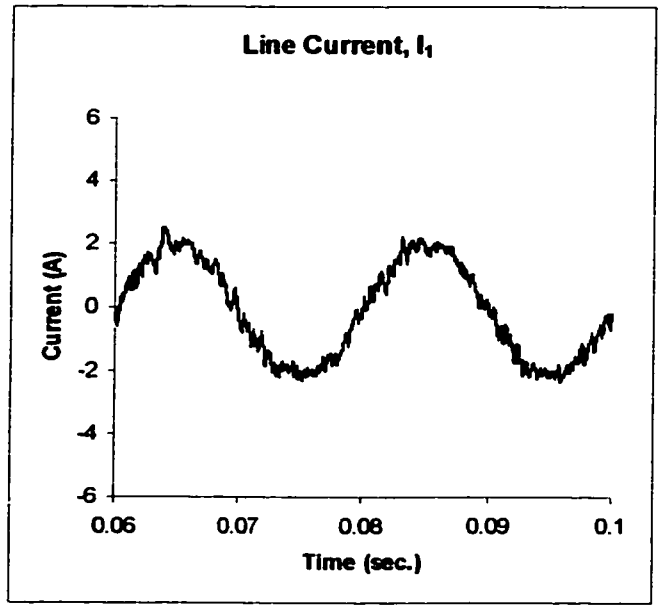
Line Current, I_1
Current (A)
Time (sec.)
6
4
2
0
-2
-4
-6
0.06
0.07
0.08
0.09
0.1

(b)

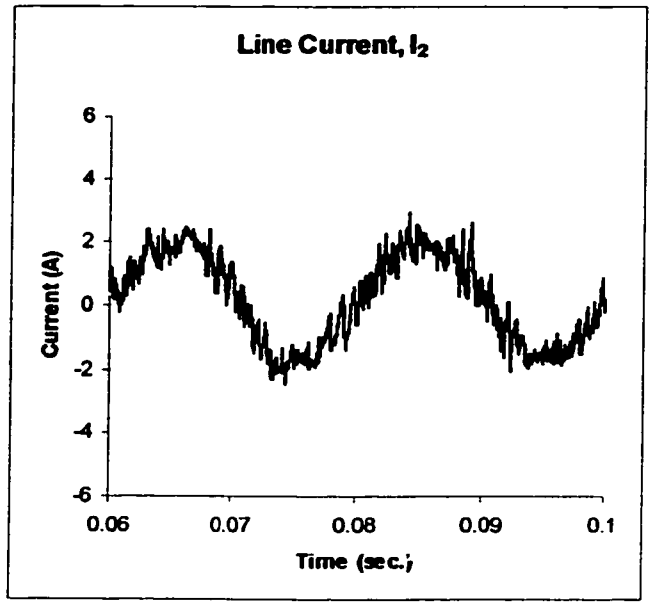
Line Current, I_2
Current (A)
6
4
2
0
-2
-4
-6
0.06
0.07
0.08
0.09
0.1
Time (sec.)

(c)

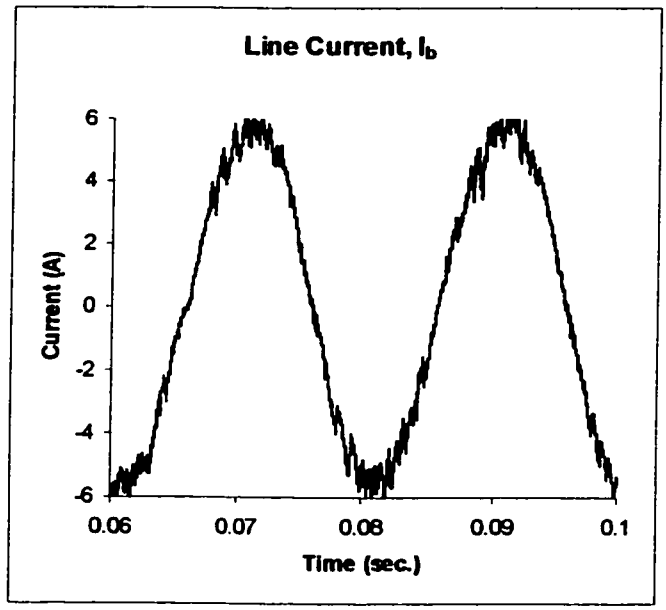
Line Current, I_b
Current (A)
6
4
2
0
-2
-4
-6
0.06
0.07
0.08
0.09
0.1
Time (sec.)

(d)

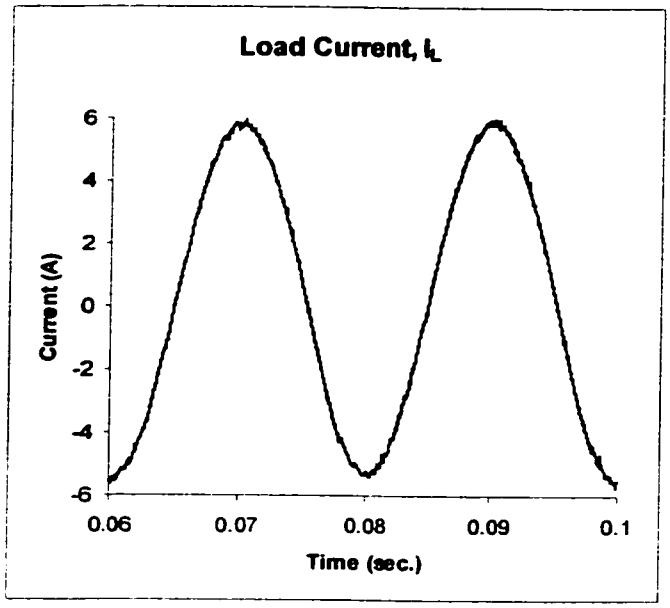

(e)

Figure 5.20 (a) Source Current, I_s; (b) Line Current, I_1; (c) Line Current, I_2; (d) Line Current, I_b; (e) Load Current, I_L.

5.4.5 The benefits of SPFC3 to that of UPFC in Power System Applications

In the previous section, it was demonstrated that SPFC3 could provide all the available functions of UPFC such as voltage drop compensation, phase angle control and shunt reactive power compensation. In addition, it can also provide real power support that is very useful for power system operations, frequency control and damping load fluctuations. Besides, with the direct control of two line currents, it provides two lines power flow control instead of only one that UPFC does. On the other hand, it can also provide instantaneous filtering action to a distorted load. Since SPFC3 is an energy storage device that can provide both real and reactive power support to the utility grid, unlike FACTS devices that can only provide reactive power support and divert real

power, a great flexibility can be obtained not only to delay the need to build more transmission lines but also to delay the need to build power plants and enable neighboring utilities and regions to economically and reliably exchange power.

5.5 Conclusions and discussions

This chapter discusses several topologies of the BESS connection to the grid that provide UPFC functions while at the same time makes use of the high-speed control of the active and reactive power of the BESS to provide load leveling for energy management purposes. The chapter demonstrated that SPFC3 can provide all the standard functions in UPFC such as voltage drop compensation, fully controllable series voltage (both magnitude and angle) and shunt reactive power compensation. Further, it can also provide other functions not currently available in conventional UPFC. Acting as a static generator it can also provide back-up support and 'negative load-shedding' or spinning reserve capability. The control strategy provides inherent active filtering and reactive power compensation to the power system. When sufficient numbers are placed at the distribution level, the load demand seen by the transmission system can be controlled in a predetermined manner to reduce operating cost, improve load factor, provide improved power system operation and control and increase reliability of the power system, particularly, during system collapse or voltage instability. Having a single device that can provide all these functions provides a real flexible AC system – a storage form of the Power Flow Controller.

CHAPTER 6 NOVEL TECHNIQUES TO IMPROVE THE PERFORMANCE OF BESS

One of the greatest pains to human nature is the pain of a new idea.

Bagehot, Walter

Physics and Politics

CHAPTER 6 NOVEL TECHNIQUES TO IMPROVE THE PERFORMANCE OF BESS

6.1 Introduction

Having demonstrated the multi-function capability of the proposed BESS, the next stage of the research involves means on improving the performance of the BESS. There are two areas where the performance can be improved:

a) Improving the efficiency of the BESS by reducing the switching losses using soft switching technique.

b) Reducing the spread of high frequency harmonics in the source current due to the hysteresis control of the BESS.

6.2 Soft-switched battery energy storage system

Traditional hard-switching inverters inherently present several problems during switching. More specifically, current spike will occur due to the diode recovery and stray capacitor charging and discharging during turn-on. While during turn-off, the device voltage rises over the dc bus voltage owing to the leakage inductance in the circuit. This turn-off effect varies among the types of devices, depending upon the turn-off delay and current fall time can be reduced by paralleling a capacitor across the device. However, adding a capacitor across the device will, on the other hand,

significantly increase the turn-on current. The high turn-on current, as a result, increases the turn-on loss and causes switching noise.

To eliminate the switching losses and to reduce the switching noise, the state-of-the-art soft-switching inverter is employed. The soft-switching inverters have been in use for more than a decade, among them, the resonant dc link inverter is the most well known. The resonant dc link (RDCL) inverter employs a resonant inductor-capacitor circuit between the dc source and the inverter to create zero voltage intervals across the inverter. However, the peak voltage can reach twice of the supply voltage, and as a result, can increase the conduction loss of the inverter. Several improvements have been proposed to overcome the drawback of the ordinary RDCL inverter (Divan, D.M., 1989), but they all suffered from over-voltage and reliability problems.

To avoid the over-voltage problem in RDCL inverters, several resonant methods have been proposed (He, J. and Mohan, N., 1989; Lai, J.S., Young, R.W., Ott, G.W., Mckeever, J.W. and Peng, F.Z., 1996). They employ one or more auxiliary switches for zero-voltage excitation. For instance, the auxiliary resonant commutated pole (ARCP) inverter uses three sets of auxiliary circuits connected across the ac terminals of the inverter. Although the voltage stress and the current stress can be reduced, the number of devices required makes the system unreliable as well as complicated the control. Another approach, so called the parallel resonant dc link inverter (PRDCL), like the RDCL creates zero voltage intervals across the dc terminals. The auxiliary circuit is connected in parallel with the inverter but more devices are required. This type of soft-switching technique has a voltage stress equal to the supply voltage. However, the

control is dependent on the design of the resonant circuit, but once designed, it provides a great flexibility in the control process.

6.2.1 Soft-switching for PWM converter

In the overall design, the resonant circuit mainly creates resonant swing across switches before it turns on/off. There are two things that have to be achieved during the resonant swing. First, the resonant period should be as short as possible, so that high frequency switching can be obtained (Wei, H. and Ioinovici, A., 1998). At the same time the voltage and current stress on the switches should be minimized. These two things are very dependent on the design of the resonant circuit.

A resonant circuit basically comprises of a L-C tank that falls into two modes of operation, the parallel mode and the series mode as shown in Figure 6.1.

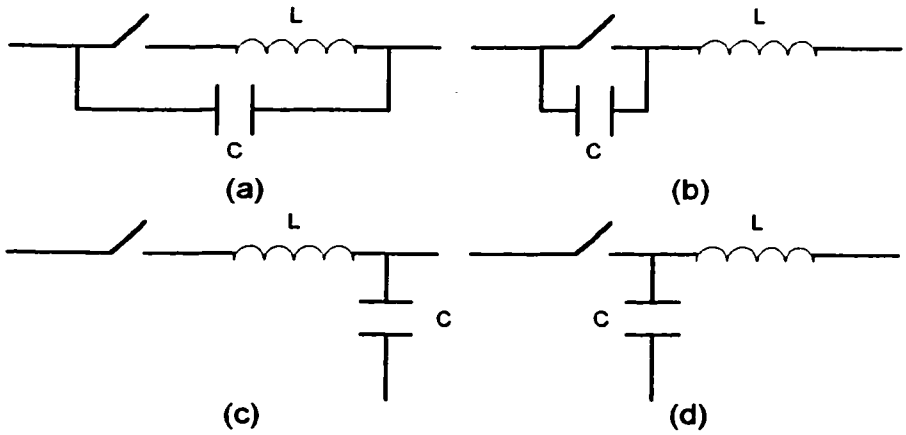

Figure 6.1 Basic resonant tanks

From Figure 6.1, only the parallel resonant circuit shown in Figure 6.1(a) will be discussed. The initial inductor-current direction, the polarity of the capacitor voltage and the current direction of the inverter determine the resonant time and the voltage/current stress on the switch. Since there are inductors connected between the inverter and the ac system can be considered as a current source that can flow in two directions, one going out of the battery bank to discharge the energy in BESS, and the other going into the battery bank to charge the batteries. Let us initially assume that the BESS current is going into the batteries as shown in Figure 6.2, which is referred to as the Type A direction. Figure 6.2 shows the BESS is connected to a resonant L-C circuit.

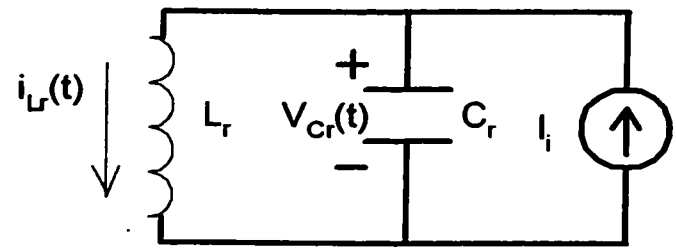

Figure 6.2 Equivalent circuit of the resonant stage (Type A direction)

Using the KCL, the following differential equations can be obtained:

$$I_i = L_r C_r \frac{d^2 I_{Lr}(t)}{dt^2} + I_{Lr}(t) \tag{6.1}$$

$$V_{Cr}(0) = V_{Co} \tag{6.2}$$

$$\frac{dI_{Lr}(t)}{dt}_{|t=0} = \frac{V_{Co}}{L_r} \tag{6.3}$$

Solving Equations (6.1), (6.2) & (6.3), we find

$$I_{Lr}(t) = I_i - \sqrt{(I_i - I_{Lo})^2 + (V_{co}/wL_r)^2}\cos(wt + \beta) \tag{6.4}$$

$$V_{Cr}(t) = wL_r\sqrt{(I_i - I_{Lo})^2 + (V_{co}/wL_r)^2}\sin(wt + \beta) \tag{6.5}$$

Here

$$\beta = \tan^{-1}\frac{V_{co}}{wL_r(I_i - I_{Lo})} \tag{6.6}$$

In a parallel resonant link, the aim of the resonant circuit is to create a zero voltage interval at the dc-link. So the time required to achieve the zero voltage across the dc-link is dependent on Equation (6.5) with the condition that $V_{Cr}(T_a)=0$.

By calculation, we have

$$T_a|_{V_{Co}=0} = \frac{-1}{w}\tan^{-1}\frac{V_{co}}{wL_r(I_i - I_{Lo})} \tag{6.7}$$

The peak resonant inductor current I_p can be obtained by

$$I_p = I_{Lr}(T_a) = I_i - \sqrt{(I_i - I_{Lo})^2 + (V_{co}/wL_r)^2} \tag{6.8}$$

However, the BESS current can have the opposite direction when it is discharging which is referred to the Type B direction.

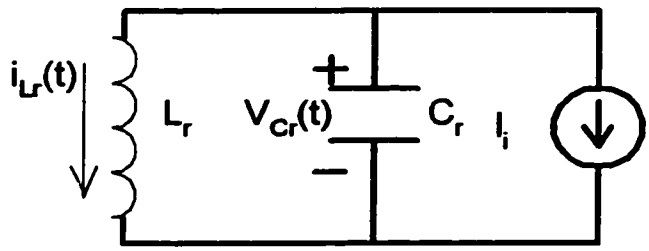

Figure 6.3 Equivalent circuit of the resonant stage (Type B direction)

From Figure 6.3, employing KCL again, the following differential equations can be obtained:

$$-I_i = L_r C_r \frac{d^2 I_{Lr}(t)}{dt^2} + I_{Lr}(t) \tag{6.9}$$

$$V_{Cr}(0) = V_{Co} \tag{6.10}$$

$$\frac{dI_{Lr}(t)}{dt}_{|t=0} = \frac{V_{Co}}{L_r} \tag{6.11}$$

Solving Equations (6.9), (6.10) & (6.11),

$$I_{Lr}(t) = -I_i + \sqrt{(I_i + I_{Lo})^2 + (V_{co} / wL_r)^2}\cos(wt - \beta) \tag{6.12}$$

$$V_{Cr}(t) = -wL_r\sqrt{(I_i + I_{Lo})^2 + (V_{co}/wL_r)^2}\sin(wt - \beta) \quad (6.13)$$

Here

$$\beta = \tan^{-1}\frac{V_{co}}{wL_r(I_i + I_{Lo})} \quad (6.14)$$

Again, the aim of the resonant circuit is to create a zero voltage interval at the dc-link. So, the time required to achieve the zero voltage across the dc-link is dependent on Equation (6.13) with the condition of $V_{Cr}(T_b)=0$.

By calculation,

$$T_b\,|_{V_{Cr}=0} = \frac{1}{w}\tan^{-1}\frac{V_{co}}{wL_r(I_i + I_{Lo})} \quad (6.15)$$

The peak resonant inductor current I_p is also obtained by

$$I_p = I_{Lr}(T_b) = -I_i + \sqrt{(I_i + I_{Lo})^2 + (V_{co}/wL_r)^2} \quad (6.16)$$

In this analysis, the time required for the dc-link to reach zero voltage in both cases is different. By substituting the following BESS and the proposed resonant circuit parameters into Equations (6.7) and (6.15) respectively: V_{CO}=230 V; L_r=2uH; C_r=18nF; I_i=10A; I_{LO}=40A; w=5.27x10^{6}rad, it is clear that the time required by Type A is longer than that by Type B. So care has to be taken to ensure that the dc link voltage actually reaches zero while performing the zero voltage switching of the main circuit in both directions.

The next section describes the whole process of the soft-switched inverter operation assuming that the BESS current is in Type B direction.

6.2.2 Configuration of the soft-switched battery energy storage system

Figure 6.4 shows a single-phase soft-switched battery energy storage system. The soft switching circuit comprises of three active switches, two diodes, a resonant inductor and a resonant capacitor connected between the dc source and the inverter. One active switch, S, is connected in series with the dc source and the other switches (Sa1, Sa2, Da3 and Da4) form an auxiliary circuit connected across the inverter. The aim of this circuit is to provide a parallel resonant across the dc link. In addition, the switches create zero turn on and zero turn off for themselves by means of soft switching.

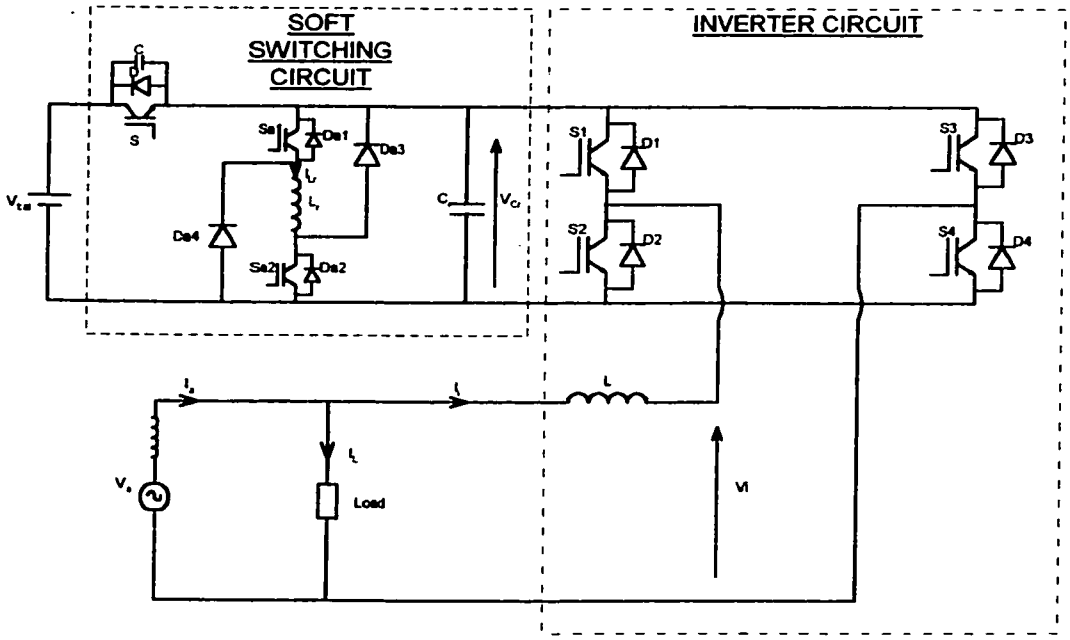

Figure 6.4 Circuit diagram of single-phase soft switched storage system

6.2.2.1 The operating principle of the soft-switching circuit

The equivalent circuit of Figure 6.4 is shown in Figure 6.5 by assuming that:

(1) The inductor L is much larger than the resonant inductor L_r.

(2) The battery capacitance is much larger than both the resonant capacitor C_r and the snubber capacitor C.

The characteristic impedance and the resonant frequency are:

$$z = \sqrt{\frac{L_r}{C_r}} \tag{6.17}$$

$$w_r = \frac{1}{\sqrt{L_r C_r}} \tag{6.18}$$

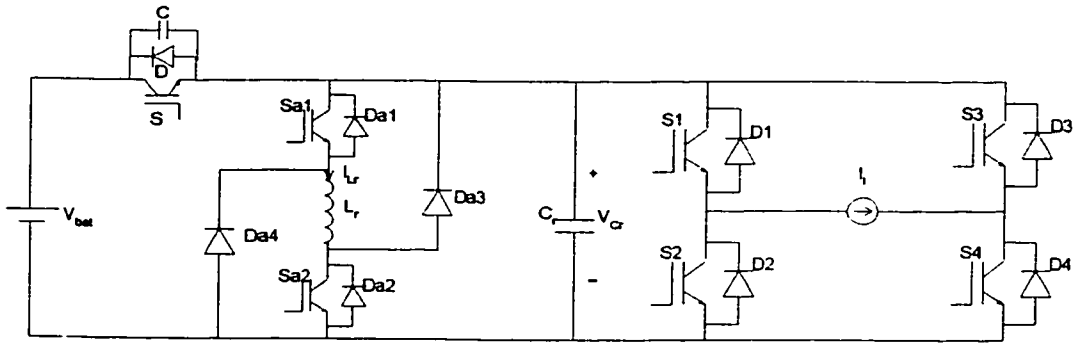

Figure 6.5 Equivalent circuit of soft-switched BESS

Based on the circuit shown in Figure 6.5, it is possible to describe the mode of transition step by step. Figure 6.6 shows the ideal gate signals including switches S1, S2, S and Sa1. Based on these switching strategies, the resonant inductor current and the resonant

capacitor voltage can be created. These switching actions can be further divided into six modes and each mode will be discussed accordingly.

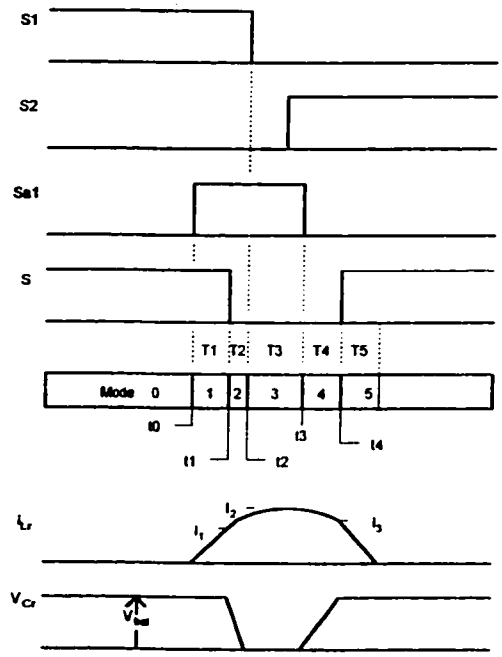

Figure 6.6 Switching strategies of the operating modes

The soft-switched BESS operation can be divided into six modes and the diagrams for each mode are shown in Figures 6.7(a) – (f).

Mode 0: - This is the initial stage of the circuit when main switches, S, S1 and S4, are ON (S, S1, S4 – ON) and auxiliary switches, Sa1 and Sa2, are OFF (Sa – OFF) as shown in Figure 6.7(a). In this mode:

$$I_{Lr}(t) = 0 \tag{6.19}$$

$$V_{cr}(t) = V_{bat} \tag{6.20}$$

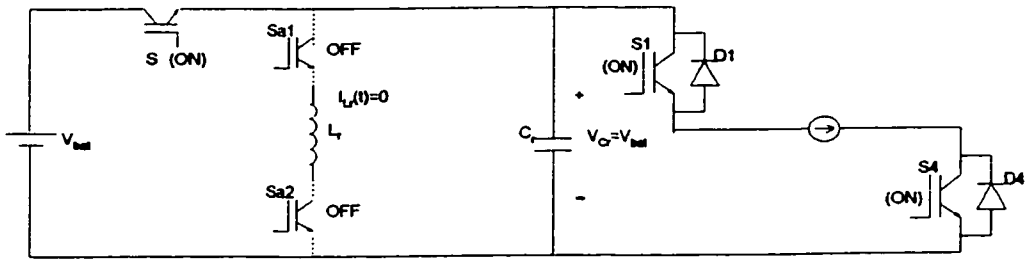

(a)

Mode 1: - The transition process starts at time t0, when the auxiliary switches gate signals are high, and Sa1 and Sa2 are ON as shown in Figure 6.7(b). In this mode resonant inductor current, I_{Lr}, increases linearly.

$$I_{Lr}(t)=\frac{V_{bat}}{L_r}t \tag{6.21}$$

$$V_{cr}(t)=V_{bat} \tag{6.22}$$

The time for L_r to charge up from 0 A to I_1 ($I_{Lr}(T_1)=I_1$) is:

$$T_1=\frac{L_r I_1}{V_{bat}} \tag{6.23}$$

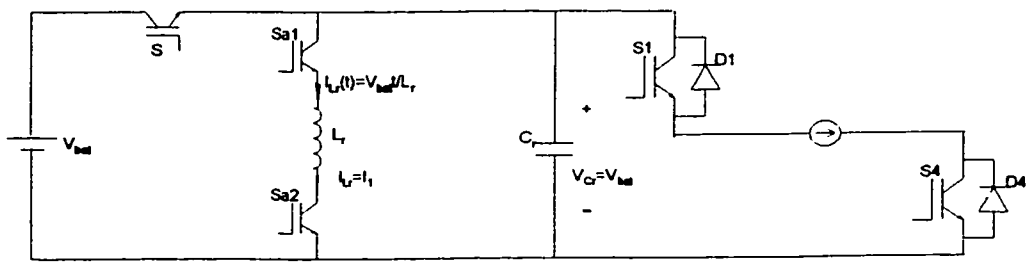

(b)

Mode 2: - This mode starts at time t1, when the inductor current is already charged to I_1, and the switch S is then turned off at zero current as shown in Figure 6.7(c) (S – OFF). In this mode resonance between L_r and C_r drives the resonant capacitor voltage, V_{Cr}, to zero. From Equations 6.12 – 6.14,

$$I_{Lr}(t) = -I_i + \sqrt{(I_i + I_1)^2 + (V_{bat} / w_r L_r)^2}\cos(w_r t - \beta) \tag{6.24}$$

$$V_{Cr}(t) = -w_r L_r \sqrt{(I_i + I_1)^2 + (V_{bat} / w_r L_r)^2}\sin(w_r t - \beta) \tag{6.25}$$

The time required for V_{cr} to resonate from V_{bat} to 0 V

$$V_{cr}(T_2) = 0 \Rightarrow T_2 = \frac{1}{w_r}\tan^{-1}\frac{V_{bat}}{w_r L_r (I_i + I_1)} \tag{6.26}$$

and the peak resonant inductor current,

$$I_2 = I_p = I_{Lr}(T_2) \tag{6.27}$$

$$I_2 = I_p = \sqrt{(I_i + I_1)^2 + (V_{bat}/Z)^2} - I_i \tag{6.28}$$

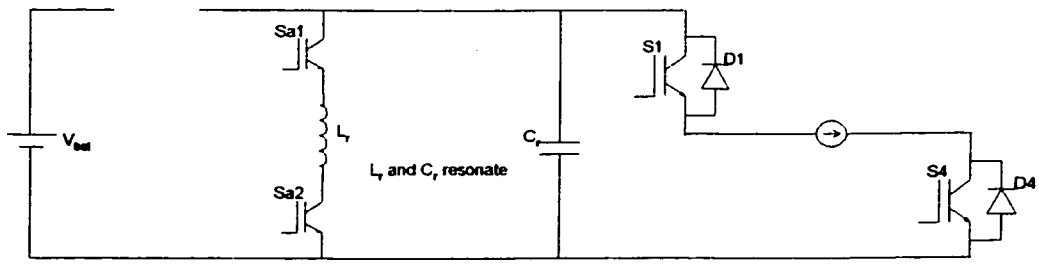

(c)

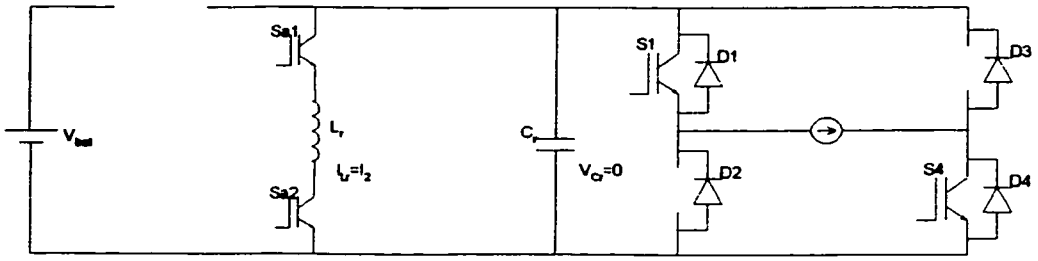

(d)

Mode 3: - When V_{Cr} reaches zero as shown in Figure 6.7(d), S1 turns OFF at time t2 (see Figure 6.7(e)) and then S2 turns ON with zero voltage switching after the dead time as shown in Figure 6.7(f). In this mode:

$$I_{Lr}(t) = I_p = I_2 \tag{6.29}$$

$$V_{cr}(t) = 0 \tag{6.30}$$

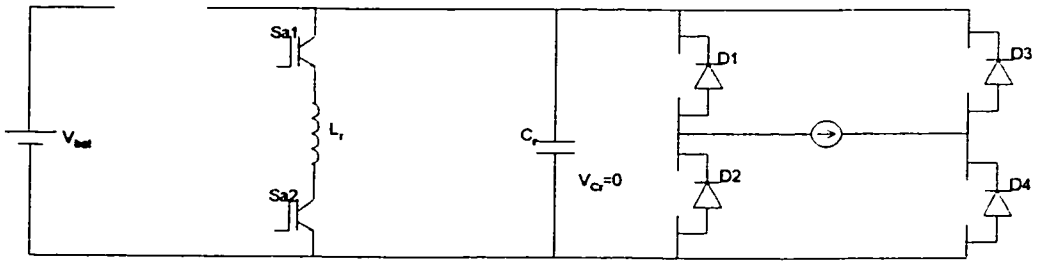

(e)

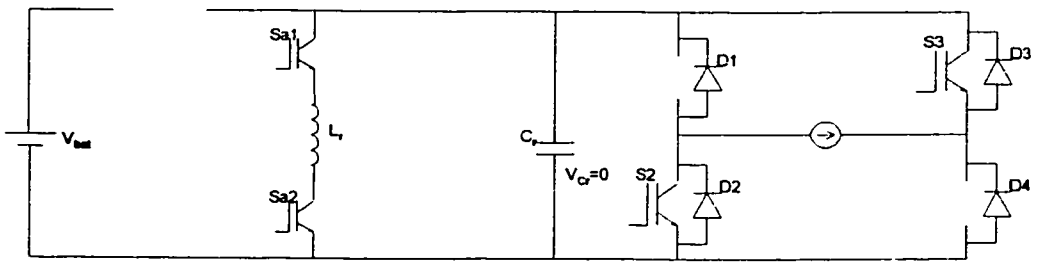

(f)

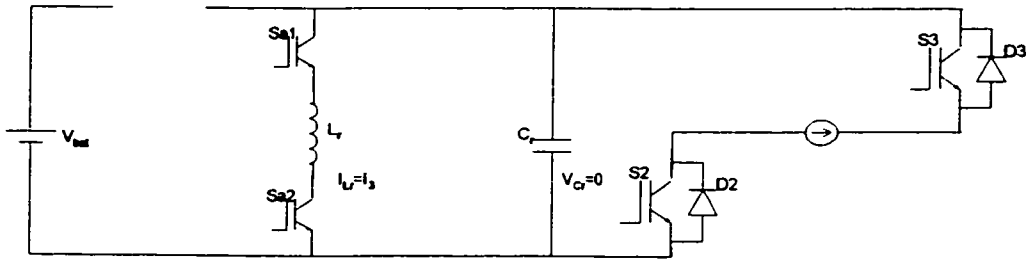

(g)

Mode 4: - After the zero voltage transition between the switches S1 and S2 (S4 and S3 also), auxiliary switches Sa1 and Sa2 turn OFF with zero current (Sa – OFF) simultaneously at time t3 as shown in Figure 6.7(h). The current in the resonant inductor drives the diodes Da3 and Da4 to conduct and energy is released to charge the resonant capacitor.

$$I_{Lr}(t) = (I_2 - I_i)\cos(w_r t) + I_i \tag{6.31}$$

$$V_{cr}(t) = (I_2 - I_i)Z\sin(w_r t) \tag{6.32}$$

$$V_{cr}(T_4) = V_{bat} \tag{6.33}$$

$$I_{Lr}(T_4) = I_3 \tag{6.34}$$

The time required for V_{cr} to resonate from 0 V to V_{bat} can be formulated as:

$$T_4 = \frac{1}{w_r}\sin^{-1}\frac{V_{bat}}{w_r L_r (I_2 - I_i)} \tag{6.35}$$

The resonant inductor current now equals to:

$$I_3 = I_{Lr}(T_4) \tag{6.36}$$

$$I_3 = \sqrt{(I_2 - I_i)^2 - (V_{bat}/Z)^2} + I_i \tag{6.37}$$

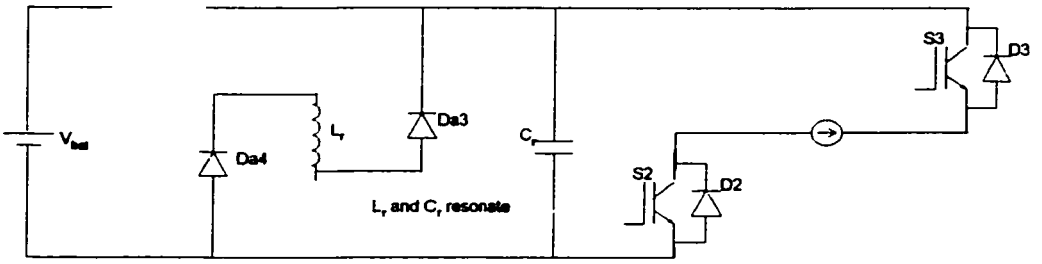

(h)

Mode 5: - When V_{Cr} rises to the battery voltage, V_{bat}, at time t4, diode D turns on naturally (see Figure 6.7(i)), then the main switch S can be turned ON at zero voltage as shown in Figure 6.7(j). In this mode:

$$V_{cr}(t) \geq V_{bat} \tag{6.38}$$

$$I_{Lr}(t) = -\frac{V_{bat}}{L_r} t + I_3 \tag{6.39}$$

$$I_{Lr}(T_5) = 0 \tag{6.40}$$

$$T_5 = \frac{L_r I_3}{V_{bat}} \tag{6.41}$$

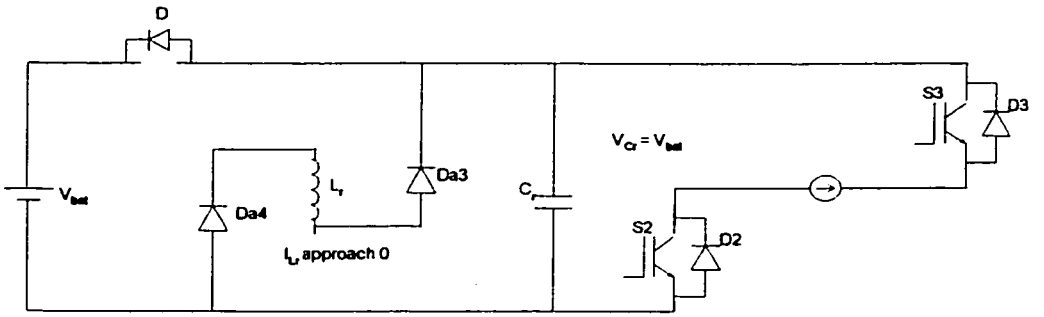

(i)

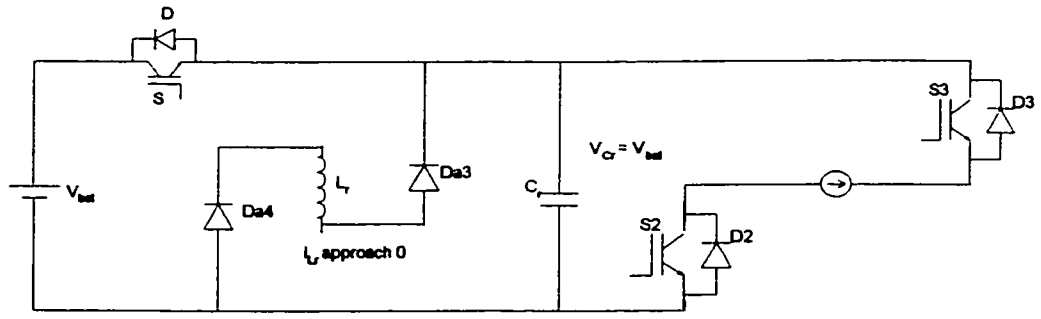

(j)

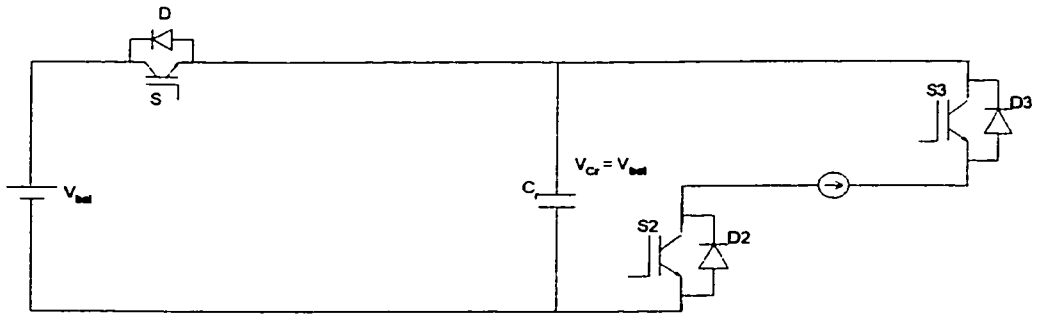

(k)

Figure 6.7 Mode diagrams of the soft switched BESS operation

Figures 6.7(a) – (k) show the operation of one switching cycle of the soft-switched BESS. In the next section the operation is simulated using the Pspice simulation package.

6.2.3 Simulation results of the soft-switched BESS using PSPICE

Figure 6.8(a) shows the switching waveforms of the gate signals S1 and S2. In Figure 6.8(b) the dc-link voltage and the resonant inductor current are shown. It shows that the

inductor current first rises to I_1, and then due to resonance reaches to its peak current value I_2, while at the same time the dc-link voltage drops to zero which is sustained until the successful transition of switches S1 and S2. After that, the auxiliary switches (Sa1 and Sa2) are turned off and the energy stored in the inductor is released to charge the resonant capacitor. When the dc-link voltage is slightly higher than the dc source, the diode, D, turns on naturally at zero current. Then the main switch can be turned on with zero voltage across it. This process repeats even if the reverse transition of switch from S2 to S1 happens. As described in section 6.2.1, the direction of inverter current, I_i, will influence the time required for resonant capacitor, C_r, to reach zero voltage. Before the transition from switch S2 to S1 (S3 to S4), the initial state of the inverter current direction is in Type A (i.e. requires longer time for C_r to reach zero voltage). That is why the time setting should satisfy I_i for both Type A and B as mentioned in section 6.2.1.

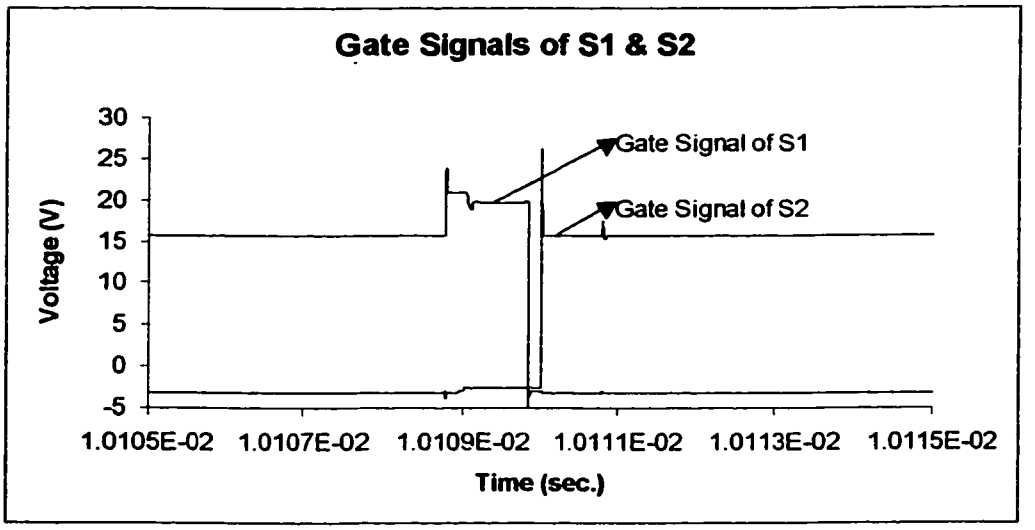

(a)

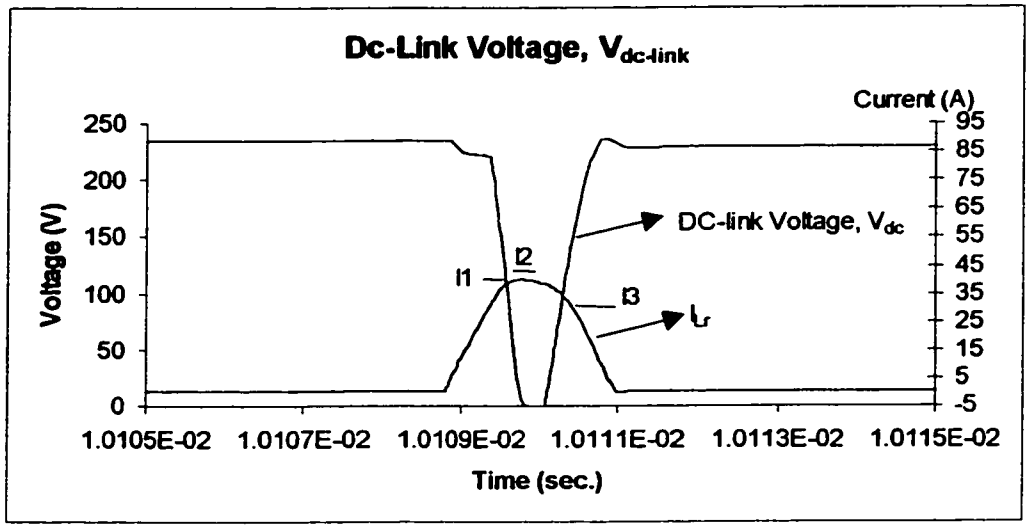

(b)

Figure 6.8 Simulation waveforms of one switching period (a) Gate Signals S1 & S2; (b) DC-link voltage

6.2.3.1 Comparison between the hard and soft switching performances of the inverter switches

Without the soft switching circuit, the system shown in Figure 6.4 becomes a conventional hard switching inverter. With all other parameters remaining the same, the switching conditions of switches S1 and S2 can be compared. Figures 6.9(a) and (b) show the plot of the voltages of the inverter switches S1 and S2, against currents under hard switching condition for one fundamental cycle (20m sec). Figure 6.9(a) shows that switch S1 is turning on and off with significant switching loss, since during the switching process in most of the time the voltage across the switch is still high when there is current flowing through the switches. At each switching point, there is switching loss represented by voltage times current. The higher the switching frequency is, the

worse the switching losses become. Figure 6.10 shows the area of the overlap of voltage and current during switching on operation which causes this phenomenon.

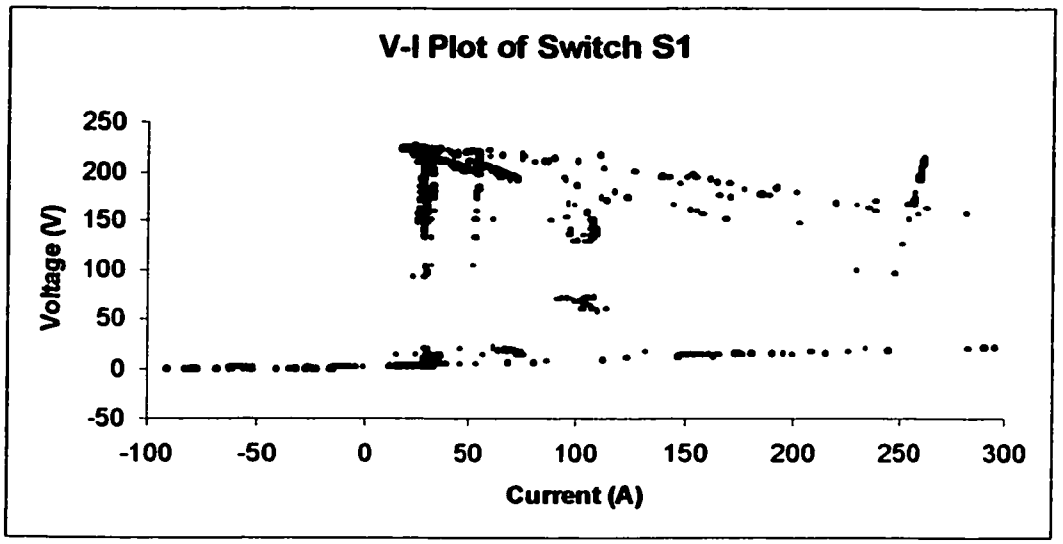

(a)

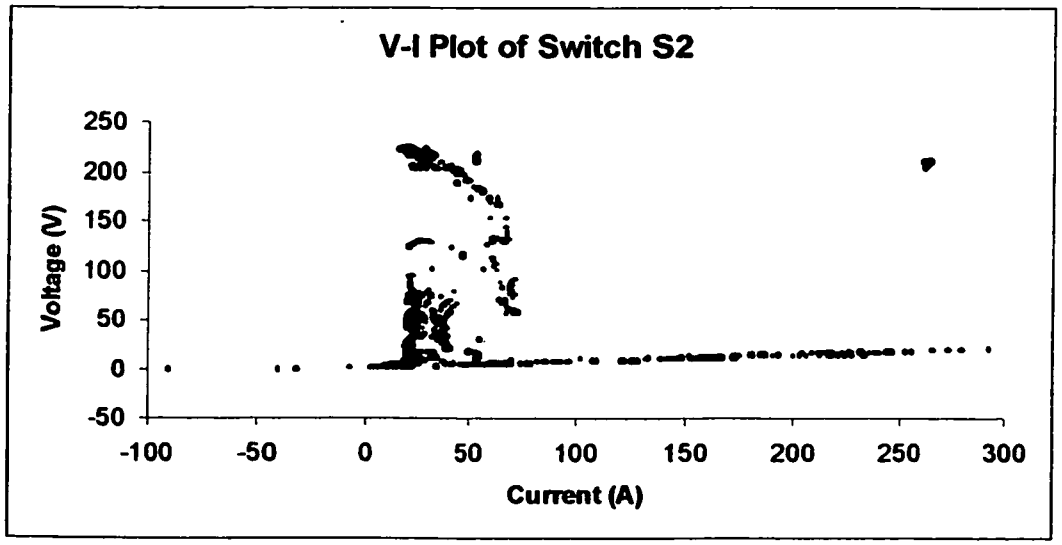

(b)

Figure 6.9 V-I plot of switch (a) S1 (b) S2 under hard switching condition

Figures 6.11(a) and (b) show the plot of the voltages across the inverter switches S1 and S2 against current under soft-switching condition for one fundamental cycle. Under the soft-switching condition, the switch is only operated when the voltage is zero (practically near zero), so very little switching losses can be observed. Figure 6.12 also shows there is no voltage and current overlap during switching.

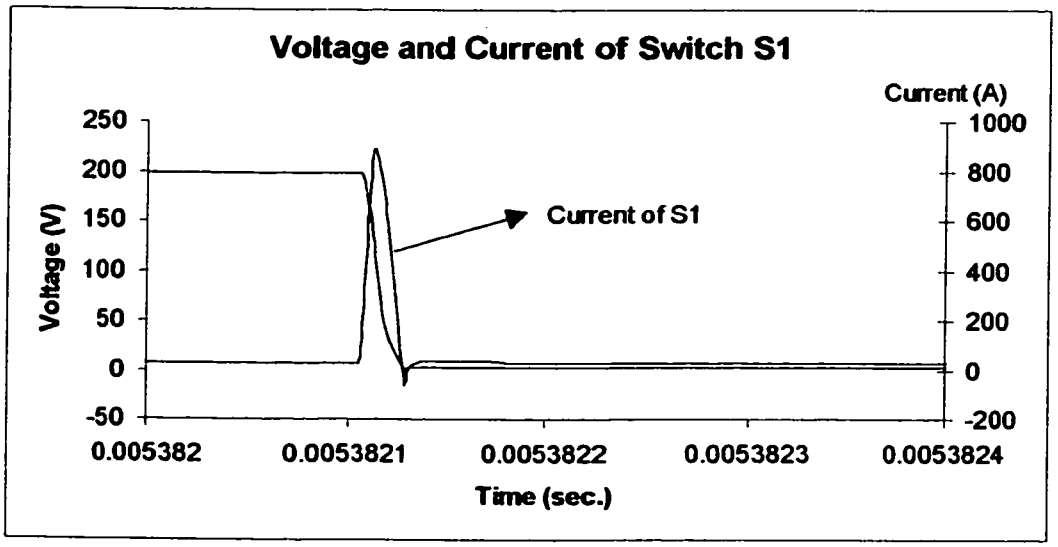

Figure 6.10 Hard switching characteristic

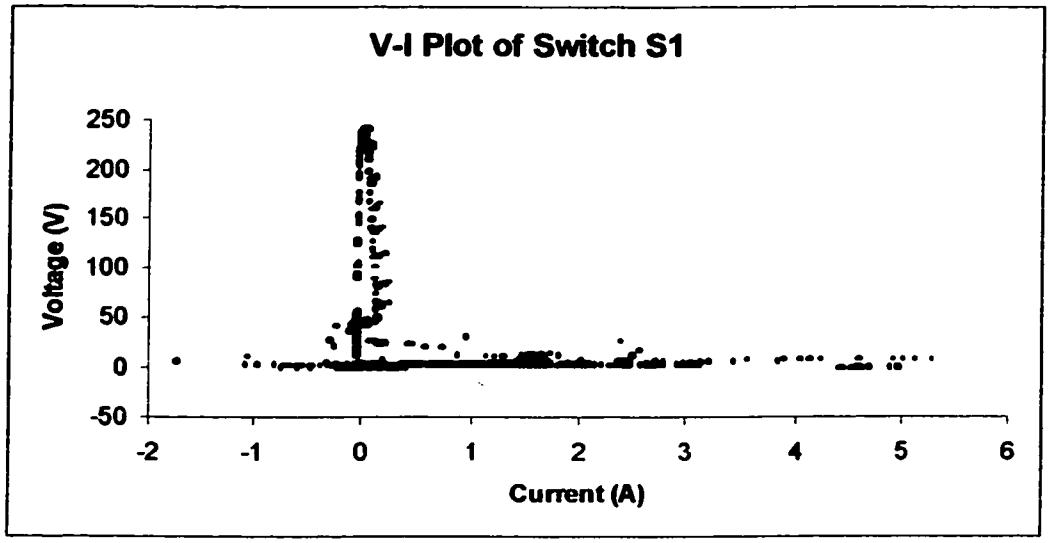

(a)

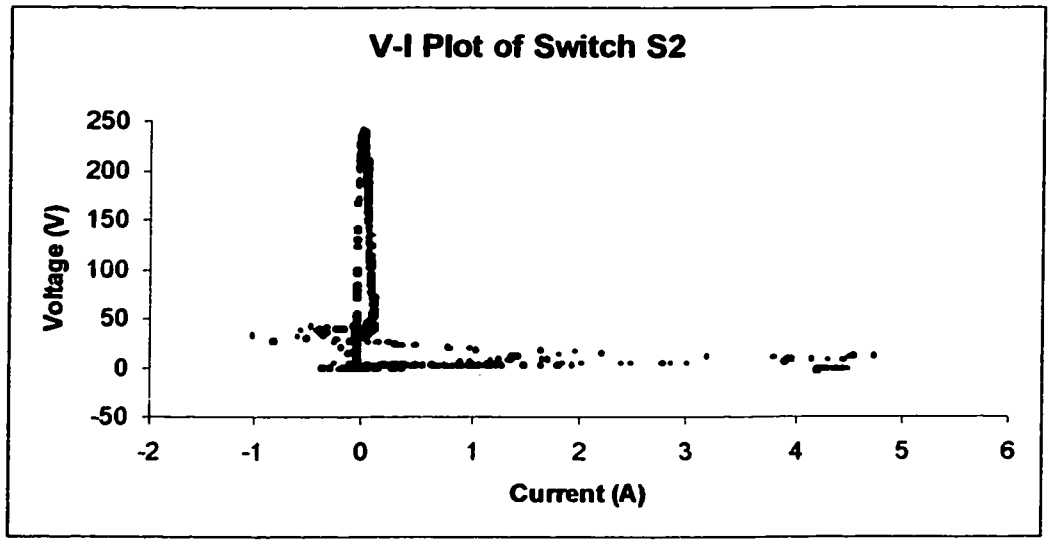

(b)

Figure 6.11 V-I plot of switches (a) S1 (b) S2

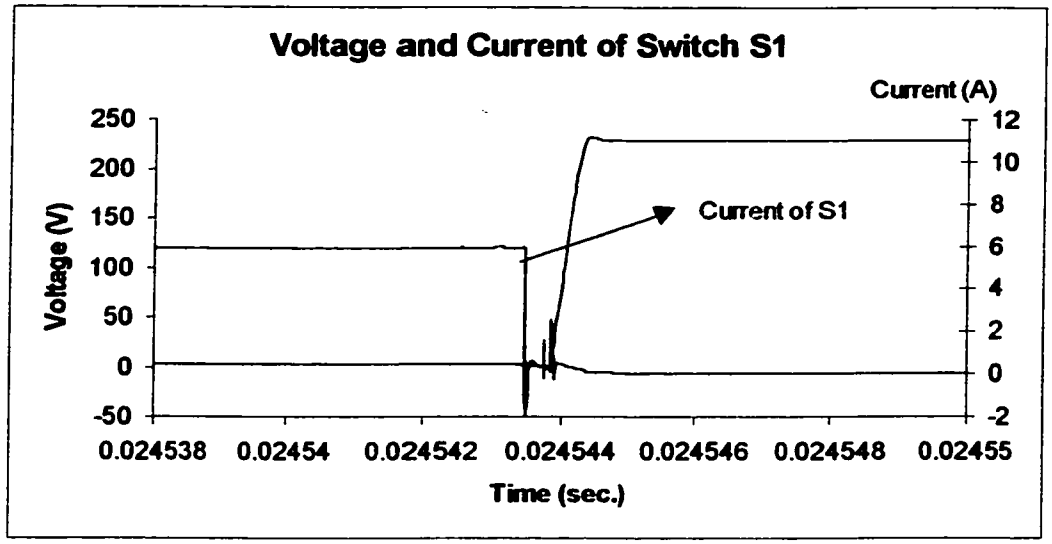

Figure 6.12 Zero Voltage Interval

Although there are three additional switches required in the soft switching circuit, the significant reduction in switching losses justifies their use.

To make sure that switch S and the other two switches (Sa1 & Sa2) are turned on at zero voltage and zero current, respectively, the V-I plots of switch S and one of the auxiliary switches are shown in Figure 6.13. The V-I plot in Figure 6.13(a) clearly shows that S can turn on close to zero voltage and also turn off with little switching losses.

Figure 6.13(a) shows that the switch S is turning on with zero voltage, however there is some loss when turning off. It is because when switch S is turned off, the current originally flowing through is directed to the snubber capacitor. If the capacitance is not large enough, some current still flows in the switch S, resulting in the turn off losses.

Figure 6.13(b) shows that switch Sa also has this problem. Although this can be avoided by increasing the capacitance across the switches, resonant time required will be longer thus reducing the switching frequency. Therefore, a tradeoff should be made here.

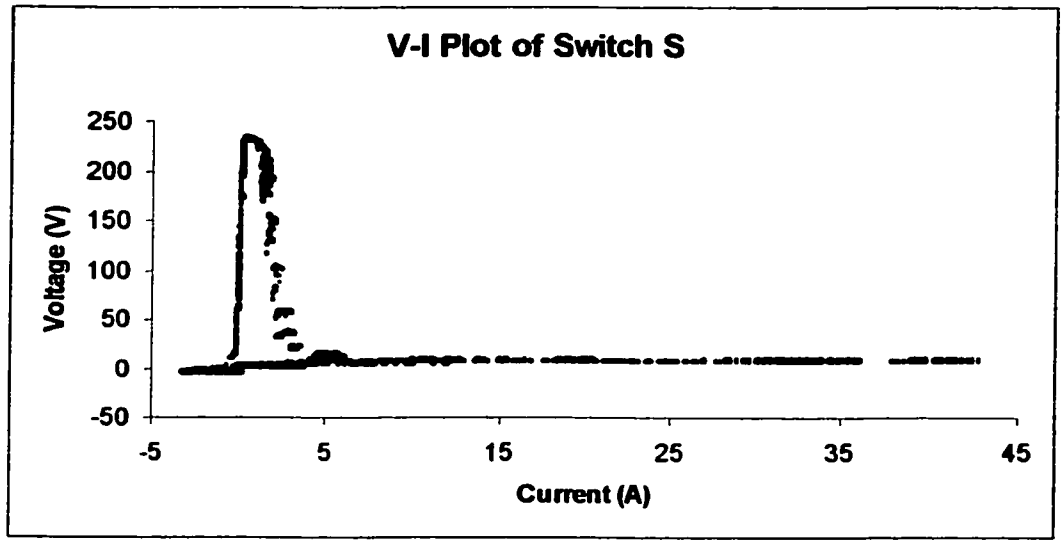

(a)

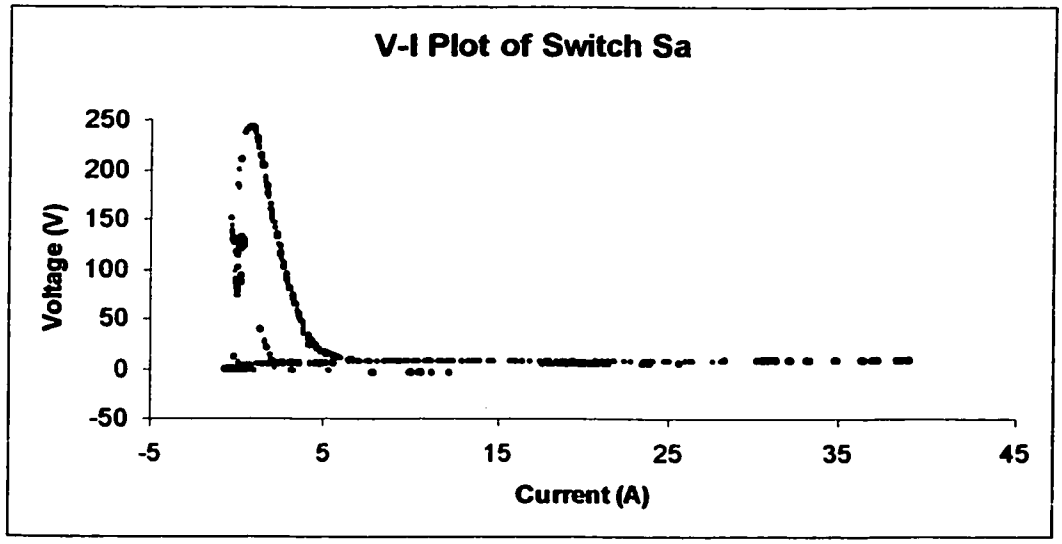

(b)

Figure 6.13 V-I plot of switches (a) S (b) Sa1

6.2.4 Control strategy of the proposed inverter

The control circuit consists of time delay devices, pulse generating devices and logic circuits. Figure 6.14 shows how the gate signals are generated. Figures 6.14(a)-(b) show the original signals generated by the hysteresis controller, Figures 6.14(c)-(f) show some of the logic signals for the gates of the switches and Figures 6.14(g)-(j) show the final control signals for the switches.

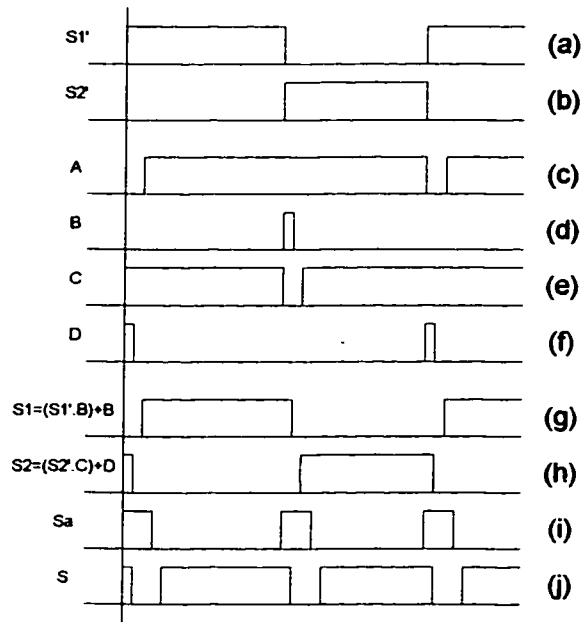

Figure 6.14 Logic signals

Figure 6.14(c) shows a signal A generated by a pulse triggered device. When the device senses a rising pulse in S1' (see Figure 6.14(a)), it will generate a low signal with a defined time period (1.2u sec.) otherwise the output is kept high. On the other hand, signal B (see Figure 6.14(d)) is triggered to be high level for a defined period (0.9u sec.)

when a falling pulse of signal S1' is sensed. Signals C and D (see Figures 6.14(e) and (f)) are generated with the same logic with reference to signal S2'. In this way, the gate signals S1 and S2 can be generated according to the logic equation, as shown in Figures 6.14 (g) and (h), where signal Sa is dependent on the rising pulse of the signals S1' and S2', and signal S is dependent on the rising pulse of B and D.

Based on this control logic, the converter can be controlled using the hysteresis technique while at the same time ensuring that the switches are operated in soft-switched mode. Figures 6.15 and 6.16 show a portion of the voltage and current of switches S1 and S2 respectively. It is noticed that in Figure 6.15, there are short zero voltage intervals across the dc-link and each interval corresponded to the turning point of the source current as shown in Figure 6.16.

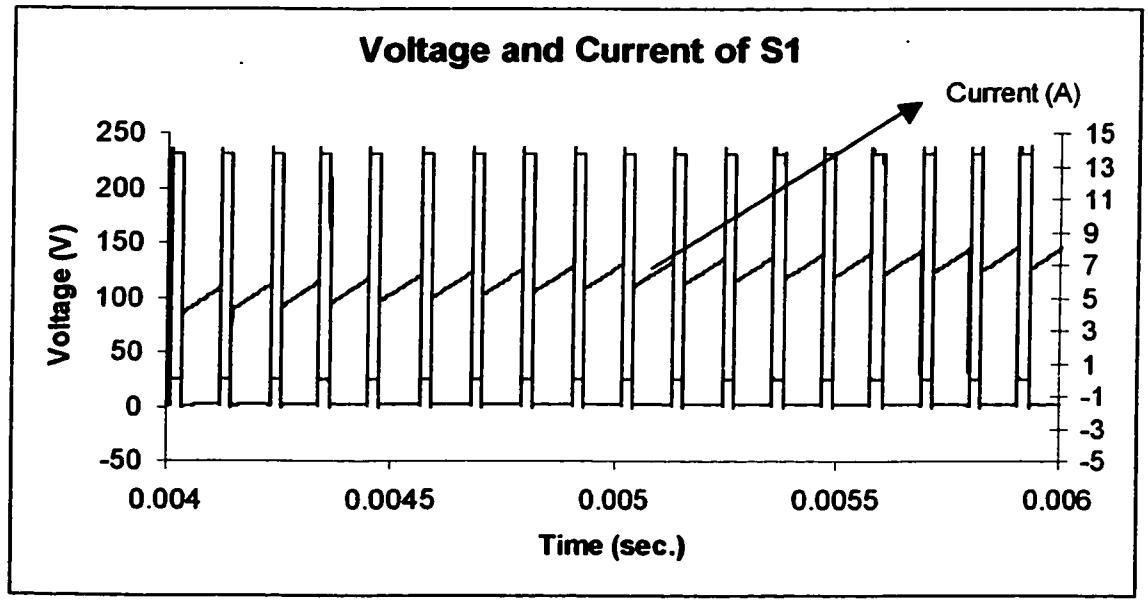

Figure 6.15 Voltage and current of S1

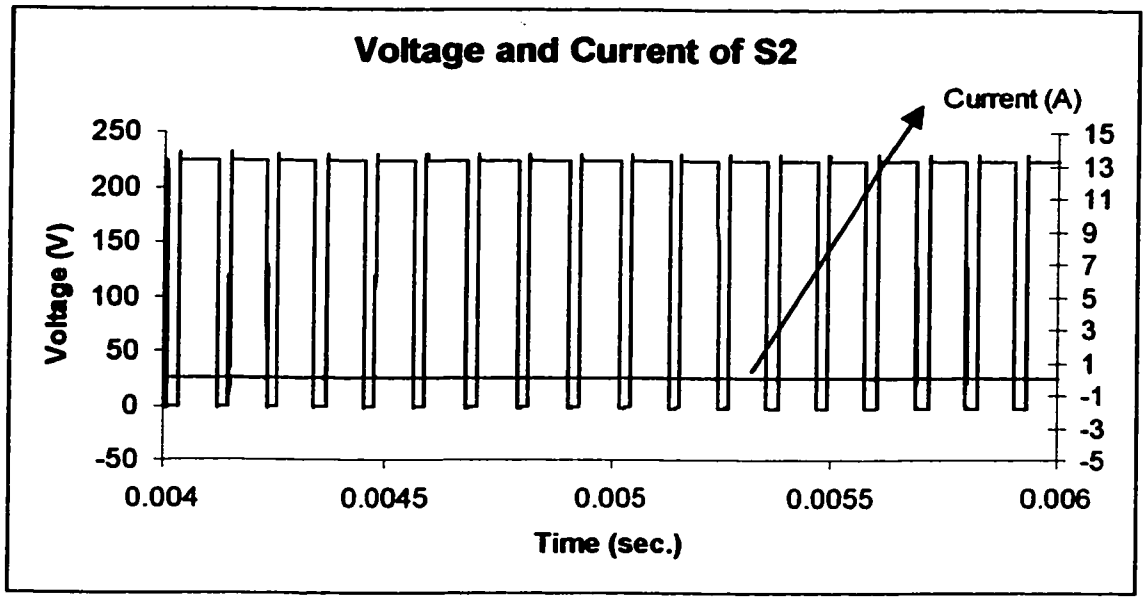

Figure 6.16 Voltage and current of S2

6.3 Development of Current Controller for Battery Energy Storage Systems (BESS) With Fixed-Hysteresis Band and Constant Modulation Frequency

When a hysteresis controller is used to control the supply line current, the ripple magnitude and frequency of the controlled current is highly dependent on the battery voltage, line inductance and the band limits of the controller. When these parameters are constant, the switching frequency can vary over quite a large range. By varying the hysteresis band limits, a constant switching frequency can be obtained without violating its fast dynamic performance (Bose, B.K., Oct. 1990) as long as the other parameters remain fixed. This method has been applied in AC drive control (Malesani, L. and Tenti, P., 1990). However these techniques assume that the battery voltage is always constant. However, in practice, the battery terminal voltage fluctuates significantly as large

current is being supplied or absorbed by the battery bank. As a result, this will create current overshoot and variable switching frequency.

This section presents a novel method of obtaining a constant switching frequency using hysteresis control with a fixed hysteresis band, by means of a DC-DC converter, to provide a controllable voltage at the inverter dc terminal. Since the output of the DC-DC converter is tightly controlled irrespective of the battery voltage variations, the inverter can be specifically designed to optimize the overall design of the BESS such that output load range and inverter efficiency can be increased, thereby reducing the total cost of the BESS.

In order to prevent the variable switching frequencies generated by a fixed hysteresis band controller, the DC-DC converter output voltage is controlled in a predetermined manner with a specified voltage magnitude and waveform. In this section, an investigation in the use of both buck- and boost- DC-DC converter will be present, and will show how the proposed method to achieve an excellent control of the supply line current with pre-determined switching frequency and fixed hysteresis band.

6.3.1 Analysis of a hysteresis controlled BESS

6.3.1.1 Traditional Battery Energy Storage System

A simplified block diagram of a BESS is shown in Figure 6.17, comprising a battery bank and a voltage source inverter connected to the grid through a transformer. Using the hysteresis current controller, the ac supply line current can be controlled both in its

magnitude and waveform to provide load leveling and power factor correction. Since the line current is tightly controlled to follow a sinusoidal reference signal, the system can also provide active filtering, irrespective of the waveform of the load connected to the grid. As far as the supply system is concerned, the total load, comprising the BESS and the actual system load, appears to be constant and sinusoidal. A simple and reliable controller based on the hysteresis controller is shown in Figure 6.17.

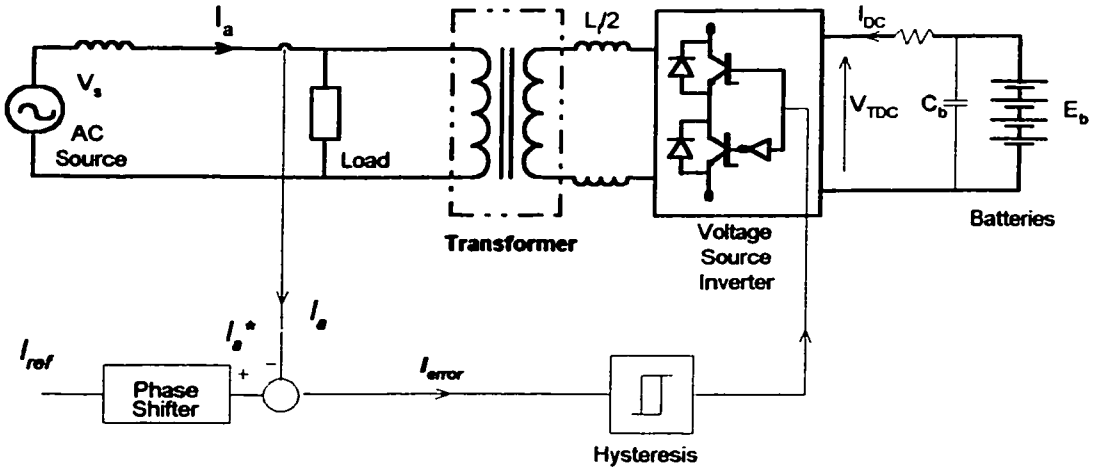

Figure 6.17 Block diagram of a BESS

The controller consists of a phase shifter and a fixed hysteresis band controller. A reference signal is compared with the instantaneous supply current, I_a, from which the appropriate switching action is taken based on the hysteresis control strategy.

The above BESS is simulated using the following data:

$V_m = 78 \sin(wt)$ V; hysteresis band: $2h_i = 1.0$ A;

$E_b = 140$ V; $L_i = 6$ mH;

I_{ref} = 3 sin (wt) A.

Figures 6.18(a) - (b) show the ac supply current waveform I_a and its frequency spectrum. Figure 6.18(b) clearly shows that there is a wide band of modulation frequency, whose range cannot be easily evaluated before hand. This has always been considered as one of the main disadvantages of the hysteresis current controller.

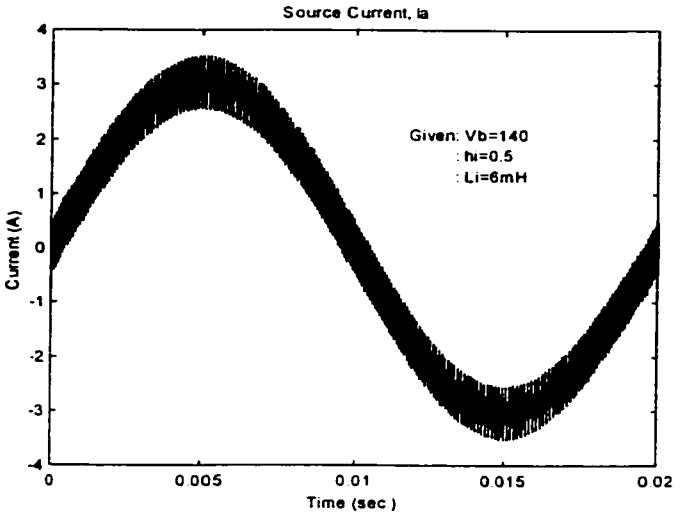

(a)

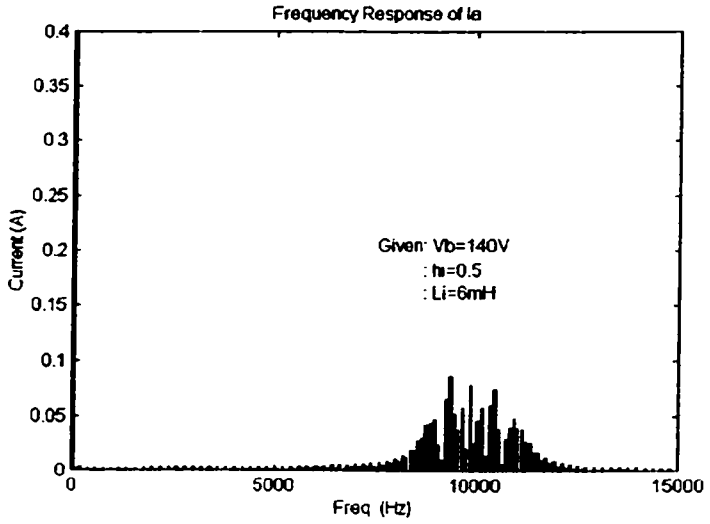

(b)

Figure 6.18 Ideal case conventional fixed-band hysteresis BESS E_b=140V. (a) Source current, Ia; (b) Frequency Spectrum of Ia.

6.3.1.2 Proposed improvement to the traditional BESS

A new improved design of the BESS using DC-DC converter, in which we can accurately pre-determine a fixed switching frequency while maintaining the fixed hysteresis band will be proposed in this section. The proposed improved BESS is shown in Figure 6.19. A DC-DC converter is inserted between the battery bank and the inverter to provide a variable DC voltage to the inverter. To understand how the voltage output of the DC-DC converter is controlled, we need to have a detailed analysis of the hysteresis controller.

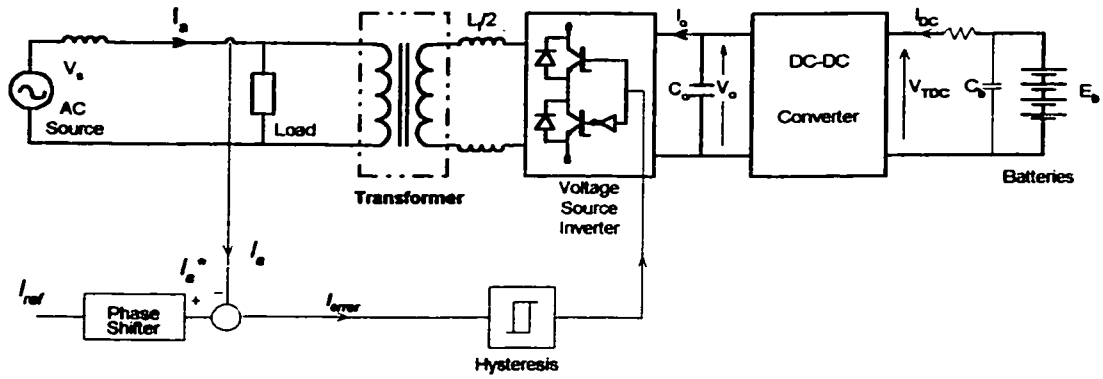

Figure 6.19 Block diagram of a BESS with DC-DC converter inserted between the battery bank and the inverter

6.3.1.3 Analysis of the Hysteresis Current Controller

The simplest equivalent circuit of a hysteresis current controlled BESS is shown in Figure 6.20. Depending on the current magnitude at any particuiar time, the upper or the lower switch will be turned on, connecting positive or negative DC voltage to the AC system through the inductance L_i.

E_b, E_i and V_s represent the battery voltage, inverter voltage and ac source voltage, respectively.

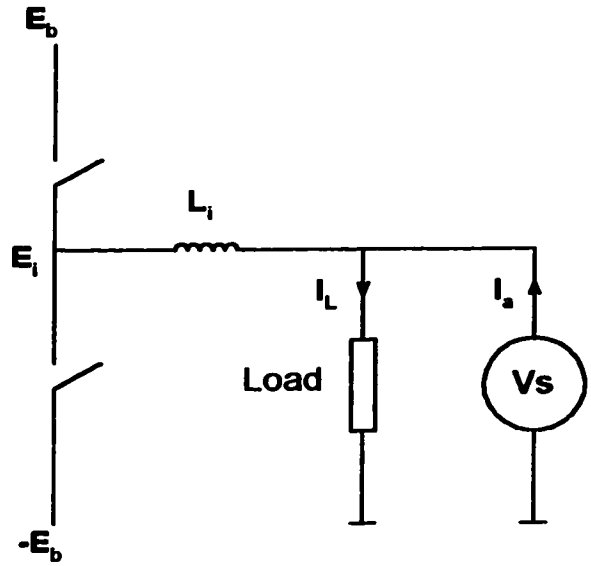

Figure 6.20 Equivalent circuit of BESS

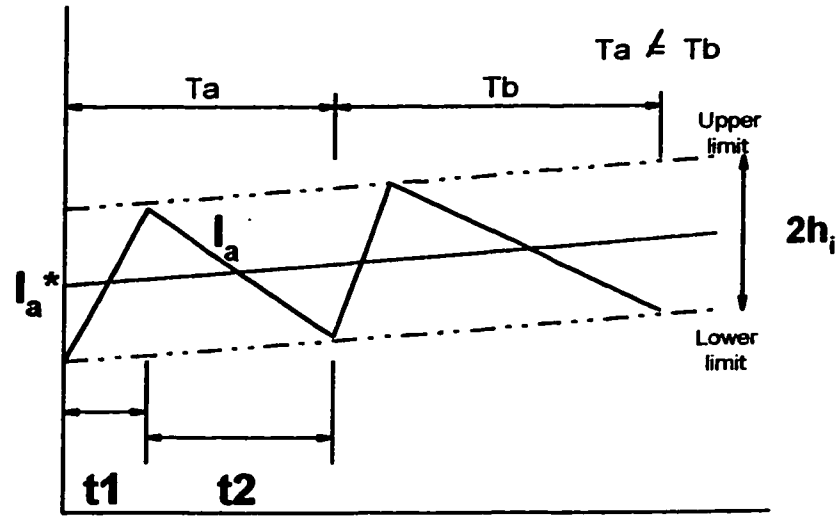

Figure 6.21 Expanded current waveform

The resulting current waveform in the first two cycles is shown in Figure 6.21. When the instantaneous current I_a is less than the reference current, I_a^*, and is below the lower band limit, the lower switch will be closed (the upper switch will be opened), causing I_a

to increase until it reaches the upper band limits at t_1. The slope is given by $(E_b+V_s)/L_i$. At time t_1, the lower switch is opened (the upper switch is closed), causing I_a to decrease until it reaches the lower band limit at t_2. The slope is given by $(E_b-V_s)/L_i$. The differential equation can be expressed as Equation (6.42) & (6.43). With the current rise represented by Equation 6.42, and the current fall represented by Equation 6.43 respectively, assuming that E_b and V_m remain constant.

$$E_b + V_s = L_i \frac{di_a}{dt} \tag{6.42}$$

$$E_b - V_s = L_i \frac{di_a}{dt} \tag{6.43}$$

where $V_s = V_m \sin(wt)$

E_b is the battery terminal voltage, $E_b > V_m$

The time period required for one switching cycle of the hysteresis loop can be calculated as:

$$T_s = \frac{4L_i h_i E_b}{E_b^2 - V_s^2} \tag{6.44}$$

where $T_s = t_1+t_2$, switching period

and t_1 is the rise time of the current

t_2 is the fall time of the current

h_i = half of the hysteresis band

The switching frequency is:

$$f_s = \frac{1}{T_s} \tag{6.45}$$

In Equation 6.44, if the battery voltage, E_b, is constant, all other terms will be constant, except for V_s, which is varying with time. It is possible to conclude therefore that this is the term that is responsible for the range of switching frequency encountered in a hysteresis controller with fixed hysteresis band. The frequency range can therefore be calculated as:

$$\frac{E_b^{\,2}}{4L_i h_i E_b} \geq f_s \geq \frac{E_b^{\,2} - V_m^{\,2}}{4L_i h_i E_b} \tag{6.46}$$

Equation 6.46 provides a means of determining the expected frequency spectrum of any BESS system controlled using hysteresis scheme with constants E_b, L_i, h_i, and V_m.

For example for the BESS whose data is given in Section 6.3.1.1, the range of the frequency spectrum can be calculated from Equation 6.46 as:

$$11.67 \text{ kHz} > f_s > 8 \text{ kHz}$$

Figure 6.18(b) confirms that the range of switching frequency is close to the above calculation.

In a similar manner, it is now having in a disposal means to shift the frequency to any value as desired by either changing h_i, L_i, E_b or a combination of these variables. For

example, if the frequency range is somewhere in 15kHz range it is possible to increase E_b to 200V. Figures 6.22(a) and (b) show the current waveform and its frequency spectrum for the BESS whose data is given in Section 6.3.1.1 when E_b is set to 200V. The range of switching frequency as shown in Figure 6.22(b) can be calculated from Equation 6.46 as:

$$16.67 \text{ kHz} > f_s > 14.13 \text{ kHz}$$

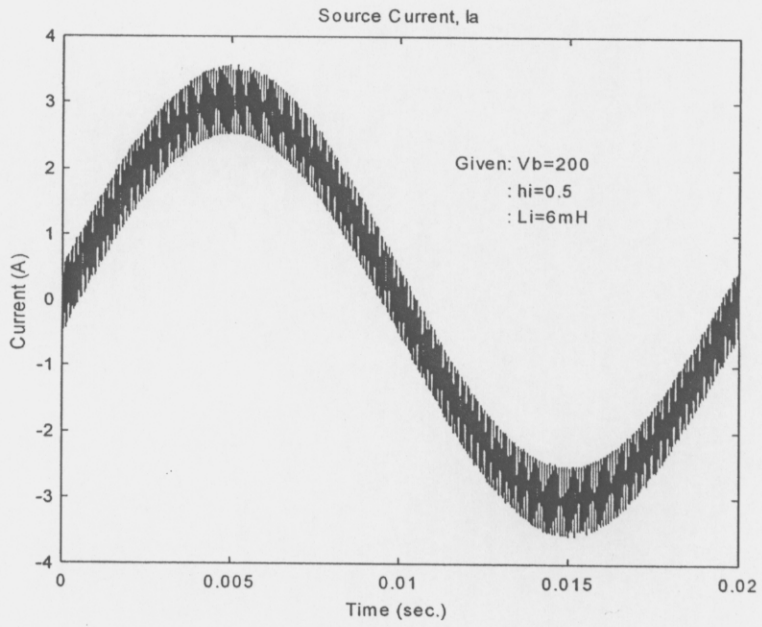

(a)

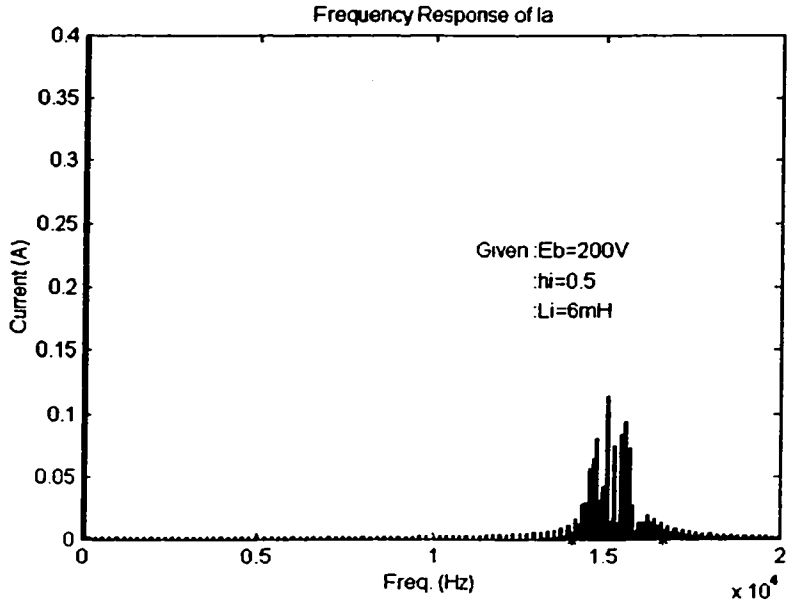

(b)

Figure 6.22 Ideal case conventional fixed-band hysteresis BESS E_b=200V (a) Source current, Ia; (b) Frequency Spectrum of Ia.

Equation (6.46), however, assumes that the terminal voltage of the battery, E_b, is constant, but actually it is not constant due to the voltage drop across the battery internal impedance. The battery terminal voltage can actually vary in the worst case up to a factor of two. The BESS given in Section 6.3.1.1 is then re-simulated with the battery bank represented by a constant voltage source behind an internal impedance of 1Ω. Figures 6.23(a)-(d) show the final current waveform, its frequency spectrum, the battery terminal voltage and the battery current. Figures 6.23(c) and (d) show that the battery voltage and current vary quite significantly from the charging to discharging mode.

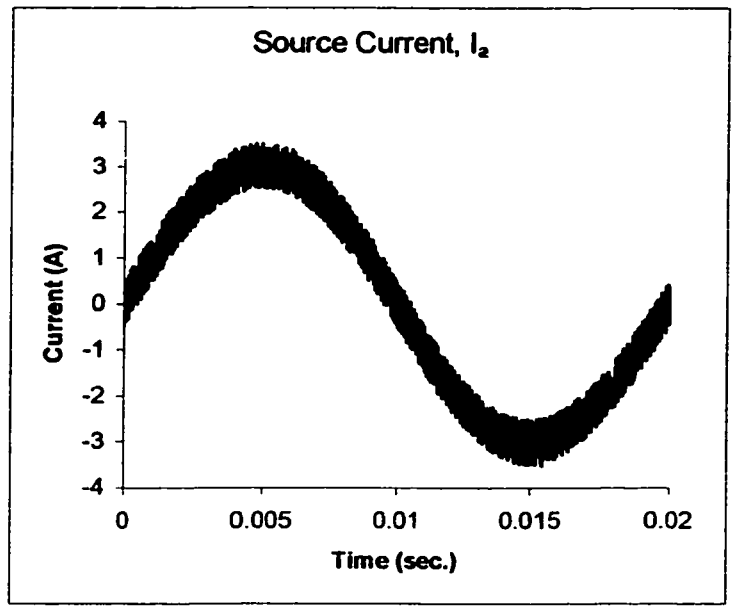
Source Current, I_2
Current (A)
4
3
2
1
0
-1
-2
-3
-4
0
0.005
0.01
0.015
0.02
Time (sec.)

(a)

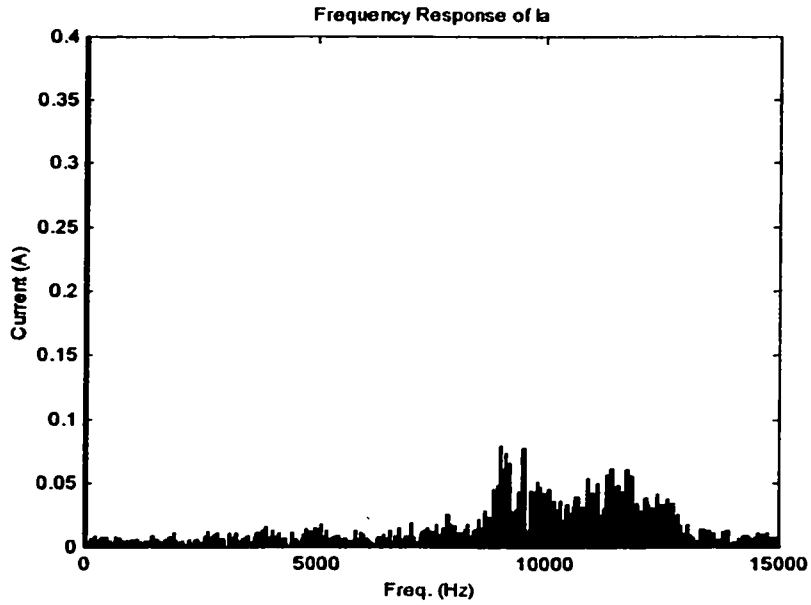
Frequency Response of Ia
Current (A)
0.4
0.35
0.3
0.25
0.2
0.15
0.1
0.05
0
0
5000
10000
15000
Freq. (Hz)

(b)

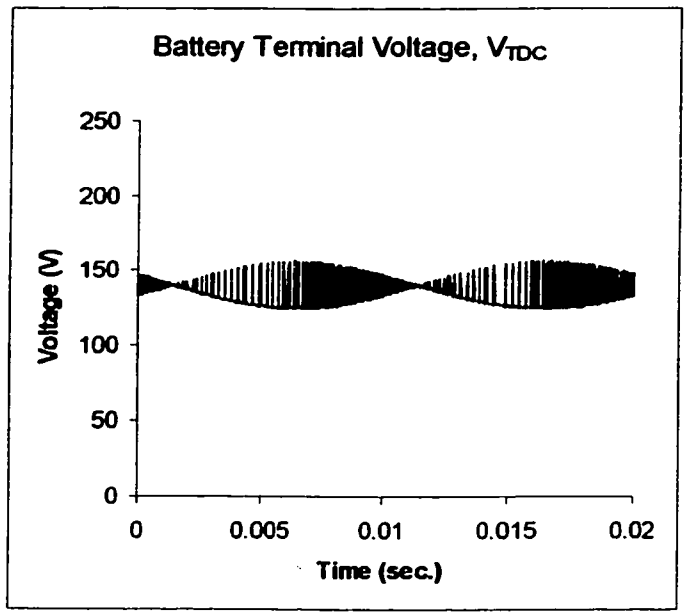

(c)

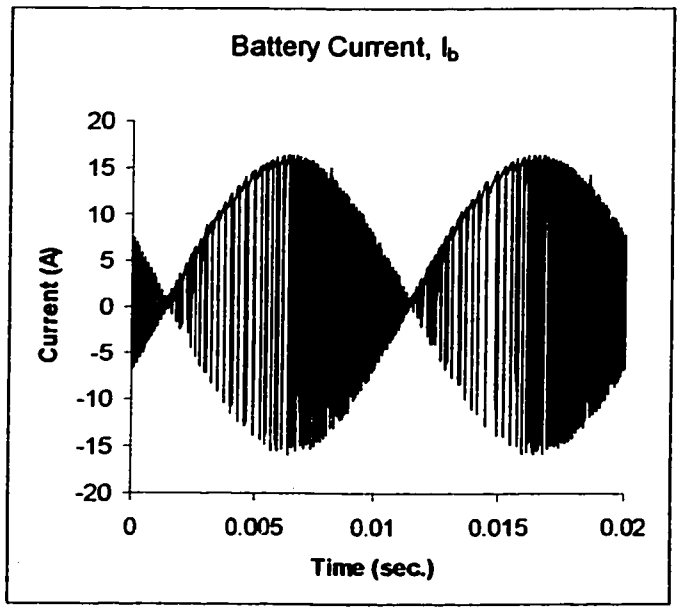

(d)

Figure 6.23 Practical case conventional fixed-band hysteresis BESS Vb=140V. (a) Source current, Ia; (b) Frequency Spectrum of Ia; (c) Battery terminal voltage, V_{TDC}; (d) Battery current, I_b.

Figures 6.18(b) and 6.22(b) show that a current controller with a fixed hysteresis band has the disadvantage that the modulation frequency varies in a band, because the peak-to-peak current ripple is required to be controlled at all points of the fundamental frequency waveform and, as a result, creates non-optimum current ripple with excessive harmonics. It is desirable to have a constant switching frequency. This can be achieved either by changing h_i or E_b.

6.3.1.3.1 Changing h_i

The hysteresis band, h_i could be varied as follows:

$$h_i = k_h(E_b^2 - V_m^2 \sin^2(wt)) \tag{6.47}$$

where $k_h = \dfrac{1}{4L_i f_s E_b}$

f_s is now a constant that can be pre-determined.

The upper and lower bands are then varied as follows:

$$I_a(upper) = I_a^* + k_h(E_b^2 - V_m^2 \sin^2(wt)) \tag{6.48}$$

$$I_a(lower) = I_a^* - k_h(E_b^2 - V_m^2 \sin^2(wt)) \tag{6.49}$$

For the BESS whose data is given in Section 6.3.1.1, we can changing h_i, to ensure that the frequency spectrum contains only one frequency, say 10kHz, following Equation

(6.47) while keeping the other parameters unchanged. Figures 6.24(a) – (c) show the resulting current waveform, its frequency spectrum and the variation of h_i with time.

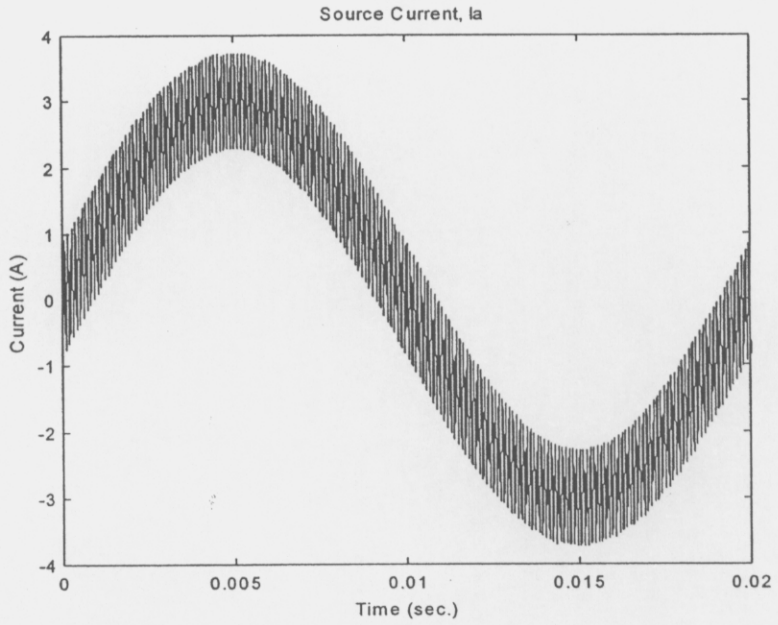

(a)

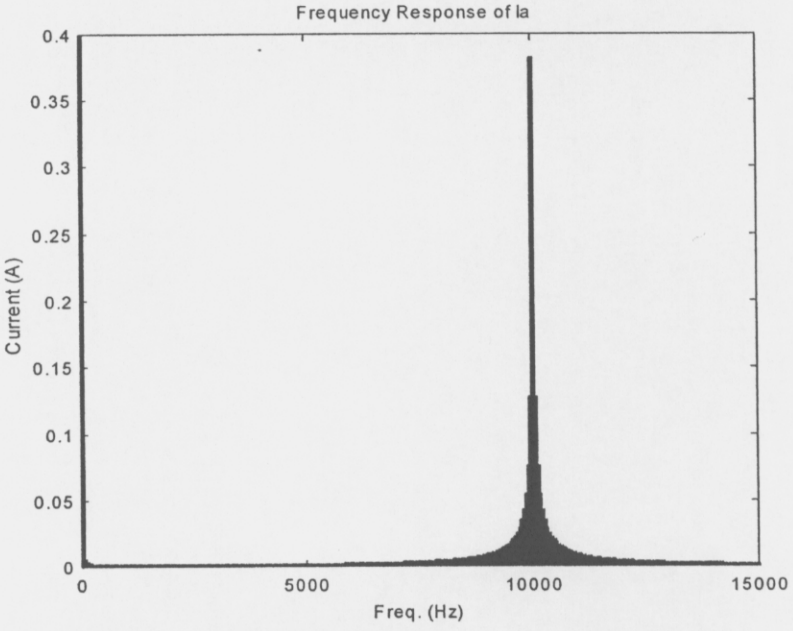

(b)

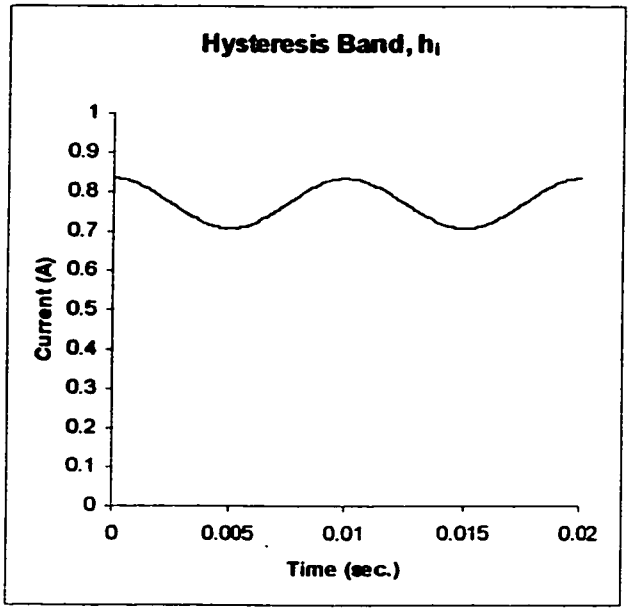

(c)

Figure 6.24 Ideal case with variable hysteresis band. (a) Source current, I_a; (b) Frequency Spectrum of I_a; (c) Hysteresis band, h_i.

6.3.1.3.2 Changing E_b

E_b can be changed to maintain $E_b^2 - V_m^2 \sin^2(wt)$ constant. This can be achieved by changing E_b using a dc-dc converter.

The instantaneous value of E_b can be calculated using Equation (6.44):

$$E_b^2 - (4L_i h_i f_s)E_b - V_s^2 = 0 \tag{6.50}$$

Solving for E_b we have,

$$E_b = 2L_i h_i f_s \pm \sqrt{(2L_i h_i f_s)^2 + V_s^2} \tag{6.51}$$

Setting $E_b = k_{dc} \pm \sqrt{{k_{dc}}^2 + {V_s}^2}$ and substituting it into Equation (6.44), a constant switching period can be obtained (and hence a constant switching frequency) as follows:

$$T_s = \frac{4L_i h_i}{2k_{dc}} \tag{6.52}$$

where k_{dc} is a constant.

For example, for the BESS whose data is given in Section 6.3.1.1, we can ensure that the frequency spectrum contains only one frequency, say 10kHz, by changing E_b using a dc-dc converter as shown in Figure 6.19, where V_o is controlled to follow Equation (6.51) and f_s is set to 10kHz. Figures 6.25(a)–(c) show the resulting current waveform, the frequency spectrum and the variation of V_o with time. Figures 6.26(a)–(c) show similar results when the frequency is set to 15kHz.

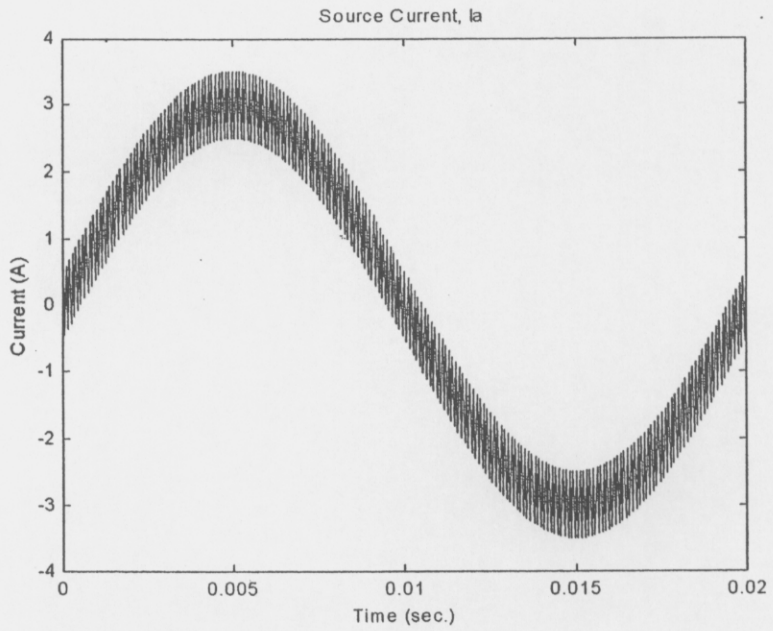

(a)

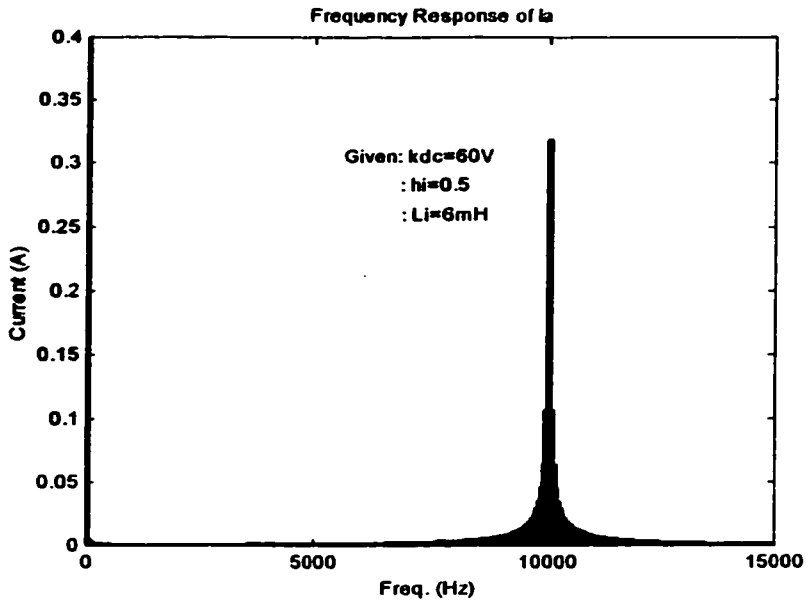

(b)

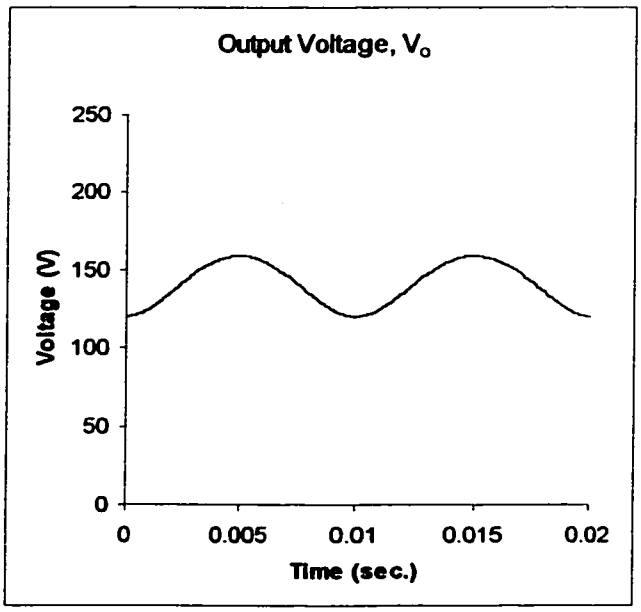

(c)

Figure 6.25 Ideal case with f_s=10kHz. (a) Source current, I_a; (b) Frequency Spectrum of I_a; (c) DC-DC converter output voltage, V_o.

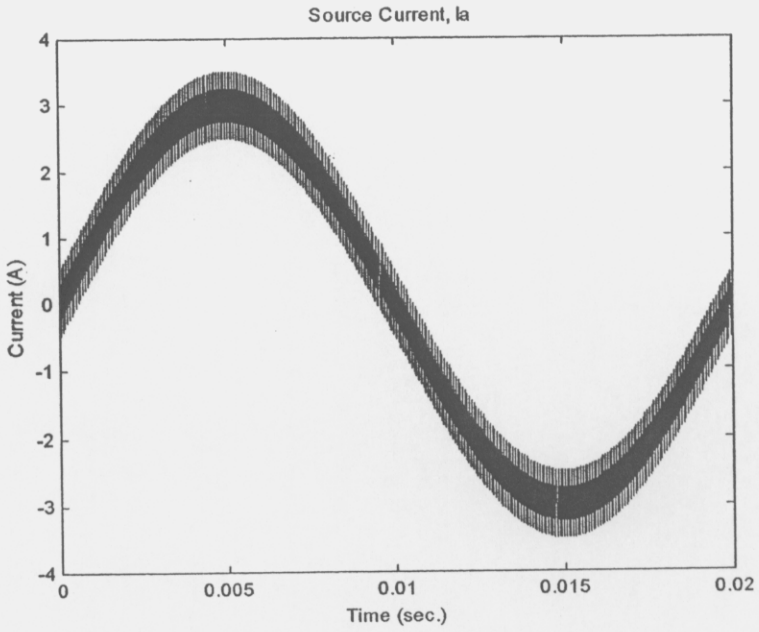
Source Current, Ia
Current (A)
Time (sec.)
4
3
2
1
0
-1
-2
-3
-4
0
0.005
0.01
0.015
0.02

(a)

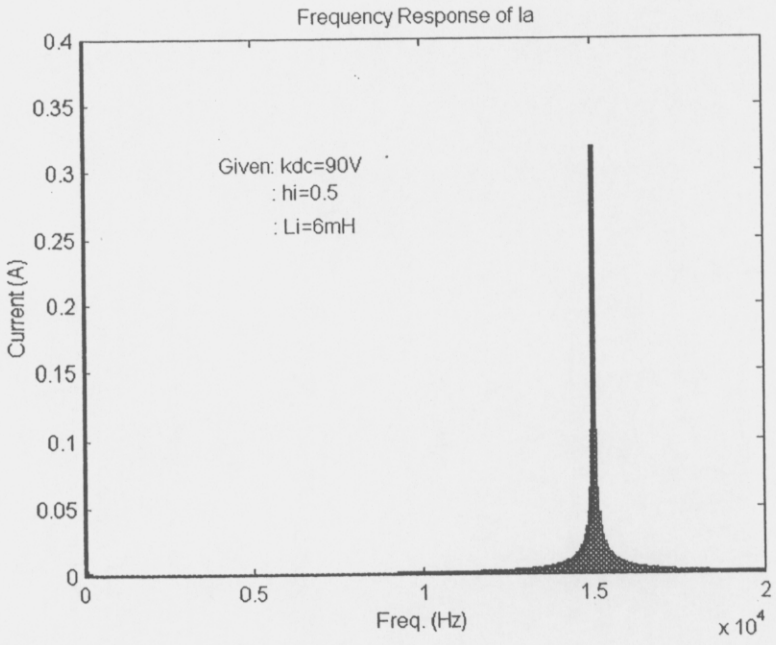
Frequency Response of Ia
Given: kdc=90V
: hi=0.5
: Li=6mH
Current (A)
Freq. (Hz)
x 10^4
0.4
0.35
0.3
0.25
0.2
0.15
0.1
0.05
0
0
0.5
1
1.5
2

(b)

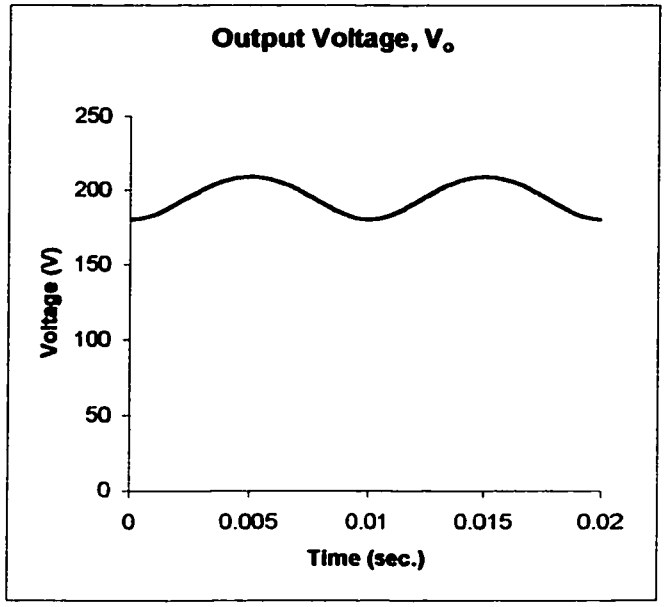

(c)

Figure 6.26 Ideal case with f_s=15kHz; (a) Source current, I_a; (b) Frequency Spectrum of I_a; (c) DC-DC converter output voltage, V_o.

Note that in obtaining the results shown in Figures 6.25(a)-(c) and Figures 6.26(a)-(c), we assume that the terminal voltage of the battery is constant, i.e. the internal resistance of the battery is zero.

Figures 6.27(a)-(d) show the resulting current waveform, the frequency spectrum, the variation of V_0 and the battery terminal voltage when a buck dc-dc converter is used, and the battery bank is rated at 240V with 2Ω internal resistance and f_s is set at 10kHz. The simulation is carried out using PSPICE with all the switches modeled as IGBT's. Note that the terminal voltage now varies as the battery bank is being charged and discharged.

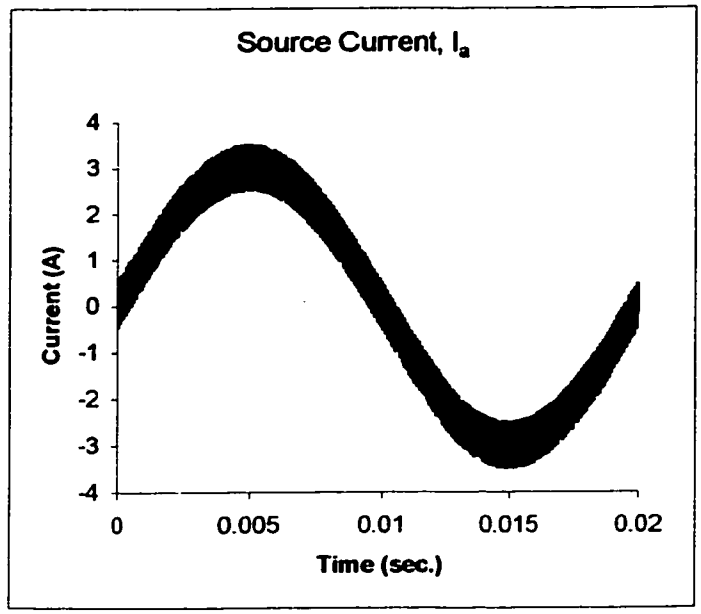
Source Current, I_a
Current (A)
4
3
2
1
0
-1
-2
-3
-4
0
0.005
0.01
0.015
0.02
Time (sec.)

(a)

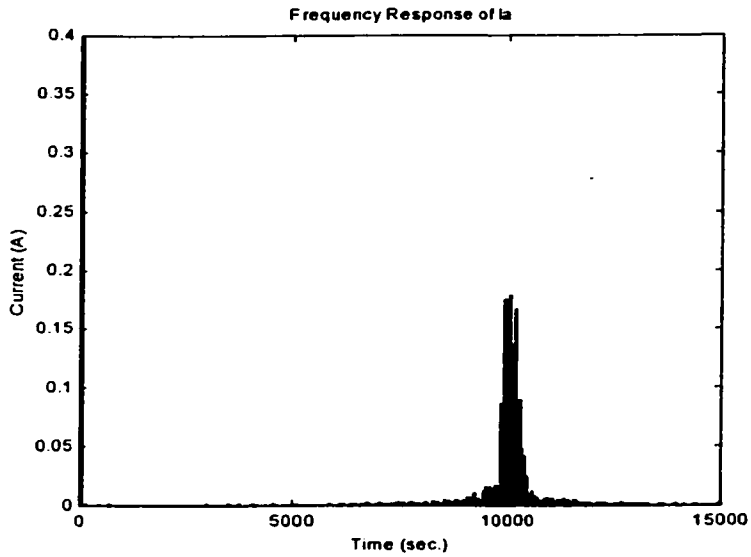
Frequency Response of Ia
Current (A)
0.4
0.35
0.3
0.25
0.2
0.15
0.1
0.05
0
0
5000
10000
15000
Time (sec.)

(b)

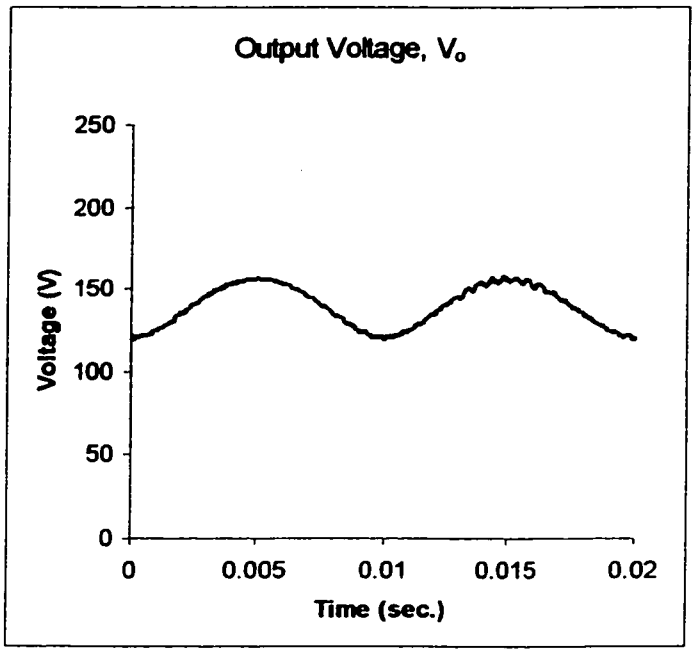

(c)

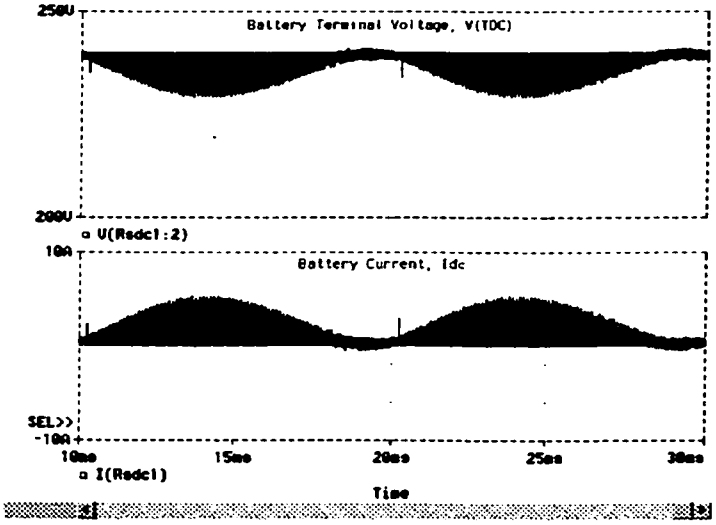

(d)

Figure 6.27 Practical case with f_s=10kHz. (a) Source current, I_a; (b) Frequency Spectrum of I_a; (c) DC-DC converter output voltage (V_o); (d) (UPPER) Battery terminal voltage, V_{TDC}; (LOWER) Battery current, I_{DC}.

By repeating the above simulation using boost dc-dc converter, when the battery bank is rated at 120V with 1Ω internal resistance and f_s is set at 15kHz, Figures 6.28(a)-(d) show the resulting current waveform, the frequency spectrum, the variation of V_0 and the battery terminal voltage.

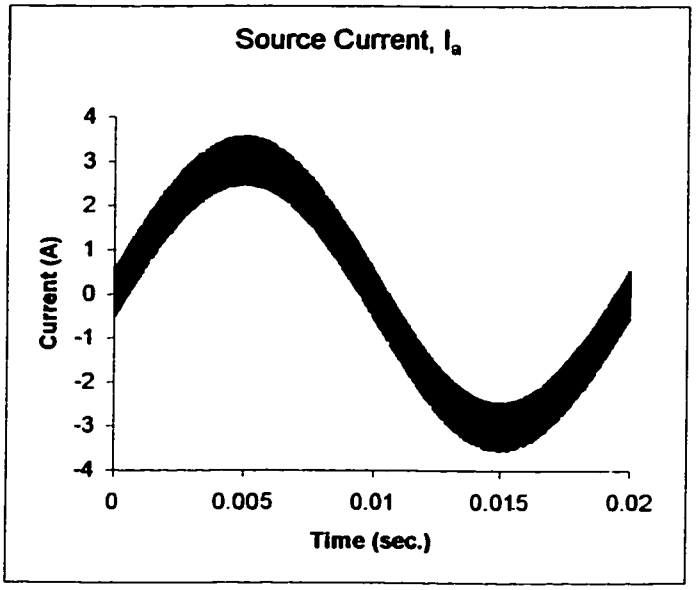

(a)

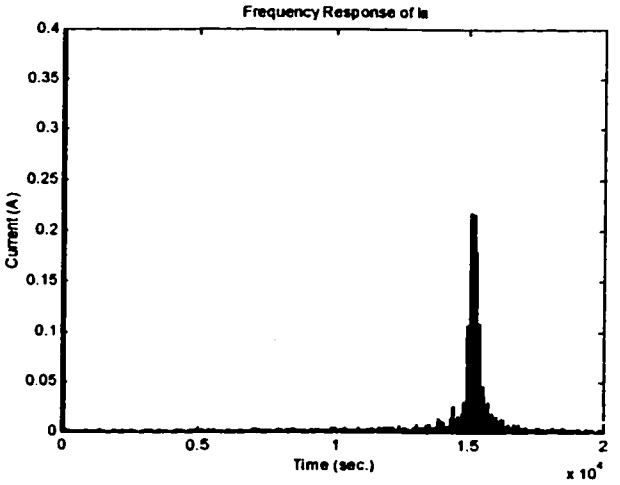

(b)

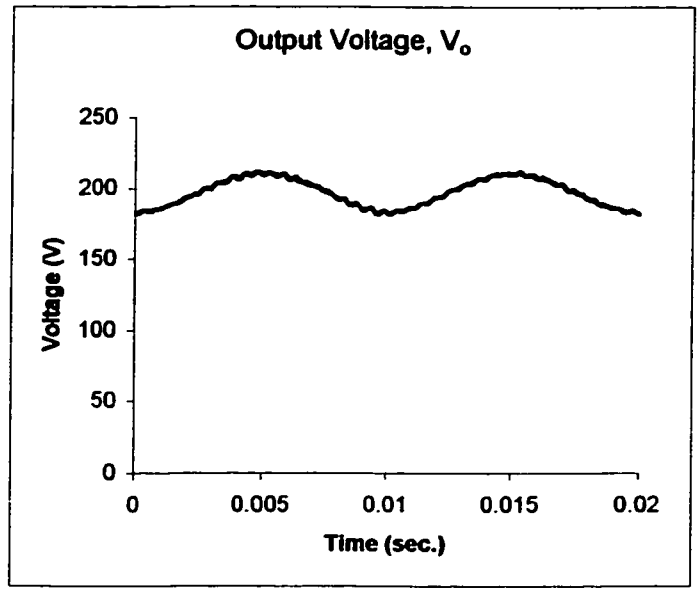

(c)

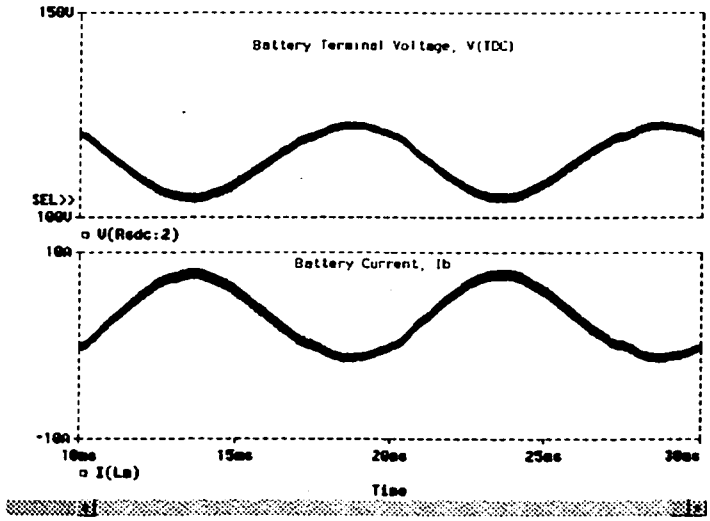

(d)

Figure 6.28 Practical case with f_s=15kHz. (a) Source current, I_s; (b) Frequency Spectrum of I_s; (c) DC-DC converter output voltage (V_o); (d) (UPPER) Battery terminal voltage, V_{TDC}; (LOWER) Battery current, I_{DC}.

As shown in Figures 6.25(b) and 6.27(b), the practical case shows a bit wider frequency range and smaller peak value, due to the non-linearity of the switching devices during switching on and switching off period, the dead-time introduced in the inverter circuit and the presence of stray capacitance and inductance in the circuit.

Note that even though the battery bank terminal voltage is still varying as shown in Figure 6.27(d) and Figure 6.28(d), the constant switching frequency is maintained.

6.3.2 DC-DC CONVERTER

There are many topologies for DC-DC conversion. A bi-directional DC-DC Buck and a bi-directional DC-DC Boost will be investigated in this section.

6.3.2.1 Buck DC-DC Converter

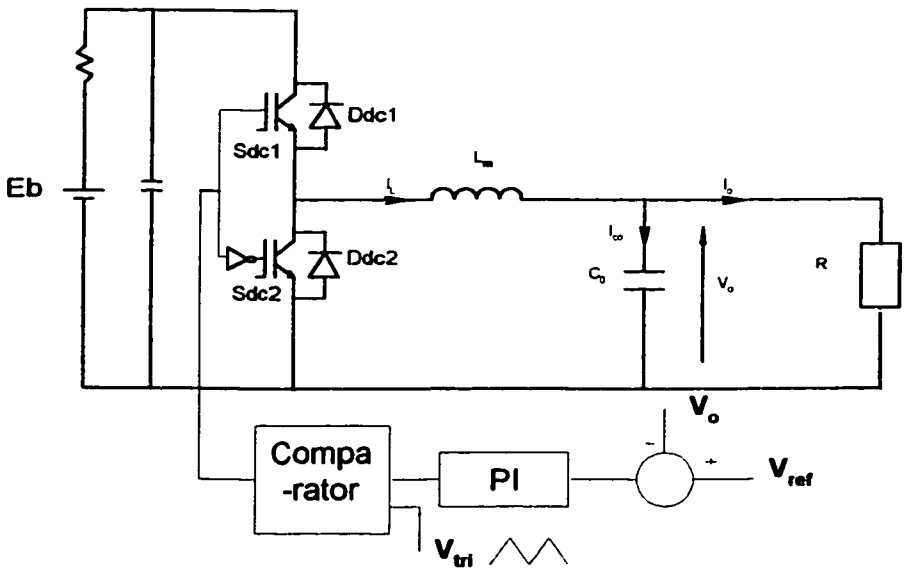

Figure 6.29 Bi-directional buck converter

A bi-directional buck dc-dc converter is shown in Figure 6.29. The converter allows the current to flow in and out of the battery bank.

The dc component of the output voltage is controlled by adjusting the duty ratio D and the average of the output voltage is:

$$V_0 = \frac{1}{T}\int_0^T v_s(t)dt$$
$$= \frac{1}{T}\int_0^{DT} v_s(t)dt$$

$$V_o = V_s D \tag{6.53}$$

The main point to the analysis for determining the change in inductor current, i_L, is known from Equations (6.54) and (6.55), when switch, S_{dc1}, is closed (S_{dc2} is opened) and when switch S_{dc1} is opened (S_{dc2} is closed), respectively.

When the switch S_{dc1} is closed in the bi-directional buck converter circuit of Figure 6.29,

$$\frac{di_L}{dt} = \frac{\Delta i_L}{DT} = \frac{E_b - V_0}{L_m}$$
$$\Delta i_{L(closed)} = \frac{E_b - V_o}{L_m} DT \tag{6.54}$$

When the switch S_{dc1} is opened in the bi-directional buck converter circuit of Figure 6.29,

$$\frac{di_L}{dt} = \frac{\Delta i_L}{(1-D)T} = \frac{-V_o}{L_m}$$

$$\Delta i_{L(opened)} = \frac{-V_o}{L_m}(1-D)T \qquad (6.55)$$

From Equation (6.54) or (6.55), the ripple of the inductor current can be rearranged as:

$$\Delta i_L = \left[\frac{V_0}{L_m}(1-D)T\right] \qquad (6.56)$$

Hence $V_o = V_s D$.

Where f = 1/T is the switching frequency in hertz.

Since this is a bi-directional dc-dc converter, there is no boundary between continuous and discontinuous current. The current can flow in both directions depending on the control strategy. The determination of the inductance, L_m, is possible by rearranging Equation (6.56) as:

$$L_m = \left[\frac{V_0}{\Delta i_L}(1-D)T\right] \qquad (6.57)$$

For a bi-directional dc-dc converter, current can flow in both directions of the inductor. When the battery is supplying the load, the inductor current flows in the positive direction and when the battery is charging, the inductor current flows in the opposite direction through the parallel diode, D_{dc1}. The charging or discharging of the battery is determined by the switching action of the two switches, S_{dc1} and S_{dc2}. The ON and OFF

ratio of the switch, S_{dc1}, is represented by the duty ratio, D, which is in turn determined by the control action.

In this converter, the output voltage, V_o, has been controlled to follow the reference voltage, V_{ref}. In order to provide a ripple free output voltage, the capacitor was assumed to be very large to keep the output voltage constant. In practice, the output voltage cannot be kept perfectly constant with a finite capacitance. The variation in output voltage, or ripple, is computed from the voltage-current relationship of the capacitor. The current in the capacitor is

$$I_{co} = I_L - I_o \tag{6.58}$$

shown in Figure 6.30(a).

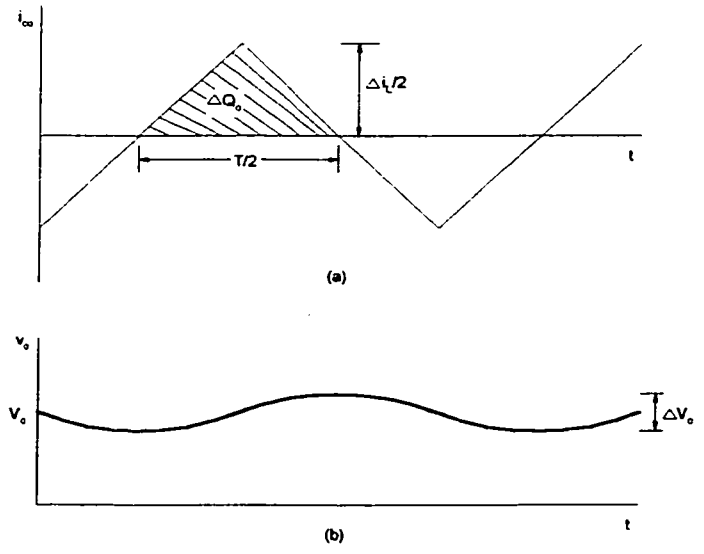

Figure 6.30 Buck converter waveform (a) Capacitor current, I_{co}. (b) Capacitor ripple voltage, V_o.

While the capacitor current is positive, the capacitor is charging. From the definition of capacitance, we have

$$Q_o = C_o V_o \tag{6.59}$$

$$\Delta Q_o = C_o \Delta V_o \tag{6.60}$$

$$\Delta V_o = \frac{\Delta Q_o}{C_o} \tag{6.61}$$

The change in charge, ΔQ_o, is the area of the triangle above the time axis:

$$\Delta Q_o = \frac{1}{2}\left(\frac{T}{2}\right)\left(\frac{\Delta i_L}{2}\right) = \frac{T\Delta i_L}{8} \tag{6.62}$$

Substituting Equation (6.62) into (6.60) yields,

$$\Delta V_o = \frac{T\Delta i_L}{8C_o} \tag{6.63}$$

Using Equation (6.56) for Δi_L,

$$\Delta V_o = \frac{V_o(1-D)}{8L_m C_o f^2} \tag{6.64}$$

In this equation, ΔV_o is the peak-to-peak ripple voltage at the output, as shown in Figure 6.30(b). It is useful to express the capacitance in terms of the ripple voltage of the dc-dc converter:

$$C_o = \frac{V_o(1-D)}{8L_m \Delta V_o f^2} \tag{6.65}$$

Based on Equations (6.57) and (6.65), the inductance and capacitance values of the converter can be designed, it is, however, necessary to first determine the power outputs at the maximum voltage level. The designed parameters are based on the duty cycle, D, output voltage, V_o, output current, I_o, and the switching frequency, f. The inductance, L_m, and capacitance, C_o, as shown in Equations (6.57) and (6.65) are rewritten as:

$$L_m \geq \frac{V_o(1-D)}{\Delta i_L f} \tag{6.66}$$

$$C_o \geq \frac{V_o(1-D)}{8L_m f^2 \Delta V_o} \tag{6.67}$$

In this application, L_m is set to 0.68mH and C_o to 6uF.

Figures 6.31 and 6.32 show the closed-loop voltage, V_o, and output current, I_o, of the buck dc-dc converter. Because the available battery bank is rated at 240V, the initial base dc voltage is chosen to be $2k_{dc}$=120V.

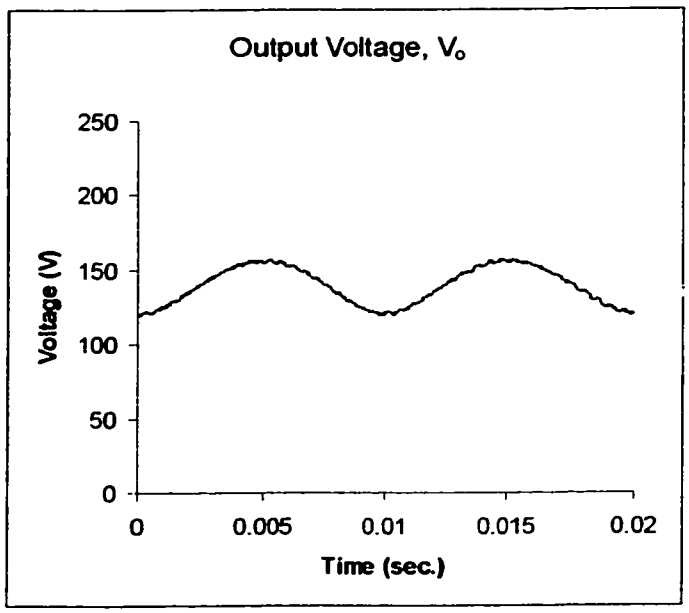

Figure 6.31 Output voltage, V_o

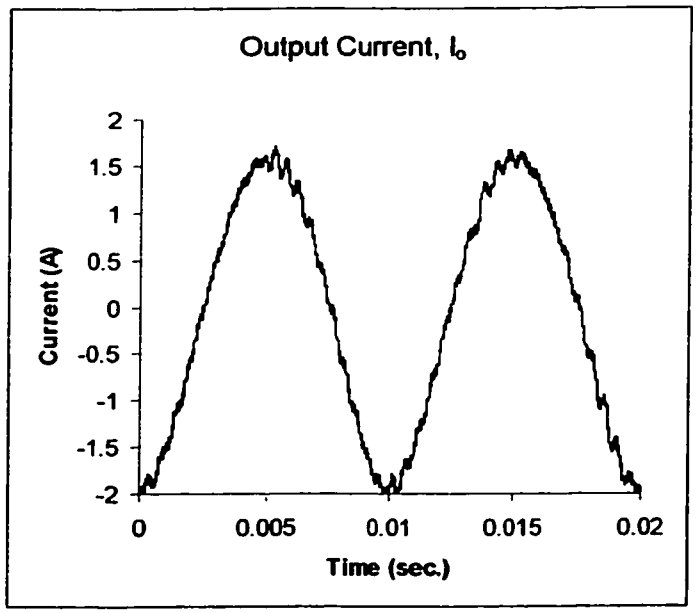

Figure 6.32 Output current, I_o

6.3.2.2 Boost DC-DC Converter

The simplified diagram of the bi-directional boost dc-dc converter is shown in Figure 6.33.

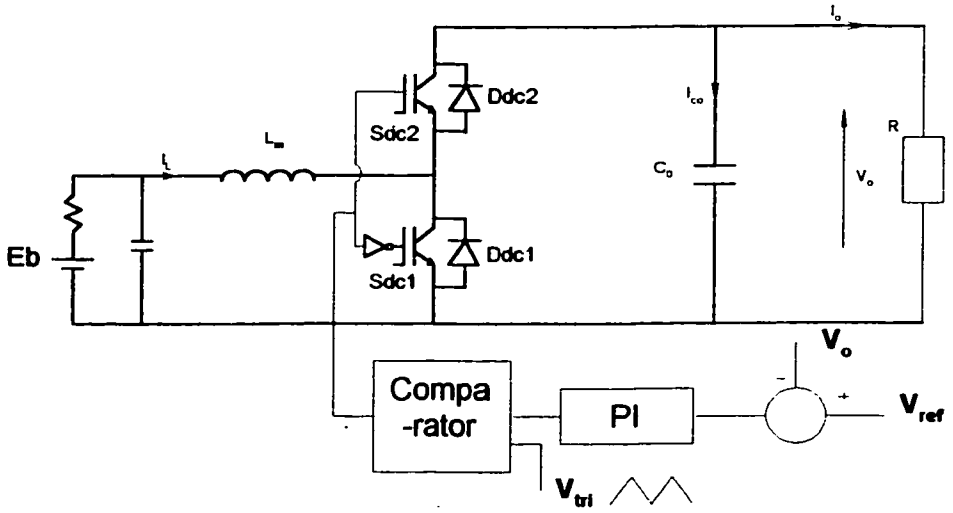

Figure 6.33 Bi-directional boost converter

The average inductor voltage must equal to zero for periodic operation. Expressing the average inductor voltage over one switching period,

$$V_L = E_b D + (E_b - V_o)(1 - D) = 0 \tag{6.68}$$

Solving for V_o yields:

$$V_o = \frac{E_b}{(1 - D)} \tag{6.69}$$

Equation (6.69) shows that if the switch is always open and D is zero, the output is the same as the input. As the duty ratio increases, the denominator of Equation (6.69) will

become smaller and the output larger than the input. The boost converter produces an output voltage that is larger than or equal to the input voltage. However, the output cannot be less than the input.

As the duty ratio of the switch approaches one, the output goes to infinity according to Equation (6.69). However, Equation (6.69) is based on ideal components. In pratical applications, the resistance of the circuit will limit the amount of voltage that can be obtained. Figure 6.34 shows the voltage and current waveforms for the boost converter,

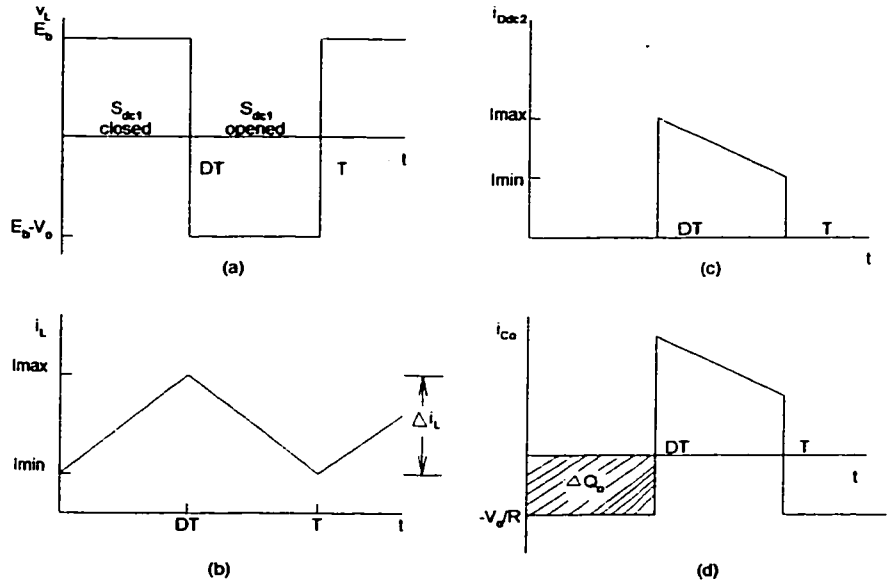

Figure 6.34 Boost converter waveforms. (a) Inductor voltage. (b) Inductor current. (c) Diode (D_{dc2}) current. (d) Capacitor (C_o) current.

the rate of change of inductor current is computed as:

$$\frac{\Delta i_L}{\Delta t} = \frac{\Delta i_L}{DT} = \frac{E_b}{L_m} \tag{6.70}$$

When switch S_{dc1} is closed.

Solving for Δi_L for the switch S_{dc1} closed (S_{dc2} opened), the change of inductor current:

$$\Delta i_{L(closed)} = \frac{E_b DT}{L_m} \tag{6.71}$$

When the switch, S_{dc1} is opened (S_{dc2} is closed), the inductor current cannot change instantly, so the diode, D_{dc2}, becomes forward biased to provide a path for inductor current. The rate of change of inductor current is computed as:

$$\frac{\Delta i_L}{\Delta t} = \frac{\Delta i_L}{(1-D)T} = \frac{E_b - V_o}{L_m} \tag{6.72}$$

Solving for Δi_L for the switch S_{dc1} opened (S_{dc2} closed), the change of inductor current:

$$\Delta i_{L(opened)} = \frac{(E_b - V_o)(1-D)T}{L_m} \tag{6.73}$$

The rate of change of the inductor current can be rearranged from Equation 6.71 or 6.73 as:

$$\Delta i_L = \frac{V_o(1-D)DT}{L_m} \tag{6.74}$$

The inductor current in the bi-directional dc-dc converter is continuous. The inductance can be found by rearranging Equation (6.74) as:

$$L_m = \frac{V_o(1-D)DT}{\Delta i_L} \tag{6.75}$$

The output voltage is assumed to be constant, implying an infinite capacitance. In practice, a finite capacitance will result in some fluctuation in output voltage, or ripple.

The peak-to-peak output voltage ripple can be calculated from the capacitor current waveform, shown in Figure 6.34(d). The changes in capacitor charge can be calculated from

$$|\Delta Q_o| = \left(\frac{V_o}{R}DT\right) = C_o \Delta V_o \tag{6.76}$$

An expression for ripple is then

$$\Delta V_o = \frac{V_o DT}{RC_o} = \frac{V_o D}{RC_o f} \tag{6.77}$$

$$\frac{\Delta V_o}{V_o} = \frac{D}{RC_o f} \tag{6.78}$$

From Equation (6.75) and (6.78), the inductance and capacitance can be rewritten as:

$$L_m \geq \frac{V_o D(1-D)}{f\Delta i_L} \tag{6.79}$$

$$C_o \geq \frac{V_o D}{\Delta V_o R f} \tag{6.80}$$

Bi-directional boost dc-dc converter has an advantage that it can step up the battery dc voltage, and hence less batteries are required and the battery cost reduced. Although the boost converter is more suitable and cost effective than the buck converter for the BESS, in general the control is not as linear as the buck converter and further it may become unstable under certain operating conditions. Larger output capacitor is also required and in this application C_0=12uF and L_m=0.6mH. In designing the boost converter for the BESS, it is important to identify the output power at peak voltage rating. If the power required is too high, the boost converter may become unstable. Figures 6.35 and 6.36 show the close-loop output voltage, V_o, and output current, I_o, of the boost converter. The converter output voltage is controlled with base voltage equal to $2k_{dc}$=180V. Figure 6.36 also shows that the current can flow freely in and out of the battery bank.

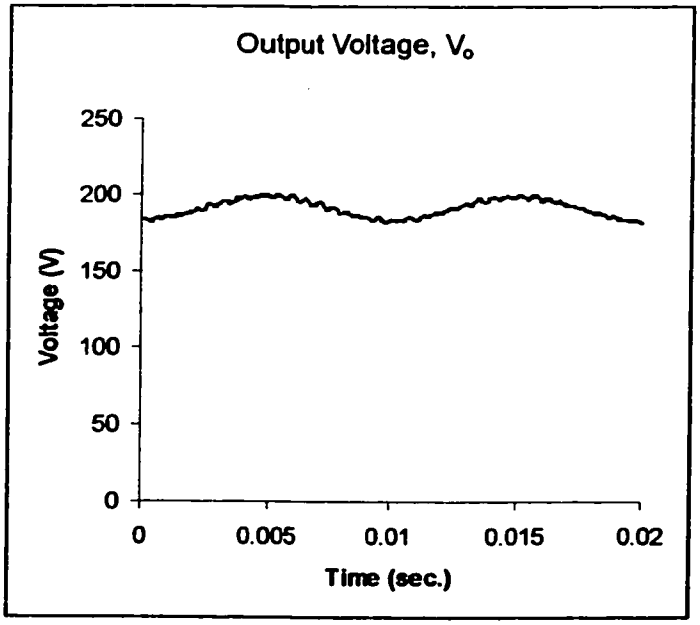

Figure 6.35 Output voltage, V_o

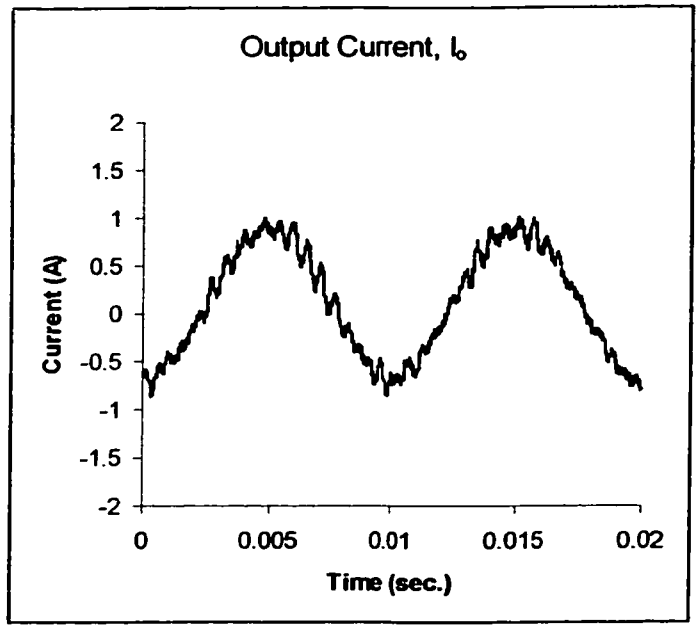

Figure 6.36 Output current, I_o

6.3.3 Improvement that can be gained by using the proposed technique

Based on the analysis made in the pervious sections, the battery voltage variation and the PWM frequency variation with the fixed-hysteresis band can be identified. With the proposed method which employs the DC-DC converter for dc terminal voltage control and the fixed-band hysteresis controller, it is possible to solve the above problems and also provide the following benefits.

6.3.3.1 Control of switching frequency

Figures 6.25(b) and 6.26(b) show that the switching frequency can be fixed by controlling the variable output voltage of the dc-dc converter. In this way, the magnitude of the variable output voltage can be controlled within a rated value to give a predefined switching frequency.

6.3.3.2 Eliminating the effect of battery voltage variation using the fixed-band hysteresis controller

Even the battery voltage in the worst case may vary by a factor of two from full charging to full discharging as shown in Figure 6.25(d) and 6.26(d), the dc-dc converter isolates the battery bank voltage from the inverter dc terminal, providing a ripple-controlled dc waveform to the inverter, so that, the battery voltage variation does not affect the fixed-band hysteresis controller.

6.3.3.3 Benefits of the Boost converter over the Buck converter

6.3.3.3.1 Reduction of battery cost

Figures 6.25(b) and 6.26(b) show the frequency spectrum at a lower and a higher output voltage, respectively controlled by a buck and a boost converter. It is noticed that when the output voltage is higher, the modulation frequency will be larger and the frequency range will be norrower. In order to achieve high switching frequency and a narrow frequency range, two approaches have been studied based on the proposed method. The first approach uses a bi-directional buck converter and the second approach employs a bi-directional boost converter. The first approach utilizing a step-down converter

requires higher battery voltage to have the same output dc voltage and hence the battery cost is higher. On the contrary, the second approach steps up the voltage level, so the number of batteries utilized can be reduced and as a result this approach is more cost effective.

6.3.3.3.2 Reduction of Current in IGBT and hence Reduction of IGBT Losses

Figures 6.37 and 6.38 show the current, I_o, flowing into the inverter. Comparing the two I_o, we notice that the current in Figure 6.38 is a half of that in Figure 6.37. Since the Boost converter stepped up the output voltage so that the transformer connected between the inverter and the ac system can be tapped up to a higher turns ratio, e.g. 2:1. Under the same power rating conditions for both of the cases, the use of boost converter provides lower current flowing to the inverter, and hence reduce the switching losses in the inverter.

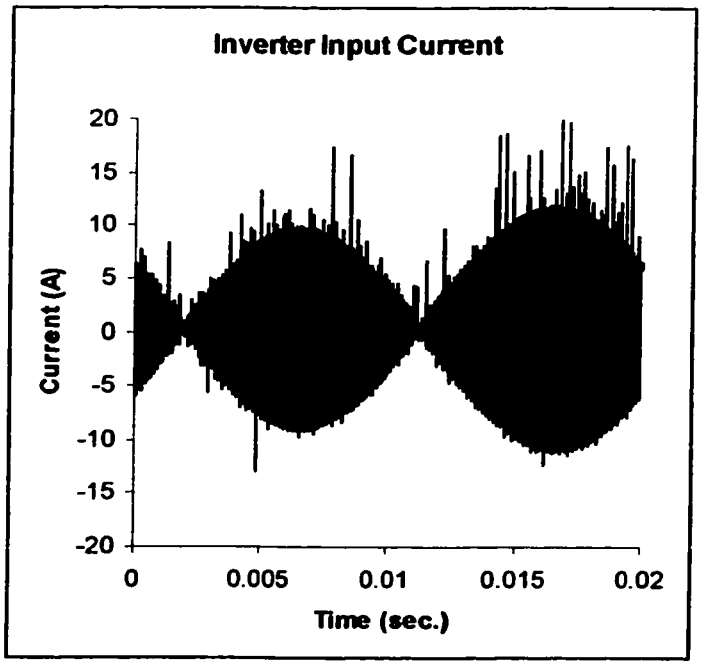

Figure 6.37 DC-Buck Inverter Current

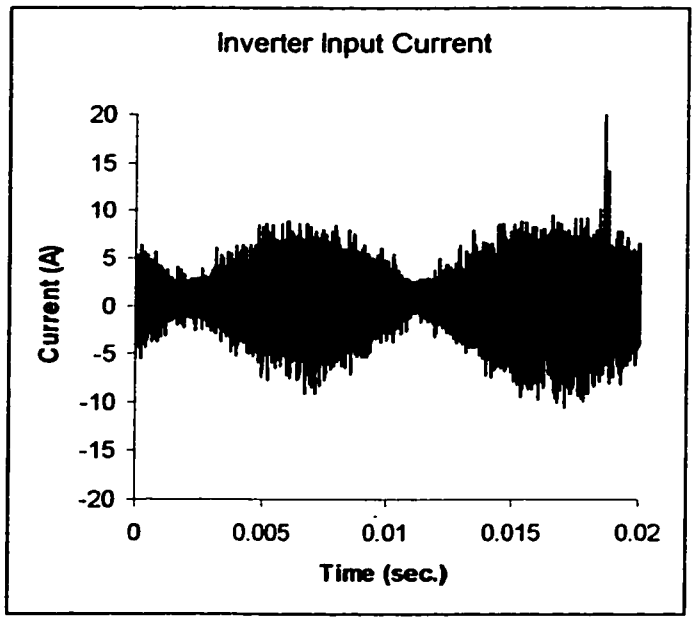

Figure 6.38 DC-Boost Inverter Current

6.3.3.3.3 Load Range Extension

The utilization of the boost converter can provide voltage control. The range of the output voltage depends on the converter design and the battery voltage. For the boost converters, the output voltage range can be adjusted from 1.6 to 2.5 times of its battery voltage. The extended voltage range provides a higher voltage difference between the inverter output voltage and the transformer terminal voltage, and a higher output current can also be obtained if the component rating is made higher, thus the output load range can be extended.

6.4 Conclusions

This chapter reviewed some of the soft switching techniques for the resonant dc link inverters and some PWM methods being used for common converter control. In section 6.2, a soft switching PWM inverter is presented by using a parallel resonant dc-link (PRDCL) and single-phase soft switching (SPSS) technique (Venkataramanan, G. and Divan, D.M., 1990). The proposed PRDCL suppresses the dc-link voltage to zero to allow zero voltage switching of inverter devices without imposing excessive device voltage and current stresses. Thus, all devices including inverters are under minimum voltage stress (V_s). The PRDCL provides not only variable link pulse width but also variable pulse position which is a quite different feature comparing to the only variable link pulse width with fixed pulse position of the other resonant dc-link (Malesani, L., Tenti, P., Divan, D.M. and Toigo, V., 1989). Thus, the PWM capability of the presented PRDCL converter can be greatly increased. For further enhancement of PWM capability of the PRDCL converter, the SPSS technique is employed by means of distributing the resonant capacitor to each inverter device. Furthermore the converter can be extended to a soft switching PWM rectifier-inverter without further excessive devices, and this is very significant for BESS applications. This is the first time that such a technique is applied for the BESS.

In section 6.3, based on the hysteresis control a newly proposed method by means of dc-dc converter provides a controllable voltage at the inverter dc terminal. The controllable voltage is designed to give a constant switching frequency even with a fixed hysteresis band. A mathematical proof has been formulated. In addition, simulation test results demonstrating the impact of dc voltage variation on the change of the controlled current frequency spectrum have been reported. Since a dc-dc converter is required to provide

the controlled voltage, some observations on the benefits and disadvantages of the dc-dc buck and the dc-dc boost converters have also been discussed.

CHAPTER 7 CONCLUSIONS

A solution is a synthesis of component elements which hurdles the obstructing difficulties and, neither exceeding the available resources nor encroaching on the limits set by the constraints, accomplishes the prescribed goals.

Asimow, Morris

Introduction to Engineering Design

CHAPTER 7 CONCLUSIONS

7.1 Main contributions

Power system operation and control problems related to uncertainty have been around the utilities for many years. Research work has been done on design and implementation of novel fast responding battery energy to remove uncertainty has given a solution to this problem. This thesis has provided a review of the various potential applications of BESS in Power Systems and actual implementations of BESS in recent years pointing out the attribute of each. Most of these implementations are, however, limited in nature, in that each BESS can provide only one or two functions. With the current technology of microprocessors and fast switching power electronic devices, the possibility of having one BESS which can provide a comprehensive multi-function capability not only remove the uncertainly but also benefit the day to day operation by curtailing the fastest demand variations, particularly at the daily peak periods was present in this thesis.

With the state-of-the-art fast acting power electronic devices and powerful microprocessors currently available in the market, the potential of having one BESS that can provide many of these functions can now become a reality. This thesis has presented the design procedure of implementing a practical BESS for use in power systems including the selection of the battery bank, the design of the power conversion system and the implementation of the control system. Building up of the whole system hinged on the application tasks and the interrelated relationship between the battery bank and

the PCS rating. In addition, the PCS construction and the implementation of the control system based on the control interface were elaborated. Moreover, the implementation of the designed control strategy with both magnitude and phase angle control based on the DSP environment has been described.

Based on the above-mentioned work, the system has been implemented initially in a single-phase configuration for physical test to demonstrate the capability of the BESS for power factor correction, active filtering, damping load fluctuations and fast control of charge and discharge conditions.

For industrial applications a three-phase configuration has been simulated and implemented in the laboratory. Experimental and simulation results show that the proposed BESS can provide a continuous control of the active and reactive power. The system also demonstrated the control ability of the BESS to maintain constant voltage at a point of common coupling irrespective of fluctuation in load demand, power quality enhancement in the form of active filtering, power factor correction, load balancing in three-phase system, load leveling for daily load management and the ability to damp any swing during transient and dynamic operation. In addition, from the BESS system point of view, the system response and the power conversion efficiency show a promising result of the BESS operation.

However, power utilities throughout the world are facing increasing financial and environmental restrictions on building new power stations and transmission lines. The distribution of power flow on paralleled transmission lines depends on the ratio of the

line impedances rather than the line thermal rating, causing uneven loading of transmission line corridors. Furthermore, reactive power losses increase rapidly as more power is transferred through a line, causing severe reactive power deficit which can lead to voltage instability. Flexible AC Transmission Systems (FACTS) have been recently introduced as a means of using power electronics to rapidly control the power flow along a transmission corridor in a predetermined manner. The thesis has discussed several topologies of BESS connection to the grid that provide FACTS flexibility while at the same time make use of the high-speed control of the active and reactive power of BESS to provide load leveling for energy management purposes. This thesis demonstrated that the SPFC3 can provide all the standard functions of UPFC such as voltage drop compensation in the form of a fully controllable series voltage source (both its magnitude and angle) and shunt reactive power compensation. Further, it can also provide other functions not currently available in the conventional UPFC such as back-up functions and 'negative load-shedding' or spinning reserve capability.

The control strategy developed for the BESS provides inherent active filtering and reactive power compensation to the power system. When sufficient numbers of the BESS are placed at the distribution level, the load demand seen by the transmission system can be controlled in a predetermined manner to reduce operating cost, improve load factor, provide improved power system operation and control and increase reliability of the power system, particularly, during system collapse or voltage instability. Having a single device that can provide all these functions provides for a real flexible AC system – a storage form of the Power Flow Controller.

To improve the performance of the BESS, a soft switching PWM inverter based on a parallel resonant dc-link (PRDCL) and soft switching technique (Venkataramanan, G. and Divan, D.M., 1990) was proposed. The proposed PRDCL suppresses the dc-link voltage to zero for a short period to allow zero voltage switching of inverter devices without imposing excessive device voltage and current stresses. Thus, all devices including inverters are under minimum voltage stress (V_s). The PRDCL provides not only variable link pulse width but also variable pulse position which is quite distinct from the traditional variable link pulse width with fixed pulse position used in other resonant dc-link circuit. (Malesani, L., Tenti, P., Divan, D.M. and Toigo, V., 1989). Thus, the PWM capability of the presented PRDCL converter is enhanced.

Finally, based on the hysteresis control a novel method is proposed where the dc voltage level at the inverter dc terminal is continuously controlled to follow a pre-set pattern, by means of a dc-dc converter. The controllable voltage is designed in such a manner that constant switching frequency in the inverter can be obtained even if a fixed hysteresis band is used. A mathematical explanation why such a procedure can provide the desired effect has been formulated. The possibility of using dc-dc converters in buck boost forms has been discussed. Advantages and disadvantages of each form were also discussed.

7.2 Recommendations for further research

As mentioned in the thesis, the BESS consists of battery system, power conversion and control systems. Although the thesis has proposed improvement on the development of the BESS, there is still many works that can be investigated.

In the system control aspect, it is possible to utilize advanced control algorithm based on artificial intelligence such as fuzzy logic control to improve the proposed hysteresis control in the BESS. However, care must be taken into account to ensure that switching losses can be minimized, particularly for use in large power applications using high frequency switching. Fuzzy logic control has been found to provide good control in many power electronics applications and it is envisaged that the use of such advanced control methodology will be valuable in future BESS development. In addition, nowadays technology allows control strategy built in a microchip for faster control, this can greatly reduce the cycle time required for processing.

In the system construction, new technologies to improve the packaging of power electronics devices have been proposed in the form of "Power Electronics Building Block". As electronic systems become more compact and complex, the interconnection of the components is more difficult. Increased density raises issues such as excessive heat generated, unplanned parasitic capacitance and inductance, thermal stresses, and bonding reliability. The integrated technology allows the designer to lay the circuit using modular components which greatly simplify the construction process. It will allow new design of soft-switching topology to be quickly laid out at the PCB board together with the inverter circuit. This will not only reduce the size of the circuit but also reduce line inductance and capacitance most often causing of EMI problem. Many kinds of combinations can be built in modular form like building blocks in construction industry that is suitable for various kinds of applications. The modular construction not only can provide inverter and soft-switching blocks, it is also possible to easily add the dc-dc converter or any other power electronics circuit to improve the performance. In this way,

parasitic loads can be reduced and in some cases the efficiency of the energy storage component can be improved, and as a result the costs and the requirement of generation capacity for charging the energy storage system can be minimized.

For system applications, the SPFCs are considered for operation in both distribution and transmission systems. However, the application of SPFCs in transmission system would require high voltage potential at the DC-link at which the batteries are connected. This may cause problems to the battery system, since it is difficult to have a high voltage DC breaker for isolation between batteries. Another difficulty is to the power conversion system have batteries operated in high voltage level. However, with advances in breaker design and the use of future innovative batteries, some of these obstacles can be overcome. At present, it seems that the SPFC could be most suitable for applications in distribution system only.

REFERENCES

Acharya, B., Divan, D.M. and Gascoigne, R.W., 1992. Active Power Filters using Resonant Pole Inverters, IEEE Transactions on Industry Applications Vol. 28, No. 6 November/December 1992, pp. 1269-1276.

Akagi, H., Tsukamoto, Y. and Nabae, A., 1990. Analysis and design of an active power filter using quad-series voltage source PMW converters, IEEE Transaction on Industry Applications, Vol. 26, No. 1 Jan./Feb. 1990.

Akagi, H., 1996. New Trends in Active Filters for Power Conditioning, IEEE Transactions on Industrial Applications, Vol. 32, No. 6, pp. 1312-1322, Nov/Dec. 1996.

Alt, J.T., Anderson, M.D. and Jungst, R.G., 1997. Assessment of Utility Side Cost Savings from Battery Energy Storage, IEEE Transactions on Power Systems, Vol. 12, No. 3, August 1997, pp. 1112-1120.

Anderson, M.D., and Carr, D.S., 1993. Battery Energy Storage Technologies, Proceedings of the IEEE, Vol. 81, No. 3, March 1993, pp.475-479.

Baker, J.N. and Collinson, A., 1999. Electrical Energy Storage at the turn of the Millennium, Power Engineering Journal, Vol.13, No.3, June 1999, pp.107-112.

Baker, M., 1997. Power transmission and how it's changing, Power Engineering Journal, Vol. 11, No. 5, October 1997, pp. 189-196.

Ball, G.J., Corey, G. and Norris, B.L., 1995. Government, Industry, and Utility Development and Evaluation of a Modular Utility Battery Energy Storage System, IEEE Transactions on Energy Conversion, Vol. 10, No. 3, Sept. 1995, pp. 549-554.

Balland J.P., Bassett, R.J. and Davidson, C.C., 1996. Power Electronic Devices and Their Impact for Power Transmission, AC and DC Power Transmission, 29 April-3 May 1996, Conference Publication No. 423, IEE 1996, pp. 245-251.

Bedford, B.D., 1975. Versatile Cycloinverter Power Converter Circuits, U.S. Patent, No. 3,742,336, 26 June, 1975.

Berdelle, J., 1932. Der elektrische Speicher in der Stromversorgung (Electric Storage for Power Supply Systems) Berlin, 1932.

Berkovici, J. and Ioinovici, A., 1998. High Efficient PWM Zero-Voltage-Transition DC-DC Boost Converter, Proceedings of the IEEE International Symposium on Circuits and System 1998 (ISCAS 98) Vol. 6, pp. 442-445.

Bernard, S. and Papoz, S., 1995. Active filter design and specification for control of harmonics in industrial and commercial facilities, Proceedings in Power Quality Solutions, September 1995.

Bhargava, B. and Dishaw, G., 1998. Application of an Energy Source Power System

Stabilizer on the 10 MW Battery Energy Storage System at Chino Substation, IEEE Transactions on Power System, Vol. 13, No. 1, Feb. 1998, pp. 145-151.

Bhattacharya, S., Frank, T.M., Divan, D.M. and Banerjee, B., 1998. Active Filter System Implementation, IEEE Industry Application Magazine, September/October, 1998, pp. 47-63.

Blasko, V. and Kaura, V., 1997. A New Mathematical Model and Control of a Three-Phase AC-DC Voltage Source Converter, IEEE Transactions on Power Electronics Vol. 12, No. 1, January 1997, pp. 116-123.

Boening, H.J. and Hauer, J.F., 1985. Commissioning test of the Bonneville power damonstration 30 MJ super-conducting magnetic energy storage unit, IEEE Transactions on PAS., Vol. 104, No. 2, 1985, pp. 302-309.

Bose, B.K., 1990. An Adaptive Hysteresis-Band Current Control Technique of a Voltage-Fed PWM Inverter for Machine Drive System, IEEE Transactions on Industrial Electronics Vol. 37, No. 5, October 1990, pp. 402-408.

Brod, D.M. and Novotny, D.W., 1984. Current control of VSI-PWM inverters, IEEE/IAS 1984 Annual Meeting, pp. 418-425.

Campbell, A. and McHattie, R., 1999. Backfilling the sine-wave, Power Engineering Journal, Vol. 13, No. 3, June 1999, pp. 153-158.

Chan, C.C. and Chau, K.T., 1993. A New Zero-Voltage-Switching DC/DC Boost

Converter, IEEE Transactions on Aerospace and Electronic Systems Vol. 29, No. 1, January 1993, pp. 125-134.

Chen, D.Y., Lee, F.C. and Carpenter, G., 1995. Nondestructive RBSOA Characterization of IGBT's and MCT's, IEEE Transactions on Power Electronics Vol. 10, No. 3, May 1995, pp. 368-372.

Cheriti, A., Al-Haddad, K., et.al., 1990. A Rugged Soft Commutated PWM Inverter for AC Drives, IEEE PESC, 1990 Records, pp. 656-662.

Chiang, S.J., Liaw, C.M., Chang, W.C. and Chang, W.Y., 1996. Multi-Module Parallel Small Battery Energy Storage System, IEEE Transactions on Energy Conversion, Vol. 11, No. 1, March 1996, pp. 146-154.

Choi, J.W. and Sul, S.K., 1997. New Current Control Concept – Minimum Time Current Control in the Three-Phase PWM Converter, IEEE Transactions on Power Electronics Vol. 12, No. 1, January 1997, pp. 124-130.

Choi, J.W. and Sul, S.K., 1998. Fast Current Controller in Three-Phase AC/DC Boost Converter Using d-q Axis Cross-coupling, IEEE Transactions on Power Electronics Vol. 13, No. 1, January 1998, pp. 179-185.

Collinson, A., 1999. Power Quality - The Volts and Amps of Electricity Supply, IEE Review, May 1999, pp. 122-130.

Dawande, M.S., Kanetkar, V.R. and Dubey, G.K., 1996. Three-Phase Switch Mode

Rectifier with Hysteresis Current Control, IEEE Transactions on Power Electronics Vol. 11, No. 3, May 1996, pp. 466-471.

De Broe, A.M., Drouilhet, S. and Gevorgian, V., 1999. A peak power tracker for small wind turbines in battery charging applications, IEEE Transactions on Energy Conversion, Vol. 14, 4 Dec. 1999, pp. 1630 –1635.

DeHaan, S.W.H. and Huisman, H., 1985. Novel Operation & Control Modes for Series-Resonant Converters, IEEE Transactions on Industrial Electronics, Vol. IE-32, No. 2, pp. 150-157.

DelMonaco, et al, 1982. Advanced Batteries for Load-Leveling; the Utility Perspective on System Integration, IEEE Transactions on Power Apparatus and Systems, Vol.101, No.9, pp.3315-3321, 1982.

Divan, D.M. and Skibinski, G., 1989. Zero-Switching-Loss Inverters for High-Power Applications, IEEE Transactions on Industry Applications Soc., Vol. 25, No, 4, July/August, 1989, pp. 634-643.

Divan, D.M., 1989. The Resonant DC Link Converter – A New Concept in Static Power Conversion, IEEE Transactions on Industry Applications, Vol. 25, No. 2, March/April, 1989, pp. 317-325.

Divan, D.M., Malesani, L., Tenti, P. and Toigo, V., 1993. A Synchronized Resonant DC Link Converter for Soft-Switched PWM, IEEE Transactions on Industry Applications Vol. 29, No. 5, September/October 1993, pp. 940-948.

Divan, D.M., Venkataramanan, G., Rik, W.A. and Doncker, A.D., 1993. Design Methodologies for Soft Switched Inverters, IEEE Transactions on Industry Applications Vol. 29, No. 1, January/February 1993, pp. 126-135.

Divan, Deepakraj M. and Skibinski, G., 1989. Zero-Switching-Loss Inverters for high-power applications, IEEE Transactions on Industry Application, Vol.25, No.4, July/August 1989, pp.634-643.

Dobie, W.C., 1998. Electrical energy storage, Power Engineering Journal, Vol.12, No.4, August 1998, pp.177-181.

Eckroad, S. and Radimer, B., 1991. Review of Engineering Design Considerations for Battery Energy Management Systems, IEEE Transactions on Energy Conversion Vol. 6, No. 2, June 1991, pp. 303-9.

Edris, A.A., 1997. Proposed Terms and Definitions for Flexible AC Transmission System (FACTS), IEEE Transactions on Power Delivery, Vol. 12, No. 4, October 1997, pp. 1848-1853.

Edris, A.A., Mehraban, A.S., Rahman, M., Gyugyi, L., Arabi S. and Rietman, T.R., 1998. Controlling the Flow of Real and Reactive Power, IEEE Computer Applications in Power, January 1998, pp. 20-25.

EESAT, 1998. (Electrical Energy Storage Systems, Applications and Technologies), Chester, United Kingdom, Conference proceedings, EA Technology, June 1998.

Enjeti, P., Ziogas, P.D., Lindsay, J.F. and Rashid, M.H., 1986. A novel current controlled PWM inverter for variable speed ac drive, IEEE/IAS 1986 Annual Meeting, pp. 235-243.

Enslin, J.H.R., Zhao, J. and Spee, R. Operation of the Unified Power Controller as Harmonic Isolator.

Eric, G.C., Yang, X., Jiang, Y.M. and Lee, F.C., 1994. Novel Zero-Current-Transition PWM Converters, IEEE Transactions on Power Electronics Vol. 9, No. 6, November 1994, pp. 601-606.

Espelage, P.M. and Bose, B.K., 1975. High Frequency Link Power Conversion, IEEE-IAS Auunal Meeting Records, pp. 802-808.

Exide Management and Technology Company, 1983. Research, Development, and Demonstration of Advanced Lead-Acid Batteries for Utility Load Leveling, Yardley, PA, for Argonne National Laboratory, Report No. ANL/OEPM-83-6, August 1983, pp2-4.

Finney, S.J., Green, T.C. and Williams, B.W., 1993. Review of Resonant Link Topologies for Inverters, IEE Proceedings on Electric Power Applications Vol. 140, No. 2, March 1993, pp. 103-113.

Fuerte-Esquivel, C.R. and Acha, E., 1997. Unified Power Flow Controller: a critical comparison of Newton-Raphson UPFC algorithms in power flow studies, IEE

Proceedings on Generation, Transmission and Distribution, Vol. 144, No. 5, September 1997, pp. 437-444.

Fujita, H. and Askagi, H., 1991. A practical approach to harmonic compensation in power systems - series connection of passive and active filters, IEEE Transaction on Industry Applications, Vol. 27, No. 6, Nov./Dec. 1991.

Funabiki, S. and Fuji, T., 1993. Fuzzy control of SMES for leveling load power fluctuation based on lukasiewicz logic, IEE Proceedings, Part C, Vol. 140, No. 2, 1993, pp. 91-95.

Gaio, E., Piovan, R. and Malesani, L., 1988. Evaluation of Current Control Methods for Voltage Source Inverters, ICEM 88, pp. 345-351.

Galiana, F.D., Almeida, K., Toussaint, M., Griffin, J., Atanackovic, D., Ooi, B.T. and McGillis, D.T., 1996. Assessment and Control of the Impact of FACTS Devices on Power System Performance, IEEE Transactions on Power Systems, Vol. 11, No. 4, November 1996, pp. 1931-1936.

Garcia, P.D. and Barbi, I., 1990. A Family of Resonant DC-link Voltage Source Inverters, IEEE IECON, 1990 Rec., pp. 844-849.

Gavrilovic, M.M., 1995. Optimum control of SMES systems for maximum power system stability and damping, Electrical Power & Energy Systems, Vol. 17, No. 3, 1995, pp. 199-205.

Gotham, D.J. and Heydt, G.T., 1998. Power Flow Control and Power Flow Studies for Systems with FACTS Devices, IEEE Transactions on power Systems, Vol. 13, No. 1, February 1998, pp. 60-65.

Gruzs, T.M. An Optimized Three-Phase Power Conditioner Featuring Deep Sag Protection and Harmonic Isolation.

Gyugi, L., 1992. Unified Power-flow Control Concept for Flexible AC Transmission Systems, IEE Proceedings Part C, Vol. 139, No. 4, July 1992, pp. 323-331.

Gyugi, L., Rietman, T.R., Edris, A., Schauder, C.D., Torgerson, D.R. and Williams, S.L., 1995. The Unified Power Flow Controller: A New Approach to Power Transmission Control, IEEE Transactions on Power Delivery, Vol. 10, No. 2, April 1995, pp. 1085-1097.

Gyugyi, L. and Cibulka, F., 1979. The High-Frequency Base Converter – A New Approach to Static High-Power Conversion, IEEE Transactions on Industry Applications, Vol. IA-15, No. 4, pp. 420-429.

Habetler, T.G., 1993. A Space Vector-Based Rectifier Regulator for AC/DC/AC Converters, IEEE Transactions on Power Electronics Vol. 8, No. 1, January 1993, pp. 30-36.

Haffmann, E., Alcorn, J., Chen, W., Hsu, Y.H., Purcell, J. and Schermer, R., 1981. Design of the BPA superconducting 30 MJ magnetic energy storage coil, IEEE Transactions on MAG., Vol. 17, 1981, pp. 521-524.

Hauth, R.L. and Moran, R.J., 1978. Introduction to Static Var Systems for Voltage and Var Control, General Electric Company, IEEE Tutorial Course, Power Electronics Applications in Power Systems, 1978, pp. 48-55.

He, J. and Mohan, N., 1989. Parallel Resonant DC Link Circuit – A Novel Zero Switching Loss Topology with Minimum Voltage Stresses, IEEE PESC, 1989, Res., pp.1006-1012.

He, J. and Mohan, N., 1990. Zero Voltage Switching PWM Inverter for High Frequency DC-AC Power Conversion, IEEE IAS, 1990, Res., pp.1215-1221.

He, J. and Mohan, N., 1991. Parallel Resonant DC Link Circuit – A Novel Zero Switching Loss Topology with Minimum Voltage Stresses, IEEE Transactions on Power Electronics Vol. 6, No. 4, October 1991, pp. 687-694.

He, J., Mohan, N. and Wold, B., 1993. Zero-Voltage-Switching PWM Inverter for High-Frequency DC-AC Power Conversion, IEEE Transactions on Industry Applications Vol. 29, No. 5, September/October 1993, pp. 959-968.

Hingorani, N.G., 1991. FACTS – Flexible AC Transmission System, Proceedings of the 5th 1991 IEE International Conference on AC and DC Transmission, Publ. 345, pp. 1-7, September 1991.

Hingorani, N.G., 1993. Flexible AC Transmission, IEEE Spectrum, Vol. 30, No. 4, April 1993, pp. 40-45.

Hingorani, N.G., 1994. IEE Colloquium on FACTS – The key to increased the utilization of Power Systems, No. 1994/005, pp. 4/1-10.

Hingorani, N.G., 1996. The Rise of High-Voltage, Direct-Current Systems, IEEE Spectrum, 1996.

Holtz, J. and Stadtfeld, S., 1983. A predictive controller for the stator current vector of ac machine-fed from a switched voltage source, Proceedings in International Power Electronic Conference Rec., (Tokyo), pp. 1665-1675.

Holtz, J., 1992. Pulsewidth Modulation – A Survey, IEEE PESC '92, Conf. Rec. Vol. 1, pp. 11-18.

Hsu, C.Y. and Wu, H.Y. A New Single-Phase Active Power Filter with Reduced Energy Storage Capacitor.

Hu, L. and Morrison, R.E., 1996. Simulation study of a transmission system containing two unequally rated parallel lines and a UPFC, IEE AC and DC Power Transmission, No. 423, 29 April-3 May 1996, pp. 346-350.

Hua, G.C., Leu, C.S., Jiang, Y.M. and Lee, F.C., 1994. Novel Zero-Voltage-Transition PWM Converters, IEEE Transactions on Power Electronics Vol. 9, No. 2, March 1994, pp. 213-219.

Hung, S.T., Hopkins, D.C. and Mosling, C.R., 1993. Extension of Battery Life Via

Charge Equalization Control, IEEE Transactions on Industrial Electronics Vol. 40, No. 1, February 1993, pp. 96-104.

Hunt, G.W., 1999. Valve-regulated lead/acid battery systems, Power Engineering Journal, Vol. 13, No. 3, June 1999, pp.113-116.

Hurwitch, H.J. and Carpenter, C.A., 1991. Technology and application options for future battery power regulation, IEEE Transactions on Energy Conversion, Vol. 6, No. 1, 1991, pp. 724-731.

Iglesias, I.J., Bautista, A. and Visiers, M., 1997. Experimental and simulated results of a SMES fed by a current source inverter, IEEE Transactions on A.S., Vol. 7, No. 2, 1997, pp. 861-864.

Irei, F., Takeo, M and et al, 1992. A field experiment on power line stabilization by a SMES system, IEEE Transactions on MAG, Vol. 28, No. 1, 1992, pp. 426-429.

Ise, T., Murakami, Y. and Tsuji, K., 1986. Simultaneous active and reactive power control of superconducting magnetic energy storage using GTO converter, IEEE Transactions on PWRD, Vol. 1, No. 1, 1986, pp. 143-149.

Jou, H.L., Wu, J.C. and Chu, H.Y., 1994. New single-phase active power filter, IEE Proceedings on Electrical Power Applications Vol. 141, No. 3, May 1994.

Jung, K.H., Kim, H.Y. and Rho, D., 1996. Determination of the Installation Site and Optimal Capacity of the Battery Energy Storage System for Load Leveling, IEEE

Transactions on Energy Conversion, Vol. 11, No. 1, March 1996, pp. 162-167.

Jung, Y.C. and Cho, G.H., 1994. Quasi-parallel Resonant DC Link Inverter with Improved PWM Capability, Electronics Letters, Vol. 30, No. 22, 27th October 1994, pp. 1827-1828.

Jung, Y.C., Liu, H.L., Cho, G.C. and Cho, G.H., 1996. Soft Switching Space Vector PWM Inverter Using a New Quasi-Parallel Resonant DC Link, IEEE Transactions on Power Electronics Vol. 11, No. 3, May 1996, pp. 503-511.

Kanazawa, A.Y., Nabae, A., 1984. Instantaneous Reactive Power Compensator Comparing Switching Devices Without Energy Storage Components, IEEE Transactions on Industrial Applications, Vol. IA-20, pp. 625- 630, 1984.

Kazmierkowski, M.P., and Malesani, L., 1998. Current Control Techniques for Three-Phase Voltage-Source PWM Converters: A Survey, IEEE Transactions on Industrial Electronics Vol. 45, No. 5, October 1998, pp. 691-703.

Kheraluwala, M.H. and Divan, D.M., 1990. Delta Modulation Strategies for Resonant Link Inverters, IEEE Transactions on Power Electronics Vol. 5, No. 2, April 1990, pp. 220-228.

Klaassens, J.B., 1984. DC to AC Series-Resonant Converter System with High Internal Frequency Generating Synthesized Waveforms for Multikilowatt Power Levels, IEEE Power Electronics Specialists Conference, pp. 99-110.

Kodama, E. and Kurashima, Y., 1999. Development of a compact sodium-sulphur battery, Power Engineering Journal, Vol. 13, No. 3, June 1999, pp. 136-141.

Kottick, D., Blau, M. and Edelstein, D., 1993. Battery energy storage system for frequency regulation in an island power system, IEEE Transactions on Energy Conversion, Vol. 8, No.3, 1993, pp. 455-459.

Kottick, D. and Blau, M., 1993. Operational and economic benefits of battery energy storage plants, International Journal of Electrical Power & Energy Systems, Vol. 15, No. 6, 1993, pp.345-349.

Kunisch, H.J. and Kramer, K.G., 1981. Utilization of Electro-Chemical Storage Systems in the Insular Power Supply System of Berlin (West), Proc. IEA Conference on New Energy Conservation Technologies, Berlin 1981.

Kurnia, A., Cherradi, H. and Divan, D.M., 1995. Impact of IGBT Behavior on Design Optimization of Soft Switching Inverter Topologies, IEEE Transactions on Industry Applications Vol. 31, No. 2, March/April 1995, pp. 280-286.

Kutkut, N.H., Divan, D.M. and Gascoigne, R.W., 1995. An Improved Full-Bridge Zero-Voltage Switching PWM Converter Using a Two-Inductor Rectifier, IEEE Transactions on Industry Applications Vol. 31, No. 1, January/February 1995, pp. 119-126.

Kutkut, N.H., Divan, D.M. and Novotny, D.W., 1995. Charge Equalization for Series Connected Battery Strings, IEEE Transactions on Industry Applications Vol. 31, No. 3,

May/June 1995, pp. 562-568.

Kutkut, N.H., Divan, D.M., Novotny, D.W. and Marion, R.H., 1998. Design Considerations and Topology Selection for a 120-kW IGBT Converter for EV Fast Charging, IEEE Transactions on Power Electronics Vol. 13, No. 1, January 1998, pp. 169-178.

Kutkut, N.H., Wiegman, H.L.N., Divan, D.M. and Novotny, D.W. Design Considerations for Charge Equalization of an Electric Vehicle Battery System, Department of Electrical and Computer Engineering, University of Wisconsin – Madison, pp. 96-103.

Kutkut, N.H., Wiegman, H.L.N., Divan, D.M. and Novotny, D.W., 1998. Charge Equalization for an Electric Vehicle Battery System, IEEE Transactions on Aerospace and Electronic Systems Vol. 34, No. 1, January 1998, pp. 235-246.

Lachs, W.R. and Sutanto, D. Voltage Instability in Interconnected Power Systems: A Simulation Approach, IEEE Transactions on Power Systems (PWRS), Vol. 7, No 2, pp. 753-761.

Lachs, W.R. and Sutanto, D., 1992. Battery Storage Plant Within Large Load Centres, IEEE Transactions on Power Systems, Vol. 7, No. 2, May 1992, pp. 762-769.

Lachs, W.R. and Sutanto, D., 1994. A New Load Sheding Scheme for Limiting Under-frequency, IEEE Transactions on Power Systems Vol. 9, No. 3, August 1994, pp. 1371-1378.

Lachs, W.R. and Sutanto, D., 1994. Different Types of Voltage Instability, IEEE Transactions on Power Systems Vol. 9, No. 2, May 1994, pp. 1126-1134.

Lai, J.S. and Bose, B.K., 1990. High Frequency Quasi-Resonant DC Voltage Notching Inverter for AC Motor Drives, IEEE IAS, 1990, Rec., pp.1202-1207.

Lai, J.S., 1997. Resonant Snubber-Based Soft-Switching Inverters for Electric Propulsion Drives, IEEE Transactions on Industrial Electronics Vol. 44, No. 1 February 1997, pp. 71-80.

Lai, J.S., Young, R.W., Ott, G.W., Mckeever, J.W. and Peng, F.Z., 1996. A Delta-Configured Auxiliary Resonant Snubber Inverter, IEEE Transactions on Industry Applications Vol. 32, No. 3, May/June 1996, pp. 518-525.

Lee, F.C., 1988. High-Frequency Quasi-Resonant Converter Technologies, Proceedings of the IEEE Vol. 76, No. 4, April 1988, pp. 377-390.

Lee, R.H., 1989. Eliminating harmonic currents using transformers, Power Quality Proceedings, Oct. 1989.

Lee, T.Y. and Chen, N.M., 1995. Determination of Optimal Contract Capacities and Optimal Sizes of Battery Energy Storage Systems for Time-Of-Use Rates Industrial Customers, IEEE Transactions on Energy Conversion, Vol. 10, No. 3, September 1995, pp. 562-568.

Le-Huy, H., and Dessaint, L.A., 1986. An adaptive current controller for PWM inverters, IEEE/IAS 1986 Annual Meeting, pp. 610-616.

Lex, P. and Jonshagen, B., 1999. The zinc/bromine battery system for utility and remote area applications, Power Engineering Journal, Vol. 13, No. 3, June 1999, pp. 142-148.

Liaw, C.M. and Chiang, S.J., 1994. Design and Implementation of a Single-Phase Three-Wire Transformerless Battery Energy Storage System, IEEE Transactions on Industrial Electronics, Vol.41, No.5, October 1994, pp.540-549.

Liaw, C.M., Chiang, S.J. and Huang, S.C., 1994. A Three-phase Multi-Functional Battery Energy Storage System, Proceedings of 20th Annual Conference of IEEE Industrial Electronics (IECON' 94), 5-9 September 1994, pp. 458-463.

Liaw, C.M., Jan, L.C., Wu, W.C. and Chiang, S.J., 1996. Operation Control of Paralleled Three-phase Battery Energy Storage System, IEE Proceedings of Electric Power Application Vol. 143, No. 4, July 1996, pp. 317-22.

Limyingcharoen, S., Annakkage, U.D. and Pahalawaththa, N.C., 1998. Effects of Unified Power Flow Controllers on Transient Stability, IEE Proceedings on Generation, Transmission and Distribution Vol. 145, No. 2, March 1998, pp. 182-188.

Lin, C.E., Tsai, M.T., Shiao, Y.S. and Huang, C.L. An Active Filter for Reactive and Harmonic Compensation Using Voltage Source Inverter.

Lin, C.E., Tsai, M.T., Tsai, W.I. and Huang, C.L., 1995. Development of a General-Purpose Demand-Side Battery Energy Storage System, IEEE 1995, pp. 1893-1899.

Ling, J.A. and Eldriridge, C.J. Designing modern electrical systems with transformers that inherently reduce harmonic distortion in a PC-Rich Environment.

Lo, C.H. and Anderson, M.D., 1999. Economic Dispatch and Optimal Sizing of Battery Energy Storage Systems In Utility Load-Leveling Operations, IEEE Transactions on Energy Conversion, Vol. 14, No. 3, September 1999, pp. 824-829.

Long, W.F., 1978. HVDC Power Transmission, University of Wisconsin Madison, Wisconsin, IEEE Tutorial Course, Power Electronics Applications in Power Systems, 1978, pp. 38-47.

Lu, C.F., Liu, C.C. and Wu, C.J., 1995. Dynamic Modeling of Battery Energy Storage System and Application to Power System Stability, IEE Proceedings on Generation, Transmission and Distribution, Vol. 142, No. 4, July 1995, pp. 429-435.

Lu, C.F., Liu, C.C. and Wu, C.J., 1995. Effect of Battery Energy Storage System on Load Frequency Control Considering Governor Dead-band and Generation Rate Constraint, IEEE Transactions on Energy Conversion, Vol. 10, No. 3, September 1995, pp. 555-561.

Malesani, L. and Tenti, P., 1987. A novel hysteresis control method for current-controlled VSI PWM inverters with constant modulation frequency,

Proceedings in Conference Rec. IEEE/IAS Annual Meeting, 1987, pp. 851-855.

Malesani, L., Tenti, P., Divan, D.M. and Toigo, V., 1989. A Synchronized Resonant DC Link Converter for Soft-Switched PWM, IEEE-IAS Annual Meeting 1989, pp.1037-1044.

Malesani, L., Tenti, P., Tomasin, P. and Toigo, V., 1995. High Efficiency Quasi-Resonant DC Link Three-Phase Power Inverter for Full-Range PWM, IEEE Transactions on Industry Applications Vol. 31, No. 1, January/February 1995, pp. 141-148.

Maly, D.K. and Kwan, K.S., 1995. Optimal Battery Energy Storage System (BESS) Charge Scheduling with dynamic programming, IEE Proceedings on Science, Measurement and Technology, Vol. 142, No. 6, November 1995, pp. 453-458.

Mao, H.C., Lee, F.C., Zhou, X.W., Dai, H.P., Cosan, M. and Boroyevich, D. Improved Zero-Current Transition Converters for High-Power Applications, IEEE Transactions on Industry Applications Vol. 33, No. 5, September/October 1997, pp. 1220-1232.

Massey, G.W. Design Solutions for Harmonic Load Current Effects on Electrical Power Distribution Equipment.

Miller, N.W., Zrebiec, R.S., Delmerico, R.W. and Hunt, G., 1996. Design and Commissioning of a 5MVA, 2.5MWH Battery Energy Storage System, Proceedings of 1996 Transmission and Distribution Conference and Exposition IEEE, pp. 339-345.

Mitani, Y., Tsuji, K. and Murakami, Y., 1988. Application of superconducting magnet energy storage to improve power system dynamic performance, IEEE Transactions on Power System, Vol. 3, No. 4, 1988, pp. 1418-1424.

Mohan, N., Underland, T.M., Robbins, W.P., 1989. Power Electronics: Converters, Applications, and Design, Wiley, 1989.

Moore, P. and Ashmole, P., 1995. Flexible AC transmission systems, IEE Power Engineering Journal Vol. 9, No. 6, Dec. 1995, pp. 282-286.

Moore, P. and Ashmole, P., 1996. Flexible AC transmission systems – Part 2 Methods of transmission line compensation, IEE Power Engineering Journal Vol. 10, No. 6, Dec. 1996, pp. 273-278.

Moore, P. and Ashmole, P., 1997. Flexible AC transmission systems – Part 3 Conventional FACTS controllers, IEE Power Engineering Journal Vol. 11, No. 4, Aug. 1997, pp. 177-183.

Moore, P. and Ashmole, P., 1998. Flexible AC transmission systems – Part 4 Advanced FACTS controllers, IEE Power Engineering Journal Vol. 12, No. 2, April 1998, pp. 95-100.

Murai, Y. and Lipo, T.A., 1988. High Frequency Series Resonant DC Link Power Conversion, IEEE IAS Annual Meeting Records, pp. 772-779.

Nedderman, J., 1997. The most of Energy Storage, Asian Electricity, March 1997, pp.

21-23.

Nitschke, H.J., 1987. The Power Conditioning System for BEWAG's Steglitz Battery Plant, Proceedings International Conference Batteries for Utility Energy Storage, West Berlin, FRG, 9-11 November 1987, pp. 479-501.

Oh, D.S. and Youn, M.J., 1990. Automated adaptive Hysteresis Current Control Technique for a Voltage-Fed PWM Inverter, Electronics Letters 22nd Vol. 26, No. 24, November 1990, pp. 2044-2046.

Oruganti, R., Nagaswamy, K. and Sang, L.K., 1998. Predicted (On-Time) Equal-Charge Criterion Scheme for Constant-Frequency Control of Single-Phase Boost-Type AC-DC Converters, IEEE Transactions on Power Electronics Vol. 13, No. 1, January 1998, pp. 47-57.

Pahmer, C., Caspolino, G.A. and Henao, H. Computer-Aided Design for Control of Shunt Active Filter.

Palomino, E., Stevens, J. and Wiles, J., 1996. A Control System for Improved Battery Utilization in a PV-Powered Peak-Shaving System, IEEE 25th Photovoltaic Specialists Conference, Washington, D.C., 13-17 May 1996, pp. 1525-1528.

Pan, C.T. and Chang, T.Y., 1994. An Improved Hystersis Current Controller for Reducing Switching Frequency, IEEE Transactions on Power Electronics Vol. 9, No. 1, January 1994, pp. 97-104.

Patterson, O.D. and Divan, D.M., 1991. Pseudo-Resonant Full Bridge DC/DC Converter, IEEE Transactions on Power Electronics, Vol. 6, No. 4, October 1991, pp. 671-678.

Pelly, B.R. and Gyugyi, L., 1977. Naturally Commutated Cycloconverter with Controlled Input Displacement Power Factor, U.S. Patent, No. 4,013,937, 22 March 1977.

Pfaff, G., Weschta, A and Wick, A., 1982. Design and experimental results of a brushless ac servo drive, IEEE/IAS 1982 Annual Meeting, pp. 692-697.

Power Systems Engineering Department. HVDC Handbook, GE Industrial and Power Systems, 1st Edition.

Price, A., Bartley, S., Male, S. and Cooley G., 1999. A novel approach to utility scale energy storage, Power Engineering Journal, Vol. 13, No. 3, June 1999, pp. 122-129. Private communication, San Diego Gas & Electric, Jim Wight, Project Manager.

Quinn, C.A. and Persson, E.G. Overview of Filtering Techniques for the Reduction of Harmonic Distortion Levels on AC Distribution Systems.

Rahim, A.H.M.A., and Mohammad, A.M., 1994. Improvement of synchronous generator damping through superconducting magnetic energy storage systems, IEEE Transactions on Energy Conversion, Vol. 9, No. 4, 1994, pp. 736-742.

Rahim, A.H.M.A., Mohammad, A.M. and Khan, M.R., 1996. Control of

sub-synchronous resonant modes in a series compensated system through superconducting magnetic energy storage units, IEEE Transactions on Energy Conversion, Vol. 11, No. 1, 1996, pp. 175-180.

Rahman, K.M., Khan, M.R., Choudhury, M.A. and Rahman, M.A., 1997. Variable-Band Hysteresis Current Controllers for PWM Voltage-Source Inverters, IEEE Transactions on Power Electronics, Vol. 12, No. 6, November 1997, pp. 964-970.

Rahman, M.A., Radwan, T.S., Osheiba, A.M. and Lashine, A.E., 1997. Analysis of Current Controllers for Voltage-Source Inverter, IEEE Transactions on Industriai Electronics Vol. 44, No. 4, August 1997, pp. 477-485.

Raju, N.R., Venkata, S.S., Kagalwala, R.A. and Sastry, V.V. An Active Power Quality Conditioner for Reactive Power and Harmonics Compensation.

Rau, N.S. and Short, W.D., 1996. Opportunities for the Integration of Intermittent Renewable Resources into Networks Using Existing Storage, IEEE Transactions on Energy Conversion, Vol. 11, No.1, March 1996, pp. 181-187.

Reckrodt, R.C., Anderson, M.D. and Kluczny, R.M., 1990. Economic Models for Battery Energy Storage: Improvements for Existing Methods, IEEE Transaction on Energy Conversion, Vol. 5, No. 4, December 1990, pp. 659-665.

Redl, R., Tenti, P. and WYK, J.D.V., 1997. Power Electronics' Polluting Effects, IEEE Spectrum May 1997, pp. 33-39.

Rossetto, L., Tenti, P. and Zuccato, A., 1997. Integrated Optimum Control of Quasi-Direct Converters, IEEE Transactions on Power Electronics Vol. 12, No. 6 November 1997, pp. 993-999.

Saetieo, S. and Torrey, D.A., 1997. Fuzzy Logic Control of a Space Vector PWM Current Regulator for Three Phase Power Converters, APEC 97, 23-27 Feb., pp. 879-885.

Salameh, Z.M., Casacca, M.A. and Lynch, W.A., 1992. A mathematical model for lead-acid batteries, IEEE Transactions on Energy Conversion, Vol. 7, No. 1, pp. 93-97, March 1992.

Schonung, A. and Stemmler, H., 1964. Static frequency changers with subharmonic control in conjunction with reversible variable speed ac drives, Brown Boveri Rev., pp. 555-577.

Schottler, R. and Coney, R.G., 1999. Commercial application experiences with SMES, Power Engineering Journal, Vol. 13, No. 3, June 1999, pp. 149-152.

Schwarz, F.C., 1981. A Doublesided Cycloconverter, IEEE Transactions on Industry Electronics and Control Instrumentation, Vol. IECI-28, No. 4, pp. 282-291.

Shaughnessy, T. Power Factor, Harmonics and Harmonic Filters.

Shibata, A. and Sato, K., 1999. Development of vanadium redox flow battery for

electricity storage, Power Engineering Journal, Vol. 13, No. 3, June 1999, pp. 130-135.

Shimizu, T., Kurokawa, M., Nishida, Y., Nakaoka, M., Sugawara, Y and Horiuchi, T., 1997. Utility-Interactive Instantaneous Sine-wave Space Vector Modulated Bi-directional Three Phase Power Conditioner Using Resonant DC Link, IEEE Industry Application Society the 32nd Annual Meeting New Orleans, LA USA, 5-9 October 1997, pp. 1681-1688.

Simo, J.B. and Kamwa, I., 1995. Exploratory assessment of the dynamic behavior of multi-machine system stabilized by a SMES unit, IEEE Transactions on Power System, Vol. 10, No. 3, 1995, pp. 1566-1571.

Smale, M.J., Jenkins, N., Collinson, A., 1997. FACTS for Improved Power Quality, Proceeding of the 32nd Universities Power Engineering Conference (UPEC'97), Vol. 2, pp. 855-858, September 1997.

Sobieski, D.W. and Bhavarju, M.P., 1985. An Economic Assessment of Battery Storage in Electric Utility Systems, IEEE Transactions on Power Apparatus and Systems, Vol.PAS-104, No.12, pp.3453-3459, December, 1985.

Sood, P.K. and Lipo, T.A., 1986. Power Conversion Distribution System Using a High Frequency AC Link, IEEE IAS Annual Meeting Records, pp. 648-656.

Stillman, H.M., 1997. IGCTs – Megawatt Power Switches for Medium-Voltage Applications, ABB Review, pp. 12-17, March 1997.

Sutanto, D., Bou-rabee, M., Tam, K.S. and Chang, C.S., 1991. Harmonic filters for industrial power systems, IEEE International Conference on Advances in Power System Control, Operation and Management, Nov. 1991, Hong Kong.

Tang, W., Lee, F.C., Ridley, R.B. and Cohen, I., 1993. Charge Control: Modeling, Analysis, and Design, IEEE Transactions on Power Electronics Vol. 8, No. 4, October 1993, pp. 396-403.

Tang, Y.S and Meliopoulos, A.P., 1997. Power System Small Signal Stability Analysis with FACTS Elements, IEEE Transactions on Power Delivery, Vol. 12, No. 3, July 1997, pp. 1352-1361.

Tao, G. and Kokotovic, P.V., 1995. Adaptive Control of Plants with Unknown Hystereses, IEEE Transactions on Automatic Control, Vol. 40, No. 2, February 1995, pp. 200-212.

Tarrant, C., 1999. Revolutionary flywheel energy storage system for quality power, Power Engineering Journal, Vol. 13, No. 3, June 1999, pp. 159-163.

Ter-Gazarian, A.G., Kagan, N., 1992. Design model for electrical distribution systems considering renewable, conventional and energy storage units, IEE Proceedings on Generation, Transmission and Distribution, Vol. 139, 6 Nov. 1992, pp. 499 –504.

Torres, W., Sanchez, J., Ruiz, R., 1995. Outline of the new PREPA 20 MW battery facility, A Report by Puerto Rico Electric Authority, San Juan, Puerto Rico, 1995.

Tripathi, A. and Sen, P.C., 1992. Comparative Analysis of Fixed and Sinusoidal Band Hysteresis Current Controllers for Voltage Source Inverters, IEEE Transactions on Industrial Electronics, Vol. 39, No. 1, February 1992, pp. 63-73.

Venkataramanan, G. and Divan, D.M., 1993. Pulse Width Modulation with Resonant DC Link Converters, IEEE Transactions on Industry Applications, Vol. 29, No. 1, January/February 1993, pp. 113-120.

Voigt, B., Kunisch, H.J. and Kramer, K.G., 1989. On the operation of large scale battery storage systems, CIGRE Symposium Bangkok 1989.

Walker, L.H., 1990. 10-MW GTO Converter for Battery Peaking Service, IEEE Transactions on Industry Applications, Vol. 26, No. 1, January/February 1990, pp. 63-72.

Wang, H.F. and Swift, F.J., 1997. A unified Model for the Analysis of FACTS Devices in Damping Power System Oscillations Part I: Single-machine Infinite-bus Power Systems, IEEE Transactions on Power Delivery, Vol. 12, No. 2, April 1997, pp. 941-946.

Watanabe, E.H., Aredes, M., 1993. New Concepts of Instantaneous Active and Reactive Power in Electrical Systems with Generic Loads, IEEE Transactions on Power Delivery, Vol. 8, No. 2, pp. 697-703, 1993.

Watanabe, E.H., Aredes, M., 1995. New Control Algorithms for Series and Shunt Three-Phase Four-Wire Active Power Filters, IEEE Transactions on Power Delivery,

Vol. 10, No. 3, pp. 1649-1656, July 1995.

Wei, H. and Ioinovici, A., 1998. Zero-Voltage Transition Converter with High Efficiency Operating at Constant Switching Frequency, IEEE Transactions on Circuits and Systems—1: Fundamental Theory and Applications, Vol. 45, No. 11 November 1998, pp. 1121-1128.

Weinmann, O., 1999. Hydrogen – the flexible storage for electrical energy, Power Engineering Journal, Vol. 13, No. 3, June 1999, pp. 164-170.

Widjaja, I., Kurnia, A., Shenai, K. and Divan, D.M., 1995. Switching Dynamics of IGBT's in Soft-Switching Converters, IEEE Transactions on Electron Devices Vol. 42, No. 3, March 1995, pp. 445-454.

Windpower monthly, 1997, "Utilities identify five offshore sites", WINDPOWER MONTHLY, July 1997, pp.24-25.

Woodbridge, J.L., 1909. Utilization of Accumulator Batteries for Control of AC Networks, Elektrotechnische Zeitung (ETZ), 1909, pp.102.

Wu, C.J. and Lee, T.S., 1991. Application of superconducting magnetic energy storage unit to improve the damping of synchronous generator, IEEE Transactions on Energy Conversions, Vol. 6, No. 4, 1991, pp. 573-578.

Wu, C.J. and Lee, T.S., 1993. Application of simultaneous active and reactive power modulation of superconducting magnetic energy storage unit to damp turbine

generator sub-synchronous oscillations, IEEE Transactions on Energy Conversions, Vol. 8, No. 1, 1993, pp. 63-70.

Wu, C.J. and Wang, C.H., 1992. Damping of power system oscillation by an active power modulation superconducting magnetic energy storage unit, Electric Power Systems Research, No. 24, 1992, pp. 65-72.

Wu, R.S., Dewn, S.B. and Slemon, G.R., 1991. Analysis of an ac-to-dc Voltage Source Converter Using PWM with Phase and Amplitude Control, IEEE Transactions on Industry Application Vol. 27, No. 2, March/April, 1991, pp. 355-364.

Yazdian-Varjani, A., Perera, S. and Chicharo, J.F., 1998. A Centroid-Based PWM Switching Technique for Full-Bridge Inverter Applications, IEEE Transactions on Power Electronics Vol. 13, No. 1, January 1998, pp. 115-124.

YMC Delegation, 1996. "Renewable Energy in Europe", Young Members Committee, The Hong Kong Institution of Engineers.

Zahedi, A., 1994. "Energy, People, Environment." Development of an integrated renewable energy and energy and energy storage system, an uninterruptible power supply for people and for better environment, IEEE International Conference on Systems, Man, and Cybernetics, 1994, Humans, Information and Technology, 1994, Vol. 3, 1994, pp. 2692 -2695.

APPENDIX 1

Data for the simulation in Section 5.4 are shown as follow. For circuit diagram, please refer to Figure 5.15.

$V_s=77.78\angle 0°$;

$I_s=12\angle -10.88°$;

$Z_s=1.2+j0.0628$;

$Z_1=0.6+j0.63$;

$Z_2=0.3+j0.315$;

$Z_L=5+j1$;

$V_1=63.5\angle 1.79°$;

$V_2=61.3\angle 0.43°$

$V_m=59.2\angle -1.02°$

$V_c=V_1-V_2$

$=2.6\angle 35.52°$

$V_d=V_1-V_m$

$=5.2\angle 35.52°$

$V_c=V_m-V_2$

$=2.6\angle -144.48°$

$I_1=6.\angle -10.88°$

$I_2=6\angle -10.88°$

$I_b=6\angle -10.88°$

$I_L=12\angle -10.88°$